Novel Re-NO Based, Highly Efficient Hydrogenation Catalysts - Stereochemical and Electronical Tuning of the $[ReHX(L)(NO)(PR_3)_2]$ System

Dissertation

zur

Erlangung der naturwissenschaftlichen Doktorwürde

(Dr. sc. nat.)

vorgelegt der

Mathematisch-naturwissenschaftlichen Fakultät

der

Universität Zürich

von

Balthasar Dudle

aus Bütschwil, SG

Promotionskomitee

Prof. Dr. Heinz Berke (Vorsitz und Leitung)

Prof. Dr. Roland K. O. Siegel

Zürich, 2011

Summary

Homogeneous hydrogenations catalysts based on platinum group metals were found to be highly effective, selective and easily tunable for a wide range of substrates and are therefore the workhorses in application. Other transition metals were also successfully employed in hydrogenations, but are usually not as versatile and easy in use. However, for rhenium based catalysts only little is known and reported on their applications in hydrogenation although rhenium is bordering the platinum group metals and thus retains a great deal of the properties of these metals, like for instance, its affinity to hydrogen and olefins. Therefore it was the aim of this PhD Thesis to explore the potential of catalysts containing the Re-NO fragment, which is isoelectronic to Rh-X, Ru-CO or Ru-PR_3 fragments often encountered in hydrogenation catalysts.

Prior to the presentation of the results of this PhD Thesis in chapters 2-6, selected fundamental aspects of homogeneous hydrogenations are discussed in chapter 1. In chapter 2 Re complexes of the type $[ReH_2(olefin)(NO)(PR_3)_2]$ are compared with the intermediate $[RhClH_2(olefin)(PPh_3)_2]$ occurring in the catalytic cycle of the Wilkinson catalyst. This studies revealed an exceptionally stable cis-hydrido ethyl intermediate, which further reacted via oxidative ethylene coupling to the $[Re(\eta^2\text{-}C_2H_4)(\eta^4\text{-}C_4H_6)(NO)(PPh_3)]$ complex. The comparison of the Re- with related Rh-system suggested significant differences in oxidative addition/reductive elimination behavior, which complicated the direct transfer of catalytic concepts from the Rh-X fragments to isoelectronic Re-NO systems. In the subsequent chapter 3 the binding of the model substrate ethylene to complexes of the form $[ReX_2(\eta^2\text{-}C_2H_4)(NO)(PPh_3)_2]$ was investigated. High ethylene affinities and rotational barriers were found in these systems. Therefore hydrogenation experiments with $[ReHX(\eta^2\text{-}C_2H_4)(NO)(PPh_3)_2]$ complexes described in chapter 4 revealed that this olefin binding properties had some general implications on the hydrogenation catalysis. As a consequence, it was concluded from the insights gained in chapter 2-4 that a change of the stereochemistry from the trans phosphine complexes $[ReHX(\eta^2\text{-}C_2H_4)(NO)(PPh_3)_2]$ to cis-diphosphine complexes of the form $[ReBrX(L)(NO)(P\cap P)]$ ($P\cap P$ = large bite angle phosphins) should enhance their catalytic activity. Consequently $[ReBrX(L)(NO)(P\cap P)]$ systems were developed as described in chapter 5. Catalytic experiments and mechanistic studies revealed that these systems are among the most active Re-based hydrogenation catalysts. It could be shown that the catalyses follows an Osborn hydrogenation mechanism. Finally the phosphine related $Re(CO)(NO)(IMes)_2$ fragment was checked with respect to its potential application in hydrogenations. Overall this work provided new insights in the possibility to use rhenium in catalysis and improved our general understanding of rhenium based homogeneous hydrogenations.

Zusammenfassung

Homogene Hydrierkatalysatoren auf Platingruppenelementen Basis haben sich als hoch effizient, selektiv und leicht anpassbar erwiesen, und sind darum heute die Arbeitspferde in der Anwendung. Auf diversen anderen Übergangsmetallen basierende Hydrierkatalysatoren wurden ebenfalls beschrieben, aber in der Regel sind diese Systeme nicht so einfach und vielseitig im Gebrauch. Im Gegensatz dazu ist nur wenig über die Anwendung von Rhenium-basierten Hydrierkatalysatoren bekannt, obwohl das Element Rhenium im Periodensystem direkt neben der Platingruppen liegt und darum noch einige Charakteristiken dieser Elemente wie beispielsweise eine ausgeprägte Affinität zu Wasserstoff und Olefinen aufweist. Ausserdem ist das Re-NO Fragment isoelektronisch zu den Rh-X, den Ru-P und den Ru-CO Fragmenten, welche oft in aktiven Katalysatoren vorkommen. Darum war es das Ziel dieser Doktorarbeit, das Potential von Re-NO basierten Katalysatoren auszuloten.

Bevor die Resultate dieser Doktorarbeit in den Kapiteln 2-6 präsentiert werden, gibt das erste Kapitel einen Einblick in ausgewählte Aspekte der homogenen Hydrierkatalyse. Im 2. Kapitel werden dann Komplexe der Form $[ReH_2(Olefin)(NO)(PR_3)_2]$ mit dem Intermediat $[RhClH_2(Olefin)(PPh_3)_2]$ aus dem Wilkinson Hydrierzyklus verglichen. In diesen Untersuchungen wurde eine ausserordentlich stabile cis-Hydrido-Ethyl Spezies gefunden, welches via oxydative Ethylen Kupplung zum $[Re(\eta^2\text{-}C_2H_4)(\eta^4\text{-}C_4H_6)(NO)(PPh_3)]$ Komplex reagiert. Der Vergleich des Re- mit dem verwandten Rh-System weist auf signifikante Unterschiede im oxydativen Additions-/reduktive Eliminierungsverhalten hin, welche das Übertragen von Konzepten von Rh-X Systemen auf Re-NO Systeme erschweren. Im nächsten Kapitel wurde die Re-Ethylen Bindung in $[ReX_2(\eta^2\text{-}C_2H_4)(NO)(PPh_3)_2]$ Komplexen untersucht wobei eine hohe Ethylenaffinität und eine hohe Rotationsbarriere gefunden wurden. Hydrierversuche mit $[ReHX(\eta^2\text{-}C_2H_4)(NO)(PPh_3)_2]$ zeigten, dass diese Eigenschaften weitereichende Konsequenzen für die Katalyse haben. Aus den Erkenntnissen aus den Kapiteln 2-4 wurde gefolgert, dass die stereochemische Veränderung durch den Wechsel von trans-Phosphin $[ReHX(\eta^2\text{-}C_2H_4)(NO)(PPh_3)_2]$ Komplexen zu cis-phosphin Komplexen der Form $[ReBrX(L)(NO)(P\cap P)]$ ($P\cap P$ = bidentates Phosphin mit grossem Bisswinkel) zu einer Erhöhung der katalytischen Aktivität führen würde. Dementsprechend wird die Entwicklung des $[ReBrX(L)(NO)(P\cap P)]$ Systems in Kapitel 5 beschrieben. Katalytische Experimente und mechanistische Studien zeigten, dass dieses System zu den aktivsten Rhenium basierten Hydrierkatalysatoren gehört und die Katalyse einem Osborn Mechanismus folgt. Abschliessend wurde das $Re(CO)(NO)(IMes)_2$ Fragment hinsichtlich seiner Eignung für die Hydrierkatalyse untersucht. Damit wurde in dieser Doktorarbeit eine neue Familie von höchst effizienten Hydrierkatalysatoren entwickelt und das allgemeine Verständnis von Rhenium in der Hydrierkatalyse verbessert.

Acknowledgement

Science is a complex team sport - The work of an individual scientist is always interwoven into ideas and concepts ranging over time and space. It also requires a stimulating and helpful environment and a lot of material resources. In that context I want to express my gratitude to those people, who enabled me to do this research.

First of all I want to thank Prof. Dr. Heinz Berke for accepting me as a student and giving me the unique possibility to do my dissertation on a challenging and inspiring topic at the University of Zürich. But since science leads not always to the expected goal, I also want to thank him for patience, confidence and optimism.

Ideas and concepts grow best if they are shared and discussed. Experimental insights need to be assessed from different unprejudiced positions. Therefore I also want to thank Dr. Christian Frech and Dr. Thomas Fox for innumerable open minded discussions on chemistry and spectroscopy.

I also want to thank Dr. Olivier Blacque, who carried out all the structural analyses and squeezed out information from the smallest crystals. Moreover I want to thank him for numerous discussions on structures and DFT-calculations.

Furthermore I want to thank Rajesh Kunjanpillai who joined the project and established the Sixantphos chemistry of the [ReBrX(L)(NO)(P∩P)] System for his contribution to chapter 5.

Finally I want to thank all members of the group for the good and productive working atmosphere.

1. Introduction

Catalytic hydrogenation is an important part of the organic chemist's toolkit. It is employed for bulk applications like the hardening of plant oils for the food industry or the synthesis of simple raw materials as well as for very specific and sophisticated tasks as the introduction of chirality into small molecules for the preparation of pharmaceuticals or agrochemicals. Although catalytic hydrogenation has its roots in the work of Paul Sabatier, who was rewarded for this with the Nobel Prize in 1912, there is still ongoing interest in it. Over more than a century, catalytic hydrogenation inspired chemists and led to numerous innovations. Although hydrogenation has matured from fundamental science to an efficient technology in the field of synthesis, there is still room for improvement and new applications. This ongoing interest is also reflected in an exponential growth of the technical literature(Figure 1).

Figure 1: The increasing number of publications on hydrogenation and its applications reflects not only the ongoing interest but also the overall growth in research activity.

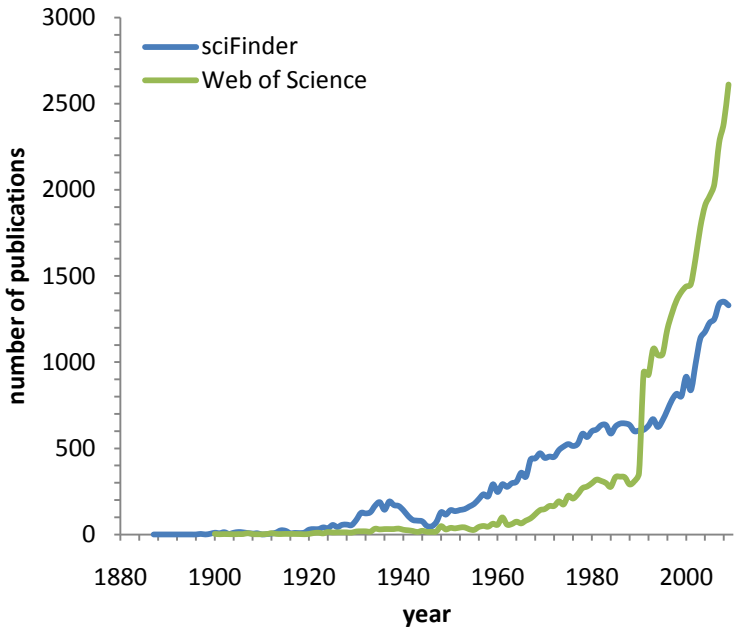

The main topic of this work is the development of novel rhenium based hydrogenation catalysts. To give an introduction into the process of hydrogenation, it will first be presented from a general point of view. Aspects such as the substrates, the catalysts, the mechanisms and related reactions will be discussed. Furthermore some related hydrogen chemistry and a few aspects on hydrogen are discussed before the novel rhenium hydrogenation chemistry is presented.

1.1 Hydrogenation

First of all the concept of hydrogenation has to be clarified. In the all-embracing definition this encompasses all reactions in which a molecule of dihydrogen (H_2) is transferred to an acceptor molecule. This comprises reactions which are usually not perceived as hydrogenations. For example the famous hydrogen-oxygen reaction, the Haber-Bosch process or the reduction of a metal oxide with H_2 could formally be called hydrogenations, but because of their exceptional nature such reactions are usually named specifically.

Scheme 1: Diverse examples of hydrogenation reactions

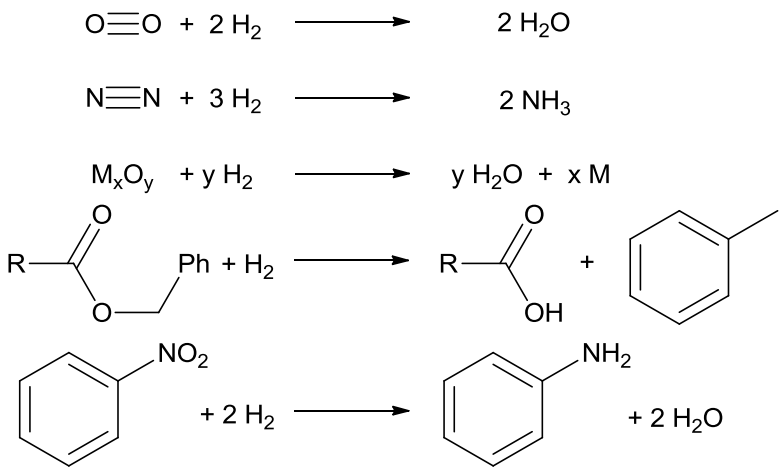

Therefore the term hydrogenation has to be defined more accurately. In the general chemical language use, hydrogenation designates a reaction in which H_2 is transferred to an unsaturated acceptor molecule[1]. Furthermore, reactions in which a single bond is disrupted by the formal insertion of H_2 are excluded from this definition. These reactions are called hydrogenolysis reactions. Another special case is the hydroformylation or oxo-reaction, in which an olefin reacts with H_2 and carbon monoxide to an aldehyde, which constitutes an own class of reactions. Typical substrates for hydrogenations are alkenes, alkynes, carbonyl compounds and imines. In the case of carbonyl and imine compounds, the hydrogenation results in the formal reduction of the involved carbon atoms. Nevertheless, the term hydrogenation should not be mixed with the term reduction.

1.1.1 The thermodynamics of hydrogenation

Hydrogenation reactions of unsaturated bonds are often strongly exothermic. The data in Table 1 gives an overview of the hydrogenation enthalpies (ΔH_{hydr}) of unsaturated C-C bonds in typical substrates. It shows that $\Delta H_{hydr.}$ for non conjugated double bonds in non strained molecules is in the range of 120-130 kJmol^{-1}. In cyclic molecules $\Delta H_{hydr.}$ depends also upon ring strain. In case of cyclopropene this leads to an increased $\Delta H_{hydr.}$ of -223.8 kJmol^{-1} while in case of cycloheptene $\Delta H_{hydr.}$

[1] Arpe, H. J.; Biekert, E.; Gerhartz, W. *Ullmann's encyclopedia of industrial chemistry*, 5th ed.; VCH Verlagsgesellschaft: Weinheim, 1996.

decreases to 108.9 kJmol^{-1}. Aromaticity is another important factor in hydrogenation reactions, which generally lowers $\Delta H_{hydr.}$. In case of naphtalene this results in the reduction of the average ΔH_{hydr} to only 66.5 kJmol^{-1} per dihydrogen molecule, which is roughly half of the ΔH_{hydr} of a typical isolated C=C double bond. The hydrogenation of C≡C triple bonds to C=C double bonds is even more exothermic with typical hydrogenation enthalpies in the range of 160-170 kJmol^{-1}, because the third bond in C≡C is thermodynamically weaker compared to the C-C or the C=C bond.

Table 1: Hydrogenation enthalpies of multiple C-C bonds calculated[2] from $\Delta H_f^{\ominus}$ or literature[3-5]

educt	**product**	**ΔH (kJmol^{-1})**
ethylene (g)	ethane (g)	-136.3
acetylene (g)	ethylene (g)	-175.7
propene (g)	propane (g)	-124.7
propine (g)	propene (g)	-164.9
allene (g)	propene (g)	-170.5
cyclopropene (g)	cyclopropane (g)	-223.8
cyclobutene (g)	cyclobutane (g)	-153.0
cyclopentene (l)	cyclopentane (l)	-109.5
cyclohexene (l)	cyclohexane (l)	-117.9
cycloheptene	cycloheptane	-108.9 (3)
butadiene (g)	1-butene (g)	-108.4
trans-hexatriene	n-hexane	-335 (4)
benzene (l)	cyclohexane (l)	-205.4
furan (l)	tetrahydrofuran (l)	-153.9
pyrrole (l)	pyrrolidine (l)	-104.1
naphtalene (g)	*trans*-decahydronaphtalene (g)	-332.4
styrene (l)	ethylbenzene (l)	-116.1
phenylacetylene	styrene	-160 (5)
acrylic acid (l)	propanonic acid (l)	-126.9
allyl alcohol (l)	1-propanol (l)	-130.8
divinyl ether (l)	ethyl vinyl ether (l)	-127.6

In general, the high $\Delta H_{hydr.}$ reflects the weaker character of multiple X-X/X-Y bonds compared to X-H/ Y-H bonds. Therefore the hydrogenation of carbonyl compounds should in general posses less negative $\Delta H_{hydr.}$ compared to olefins because the C=O double bond is stronger than the C=C double bond and the C-H and O-H bonds are comparable[6]. Unlike the strong C=O bond, the C=N bond is comparable to the C=C bond[6]. Nevertheless $\Delta H_{hydr.}$ of imines is less negative than $\Delta H_{hydr.}$ of olefins

[2] Lide, D. R. *Handbook of Chemistry and Physics*, 73th ed.; CRC Press: Boca Raton, Florida, 1993.

[3] Roth, W.R.; Lennartz, H.W., Heats of hydrogenation. I. Determination of heats of hydrogenation with an isothermal titration calorimeter. *Chemische Berichte* **1980**, 113, 1806-1817.

[4] Fang, W.; Rogers, D.W., Enthalpy of hydrogenation of the hexadienes and cis- and trans-1,3,5-hexatriene. *Journal of Organic Chemistry* **1992**, 57, 2294-2297.

[5] Davis, H.E.; Allinger, N.L.; Rogers, D.W., Enthalpies of hydrogenation of phenylalkynes: indirect determination of the enthalpy of formation of diphenylcyclopropenone. *J. Org. Chem.* **1985**, 50, 3601-3604.

[6] Riedel, E. *Anorganische Chemie*, 4. Aufl.; de Gruyter: Berlin, 1999.

because the average N-H bond is weaker than the C-H bond. The data in Table 2 illustrates this finding.

Table 2: Hydrogenation enthalpies of multiple C-O and C-N bonds calculated[2] from $\Delta H_f^{\ominus}$ or literature[7-9]

educt	**product**	**ΔH (kJmol^{-1})**
carbon dioxide (g)	formic acid (g)	+14.9
carbon monoxide (g)	methanol (g)	-91.0
dinitrogen (g)	2 ammonia (g)	-91.8
formaldehyde (g)	methanol (l)	-92.9
acetaldehyde (l)	ethanol (l)	-85.9
propanal (l)	n-propanol (l)	-87.3
isobutanal (l)	iso-butanol	-87.3
benzaldehyde (l)	benzyl alocohl (l)	-73.7
acetone (l)	2-propanol (l)	-70.0
3-pentanone (l)	3-pentanol (l)	-72.4
3-methyl-2-butanone (l)	3-methyl-2-butanol (l)	-67.2
formic acid (g)	formaldehyde (g)	+28.2
acetic acid (l)	acetaldehyde (l)	+6.9
benzoic acid (g)	benzaldehyde (g)	+12.6
N-ethylydene-propylamine	ethylpropylamine	-89 (7)
N-butylidenebutylamine	dibutylamine	-86 (8)
N-ethylydene-isopropylamine	ethylisopropylamine	-92 (8)
N-ethylydene-*tert*-butylamine	ethylisobutylamine	-96 (8)
glyoxal-bis(N-*tert*-butyl)imine	N,N'-di-*tert*-butylethylenediamine	-188 (8)
2,3-dimethyldihydropyrazine	2,3-dimethylpiperazine	-169 (8)
pyrazin	piperazine	-207 (8)
propionitrile (l)	propylamine (l)	-117.0
isobutyronitrile	isobutylamine	-118.8

It reveals that aldehydes and aldimines possess negative hydrogenation enthalpies of around -80 to -90 kJmol^{-1}. Therefore the hydrogenation of aldehydes and aldimines is about 25% less exothermic than the hydrogenation of olefins. Ketones with a $\Delta H_{hydr.}$ of around -70 kJmol^{-1} have even less negative $\Delta H_{hydr.}$ than aldehydes. Due to the lack of experimental data, hydrogenation enthalpies of ketimines cannot be compared to those of aldimines. The hydrogenation of carboxylic acids is thermodynamic less favorable compared to the hydrogenation of ketones, aldehydes and imines. The first step from the carboxylic acid to the corresponding aldehyde and water has even positive $\Delta H_{hydr.}$ of up to 28.2 kJmol^{-1} (formic acid). But the subsequent hydrogenation of the aldehydes to the alcohols is sufficiently exothermic, to act as driving force for the hydrogenation of carboxylic acids to

[7] Jackman, L.M.; Packham, D.I., The experimental resonance energy of acridine. *Proc.Chem. Soc.* **1957**, 349-350.
[8] Hafelinger, G.; Steinmann, L., Heat of hydrogenation of compounds containing isolated and conjugated C=N double bonds. *Angew. Chem. Int. Ed.* **1977**, 16, 47-48.

the corresponding alcohols. Nitriles have also similar low $\Delta H_{hydr.}$ of around -120 $kJmol^{-1}$ for the hydrogenation to corresponding amines.

1.2 Hydrogen

Hydrogen, the second substrate in hydrogenation reaction, is the lightest element and it is abundant in the universe[9]. Its elementary form is dihydrogen (H_2) which is the simplest and smallest imaginable molecule. Because it diffuses easily into space, H_2 is only present in trace amounts in the earth atmosphere. Therefore, most hydrogen on earth is chemically bound in either water or organic matter[9]. Although H_2 is such a simple molecule, it kept chemists busy for centuries and even today a lot of research is carried out in this field. Since H_2 can easily be produced by the reactions of non noble metals with acids, it has been accessible for a long time[10]. First records of H_2 generation date back to the 16th century but it was not recognized as an element[9] until 17th century. The discovery of hydrogen is attributed to the work of Henry Cavendish and Antoine Lavoisier. Dihydrogen is usually produced by the reduction of water protons[11]. The mentioned reaction with non noble metals is only feasible in laboratory scale. In large scale the "universal reducing agent" coal is much more efficient. In the so called coal gasification process water reacts with carbon in an endothermic reaction to synthesis gas - a mixture of H_2 and carbon monoxide (CO). The energy required for this reaction is provided by partial burning of coal.

$$C + H_2O(g) \leftrightarrows CO + H_2 \qquad \Delta H = +131.3\ kJmol^{-1}\ [2]$$

If CO is not required for further reactions, it can be reacted with another equivalent of water to produce another equivalent of H_2 and carbon dioxide (CO_2).

$$CO + H_2O(g) \leftrightarrows CO_2 + H_2 \quad \Delta H = -41.2\ KJmol^{-1}\ [2]$$

This reaction is called water gas shift reaction and leads formally to the formation of CO_2 and H_2 . Nevertheless, the product gases have to be purified from sulfur containing contaminants, residual CO and other impurities originating from burning coal. Alternatively, various hydrocarbons can be used. In contrast to the coal gasification process, hydrocarbons already contain hydrogen which can be obtained as H_2 by thermal decomposition:

$$C_xH_y \leftrightarrows x\ C + y/2\ H_2$$

[9] Enghag, P. *Encyclopedia of the elements*. *Technical data, history, processing, applications;* Wiley-VCH: Weinheim, 2004.
[10] Holleman, A. F.; Wiberg, E.; Wiberg, N. Holleman-Wiberg. *Lehrbuch der anorganischen Chemie*, 101. Aufl.; de Gruyter: Berlin, 1995.
[11] Holladay, J. D.; Hu, J.; King, D. L.; Wang, Y. An overview of hydrogen production technologies: Hydrogen Production - Selected papers from the Hydrogen Production Symposium at the American Chemical Society 234th National Meeting & Exposition, August 19-23, 2007, Boston, MA, USA. *Catalysis Today* **2009,** *139* (4), 244–260.

$$CH_4 \leftrightarrows C + 2\ H_2 \qquad \Delta H = +74.4\ kJmol^{-1}\ [2]$$

The formed carbon can then be reacted with water to obtain more H_2 and CO_2:

$$CH_4 + 2\ H_2O(g) \leftrightarrows CO_2 + 4\ H_2 \qquad \Delta H = +164.5\ kJmol^{-1}\ [2]$$

Alternatively, H_2 of high purity can be obtained by electrolysis of water:

$$2\ H_2O(l) \leftrightarrows O_2 + H_2 \quad \Delta H = +285.8\ kJmol^{-1}\ [2]$$

Electrolysis is only economic if the high purity of the obtained H_2 is crucial. Otherwise the production of H_2 from fossil fuels is more economic and also more environmental benign as the latter route circumvents the production of electricity (partly from fossil fuels).

1.2.1 Activation of H_2

H_2 can be split either homolytically into formally two H· radicals or heterolytically into a hydride and a proton (Scheme 2). The homolytic splitting[2] of H_2 in the gas phase requires 436 $kJmol^{-1}$. If H_2 is formally split heterolytically into a proton and a hydride, the dissociation energy decreases depending on the local electrical field and eventually ceases to exist (Scheme 8)[12]. Consequently the high binding energy of H_2 results in kinetic inertness. Therefore hydrogen chemistry depends largely on the use of catalysts to activate H_2. In the following two sections the heterolytic and the homolytic activation of H_2 are briefly discussed. For a more detailed overview on the topic, the interested reader is referred to Berke's review on the principles of H_2 activation[13].

Scheme 2: The activation of H_2 can proceed in a heterolytic and a homolytic mode.

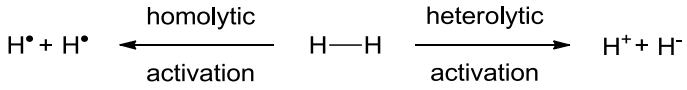

1.2.1.1 Homolytic activation of H_2

The first reported catalyst for H_2 activation was elemental platinum for the catalyzed hydrogen oxygen reaction by J. W. Döbereiner in 1823, which led to the invention of the famous Döbereiner lighter[14]. Platinum did not remain the only metal being able to activate H_2. Today the metals Ti, Zr, Hf, V, Nb, Ta, Cr, Mo, W, Fe, Ru, Os and to smaller extent Ni, Co, Rh, Pd, Pt, Ir, Mn and Cu are also known to be capable of activating H_2[15]. The mode of activation by these metals is called chemisorption. In contrast to physisorption, which refers to the mere adsorption of the sorbent to a

[12] Grimme, S.; Kruse H.; Goerigk, L.; Erker, G. The Mechanism of Dihydrogen Activation by Frustrated Lewis Pairs Revisited. *Angew. Chem. Int. Ed.* **2010,** *49*, 1402–1405.
[13] Berke, H, Conceptual approach to the Reactivity of Dihydrogen. ChemPhysChem **2010,** 11, 1837-1849.
[14] Hoffman, R. Döbereiner's Lighter. *American Scientist* **1998**, *86*, 326.
[15] Hagen, J. *Technische Katalyse*. *Eine Einführung;* VCH: Weinheim, **1996**.

surface, chemisorption is a chemical reaction, in which the sorbent forms chemical bonds with the surface atoms (Scheme 3). In some cases, hydrogen diffuses to such a high extent into the metals or alloys that these materials are considered for H_2 storage applications[16].

Scheme 3: Schematic depiction of physisorption and chemisorption by a metal surface.

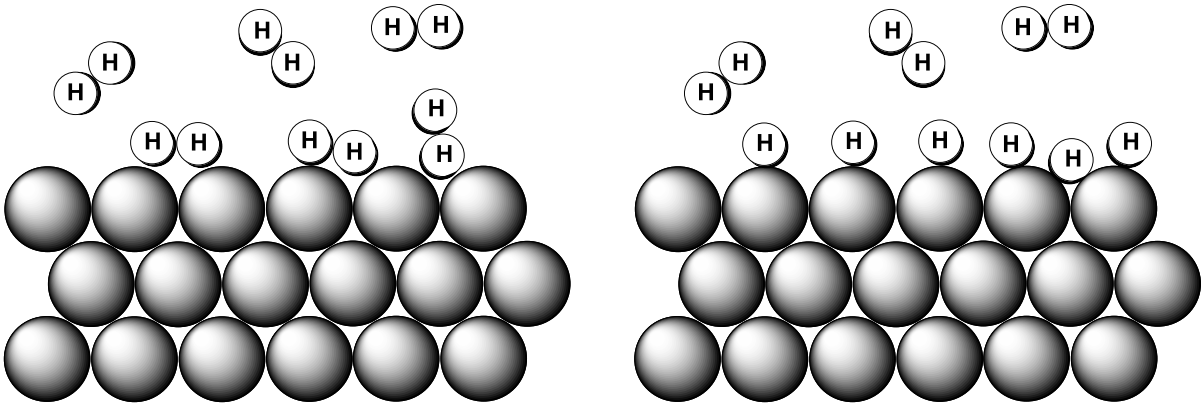

Activation of H_2 by molecular species was discovered later. In 1942 the absorption of hydrogen by cobaltous cyanide in aqueous solution was reported by M. Iguchi[17]. In the following time various complexes were found, which undergo easily oxidative addition of H_2. But it was not until 1984, when Kubas discovered the H_2 complexes[18]. This triggered an avalanche of research on the topic and a large number of H_2 complexes were found. It showed that the binding of H_2 in these complexes varies and that the transition from the H_2 complex over oxidative addition to a dihydride complex is smooth[19,20]. With this experimental data the understanding and interpretation of the homolytic activation of σ-bonds - in particular of the H-H bond - were improved fundamentally. It proved that σ-bonds could be coordinated to an unsaturated atom to form a σ-complex. Furthermore, it revealed that the ability for back donation decided over the faith of such a σ-complex (Scheme 4). If no or only little back donation is possible, the oxidative addition becomes stuck on an early stage and the σ-bond remains intact and a σ-complex is formed. If the back donation into the σ*-orbital is stronger, the σ-bond is weakened. This results then in the oxidative addition to a classical dihydride complex. These findings in molecular chemistry can be generalized, to provide a theory for the chemisorption of small molecules by metal surfaces as well.

[16] Sakintuna, B.; Lamari-Darkrim, F.; Hirscher, M. Metal hydride materials for solid hydrogen storage: A review. *Int. J. Hydrogen Energy* **2007,** *32*, 1121–1140.
[17] Kwiatek, J. Reactions Catalyzed by Pentacyanocobaltate(II). *Catal. Rev.* **1967,** *1*, 37–72.
[18] Kubas, G. J.; Ryan, R. R.; Swanson, B. I.; Vergamini, P. J.; Wasserman, H. J. Characterization of the first examples of isolable molecular hydrogen complexes, $M(CO)_3(PR_3)_2(H_2)$ (M = molybdenum or tungsten; R = Cy or isopropyl). Evidence for a side-on bonded dihydrogen ligand. *J. Am. Chem. Soc.***1984,** *106*, 451–452.
[19] Kubas, G. J. Dihydrogen complexes as prototypes for the coordination chemistry of saturated molecules. *Proc. Natl. Acad. Sc.* **2007,** *104*, 6901–6907.
[20] Kubas, G. J. Metal-dihydrogen and σ-bond coordination: the consummate extension of the Dewar-Chatt-Duncanson model for metal-olefin π-bonding. *J. Organomet. Chem.* **2001,** *635*, 37–68.

Scheme 4: The degree of back-bonding into the σ*-orbital of H_2 is decisive for the nature of the formed compound.

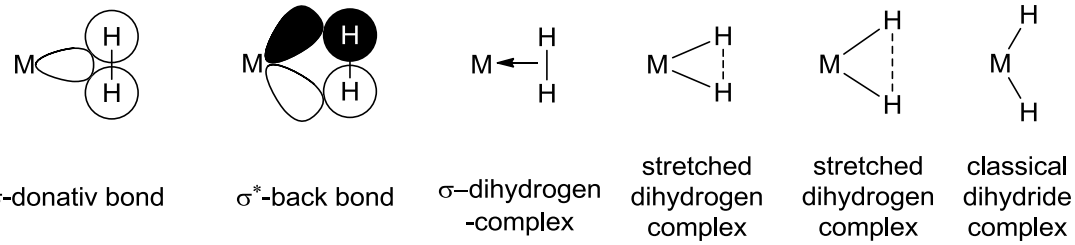

A special case of homolytic activation of H_2 is the activation by radicals. An early example of this mechanism is the activation of H_2 with chlorine radicals in a very exothermic chain reaction (HCl: $\Delta H_f^{\ominus}$ = -92 kJmol^{-1} [2]) to form hydrochloric acid. A less dangerous example is the activation with dinuclear metal complexes such as [$Co_2(CO)_8$] (ΔH = +20 kJmol^{-1})[21] or [$Mn_2(CO)_{10}$] (ΔH = +36 kJmol^{-1})[22] to the corresponding hydrides [$CoH(CO)_4$] rep. [$MnH(CO)_5$]. In these cases it is assumed that the metal-metal bond of the dinuclear complexes is homolytically cleaved and the formed radicals react with H_2 molecules in most cases via a trimolecular transition state to form the mono hydrides[23] (Scheme 5).

Scheme 5: Activation of H_2 by metal radicals.

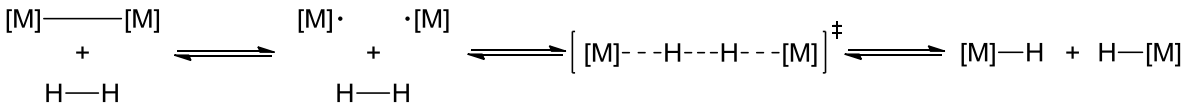

1.2.1.2 Heterolytic activation of H_2

The discovery of the σ-dihydrogen complexes revealed that the bound hydrogen can be very acidic[24,25]. The deprotonation of such acidic H_2 complexes is often possible, if a sterically hindered and sufficient basic base is employed. Since the H_2 molecule is formally split into a hydride and a proton, this mode of H_2 activation is the so called heterolytic activation. As the backbonding capabilities of metals are not required for this kind of activation, it is not confined to transition metals. An early observation of transition-metal-free H_2 activation was made by Walling and Bollyky,

[21] Rathke, J. W.; Klingler, R. J.; Krause, T. R. Thermodynamics for the hydrogenation of dicobalt octacarbonyl in supercritical carbon dioxide. *Organometallics* **1992,** *11*, 585–588.
[22] Klingler, R. J.; Rathke, J. W. Thermodynamics for the hydrogenation of dimanganese decacarbonyl. *Inorg. Chem.* **1992,** *31*, 804–808.
[23] Capps, K. B.; Bauer, A.; Kiss, G.; Hoff, C. D. The rate and mechanism of oxidative addition of H_2 to the ·$Cr(CO)_3C_5Me_5$ radical - generation of a model for reaction of H_2 with the ·$Co(CO)_4$ radical. *J.Organomet. Chem.* **1999,** *586*, 23–30.
[24] Fong, T. P.; Lough, A. J.; Morris, R. H.; Mezzetti, A.; Rocchini, E.; Rigo, P. Turning dihydrogen gas into a strong acid. Formation and reactions of the very acidic ruthenium dihydrogen complexes. *J. Chem. Soc., Dalton Trans.* **1998,** 13, 2111–2113.
[25] Luther, T. A.; Heinekey, D. M. Synthesis, Characterization, and Reactivity of Dicationic Dihydrogen Complexes of Osmium and Ruthenium. *Inorg. Chem.* **1998,** *37*, 127–132.

when they found the transition-metal-free hydrogenation of ketones in 1964[26] (Scheme 6). Later Berkessel et al. proposed a cyclic transition state for this reaction[27].

Scheme 6: Catalytic hydrogenation of benzophenone in the presence of KO*t*Bu.

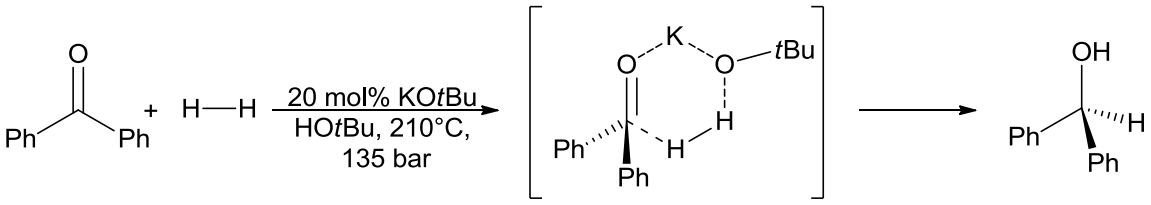

Although this is an example of transition-metal-free H_2 activation, it should require decades until the first example of a molecular main group compound was found, which was capable of reversibly bind H_2. In 2006 Stephan et al. found the remarkable phosphonium borate $[(Mes)_2PH(C_6F_4)BH(C_6F_5)_2]$ (**1**) which reversibly loses H_2 upon heating[28] to form $[(Mes)_2P(C_6F_4)B(C_6F_5)_2]$ (**2**). **2** was found to react under mild conditions without catalyst with H_2 to regenerate **1** (Scheme 7).

Scheme 7: The first reported example of reversible heterolytic activation of H_2 to produce pure main group element compounds without metal catalyst.

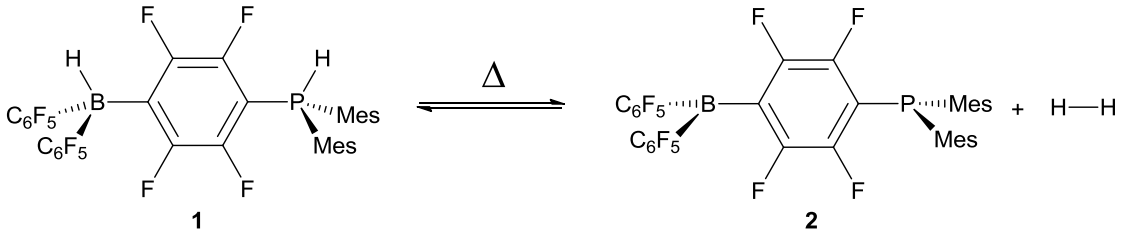

These findings triggered a great deal of research in the field of Frustrated Lewis Pairs (FLP). The FLP encounter complex refers to a couple of Lewis acid and Lewis base which cannot form stable Lewis adducts due to steric hindrance. Up to the present numerous FLPs capable for H_2 activation were developed and theoretical investigations showed that the electrical field induced by the FLP allows heterolytic dissociation of H_2 under mild conditions[12]. It should be noted that the activation of H_2 with an unsaturated electron deficient transition-metal complex and an adequate base is mechanistically hard to distinguish from an FLP and thus the mechanism of H_2 activation is fairly close to the main group FLP reaction (Scheme 8).

[26] Walling, C.; Bollyky, L. Homogeneous Hydrogenation in the Absence of Transition-Metal Catalysts. *J. Am. Chem. Soc.* **1964,** *86*, 3750–3752.
[27] Berkessel, A.; Schubert, T. J. S.; Müller, T. N. Hydrogenation without a Transition-Metal Catalyst: On the Mechanism of the Base-Catalyzed Hydrogenation of Ketones. *J. Am. Chem. Soc.* **2002,** *124*, 8693–8698.
[28] Welch, G. C.; Juan, R. R. S.; Masuda, J. D.; Stephan, D. W. Reversible, Metal-Free Hydrogen Activation. *Science* **2006,** *314*, 1124–1126.

Scheme 8: The polarization of H_2 is principally independent from the origin of the electric field.

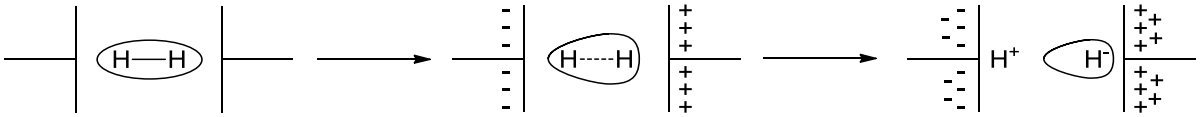

1.3 Hydrogenation catalysts and the mechanisms of hydrogenation

Hydrogenation reactions do not only require the activation of H_2 but also the activation of the acceptor substrate for facile H transfer, which is usually an unsaturated organic compound. Furthermore, the activated H_2 and the activated substrate have to be combined in an adequate way to form the products. The characteristics of substrates vary - from non-polar multiple bonds, such as the ethylene C=C bond to strongly polarized bonds, such as the carbonyl C=O bond in acetone. This substrate variety is reflected in different modes of activation and in different catalytic mechanisms for the respective substrates. Consequently, a catalyst, which is very efficient in hydrogenation of non-polar bonds, is less effective in hydrogenation of polar bonds and *vice versa*. For example the Fe^{II}/EDTA system shows high selectivity for C=C bonds[29] while the $[RuH_2(ethylenediamine)(PPh_3)_2]$ complex can hydrogenate only C=O bonds[30] (Scheme 9).

Scheme 9: Chemoselective hydrogenation of C=O and C=C bond

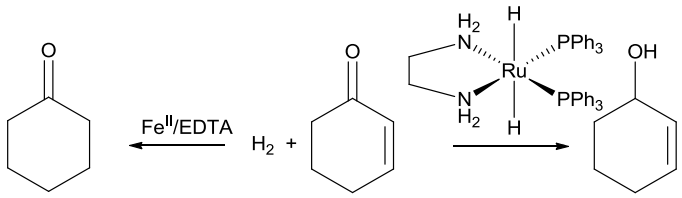

The mechanisms of catalytic hydrogenation reactions are not uniform und vary with the catalyst-substrate couple and the employed conditions. Spectroscopic observation of intermediates is usually difficult and requires often sophisticated experiments. Sometimes, especially in case of heterogeneous catalysts, the elucidation of the mechanism with the help of spectroscopic methods is almost impossible. Therefore, the scope of this introducing section is limited to a few selected and well understood catalyst systems. The catalyst systems are divided into two groups according to the nature of the hydrogen transfer. Catalysts of the homopolar group transfer H_2 formally as H· radicals, while the catalysts of the heteropolar group transfer formally H^+ and H^- to the substrate. Furthermore, a finer subdivision of the catalysts according to the sequence of H_2 transfer can be

[29] Bhor, M. D.; Bhanushali, M. J.; Nandurkar, N. S.; Bhanage, B. M. Direct reductive amination of carbonyl compounds with primary/secondary amines using recyclable water-soluble Fe-II/EDTA complex as catalyst. *Tetrahedron Lett.* **2008,** *49*, 965–969.

[30] Ohkuma, T.; Ooka, H.; Ikariya, T.; Noyori, R. Preferential hydrogenation of aldehydes and ketones. *J. Am. Chem. Soc.* **1995,** *117*, 10417–10418.

made. For a more detailed overview on these processes, the interested reader is again referred to Berke's conceptual overview on hydrogen chemistry[13].

1.3.1 Homopolar hydrogenation catalysts

The probably best-known homopolar hydrogenation catalyst is $[RuCl(PPh_3)_3]$ (**3**) - the so called Wilkinson's catalyst. It was discovered in 1966 by Wilkinson and it was the first hydrogenation catalyst, which was extensively studied by at the time very modern means such as ^1H and ^{31}P VT-NMR and various kinetic experiments[31,32,33,34]. Scheme 10 shows a simplified catalytic cycle of Wilkinson's catalyst.

Scheme 10: A simplified catalytic cycle of Wilkinson's catalyst **3**

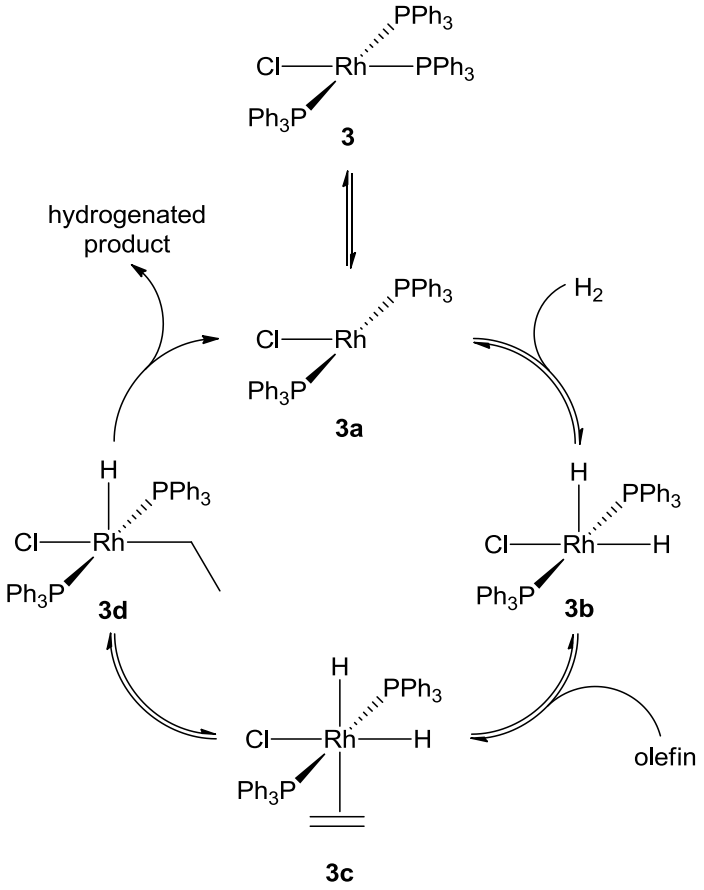

The saturation of the unsaturated intermediate species **3a,b** and **d** with solvent molecules, PPh_3 or by dimerization is not shown. These saturated species are prevailing in solution. As the catalysis is

[31]Osborn, J. A.; Jardine, F. H.; Young, J. F.; Wilkinson, G. Preparation and Properties of Tris(Triphenylphosphine)Halogeno-rhodium(I) and Some Reactions thereof including Catalytic Homogeneous Hydrogenation of Olefins and Acetylenes and their Derivatives. *J. Chem. Soc., A* **1966,** 12, 1711–1732.

[32] Tolman, C. A.; Meakin, P. Z.; Lindner, D. I.; Jesson, J. P. Triarylphosphine, hydride, and ethylene complexes or rhodium(I) chloride. *J. Am. Chem. Soc.* **1974,** *96*, 2762–2774.

[33] Meakin, P.; Jesson, J. P.; Tolman, C. A. Nature of chlorotris(triphenylphosphine)rhodium in solution and its reaction with hydrogen. *J. Am. Chem. Soc.* **1972,** *94*, 3240–3242.

[34] Eaton, D. R.; Suart, S. R. Ligand exchange and isomerization in tris(triphenylphosphine)chlororhodium(I). *J. Am. Chem. Soc.* **1968,** *90*, 4170–4172.

very efficient, none of the depicted unsaturated intermediates could be detected under catalytic conditions. The proposed dihydro-olefin complex [$RhClH_2$(olefin)(PPh_3)$_2$] (**3c**) could not be detected either. D_2 experiments with cyclic substrates revealed that the transfer of the H/D atoms to the substrate is a step wise and reversible process[35]. Nevertheless, this process is very fast for sterically less demanding substrates and therefore the hydrogen transfer to the substrates is often considered as one fast step.

We can conclude from the extensive research on the system that the characteristic features of the Wilkinson's catalyst are the following:

- H_2 is oxidatively added before the substrate is bound to the complex.
- The insertion of the olefin into the Rh-H bond is fast but principally reversible.
- The decomposition of the catalyst is prevented by the formation of 16e- complexes such as [$RhCl(PPh_3)_3$] and [{$Rh(\eta^2$-$Cl)(PPh_3)_2$}$_2$] respectively their H_2 containing 18e- counterparts.
- Repeated ligand dissociation during the course of the catalysis is necessary.
- The reaction is 1th order in the olefin and the hydrogen concentrations.

Later on, cationic complexes of the form [Ru(dien)P_2][A^-] (**4**) P= phosphines or bisphosphine, A^- = weakly coordinating anion such as BF_4^- or PF_6^-, dien = 1,5-cyclooctadiene, 1,4-cyclohexadiene or norbornadiene were prepared[36] and used as hydrogenation pre-catalysts in polar solvents. This led to improved catalyst activity, because no phosphine ligand dissociation is involved anymore. Nevertheless, it was observed that the diene ligand initially inhibits the catalyst. This leads to an initiation phase of the catalysis until the diene is fully hydrogenated to produce the solvate complex **4a**. **4a** readily absorbs H_2 to form the cationic dihydride **4b**, which is isolable (Scheme 11). As the dienes are hydrogenated very slowly this can take a long time[37]. Osborn and coworkers investigated the mechanism of these catalysts and revealed a new reaction pathway[38]. If the catalysts are used in basic environment, the deprotonation of the cationic **4b** to the neutral hydride **4c** occurs. The proposed catalytic cycle in Scheme 11 shows the schematic outline of Osborn's cycle. It needs to be mentioned that the occurrence of a particular species depends very much on the solvent and the substrate. Therefore the species **4c-f** may not necessarily posses the depicted structures under real catalytic conditions and should be considered as rough guidelines to understand the cycle.

---

[35] Hussey, A. S.; Takeuchi, Y. Hydrogenations of cycloalkenes using tris(triphenylphosphine)chlororhodium(I). *J. Am. Chem. Soc.* **1969,** *91*, 672–675.

[36] Shapley, J. R.; Schrock, R. R.; Osborn, J. A. Preparation and catalytic properties of some cationic iridium(III) and rhodium(III) dihydrido complexes. *J. Am. Chem. Soc.* **1969**, 91, 2816–2817.

[37] Heller, D; de Vries, A. H. M.; de Vries, J. G. Catalyst Inhibition and Deactivation in Homogeneous Hydrogenation. In *The handbook of homogeneous hydrogenation*; de Vries, J. G.; Elsevier, C. J. Eds.; WILEY-VCH: Weinheim, 2007; pp 1483–1516.

[38] Schrock, R. R.; Osborn, J. A. Catalytic hydrogenation using cationic rhodium complexes. I. Evolution of the catalytic system and the hydrogenation of olefins *J. Am. Chem. Soc.* **1976,** *98*, 2134–2143.

Osborn's catalytic cycle differs in the order of substrate binding from the Wilkinson's catalyst's cycle. The olefin is first bound to **4c** producing **4d**. After a β-hydride shift, the alkyl complex **4e** is formed, which adds H_2 forming **4f**. The hydrogenated product is finally eliminated from **4f** regenerating **4c**. The β-hydride shift of the hydride from the metal (**4d**) to the olefin (**4e**) and its reversal are fast processes and in addition the olefin is reversibly bound to **4d.** This may lead to olefin isomerization for this kind of catalysis.

Scheme 11: Osborn's catalytic cycle

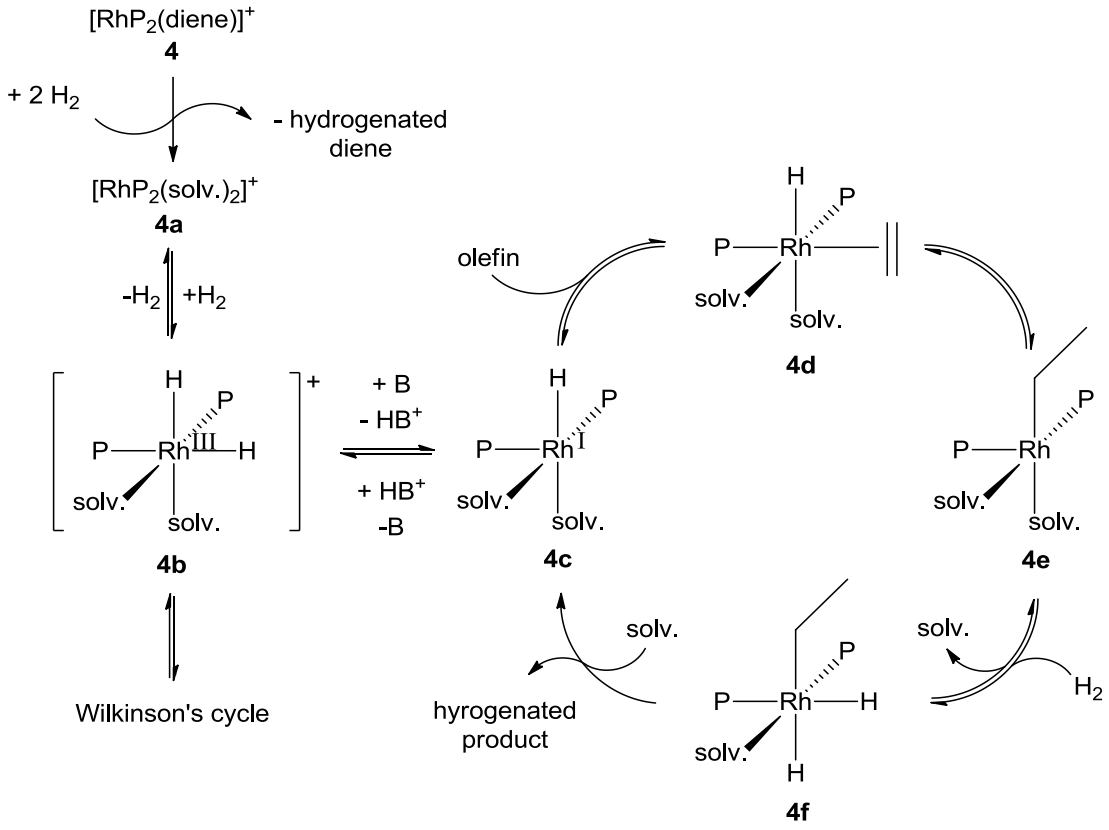

The key features of Osborn's cycle can be summarized as follows:

- Depends on pH - basic media are required.
- **4a** is more efficient than **3** because only solvent de- and re-coordination is required to initiate the cycle.
- Olefin coordinates before H_2 is oxidatively added
- Olefin isomerization.
- H_2 coordination to the alkyl-complex is crucial

Cationic $[Ru(dien)L_2][A^-]$ catalysts are prepared from commercially available $[\{Ru(dien)(\mu^2\text{-}Cl)_2\}]$ (**5**)[39] or even more convenient $[Ru(dien)_2][A^-]$ (**6**) precursors by adding 2 equivalents of a monodentate

[39] Chatt, J.; Venanzi, L. M. Olefin Coordination Compounds: 16. Diene Compleses of Rhodium(I). *J. Am. Chem. Soc.* **1957**, 79, 4735–4741.

phosphine or 1 equivalent of a bisphosphine. This facile access to the pre-catalyst together with excellent catalytic properties and high versatility make this catalyst system to one of the most preferred systems. Especially for asymmetric hydrogenation, where numerous ligands have to be tested, the ease of catalyst preparation is an important factor in the overall evaluation of the system.

Scheme 12: In situ preparation of Osborn's catalysts from commercial starting materials

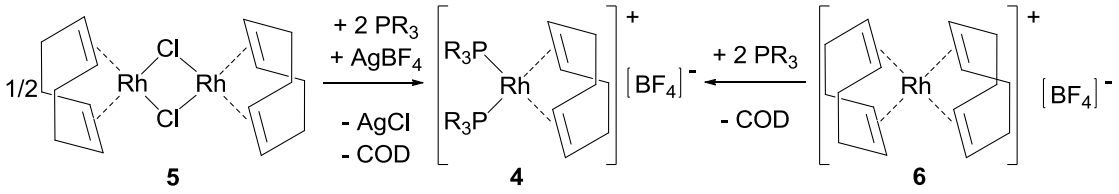

Another catalyst, which is working principally in the same way, is Crabtree's catalyst[40]. Analogous to Osborn's catalyst it is derived from the cationic $[Ir(COD)L_2][PF_6]$ (**7**) (L = 2 phosphines or phosphine and pyridine) complex. It is much more active than Wilkinson's and Osborn's catalyst and can hydrogenate also sterically more demanding substrates. But unlike Wilkinson's or Osborn's catalyst, it requires the stabilization with the substrate after the hydrogenation of the COD ligand. If either the substrate is fully consumed or the substrate olefin is sterically demanding, polynuclear hydride bridged complexes (**8a,b**) can be formed (Scheme 13).

Scheme 13: Deactivation of Crabtree's catalyst by the formation of poly-hydrides

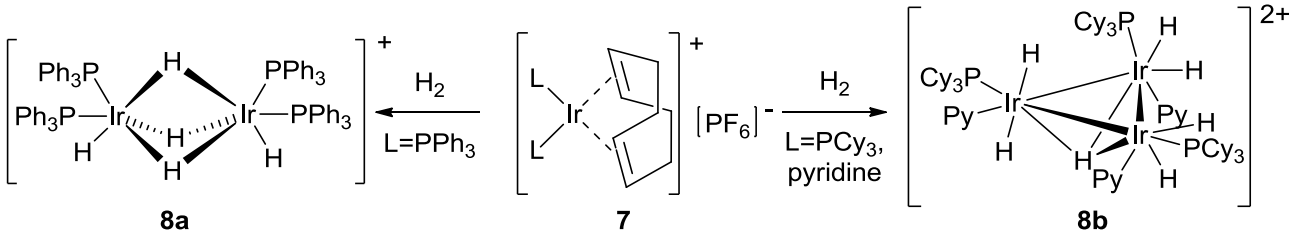

To complete the overview of the homopolar hydrogenation catalysts, it has to be mentioned that the catalysis on metal surfaces is expected to operate on a very similar[15] base. Nevertheless much less experimental data are available because the reactions take place on surfaces where the spectroscopic toolkit is very limited. This causes problems to the elucidation of the mechanisms, which is already difficult for homogenous, well defined systems. Furthermore, heterogeneous catalysts are not as uniform as their homogenous counterparts and based on this fact the reactions are generally less reproducible.

1.3.2 Heteropolar hydrogenation catalysts

As already mentioned, H_2 can be split heterolytically into H^+ and H^-. Therefore, catalysts following this route of activation are predestinated to substitute ionic hydride sources such as $NaBH_4$ or $LiAlH_4$ in

[40] Crabtree, R. Iridium compounds in catalysis. *Acc. Chem. Res.* **1979**, *12*, 331–337.

organic chemistry (Scheme 14). Such hydride sources are extensively used to reduce substrates such as carbonyl-compounds, imines, carboxylic acids and esters.

Scheme 14: Comparison of the stoechiometric two step procedure to reduce a ketone against single step hydrogenation

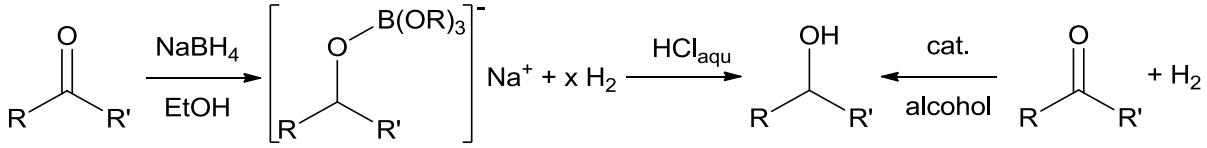

Therefore, the development of hydrogenation catalysts capable of formally delivering H^- and H^+ to a substrate is very attractive. It leads to less complex and therefore more economical and also more environmental benign processes. Despite of these amenities, the systematic research for such catalysts is a comparably young field. Although catalytic procedures for the catalytic hydrogenation of ketones were known for a long time, with early records dating back to 1903[41], the highly efficient and selective ruthenium catalysts were developed relatively late in the mid nineties. An early highly efficient catalyst for the hydrogenation of ketones is Shvo's catalyst $[RuH(CO)_2(\eta^5\text{-}C_5H_4OH)]$ (**9**)[42]. Studies on this catalyst gave in-depth insight into metal-ligand bifunctional catalysis. The catalytic cycle in Scheme 15 was longtime controversial, as it is very difficult to proof experimentally. An alternative primary coordination sphere mechanism, which was thought to proceed either via ring slippage or carbonyl dissociation steps, was discussed as well. Because experiments alone could not fully support either one of the mechanisms[43], theoretical studies were carried out, which finally supported the secondary coordination sphere mechanism[44]. In this mechanism, the proton and hydride transfers from **9** to a polar acceptor substrate (acetone in Scheme 15) were thought to proceed concerted. As the polarization of **9** and **9a** matches with that of the substrate/product compounds, hydrogen bonds are anticipated to be formed between the catalyst species and the educts/products. This leads to favorable pre-orientation and facilitates the simultaneous transfer of the hydride/proton in a concerted transition state **TS(9+carbonyl)**. The H transfer via **TS(9+carbonyl)** is thermodynamically accessible from the starting compound side as well as from the product side, thus the hydrogen transfer is reversible. Therefore, **9** catalyzes also the transfer-hydrogenation between a sacrificial H donor molecule, such as isopropanol or formic acid and an acceptor molecule. Since such reactions are usually not very exothermic (Table 2), the thermodynamics of the double H

[41] Sabatier, P.; Senderens, J. B. Transformation of aldehydes and ketones in alcohols by catalytic hydrogenation. *C. R. Hebd. Seances Acad. Sci.* **1903,** *137*, 301–303.
[42] Shvo, Y.; Czarkie, D.; Chodosh, D. F.; Rahamim, Y. A new group of ruthenium complexes: structure and catalysis. *J. Am. Chem. Soc.* **1986,** *108*, 7400–7402.
[43] Casey, C. P.; Beetner, S. E.; Johnson, J. B. Spectroscopic Determination of Hydrogenation Rates and Intermediates during Carbonyl Hydrogenation Catalyzed by Shvo's Hydroxycyclopentadienyl Diruthenium Hydride Agrees with Kinetic Modeling Based on Independently Measured Rates of Elementary Reactions. *J. Am. Chem. Soc.* **2008,** *130*, 2285–2295.
[44] Comas-Vives, A.; Ujaque, G.; Lledós, A. Hydrogen Transfer to Ketones Catalyzed by Shvo's Ruthenium Hydride Complex: A Mechanistic Insight. *Organometallics* **2007,** *26*, 4135–4144.

transfer has to be finely tuned by choosing appropriate donor and acceptor components. For catalytic hydrogenations, the regeneration of **9** from **9a** applying H_2 is crucial. Current studies suggest that an acidic H_2 intermediate is formed. Subsequently an alcohol group mediates the transfer of the acidic H_2 ligand to the carbonyl function of the cyclopentadieneone ligand[45].

Scheme 15: The catalytic cycle of Shvo's catalyst

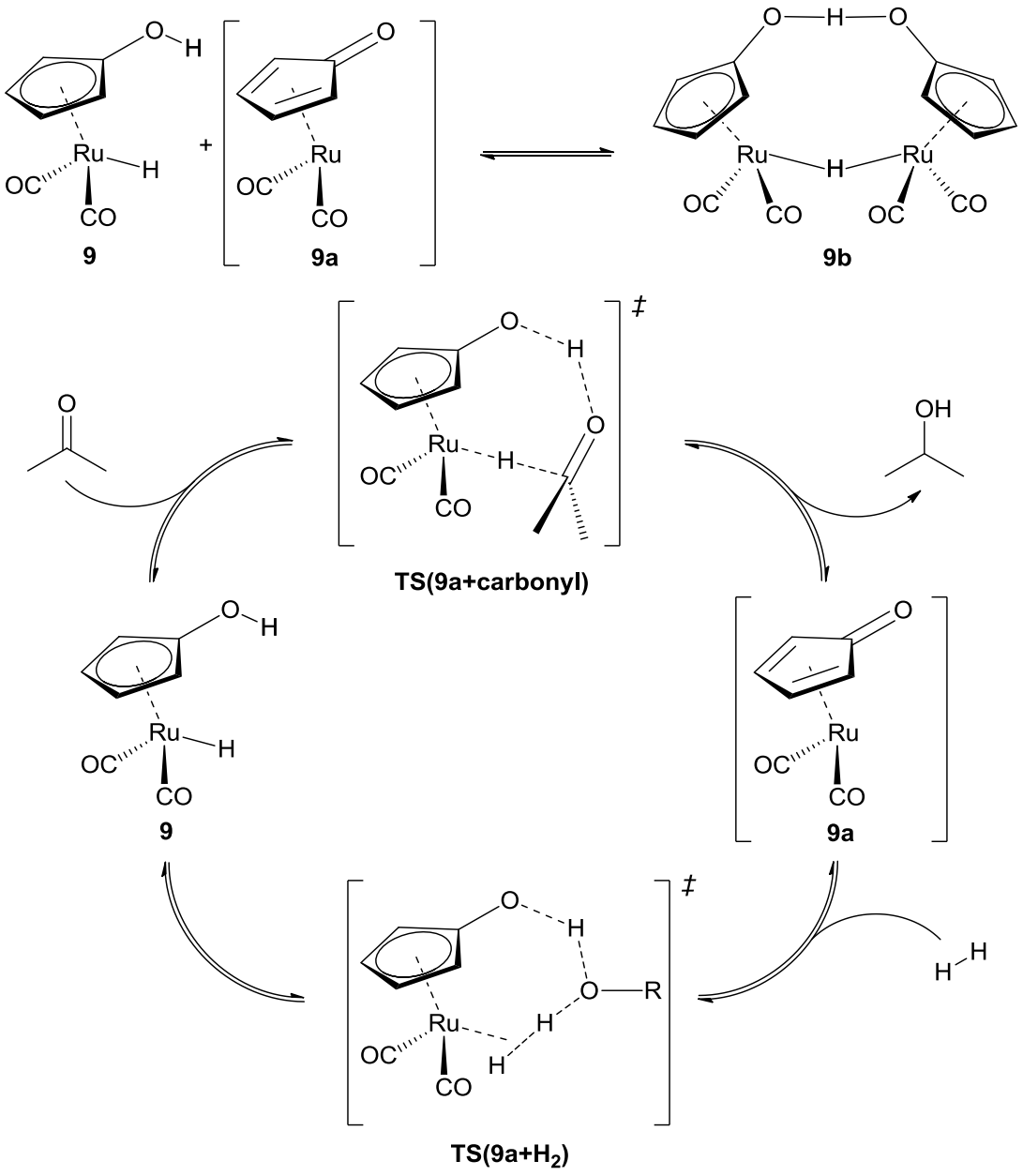

[45] Casey, C. P.; Johnson, J. B.; Singer, S. W.; Cui, Q. Hydrogen Elimination from a Hydroxycyclopentadienyl Ruthenium(II) Hydride - Study of Hydrogen Activation in a Ligand-Metal Bifunctional Hydrogenation Catalyst. *J. Am. Chem. Soc.* **2005,** *127,* 3100–3109.

Since Shvo's catalyst is also capable of hydrogenating C=C and C≡C bonds[46], it seems likely that it also is capable of homopolar hydrogenation taking place within the primary coordination sphere. The unique features of Shvo's catalyst can be summarized as follows:

- Substrate and product coordination supported by hydrogen bonds.
- Secondary coordination sphere mechanism - no metal-substrate bonding involved in the catalytic cycle.
- Simultaneous transfer of formally H^+ and H^-.
- All steps are reversible, allowing also product dehydrogenations.
- Regeneration of bifunctional catalysts via acidic H_2 complexes.

Today the probably most successful heteropolar hydrogenation/transfer hydrogenation systems are the Noyori type catalysts of the form $[RuCl_2(P\text{-}P)(N\text{-}N)]$ (**10,** P-P = binap, or other bisphosphines; N-N = diamine)[47,48] or [RuCl(arene)(N-N)] (**11**, arene = mesitylene, cymene, benzene; N-N = diamine)[49]. The catalytic active hydride species **10a,b** and **11a** are usually prepared *in situ* from commercially available $[Ru(arene)Cl_2]_2$ (**12**) and chiral diphosphines/diamines in the presence of a base and H_2 (Scheme 16).

Scheme 16: Generation of Noyori's catalysts

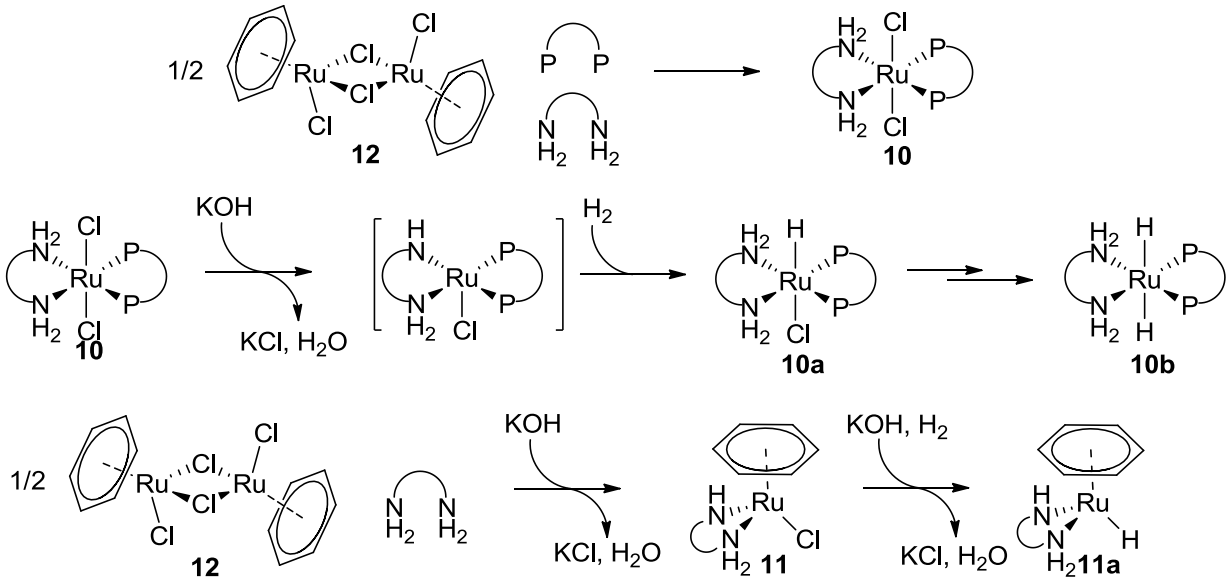

[46] Blum, Y.; Czarkie, D.; Rahamim, Y.; Shvo, Y. (Cyclopentadienone)ruthenium carbonyl complexes - a new class of homogeneous hydrogenation catalysts. *Organometallics* **1985,** *4*, 1459–1461.

[47] Ohkuma, T.; Ooka, H.; Hashiguchi, S.; Ikariya, T.; Noyori, R. Practical Enantioselective Hydrogenation of Aromatic Ketones. *J. Am. Chem. Soc.* **1995,** *117*, 2675–2676.

[48] Ohkuma, T.; Ooka, H.; Ikariya, T.; Noyori, R. Preferential hydrogenation of aldehydes and ketones. *J. Am. Chem. Soc.* **1995,** *117*, 10417–10418.

[49] Hashiguchi, S.; Fujii, A.; Takehara, J.; Ikariya, T.; Noyori, R. Asymmetric Transfer Hydrogenation of Aromatic Ketones Catalyzed by Chiral Ruthenium(II) Complexes. *J. Am. Chem. Soc.* **1995,** *117*, 7562–7563.

The catalytic cycle of Noyori's catalysts is also believed to follow the same mechanism as Shvo's catalyst. Again hydrogenation and transfer-hydrogenation are feasible. Furthermore, Noyori type catalysts have similar practical advantages as Osborn type catalysts. They are easily generated *in situ*, hydrogenate a broad scope of substrates and with appropriate chiral ligands they catalyze hydrogenations and transfer-hydrogenations with high enantioselectivity. Therefore, it is not surprising that the Noyori and Osborn systems are among the most valuable tools for the synthesis of chiral compounds.

1.3.3 Ionic hydrogenations

An alternative to the concerted transfer of H^+ and H^- in the Shvo or Noyori type mechanisms is the so-called ionic hydrogenation. The concept and the catalysts date back to earlier times than the concept of the metal ligand bifunctional catalysis[50]. Ionic hydrogenation originates from the stoechiometric reaction of olefins with an acid, such as TFA and a sacrificial hydride donor, such as $HSiEt_3$ reported by Kursanov [51].

Scheme 17: Kursanov's proposed mechanism for the stoechiometric ionic hydrogenation of styrene:

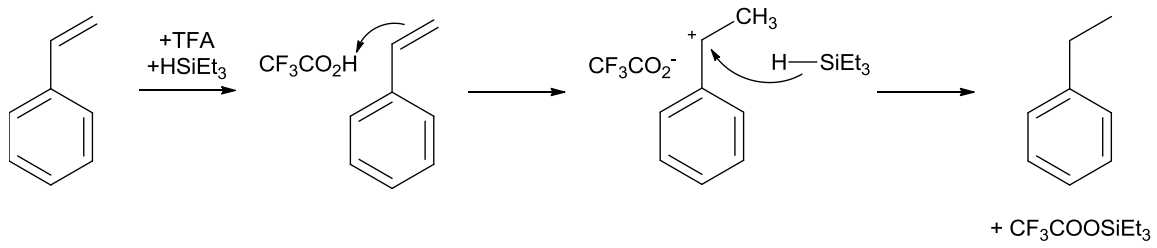

The difference between this concept and the metal bifunctional concept is subtle, as in both cases H_2 is formally transferred as H^+ and H^-. Since the metal complex in the metal ligand bifunctional catalysis provides H_2 polarized in one single molecule, the probably most obvious distinguishing feature of the ionic hydrogenation is the heterolytic splitting of an acidic H_2 complex into a metal hydride and a proton, which is stabilized by an external base, such as the solvent or the substrate. Since this can also be accomplished by the use of a FLP (*vide supra*), ionic hydrogenation is principally not limited to metal complexes. Indeed metal-free hydrogenation of imines[52], silylenolethers[53] and enamines[54] was reported soon after the discovery of the reversible H_2 activation with **1**. The mechanisms for this type

[50] M.I.Kalinkin; G.D.Kolomnikova; Z.N.Parnes; D.N.Kursanov. Catalytic Ionic Hydrogenation. *Russ. Chem. Rev.* **1979**, 612–634.
[51] Kursanov, D. N.; Parnes, Z. N.; Bassova, G. I.; Loim, N. M.; Zdanovic. VI. Ionic Hydrogenation of Ethylene Bond and Double Bond of Carbonyl Group *Tetrahedron* **1967**, *23*, 2235-2242.
[52] Preston A. Chase; Gregory C. Welch; Titel Jurca; Douglas W. Stephan. Metal-Free Catalytic Hydrogenation. *Angew. Chem. Int. Ed.* **2007**, *46*, 8050–8053.
[53] Wang, Huadong; Froehlich, Roland; Kehr, Gerald; Erker, Gerhard. Heterolytic dihydrogen activation with the 1,8-bis(diphenylphosphino)-naphthalene/$B(C_6F_5)_3$ pair and its application for metal-free catalytic hydrogenation of silyl enol ethers. *Chem. Commun.* **2008** 5966–5968.
[54] Spies, P.; Schwendemann, S.; Lange, S.; Kehr, G.; Roland Fröhlich; Erker, G. Metal-Free Catalytic Hydrogenation of Enamines, Imines, and Conjugated Phosphinoalkenylboranes. *Angew. Chem. Int. Ed.* **2008**, *47,* 7543–7546.

of hydrogenation can be distinguished by the sequence of the H^+ and H^- transfers, as well as in other involved elementary reaction steps. For a detailed discussion, the interested reader is referred to Morris review on this topic[55]. Although ionic hydrogenation is an interesting reaction from the academic point of view, it is of low practical importance, since it suffers until present date from some obvious weak points:

- Unsaturated species appear in the catalytic cycle, as a consequence there is low functional group and solvent tolerance.
- Difficult catalyst preparations involving often undesired or expensive counter ions, such as ClO_4^- or $BAr^F{}_4^-$.
- Low activities
- General applicability is suffering, since the systems are often highly specific to particular reaction conditions and substrates.

Scheme 18: Ionic hydrogenation using $[Re(CO)_2(PMe_3)_3][BAr^F{}_4]$

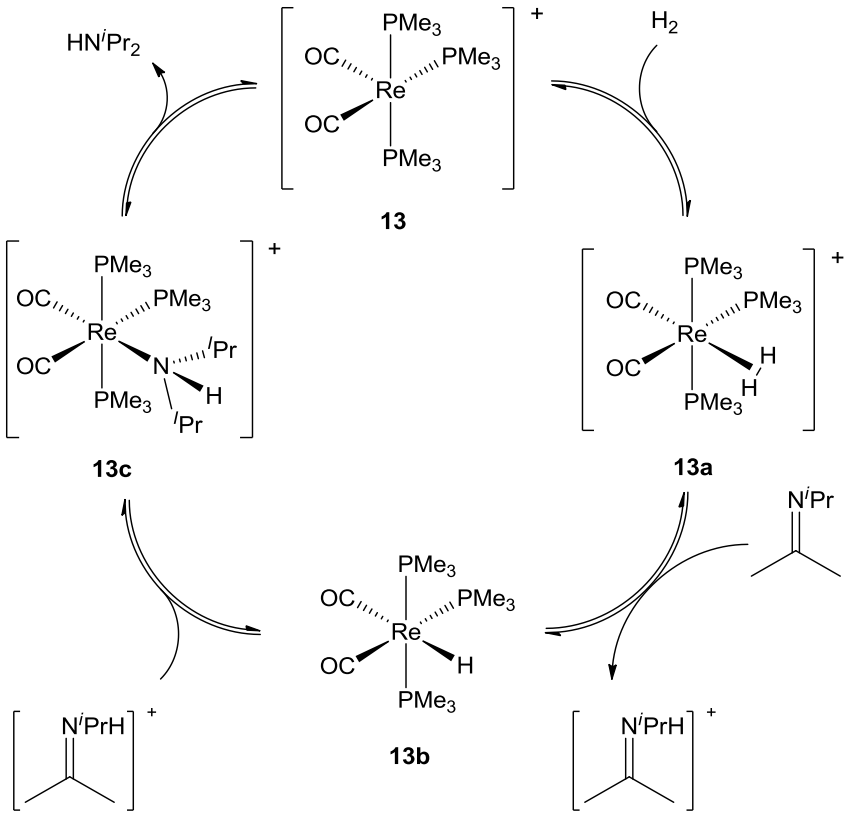

[55] Clapham, S. E.; Hadzovic, A.; Morris, R. H. Mechanisms of the H_2-hydrogenation and transfer hydrogenation of polar bonds catalyzed by ruthenium hydride complexes: Vignettes of Homogeneous Catalysis. *Coord. Chem. Rev.* **2004,** *248*, 2201–2237.

An example following the path of the ionic hydrogenation is given in Scheme 18[56] for the hydrogenation of imines with $[Re(CO)_2(PMe_3)_3][BAr^F_4]$. As outlined above, the hydrogenation mechanism starts with the unsaturated species **13**, which in the presence of H_2 forms the acidic complex **13a** . **13a** is subsequently deprotonated by the substrate N-isopropylisopropylene. The substrate undergoes then insertion into the Re-H bond. This insertion is presumably initiated by dissociation of a CO or PMe_3 ligand followed by the coordination of the substrate. After hydride migration, the intermediate amide complex is then protonated forming the amine complex **13c**. The dissociation of the product amine from **13c** finally leads back to the catalyst precursor **13**. The general features of such catalytic cycles are:

- H_2 is heterolytically split into H^+ and H^-.
- The sequence and character of the involved elementary reaction steps, in particular the H atom transfers, can vary from catalyst to catalyst.
- Up to the present transition metals catalysts are superior over "metal-free" systems.

These features cause a very wide range of possible catalytic systems and because catalytic hydrogenations following these mechanisms are strongly ligand type oriented they are not limited by the properties of the involved metal centers. For instance it is not a crucial condition to use precious transition metal centers. Even metal-free systems can be applied. Nevertheless, it turned out that these catalysts are usually quite specific to particular reaction conditions and substrates. Moreover, their activities are often low requiring high catalyst loadings. There are indeed very efficient exceptions but they are often based on precious metals, such as ruthenium. Overall, the ionic hydrogenation approach via metal ligand bifunctional systems (which can be classified as a sub-group of ionic hydrogenation) is still very promising as its range of applications is expandable to more versatile, less sensitive and more efficient catalysts. Furthermore, it has to be noted that appropriate supported ionic hydrogenation catalysts may overcome much of their limitations if they could be protected/prearranged in "enzymatic" cages. But this is currently still science fiction.

1.4 Enantioselective hydrogenation

Another important aspect of hydrogenation reactions is the enantioselective hydrogenation of prochiral substrates by chiral catalysts. For the sake of completeness a very brief overview on the origin of enantioselectivity of chiral Osborn and Noyori systems will be presented in the subsequent sections. It has to be clarified that it was not subject of this work to hydrogenate enantioselectively.

[56] Liu, X.-Y.; Venkatesan, K.; Schmalle, H. W.; Berke, H. Solvent Stabilization and Hydrogenation Catalysis of Trimethylphosphine-Substituted Carbonyl Rhenium Cations. *Organometallics* **2004,** *23*, 3153–3163.

1.4.1 Using the Osborn system for asymmetric hydrogenation

First of all, an overview on typical prochiral substrates is given in Scheme 19.

Scheme 19: Commonly employed test substrates for enantioselective catalytic hydrogenation reactions.

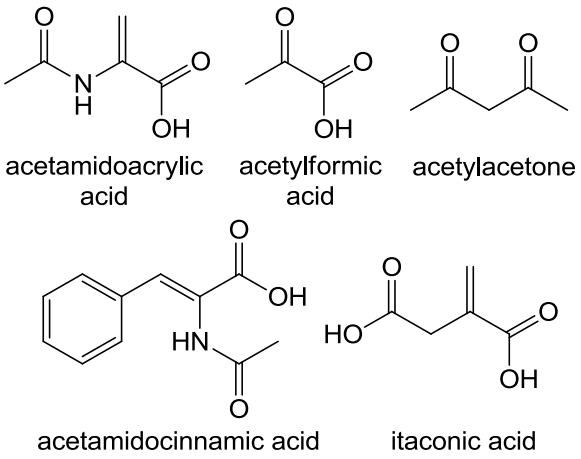

Such substrates and their derivatives are often used to demonstrate the capability of a new chiral ligand to induce asymmetric hydrogenation in combination with a Rh^+ source such as **6**. It can be seen that all of these substrates are not only prochiral, but also have a hetero atom in β-position. This allows bidentate coordination of the substrate, which is prerequisite for high asymmetric induction. The origin of the high enantioselectivity of Osborn's catalyst was investigated by Halpern in a very detailed study on the hydrogenation of methyl-(Z)-acetamidocinnamate (MAC) with $[Rh(R,R\text{-dipamp})(MeOH)_2][BF_4]$[57].

Scheme 20: Some typical chiral diphosphines

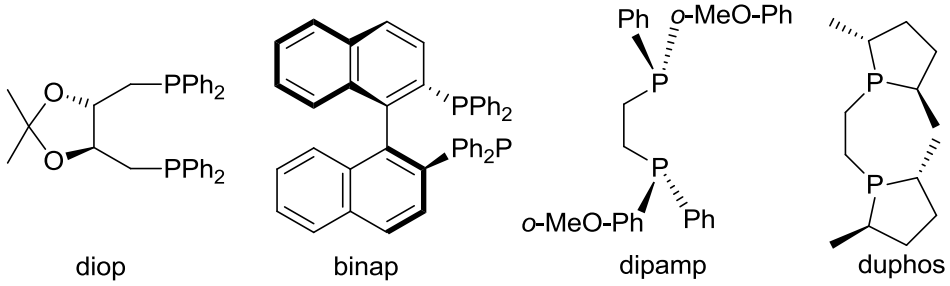

It was shown that the reaction followed basically Wilkinson's cycle (Scheme 10) with the difference that MAC is coordinated to the complex prior to the oxidative addition of H_2 (Scheme 21). The coordination of MAC is fast, reversible and leads to two diastereomeric complexes. The energetically favored isomer prevails in solution (**major**), while the less favored is called **minor** complex. At room temperature the addition of H_2 to the $[RhP_2(MAC)]^+$ complexis rate limiting for the hydrogenation. As

[57] Landis, C. R.; Halpern, J. Asymmetric hydrogenation of methyl (Z)-.alpha.-acetamidocinnamate catalyzed by [1,2-bis(phenyl-o-anisoyl)phosphino)ethane]rhodium(I): kinetics, mechanism and origin of enantioselection. *J. Am. Chem. Soc.* **1987,** *109*, 1746–1754.

the bidentate bound MAC kinetically hinders the formation of H_2, the partial MAC dissociation is crucial for further reaction. The enantioselectivity arises from the fact that the minor product is less stable and therefore reacts faster with H_2 than the major product. Furthermore, the enantioselectivity is concentration dependent. In particular high H_2 concentration/pressure results in lower selectivity since the oxidative addition of H_2 is accelerated compared to the isomerization between the **major** and the **minor** product. Although this interpretation is widely accepted, it is not generally valid. For example Noyori investigated the mechanism in [Ru(acetate)$_2$(P-P)] systems and found that under hydrogenation conditions a Ru-H system is formed, which coordinates the substrate. In that particular case the major component in the reaction mixture was found to be the more reactive one. Therefore the enantioselectivity of these catalysts was found to be opposite to the Rh catalysts with the same phosphine ligands[58]. To summarize the feature of the enantioselective hydrogenation of β-functionalized olefins, the following can be stated:

- The reversible formation of diastereomeric substrate-catalyst complexes is necessary.
- A significant energetic difference between these two diastereomers is crucial (this implies bidentate coordination of the substrate).
- The isomerization between these two diastereomers must be faster than the hydrogenation of the substrates.
- One of the diastereomers must undergo the rate limiting step significantly faster in absolute terms ($k_{Isomer1}[C_{Isomer1}]>>k_{Isomer2}[C_{Isomer2}]$).

Scheme 21: Halpern's major/minor scheme

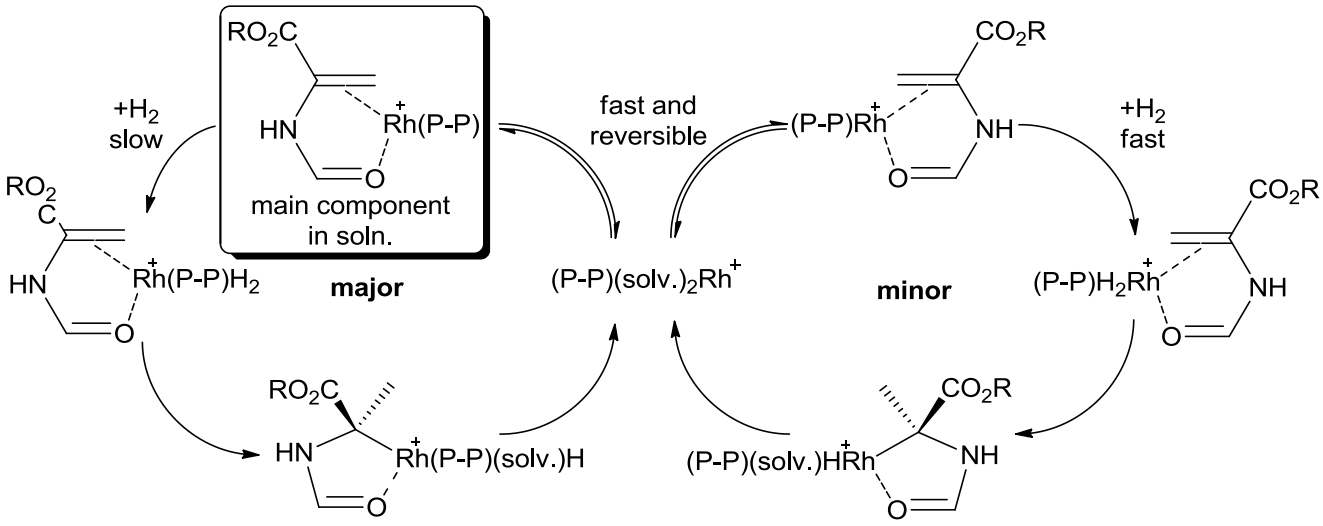

[58] Kitamura, M.; Tsukamoto, M.; Bessho, Y.; Yoshimura, M.; Kobs, U.; Widhalm, M.; Noyori, R. Mechanism of Asymmetric Hydrogenation of (Acylamino)acrylic Esters Catalyzed by BINAP Ruthenium(II) Diacetate. *J. Am. Chem. Soc.* **2002,** *124*, 6649–6667.

1.4.2 Using the Noyori system for asymmetric hydrogenations

In contrast to these rather complex mechanisms, the enantioselective hydrogenation of simple ketones with Noyori's catalysts is much easier to understand. They operate on a similar base as a highly selective enzyme with a binding pocket, which binds the substrate in a key-lock principle. In case of Noyori's catalysts a combination of a chiral diamine with a chiral diphosphine forms an asymmetric binding cleft (Scheme 22). The substrate is bound by hydrogen bonds at this cleft before the H_2 equivalent is transferred. In this state the differentiation between the two diastereomeric forms of the substrate-catalyst complex is sufficient for high enantioselectivity. As the hydrogen bonds only require a carbonyl group, also simple ketones without β-functionalization are bound strongly enough into the pocket and therefore they are recognized and react in an enantioselective way[59]. As a result these systems allow also the enantioselective hydrogenation of simple ketones, which would not be achieved satisfactorily with chiral Osborn systems.

Scheme 22: The "binding pocket" of Noyori's catalyst

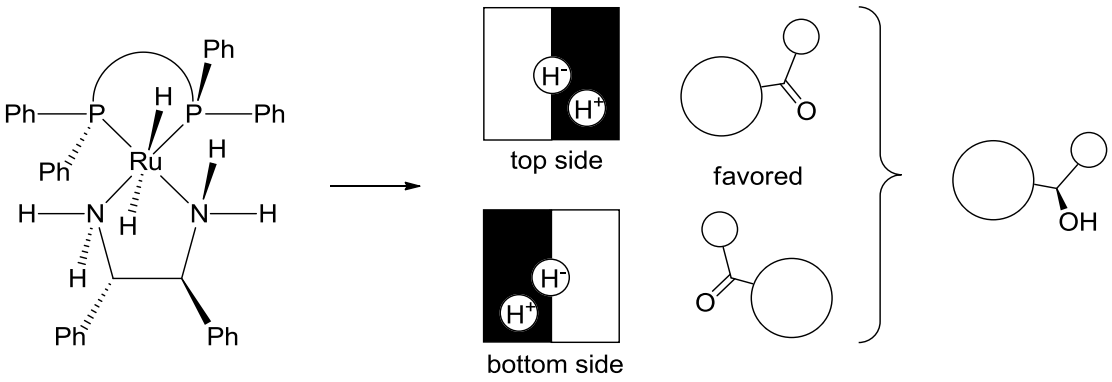

1.5 The aim of this work

It was mentioned already that the process of hydrogenation is a well developed technology. Nevertheless, especially homogeneous hydrogenation relies on only very few, very versatile and efficient systems. The working horses in homogenous hydrogenation catalysis are mainly the Rh and Ru catalysts presented in the previous sections or closely related systems. Although this platinum group element catalysts perform superior to everything else known, their use is sometimes problematic. The most obvious disadvantage is the low occurrence of these metals and consequently their high prices. Apart from that, these metals are known to be toxic[60]. For these reasons, the catalysts have to be removed from the products and recycled after the hydrogenation reaction. Additionally, precious metal catalysis often suffers from reduction of the catalytic species to the

[59] Sandoval, C. A.; Ohkuma, T.; Muñiz, K.; Noyori, R. Mechanism of Asymmetric Hydrogenation of Ketones Catalyzed by BINAP/1,2-Diamine-Ruthenium(II) Complexes *J. Am. Chem. Soc.* **2003**, 125, 13490–13503.

[60] Zimmermann, S.; Sures, B. Significance of platinum group metals emitted from automobile exhaust gas converters for the biosphere. *Environ. Sci. Pollut. Res.* **2004**, 11, 194–199. Schmid, M.; Zimmermann, S.; Krug, H. F.; Sures, B. Influence of platinum, palladium and rhodium as compared with cadmium, nickel and chromium on cell viability and oxidative stress in human bronchial epithelial cells. *Environ. Int.* **2007**, 33, 385–390.

metal under hydrogenation conditions[37,61]. This results in loss of activity and/or selectivity. Therefore, it is desirable to develop alternatives to the established catalytic systems, which don't require platinum group metals.

The element rhenium being border to the precious metals, has preserved some of its "noble" character like for example its preference for interaction with the dihydrogen molecule. In addition, the rhenium nitrosyl unit is isoelectronic to ruthenium carbonyl or phosphine fragments which comprise essential building blocks of efficient hydrogenation and hydroformylation catalysts. Therefore, we considered the rhenium nitrosyl fragment a promising starting point to develop hydrogenation catalysts. Furthermore, we were encouraged by the fact that only very few is known about homogeneous rhenium catalyzed hydrogenations. Therefore, the development of novel rhenium based hydrogenation catalysts does not only offer promising perspectives from the scientific/technical side, but also the possibility to perform some innovative work.

1.5.1 Rhenium hydride species

A key to highly active hydrogenation catalysts are compounds, which are capable to interact with H_2 and/or the unsaturated acceptor substrates. Therefore olefin, dihydrogen, and hydride complexes are potentially interesting for the development of novel catalysts. As we are especially interested in the application of the Re-NO fragment in the field of hydrogenation catalysis, the known hydrogen and olefin chemistry of compounds containing this fragment has to be considered as a starting point. According to Reaxys/Gmelin approximately 190 Re-NO complexes bearing a hydride and/or dihydrogen ligand and eventually an olefin ligand are reported in the literature. Nevertheless, a closer inspection of this type of compounds reveals only a few basic motifs (Scheme 23). The most common motif is given by complexes of the form $[ReX_2L(NO)(PR_3)_2]$ with X = $1e^-$ ligands, such as H or halide and L = $2e^-$ ligands such as PR_3, olefins, H_2 or CO. Early examples of compounds of type **21,22** and **26** have been reported already around 1975[62,63]. Later on, cyclopentadienyl complexes **29**-**31** were prepared in the eighties[64,65]. Nevertheless, the more exciting octahedral species were

[61] Widegren, J. A.; Finke, R. G. A review of the problem of distinguishing true homogeneous catalysis from soluble or other metal-particle heterogeneous catalysis under reducing conditions *J. Mol. Catal. A:Chemical* **2003**, 198, 317–341.
[62] La Monica, G.; Freni, M.; Cenini, S. New nitrosyl derivatives of rhenium. *J. Organomet. Chem.* **1974**, *71,* 57–64.
[63] Giusto, D.; Ciani, G.; Manassero, M. Synthesis and reactions of dihydridonitrosyltris(triphenylphosphine) rhenium. *J. Organomet. Chem.* **1976**, *105,* 91–95.
[64] Casey, C. P.; Andrews, M. A.; McAlister, D. R.; Rinz, J. E. Reduction of coordinated carbon monoxide. Synthesis of neutral metal formyl and hydroxymethyl derivatives of the (cyclopentadienyl)dicarbonyl(nitrosyl)rhenium(I) cation. *J. Am. Chem. soc.* **1980,** *102*, 1927–1933.
[65] Tam, W.; Lin, G. Y.; Wong, W. K.; Kiel, W. A.; Wong, V. K.; Gladysz, J. A. Synthesis and electrophile-induced disproportionation of the neutral formyl triphenylphosphinenitrosyl-.eta.-cyclopentadienylrhenium formyl ($(\eta^5$-$C_5H_5)Re(NO)(PPh_3)(CHO)$). *J. Am. Chem. soc.* **1982,** *104*, 141–152.

compounds of the form **14**,**15**,**18**,**19**,**20**,**23**,**24,25** and **32** and were prepared later in Berke's group[66,67,68,69].

Scheme 23: The most common structural motifs of ReH(NO) complexes.

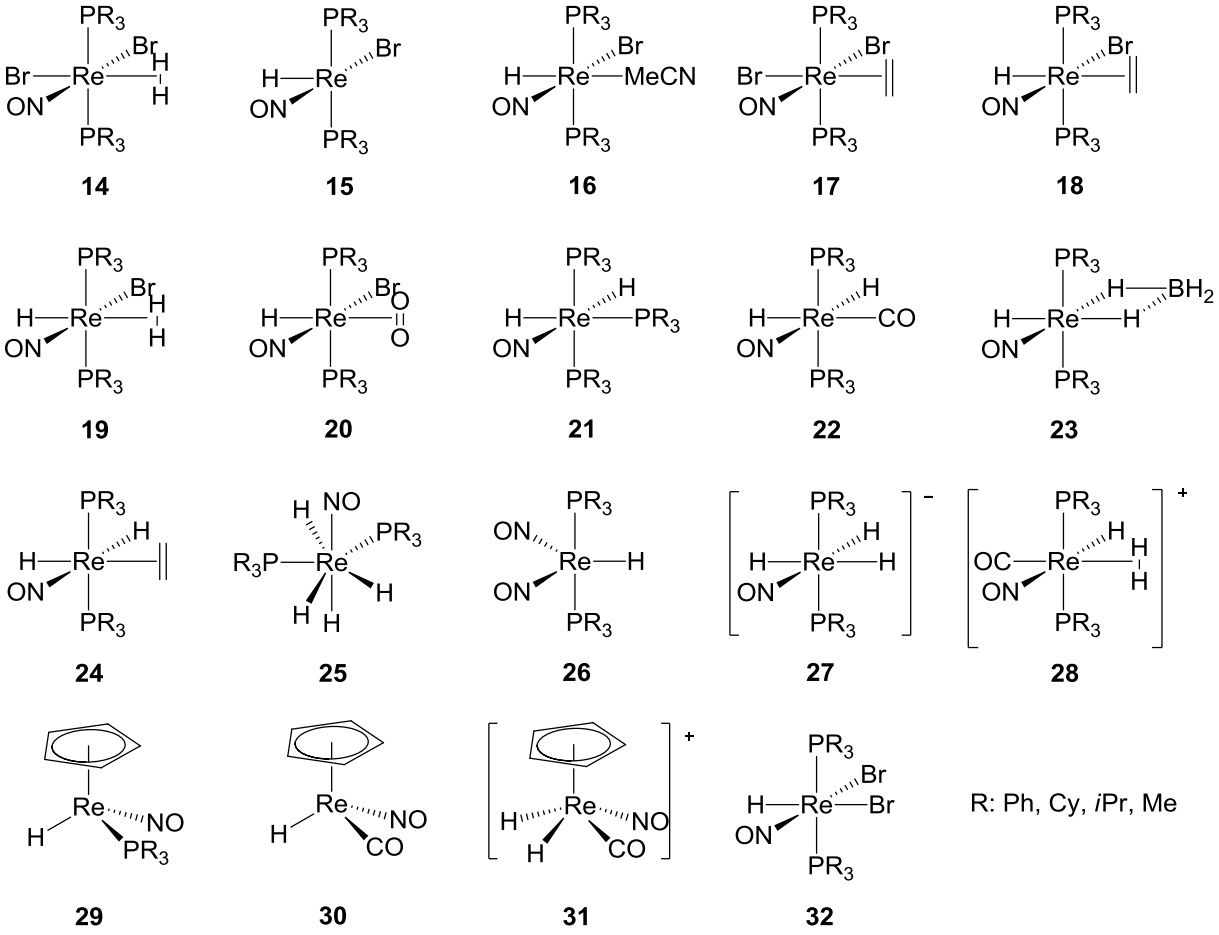

For these series of complexes, one might expect the dihydride complexes of type **21** to react in a fashion analogous to $[RhH_2Cl(PPh_3)_3]$ (**3e**) by the elimination of a phosphine followed by the addition of an olefin to form the **3c** analogue **24PPh$_3$**. Despite the striking similarity of $[ReH_2(NO)(PPh_3)_3]$ **21PPh$_3$** to **3e**, this reaction has not been reported for **21PPh$_3$**. This is not surprising as the Re d6 systems are known to be often kinetically inert. But also in case of the Wilkinson system **3a-d**, the phosphine dissociation was found to be rate limiting. Therefore the Osborn system **4a-f** was developed, where this step is circumvented by exchange of a chloride and PPh_3 with a diene ligand. Hence the removal of one of the phosphines to create a vacant coordination site is the next logical

[66] Gusev, D.; Llamazares, A.; Artus, G.; Jacobsen, H.; Berke, H. Classical and nonclassical nitrosyl hydride complexes of rhenium in various oxidation states. *Organometallics* **1999,** *18*, 75–89.
[67] Choualeb, A.; Maccaroni, E.; Blacque, O.; Schmalle, H. W.; Berke, H. Rhenium nitrosyl complexes for hydrogenations and hydrosilylations. *Organometallics* **2008,** *27*, 3474–3481.
[68] Jiang, Y.; Blacque, O.; Fox, T.; Frech, C. M.; Berke, H. Highly Selective Dehydrogenative Silylation of Alkenes Catalyzed by Rhenium Complexes. *Chem. Eur. J.* **2009,** *15,* 2121–2128.
[69] Jiang, Y.; Blacque, O.; Fox, T.; Frech, C. M.; Berke, H. Facile Synthetic Access to Rhenium(II) Complexes: Activation of Carbon-Bromine Bonds by Single-Electron Transfer. *Chem. Eur. J.* **2010**, *16,* 2240–2249.

step towards the development of an active catalyst. Indeed this modification of the system led to the first known rhenium based homogeneous hydrogenation catalysts[67] for nonpolar substrates such as 1-hexene and styrene. It was reported that $[ReH_2(\eta^2\text{-}C_2H_4)(NO)(PR_3)_2]$ with R = Cy (**24PCy$_3$**) or *i*Pr (**24P*i*Pr$_3$**) catalyzed the hydrogenation of these substrates at pressures of 60-70 bar and temperatures of 80°C. The performance of the system was found to be low with a maximal TOF of 47 h^{-1} for 1-hexene using the PCy_3 derivative of **5**. For the hydrogenation using these compounds, a monohydride mechanism was proposed by Choualeb et al.[67] (Scheme 24). It was anticipated to start from **24** with a β-hydride shift from the Re-H to the coordinated olefin to form the unsaturated alkyl complex **24a**. **24a** coordinates then a molecule of H_2 which is then oxidatively added to form an intermediate hepta-coordinated trihydride **24b**. From this dihydride the product alkane is subsequently reductively eliminated and the unsaturated intermediate dihydride complex **24c** is formed. **24c** adds an olefin to regenerate **24**. No intermediates have been reported to occur during the catalytic reaction. This strongly suggests that the first step denoted as k_1 is rate limiting. Furthermore $K=k_1/k_{-1}$ is on the side of **24**. In a theoretical study[70], this reaction mechanism has been elucidated in detail. And it has been shown that k_1 represents the rate limiting step.

Scheme 24: Proposed mechanism for the catalytic hydrogenation with **24**

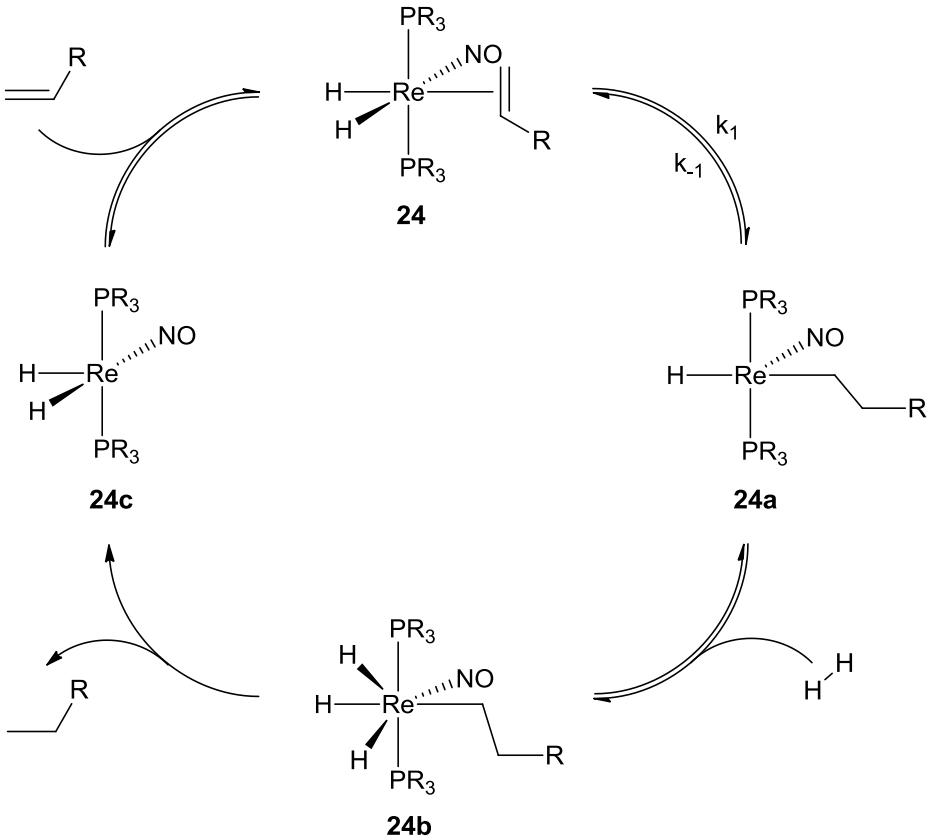

[70] Liu, L.; Bi, S.; Sun, M.; Yuan, X.; Zheng, N.; Li, P. Mechanistic investigation on hydrogenation and hydrosilylation of ethylene catalyzed by rhenium nitrosyl complex. *J. Organomet. Chem.* **2009**, 694, 3343–3348.

2. Insight into hydrogenations with the [$ReH_2(\eta^2$-$C_2H_4)(NO)(PR_3)_2$] system

After an initial promising start in the development of new Re-NO based catalysts with the pre-catalysts **24PCy$_3$** and **24P*i*Pr$_3$** the question emerged, how the system could be improved. Therefore a deeper understanding of the mechanism of the catalysis was crucial. This led us to investigate the catalysis with compounds of the form P-*trans*-P [$ReH_2(\eta^2$-olefin$)(NO)(PR_3)_2$] (**24**) in greater detail.

2.1 The preparation of [$ReH(CH_2CH_3)(\eta^2$-$C_2H_4)(NO)(PPh_3)_2$] and [$ReH_2(\eta^2$-$C_2H_4)(NO)(PPh_3)_2$] and

As Wilkinson type catalysts are known to be very sensitive to the electronic donor capability of the employed phosphines and PPh_3 was found to be optimal[71], we approached the preparation of the related P-*trans*-P [$ReH_2(\eta^2$-$C_2H_4)(NO)(PPh_3)_2$] (**24PPh$_3$**) derivative. Since the analogous **24PCy$_3$** and **24P*i*Pr$_3$**[72] complexes were conveniently prepared from the corresponding η^2-BH_4 complexes[66] we investigated the reaction of **23PPh$_3$** with ethylene (Scheme 25):

Scheme 25: Synthesis of **24PPh$_3$** and **23PPh$_3$**

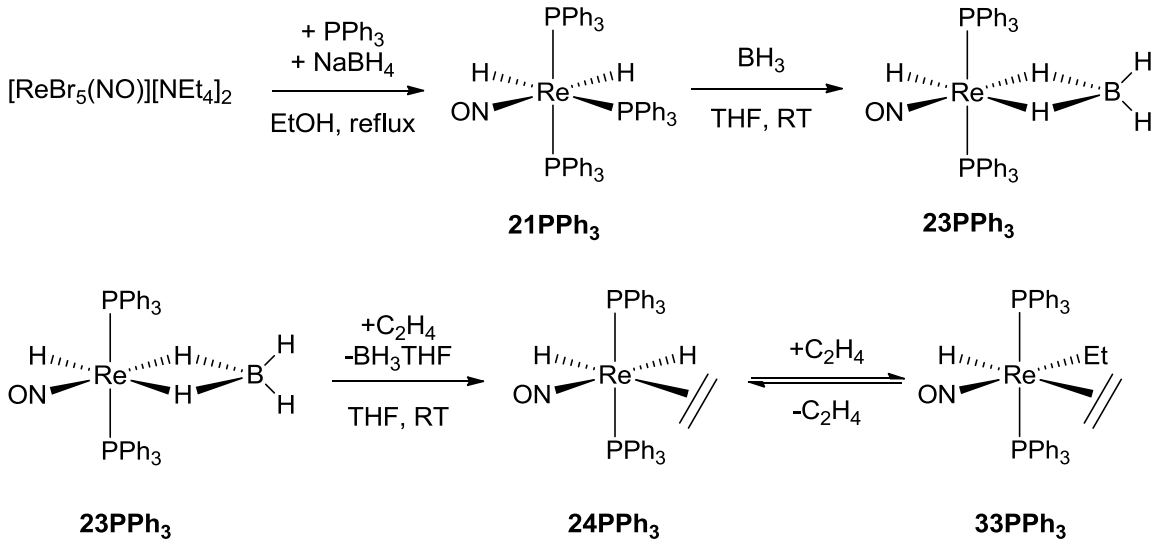

Unlike the reaction of **23P*i*Pr$_3$** and **23PCy$_3$** with ethylene, the reaction of **23PPh$_3$** with ethylene in THF led to the ethylene complex **24PPh$_3$** but also to the ethyl complex [$ReH(CH_2CH_3)(\eta^2$-$C_2H_4)(NO)(PPh_3)_2$]

[71] Montelatici, S.; van der Ent, A.; Osborn, J.A.; Wilkinson, G. Further Studies on the Homogeneous Hydrogenation of Olefins by Use of Tris(tertiary Phosphine)chlororhodium(I) Complexes. *J. Chem. Soc. A* **1968**, 1054-1058.

[72] Choualeb, A.; Blacque, O.; Schmalle, H. W.; Fox, T.; Hiltebrand, T.; Berke, H. Olefin complexes of Low-Valent Rhenium. *Eur. J. Inorg. Chem.* **2007**, 5246-5261.

(**33PPh$_3$**). This is quite unique, since *cis*-hydrido-alkyl complexes usually reductively eliminate the corresponding alkane. To our knowledge *cis*-hydrido-alkyl complexes formed by the reaction of a "masked" dihydride complex with ethylene are not known to be stable enough to be observed spectroscopically at ambient temperature.

The isolation of either one of these compounds was not possible due to their oily nature and their inherent unstable character. The attempt to convert **33PPh$_3$** into **24PPh$_3$** by repeated dissolution of the mixture in THF or toluene followed by the removal of the solvent *in vacuo* did not lead to pure **24PPh$_3$**. However **33PPh$_3$** could be transformed into **24PPh$_3$** by gently warming to ca. 50°C in solution. But this led not to pure **24PPh$_3$**, but also to a complex, not separable mixture of other decomposition products caused by the loss of ethane. In contrast **24PPh$_3$** could easily be transformed into **33PPh$_3$** by exposing it in solution to ethylene. Qualitative monitoring of the reaction of **23PPh$_3$** via ^{31}P NMR revealed that the formation of **24PPh$_3$** and **33PPh$_3$** is slowed down by kinetic barriers. Apparently, the BH_3 moiety in **23PPh$_3$** is strongly bound, which is reflected by the relative slow formation of **24PPh$_3$** (approx. 3-5 min. in an ethylene saturated 0.02 M NMR sample of **23PPh$_3$** at room temperature). The subsequent reaction with another equivalent of ethylene proceeds depending on the C_2H_4 concentration in a similar period (in the range of 10-15 min.). Since the concentration of the ethylene in solution decreased fast, the quantitative kinetics of these reactions could not be determined reliably. Therefore we approached the investigation of this reaction sequence with styrene and 1-hexene as surrogate for ethylene, but it turned out that these olefins do not react with **23PPh$_3$**. Since 1-hexene and to smaller extent styrene are electronically similar to ethylene it seems most likely that the difference in reactivity is caused by the steric differences between these olefins. Consequently no mechanistic studies could be made employing liquid olefins. As neither **24PPh$_3$** nor **33PPh$_3$** were stable compounds, the obtained mixture was characterized solely by NMR and IR spectroscopy.

In the ^{1}H NMR spectrum of **24PPh$_3$** in benzene (Figure 2), the PPh_3 ligand caused the expected multiplets in the aromatic chemical shift range. Additionally the chemically different rhenium hydrides gave rise to a set of signals at 1.507 (td, $^2J_{PH}$ = 36.5 Hz, $^2J_{HH}$ = 7.4 Hz) and -3.287 (td, $^2J_{PH}$ = 27.6 Hz, $^2J_{HH}$ = 7.4 Hz) ppm. This is in agreement with the proposed structure for **23PPh$_3$** in Scheme 25, which bears two Re-H ligands in *cis* position. The protons of the ethylene ligand are chemically different and give therefore rise to two multiplets at 2.844 ppm (2 H) and at 2.763 ppm (2 H). These multiplets are broadened at room temperature (300K, 500MHz). Increasing of the temperature of the sample to 320K leads to coalescence. This observation would be consistent with a low barrier for the rotation of the ethylene ligand around the Re-(ethylene) axis. The resulting proton exchange could not be quantified as an increase of the temperature also caused the formation of

decomposition products via ethane elimination, whose signals partially appeared in the spectral range of interest. This also prohibited the observation of a possible exchange of the ethylene protons with either one of the R-H protons. The relatively facile rotation of the ethylene ligand in complex **24PPh$_3$** is in contrast to the more strongly bound ethylene in **24PCy$_3$** and **24P*i*Pr$_3$**[67]. In the ^{31}P NMR spectrum only one broad virtual triplet at 28.5 ppm is observed. This is typical for such complexes, as the difference between couplings with the two different rhenium-hydrides is much smaller (ca. 9 Hz) than the multiplet's resolution. The appearance of only one ^{31}P NMR resonance also indicates a symmetric binding situation of the PPh_3 ligands. Together with the fact that two different signals for the Re-H ligands are observed, the structure proposed in Scheme 25 can be confirmed unambiguously. In the $^{13}C\{^1H\}$ NMR spectrum the ethylene carbon nuclei cause one signal at 35.8 ppm. The assignment of this carbon signal to the C_2H_4 ligand was confirmed by an HSQC experiment.

The ^{1}H NMR spectrum of **33PPh$_3$** is more complicated (Figure 2). It also consists of signals originating from the PPh_3 ligand, which partially overlap with those of **24PPh$_3$**. Additionally it consists of two isolated spin systems attributed to the ethylene and the ethyl ligands and a rhenium-hydride signal. The rhenium-hydride signal at 2.908 ppm (t, $^2J_{PH}$ = 31.8 Hz, 1 H) shows the typical coupling pattern originating from the coupling with two chemically equivalent phosphorus nuclei. The four protons of the ethylene ligand give rise to two broad resonances which resolve in the $^1H\{^{31}P\}$ NMR spectrum in a set of sharp resonances at 2.939 ppm (d, J_{HH} = 10.2 Hz, 2 H) and at 2.117 ppm (d, J_{HH} = 10.2 Hz, 2 H). The ethylene signals are not affected by any exchange process indicating a considerable barrier for the rotation of the ethylene ligand. Both signals were assigned with an HSQC experiment to one ^{13}C resonance at 42.9 ppm.

Figure 2: Ethyl/ethylene and hydride region of the ^{1}H NMR (C_6D_6, 300K, 500 MHz) spectra of **24PPh$_3$** (*) and **33PPh$_3$** (#).

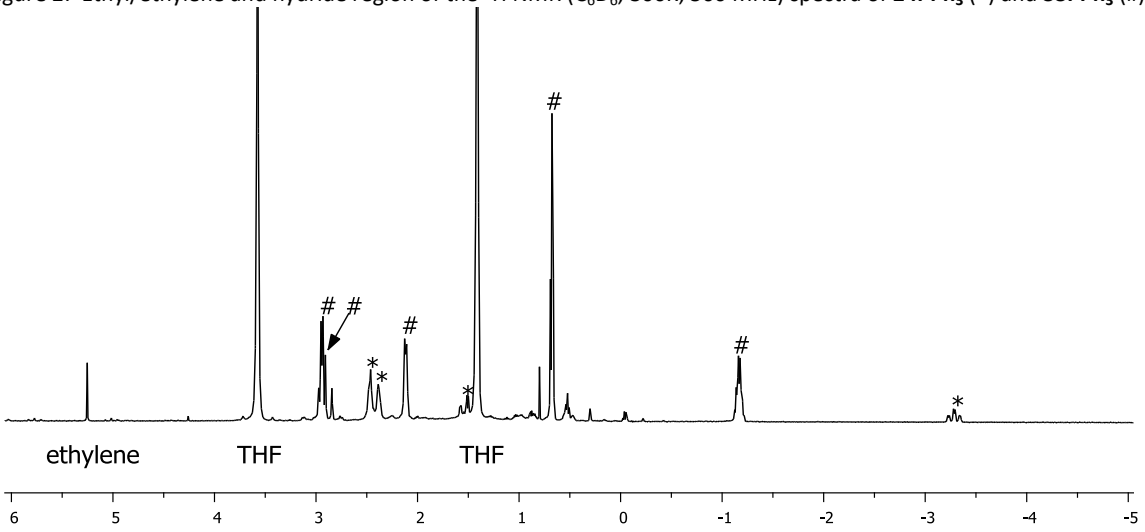

The CH_2 protons of Re-ethyl moiety give rise to a broadened resonance at -1.168 ppm (q, $^3J_{HH}$ = 7.3 Hz, 2 H). Phosphorous decoupling leads to a sharp signal. The adjacent CH_3 group causes a well

defined signal at 0.675 ppm (t, $^{3}J_{HH}$ = 7.3 Hz, 3 H). The ethyl signals were assigned via an HSQC experiment to carbon resonances at 20.0 ppm (CH_3) and at 19.0 ppm (t, $^{2}J_{PC}$ = 7 Hz, CH_2). In the ^{31}P NMR spectrum **33PPh$_3$** gave rise to a broad signal at 20.4 ppm (d, $^{2}J_{PH}$ = 31.8 Hz). From these spectroscopic data, it can be concluded that the phosphines are bound in chemically equivalent positions. The relative arrangement of the ethylene, the ethyl and the hydride ligand could not be established with these experiments. Therefore three constitutional isomers **A**, **B** and **C** (Scheme 26) have to be considered.

Scheme 26: The three constitutional isomers of **33PPh$_3$** with *trans*-phosphines.

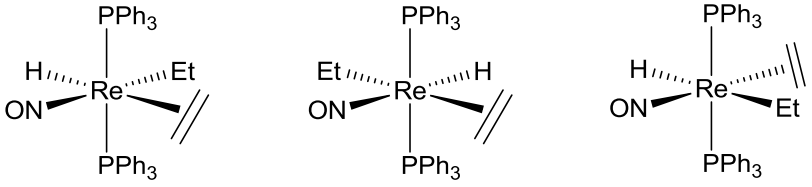

For the ligands in the plane the *trans*-influence decreases in the order of NO > C_2H_4 > H > Et. Based on the *trans*-influence concept, we can already state that **A** is more likely than **B** and **C**, since only in isomer **A** the strongest *trans*-ligand NO is in *trans* position to the weakest *trans*-ligand Et. Furthermore **C** is the most unlikely isomer of all, because the two strong π-acceptor ligands NO and ethylene would compete for the same d-orbital electron density via back bonding. A NOESY spectrum of **33PPh$_3$** was recorded (Figure 3) to support this interpretation. In this spectrum, the ligand in *trans* position to NO should give rise to cross-peaks to both of the neighboring moieties in *cis*-position, while the two ligands in *cis*-position to the NO ligand would be too far from each other to give rise to cross-peaks. Therefore, for isomer **A** two cross-peaks between the ethyl moiety and the hydride/ethylene ligand should be observable. For **B** cross-peaks between the hydride and the ethyl/ethylene ligand are expected and for isomer **C** cross-peaks between the ethylene ligand and the hydride/ethyl ligands should be observed. The NOESY spectrum in Figure 3 shows the presence of cross-peaks between the CH_3 protons of the ethyl ligand and the hydride ligand and the CH_2 group of the ethyl ligand with the ethylene ligand protons. Therefore it can be concluded that only isomer **A** is present in solution.

As only the mixtures of **24PPh$_3$** and **33PPh$_3$** could be obtained, the IR spectrum could not unambiguously be interpreted. Nevertheless the presence of the three Re-H moieties was reflected in three ν(ReH) bands at 1959 cm^{-1}, 1897 cm^{-1} and 1816 cm^{-1} but only one broad ν(NO) band was resolved at 1630 cm^{-1}. Compared to the lower wave numbers of the ν(NO) of **24PCy$_3$** (1614 cm^{-1}) and **24P*i*Pr$_3$** (1619 cm^{-1}) [67] the less electron donating character of the PPh_3 ligand became obvious.

Figure 3: NOESY spectrum of **33PPh$_3$** (C_6D_6, 298K, 500 MHz).

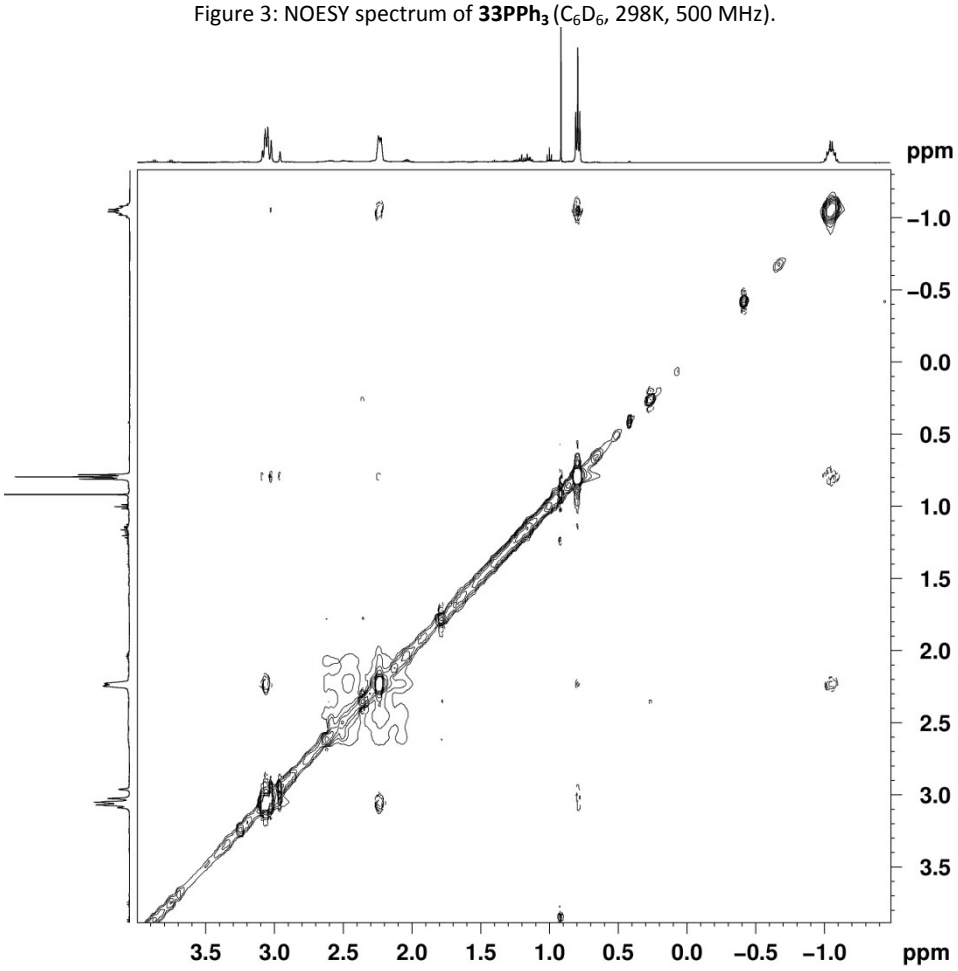

2.2 The fate of the catalyst: formation of [Re(η^2-C_2H_4)(η^4-butadiene)(NO)(PPh_3)]

As mentioned above, neither **24PPh$_3$** nor **33PPh$_3$** are stable compounds. They are sensitive to air in solution or as oils. In solution the slow reductive elimination of ethane is observed already at room temperature. Keeping a THF solution of **24PPh$_3$** and **33PPh$_3$** under an atmosphere of ethylene results first in the reaction of **24PPh$_3$** to **33PPh$_3$**, which is converted within 16 h at room temperature into the butadiene complex [Re(η^2-C_2H_4)(η^4-butadiene)(NO)(PPh_3)] (**34PPh$_3$**), which could not be isolated due to its oily nature. Nevertheless the formed **34PPh$_3$** is sufficiently pure (>80% by ^{31}P NMR, virtually no impurities in the ^{1}H NMR) to unambiguously derive the nature of it by NMR spectroscopy. Other species are formed in too low amounts to be spectroscopically characterized. The formation of **34PPh$_3$** is suggested to parallel the formation of the already known P*i*Pr$_3$ (**34P*i*Pr$_3$**) and PCy_3 (**34PCy$_3$**) analogues[72], which are obtained via the reduction of [$ReBr_2$(MeCN)(NO)(PR_3)] over sodium amalgam under an atmosphere of ethylene (Scheme 27).

Scheme 27: Formation of **34PPh$_3$**

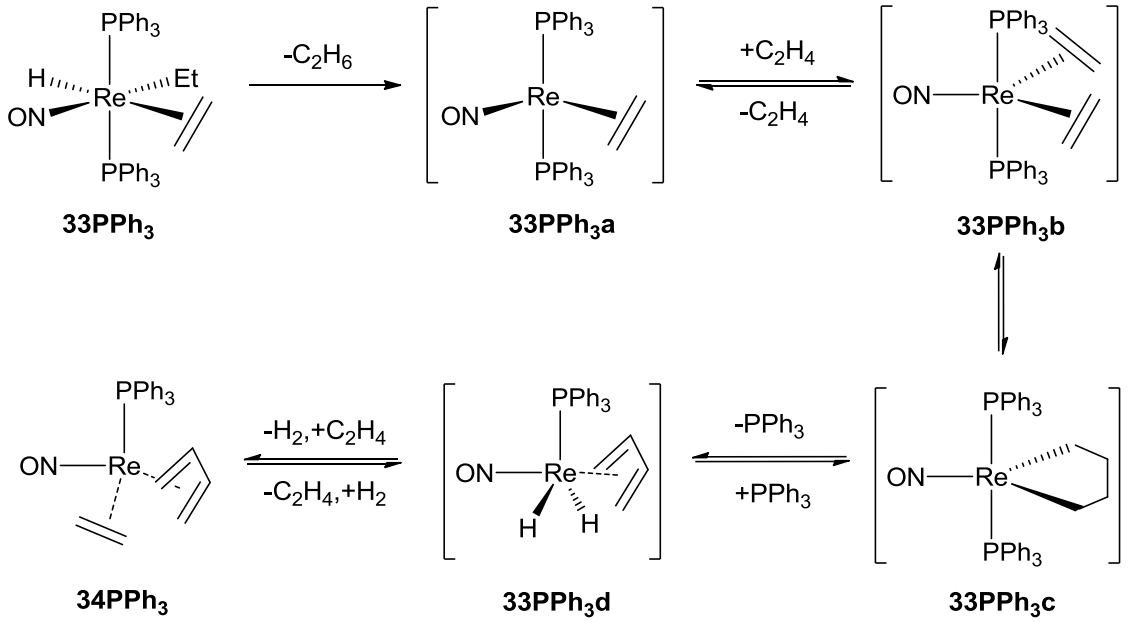

The depicted reaction pathway in Scheme 27 starts from **33PPh$_3$** with reductive elimination of ethane to form the 16e- complex [Re(η^2-C_2H_4)(NO)(PPh_3)] (**33PPh$_3$a**), which binds ethylene to form an intermediate bis-ethylene complex [Re(η^2-C_2H_4)$_2$(NO)(PPh_3)] (**33PPh$_3$b**). **33PPh$_3$b** undergoes oxidative coupling of the ethylene ligands to the metalla-cyclopentane compound **33PPh$_3$c** followed by release of PPh_3 and two C-H activation steps, which led to the intermediate dihydride or H_2 complex **33PPh$_3$d**. In the last step the H_2 ligand of **33PPh$_3$d** is exchanged with ethylene leading to the end product [Re(η^2-C_2H_4)(η^4-butadiene)(NO)(PPh_3)] **33PPh$_3$d**. The ^{1}H NMR spectrum of **34PPh$_3$** consists apart from the PPh_3 signals in the aromatic region of two spin systems which were assigned with the help of COSY, HSQC and HMBC spectra to the butadiene and the ethylene ligands (Scheme 28).

Scheme 28: The assignment of the ^{1}H and ^{13}C signals of **34PPh$_3$**.

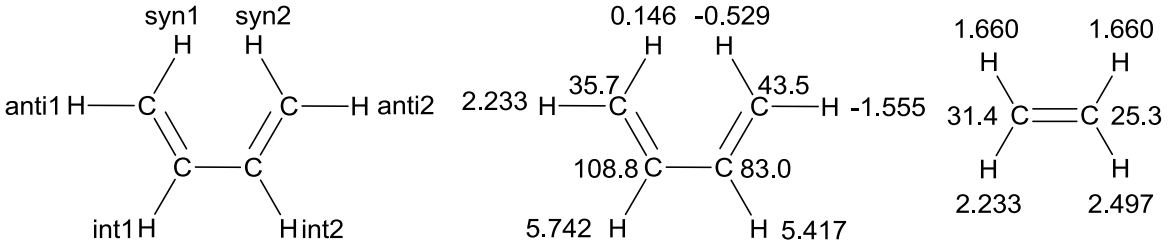

The internal protons of the butadiene ligand give rise to a set of resonances at 5.742 ppm (q, $^3J_{HH}$ = 7.0 Hz, 1 H, int1) and 5.417 ppm (q, $^3J_{HH}$ = 7.0 Hz, 1 H, int2). The observed coupling patterns arise from similar coupling constants between int1/2 and adjacent terminal and neighboring internal protons. The terminal protons syn1 and anti1, respectively syn2 and anti2 are subject to mutual geminal coupling of 3 Hz and vicinal coupling to the corresponding internal protons of 7 Hz. The

terminal protons give rise to signals at -1.555 ppm (dd, $^{3}J_{anti2int2}$ = 7 Hz, $^{2}J_{anti2syn2}$ = 3 Hz, 1 H, anti2), -0.529 ppm (dd, $^{3}J_{syn2int2}$ = 7 Hz, $^{2}J_{anti2syn2}$ = 3 Hz, 1 H, syn2), 0.146 ppm (dd, $^{3}J_{syn1int1}$ = 7 Hz, $^{2}J_{anti1syn1}$ = 3 Hz, 1 H, syn1) and 2.233 ppm (m, 1 H, overlapping with the ethylene ligand, anti1). The protons of the ethylene ligand give rise to three sets of multiplets at 2.497 ppm (m, 1 H), 2.233 ppm (m, 1 H) and 1.660 ppm (m, 2 H). The ethylene and butadiene signal of the proton spectrum are slightly broadened by weak coupling to the phosphorus nuclei. ^{31}P decoupling leads to sharp multiplets. Dynamic behavior of the penta-coordinate d8 system could not be observed at room temperature. Therefore the butadiene and the ethylene ligand are assumed to be strongly bound to the rhenium center and neither ligand rotation nor other rearrangement processes takes place on the NMR time scale. As already discussed in the literature[72], three different rotamers of **34PPh$_3$** are conceivable as structural isomers (Scheme 29).

Scheme 29: The three possible rotamers of **34PPh3**.

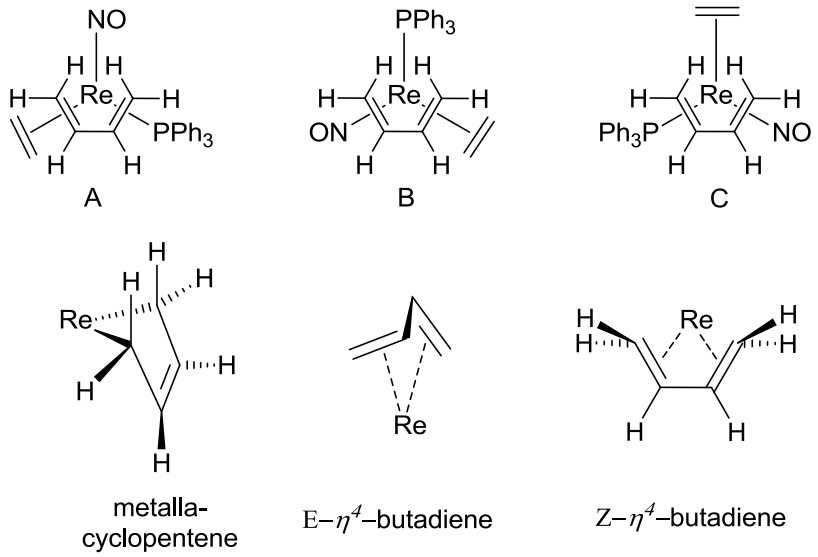

Furthermore a cyclopentene complex or an E-η^4-butadiene complex would constitute alternative isomers to the Z-η^4-butadiene complex (Scheme 29). The formation of an E-butadiene complex could be ruled out by the NOESY experiment, which confirmed the spacial proximity of the H_{syn1} and H_{syn2} protons. Furthermore the geminal coupling between the *syn* and the *anti* protons is only 3 Hz, suggesting rather a sp^2 than a sp^3 carbon[73] atom, therefore a metalla-cyclopentene complex seemed unlikely. In accordance to that, all vicinal coupling constants are approx. 7 Hz. This indicates that the butadiene ligand is rather η^4 than η^2 bound, as otherwise the coupling pattern in the metalla-cyclopentene envelope structure would lead to different coupling constants[74] for the coupling

[73] Hesse, M.; Meier, H.; Zeeh, B. *Spektroskopische Methoden in der organischen Chemie*, 7. Aufl.; Thieme: Stuttgart, 2005.
[74] Yasuda, H.; Kajihara, Y.; Mashima, K.; Nagasuna, K.; Lee, K.; Nakamura, A. 1,3-Diene complexes of zirconium and hafnium prepared by the reaction of enediylmagnesium with MCl_2Cp_2. A remarkable difference between the zirconium and hafnium analogs as revealed by proton NMR and electronic spectra. *Organometallics* **1982**, *1,* 388–396.

between the internal and the two different terminal protons. We indeed propose a Z-η^4-butadiene complex structure for **34PPh$_3$**. Furthermore we can rule out rotamer **C**, as in the NOESY experiment cross-peaks between the ethylene multiplet at 1.660 ppm and the int1/anti1 protons are visible. This indicates that **34PPh$_3$** possesses either the structure of rotamer **A** or rotamer **B**. As DFT-calculations on the model system [Re(η^2-C_2H_4)(η^4-butadiene)(NO)(PMe_3)] have revealed rotamer **B** is the thermodynamically most favorable isomer[72]. Consequently we postulate an analogous structure for **34PPh$_3$**. In the $^{13}C\{^1H\}$ NMR spectrum of **34PPh$_3$** the PPh_3 ligand caused the expected signals in the region of 125-140 ppm. The four chemically different carbon nuclei of the butadiene and the two chemically different carbon nuclei of the ethylene ligand were assigned by aid of HSQC and HMBC experiments (Scheme 28). The signals of the terminal butadiene carbon nuclei and of the ethylene carbon nuclei showed coupling with the PPh_3 phosphorus nucleus (3-7 Hz) whereas the internal carbon atoms showed no coupling. In the $^{31}P\{^1H\}$ NMR spectrum compound **34PPh$_3$** is giving rise to a single resonance at 22.4 ppm. In the IR spectrum of **34PPh$_3$** an intense, sharp ν(NO) band was observed at 1641 cm^{-1}.

2.3 Mechanistic aspects of the hydrogenation with of [ReH$_2$(η^2-C_2H_4)(NO)(PPh_3)$_2$]/[ReH(CH_2CH_3)(η^2-C_2H_4)(NO)(PPh_3)$_2$]

As mentioned in the previous sections, neither **24PPh$_3$** nor **33PPh$_3$** are stable compounds. Both tend to release ethane. In the presence of ethylene **34PPh$_3$** is formed as main product. The release of ethane from **33PPh$_3$** can be interpreted in the context of the Wilkinson cycle (Scheme 10) as reductive elimination of the hydrogenated olefin from a dihydride-olefin complex. Therefore the proposed mono hydride mechanism has at least in the case of **24PPh$_3$**/**33PPh$_3$** to be adapted to these results. However the mechanism proposed by Choualeb et al. cannot be excluded. The hydrogenation with **24PPh$_3$**/**33PPh$_3$** could proceed even via both reaction pathways (Scheme 30). The catalytic cycle proposed by Choualeb would involve the change of the oxidation state of the rhenium center from Re(+I) in compound **24PPh$_3$** and the postulated intermediates **24PPh$_3$a** and **23PPh$_3$c** to Re(+III) in the intermediate trihydride complex **23PPh$_3$b** and the proposed transition state **24PPh$_3$TS**. Therefore this cycle is denoted as Re(+I)/Re(+III) cycle in Scheme 30. In contrast to this the reaction pathway following the Wilkinson scheme involves the formal oxidation states Re(+I) for the complexes **24PPh$_3$**, **33PPh$_3$** and the proposed intermediate **24PPh$_3$a** and Re(-1) for the proposed intermediate **33PPh$_3$a**. Therefore the corresponding cycle is denoted as Re(+I)/Re(-I) cycle. Both catalytic cycles have two common species. The first one is the spectroscopically detectable **24PPh$_3$**, of which the PCy_3 and P*i*Pr_3 derivatives **24PCy$_3$** and **23P*i*Pr$_3$** can be isolated[67]. The second one is the anticipated intermediate **24PPh$_3$a**, for which no spectroscopic evidence was found. However, the fact

that **24PPh$_3$** and ethylene react to form **33PPh$_3$** suggests that such an intermediate (**24PPh$_3$a**) exists and that it is thermodynamically accessible.

Scheme 30: **24PPh$_3$** and **33PPh$_3$** as catalyst for ethylene hydrogenation.

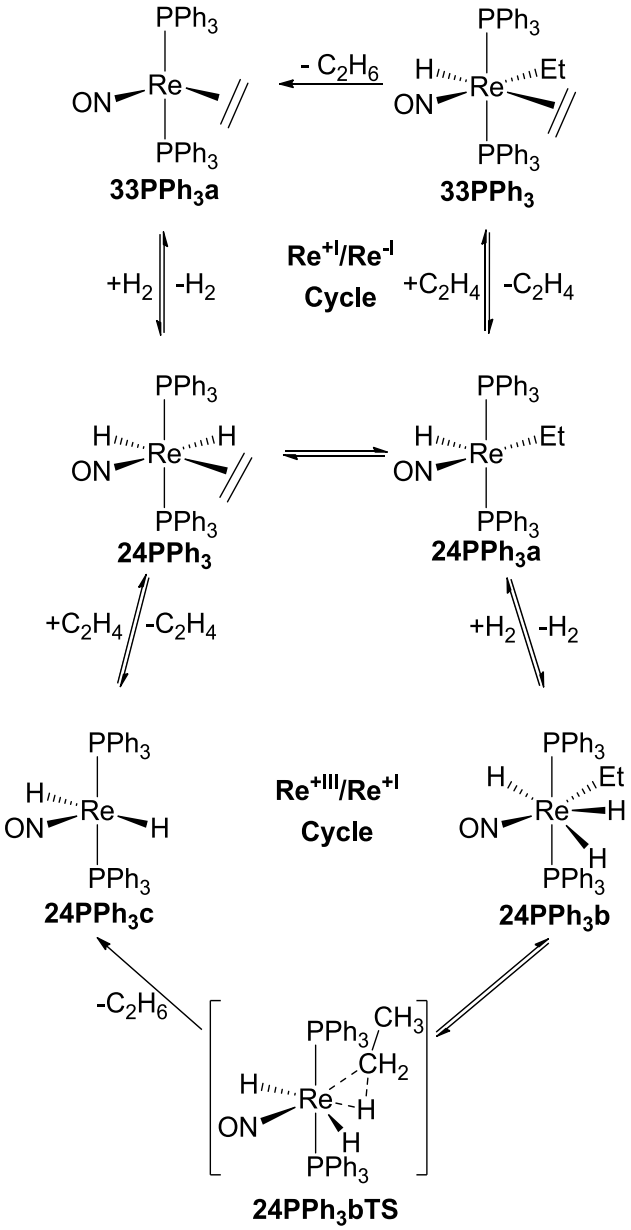

In the case of the Re(+I)/Re(+III) cycle, **24PPh$_3$a** is assumed to bind H_2 to form the hepta-coordinated trihydride complex **24PPh$_3$b**. After the oxidative addition of H_2 to **24PPh$_3$b**, the product (ethane in Scheme 30) is then reductively eliminated to form the unsaturated dihydride **24PPh$_3$c**. The addition of an olefin to **24PPh$_3$c** finally closes the cycle by regenerating the catalyst. The second anticipated catalytic cycle - the Re(+I)/Re(-I) cycle - starts as well from **24PPh$_3$** and proceeds with the Re(+I)/Re(+III) cycle via **24PPh$_3$a**. **24PPh$_3$a** adds then another equivalent of the substrate to form the spectroscopically characterized **33PPh$_3$** complex, which is then assumed to reductively eliminate the product alkane forming the intermediate **33PPh$_3$a**. Finally, the oxidative addition of H_2 to **33PPh$_3$a**

regenerates **24PPh$_3$**. Although the intermediate **33PPh$_3$a** could not be detected spectroscopically, it is likely to exist, as the reaction in absence of H_2 leads to the formation of **34PPh$_3$** which is thought to be formed starting from **33PPh$_3$a** (Scheme 27). To some extent both catalytic cycles are likely to be operative in the hydrogenation catalysis with **24PPh$_3$/33PPh$_3$** catalysts. However, the most striking argument for the Re(+I)/Re(-I) cycle is the fact that **24PPh$_3$/33PPh$_3$** release ethane in the absence of H_2 presumably forming the highly reactive intermediate **33PPh$_3$a**.

Scheme 31: Comparison of the rhodium based key intermediate **3c** with the related isoelectronic Re dihydrides **24**

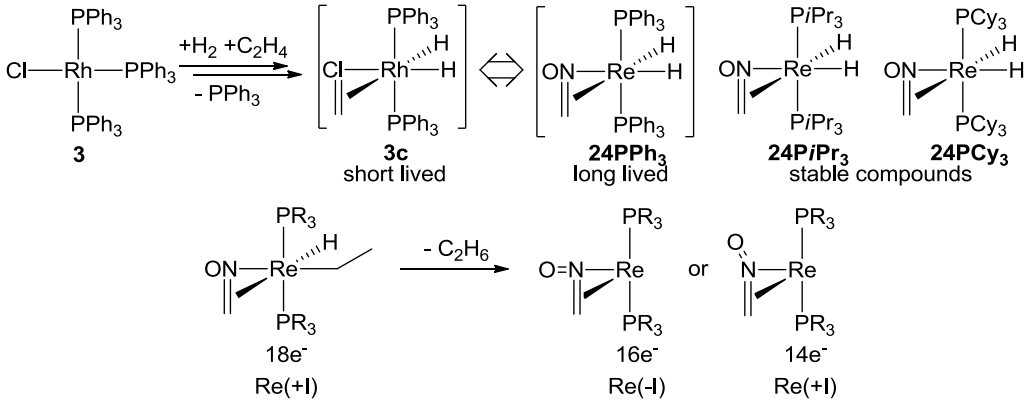

The structural relation between the intermediate **3c** of the Wilkinson-type cycle to **24PPh$_3$** is obvious (Scheme 31). However, the formal exchange of the Rh-Cl fragment with the Re-NO fragment is accompanied by the change of the oxidation state of the metal fragment from Rh(+I) to Re(-I). This has the consequence that **3c** is a Rh(+III) complex while, **24PPh$_3$** is a Re(+I) complex. The product release from these intermediates goes along with the change of the oxidation states to Rh(+I) and Re(-I). This could explain the drastic difference in activity between the highly efficient Rh system and the slower Re system, since the reductive elimination is driven by the electron density on the metal center. Electron deficient metal centers, such as Rh(+III) in **3c**, undergo reductive elimination with greater ease than electron rich ones, such as Re(+I) in **24PPh$_3$**, because in this way the electron rich centers would get reduced further to quite negative and less stabilized oxidation states. The very electron rich Re(-I) metal centers in the intermediate **24PPh$_3$a** tend to favor rather the reverse reaction which is oxidative addition[75]. Therefore one might be inclined to state that the Re(+I)/Re(-I) cycle is unlikely of importance for catalysis. However, the nitrosyl ligand is known to be a non-innocent ligand[76], which can stabilize also low oxidation states. This might be the cause, why the reductive elimination of ethane from **33PPh$_3$** is observed. Moreover, since the PPh_3 ligand is the weakest donor in the given series of phosphorus ligands, one would expect the reductive elimination

[75] Huheey, J. E.; Keiter, E. A; Keiter, R. L. *Anorganische Chemie: Prinzipien von Struktur und Reaktivität*, 2. Aufl. de Gruyter: Berlin, 1995.

[76] Kaim, W.; Schwederski, B. Non-innocent ligands in bioinorganic chemistry - An overview. Dithiolenes and non-innocent redox-active ligands. *Coord. Chem. Rev.* **2010**, *254,* 1580–1588.

to be faster in the **24PPh$_3$** system than in the **24PCy$_3$** and **24P*i*Pr$_3$** systems. And indeed using **23PPh$_3$** as pre-catalyst in the hydrogenation of 1-hexene, a TOF of 75 h^{-1} was observed, while in the case of **23PCy$_3$** only a TOF of 10 h^{-1} could be determined (10 bar H_2, 60°C, 1 mol% catalyst). Nevertheless the hydrogenation catalysis is not very efficient with compounds of type **24**, since the reductive elimination of the products is obviously disfavored in all cases. To overcome this problem, different approaches could be envisaged:

- Employing phosphines with lower donor capabilities to facilitate the reductive elimination.
- Changing the oxidation state of the ReH_2(olefin) species.
- Tuning of the catalytic cycle, such that the reductive elimination from Re(+I)is avoided.

Scheme 32: Reductive elimination as competitive reaction step to migration onto an olefin ligand:

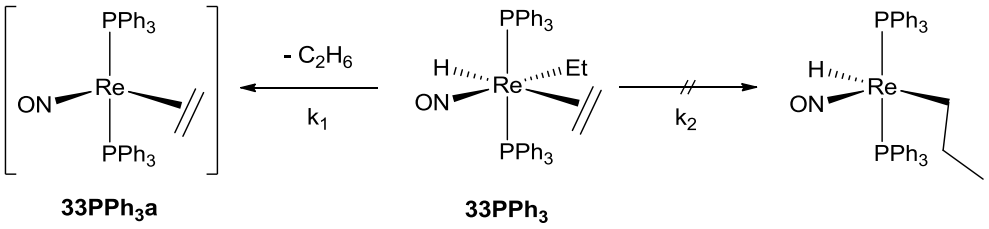

An alternative catalytic reaction pathway to the hydrogenation of the olefin would be the olefin polymerization reaction with the **24PPh$_3$/33PPh$_3$** system (Scheme 32), which however was not observed. This can be explained by the fact that the migration of the rhenium-hydride is kinetically more feasible than the migration of the ethyl-carbon onto a coordinated olefin (k_1>>k_2).

2.4 DFT-model studies of the [ReH$_2$(olefin)(NO)(PMe$_3$)$_2$] system

Liu et al.[70] studied the Re(+I)/Re(+III) cycle in Scheme 30 extensively for the model compound **24PMe$_3$**. They found a reaction pathway, which proceeds from **24PMe$_3$** over a transition state (**24PMe$_3$TS**) to the 16e- complex **24PMe$_3$a**, which in turn oxidatively adds H_2 via a an intermediate H_2 complex to form **24PMe$_3$b**. In the last step the product is released from **24PMe$_3$b** over a reductive elimination proceeding via **24PMe-TS**. The free energy profile of this sequence is depicted in Figure 4. Even though they investigated this reaction pathway very carefully, they did not investigate the reaction via the Re(+I)/Re(-I) cycle, because no experimental data indicated the feasibility of this pathway (The interested reader is referred to lit. 70 since only the most important species of the free energy pathway are shown in Figure 4). Therefore the investigation of Re(+I)/Re(-I) pathway was approached employing the same computational methods.

Figure 4: Facilitated free energy profile of the Re(+I)/Re(+III) cycle according to Liu et al. The crossed connections indicate intermediates of minor importance.

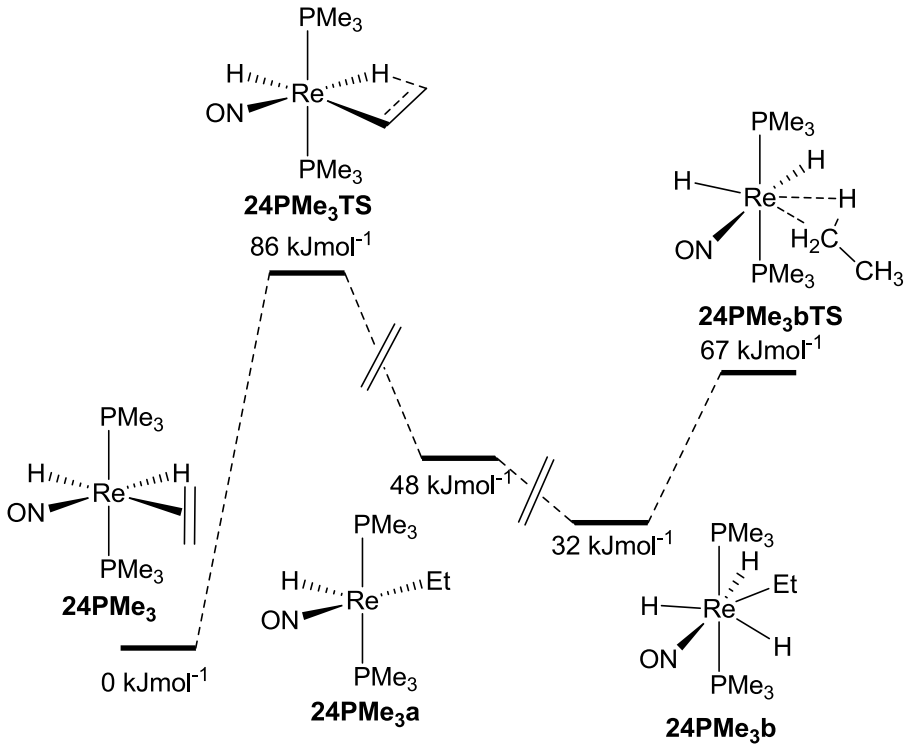

First of all the important species **24PMe$_3$**, **24PMe$_3$TS** and **24PMe$_3$a** were recomputed in order to gauge the comparability of our computations. The obtained structures (depicted in Figure 5) are structurally and energetically in good agreement with those of lit. 70. As expected the ethylene ligand of **24PMe$_3$** is aligned collinear to the P-P axis . The C=C bond is widened up to 1.421 Å and the Re-C distances are in the typical range of Re-C single bonds (Re-C1: 2.258 Å, Re-C2: 2.257 Å). The Re-H bonds are 1.698 Å (Re-H1) and 1.747 Å (Re-H2). The slight difference between Re-H1 and Re-H2 is attributed to the *trans* influence of the NO moiety on H2. In order to undergo the β-hydride shift from the Re-H to the ethylene moiety, the transition state **24PMe$_3$TS** has to be crossed which is in the model 89.9 kJmol^{-1} higher in free energy than **24PMe$_3$**. In this transition state the ethylene C=C axis is almost perpendicular to the P-P axis (torsion angles: C1-C2-Re-P1 102°, C1-C2-Re-P2 -70°). The C=C (1.409 Å) the Re-H1 (1.688 Å) and the Re-C1 (2.316 Å) distances remain almost unchanged while the Re-C2 (2.447 Å) and the Re-H2 (1.793 Å) distances are already elongated and the C2-H2 distance is shortened (1.756 Å). However, the structural features of the transition state are still closer to an ethylene hydride complex than to the agostic stabilized ethyl complex **24PMe$_3$a-ag**. This indicates an early transition state. The β-hydride shift leads to the ethyl complex **24PMe$_3$a-ag** which is stabilized by an agostic interaction of the *H*-CH_2CH_2 bond with the Re-center and which is 41.6 kJmol^{-1} higher in free energy than **24PMe$_3$**. The ethyl moiety of **24PMe$_3$a-ag** and the Re-center form a four membered ring with Re-C1 (2.197 Å) and C1-C2 (1.537 Å) distances in the range of normal single bonds and a slightly elongated C2-H1 (1.142 Å) bond. The agostic interaction causes ring strain which manifests in

a Re-C1-C2 angle of only 86°. This reduces the Re-H1 distance to 2.149 Å. In contrast to that, structure **24PMe$_3$a** is not stabilized by an agostic interaction. Therefore it is not surprising that **24PMe$_3$a** is 12.9 kJmol^{-1} higher in free energy than **24PMe$_3$a-ag** (respectively 54 kJmol^{-1} higher than **24PMe$_3$**), the Re-C1-C2 (111°) angle is relaxed and the closest *H*-CH_2CH_2*Re* distance is 3.299 Å while the Re-C1 (2.209 Å) and the C1-C2 (1.550 Å) distances remain almost identical. In **24PMe$_3$a** and **24PMe$_3$a-ag** the ethyl moiety is located *trans* to the NO ligand. This is in both cases thermodynamically favored over an ethyl-*trans*-H arrangement (for which no energetic minimum could be found).

Figure 5: Diagrams of the optimized structures of **24PMe$_3$**, **24PMe$_3$TS**, **24PMe$_3$a-ag** and **24PMe$_3$a** their relative free energies with respect to **24PMe$_3$**.

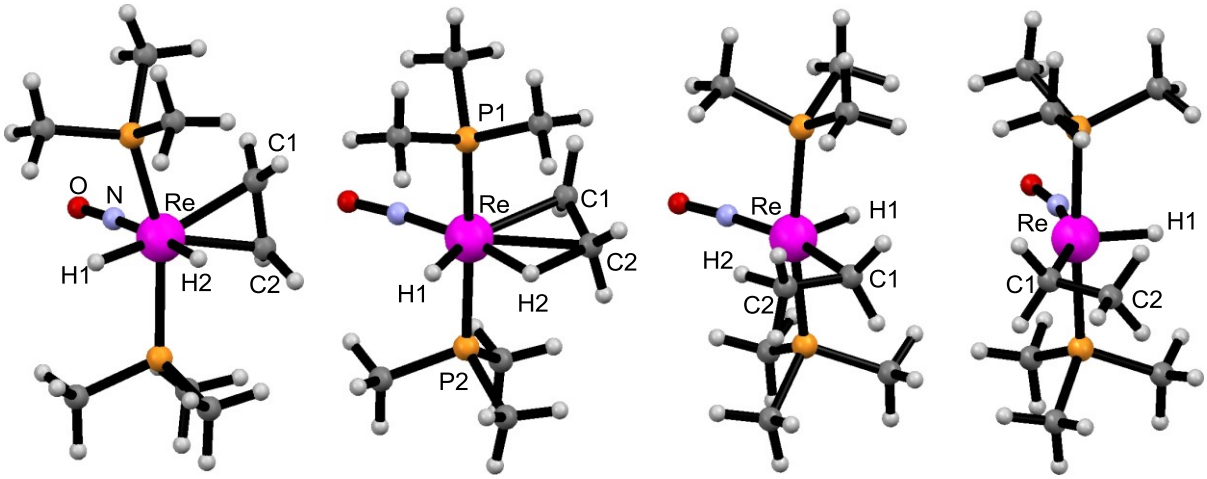

24PMe$_3$ 0.0 kJmol^{-1} | **24PMe$_3$TS** 89.9 kJmol^{-1} | **24PMe$_3$a-ag** 41.6 kJmol^{-1} | **24PMe$_3$a** 54.5 kJmol^{-1}

Selected bond lengths [Å]: **24PMe$_3$** C1-C2 1.421, C1-Re 2.257, C2-Re 2.258, H1-Re 1.698, H2-Re 1.747; **24PMe$_3$TS** C1-C2 1.409, C2-H2 1.756, C1-Re 2.316, C2-Re 2.447, H1-Re 688, H2-Re 1.793; **24PMe$_3$a-ag** C1-C2 1.537, C1-Re 2.107, C2-Re 2.592, C2-H2 1.142, H1-Re 1.661, H2-Re 2.149; **24PMe$_3$a** C1-C2 1.550, C1-Re 2.205, C2-Re 3.134, C2-H2 1.099, H1-Re 1.1.684, H2-Re 3.299. Selected bond angles [°]: **24PMe$_3$** C1-Re-C2 36.7, C2-Re-H2 84.7, H1-Re-H2 76.8; **24PMe$_3$TS** C1-Re-C2 34.3, C2-Re-H2 47.8, H1-Re-H2 69.9; **24PMe$_3$a-ag** C1-Re-C2 36.3, C2-Re-H2 25.8, H1-Re-H2 163.3; **24PMe$_3$a** C1-Re-H1 112.5 C2-C1-Re 111.8.

The reaction pathway of the Re(+I)/Re(+III) and the Re(+I)/Re(-I) cycle are identical in this first steps from **24PMe$_3$** via **24PMe$_3$TS** to **24PMe$_3$a**. However the question, whether a reductive elimination of ethane from **24PMe$_3$a** is possible was not discussed in lit. 70. Therefore the transition state for this reductive elimination (**24PMe$_3$aTS**) was optimized. However it is 121.8 kJmol^{-1} higher in free energy than **24PMe$_3$a** (and 176.3 kJmol^{-1} higher than **24PMe$_3$**). This indicates that **24PMe$_3$aTS** is probably of minor importance for the catalytic hydrogenation of olefinic compounds and for the observed reductive elimination of ethane from **33PPh$_3$**. Structurally **24PMe$_3$aTS** is in agreement with our expectations. The Re-H1 (1.741 Å) and the Re-C1 (2.257) bonds are stretched somewhat and the H1-Re-C1 angle is compressed from 112.5° to 39.8° resulting in a H1-C1 distance of 1.445 Å. Therefore **24PMe$_3$TS** can be characterized as an early transition state.

Since **24PMe$_3$a** unlikely undergoes reductive elimination, it could react either with another olefin or H_2 to form a stabilized intermediate. Liu et al. investigated the oxidative addition of H_2 to **24PMe$_3$a** and found two isomers of the trihydride complex **24PMe$_3$(H)$_3$**, which are formed via transition states from H_2 complex precursors. From these Re(+III) trihydrides the product alkane can be reductively eliminated with greater ease than from the Re(+I) complex **24PMe$_3$a**. Alternatively **24PMe$_3$a** could also react with a further equivalent of the substrate (ethylene in the model). Therefore the structure of the ethylene complex **33PMe$_3$** and the reductive elimination of ethane thereof were investigated. As in the case of the formation of **24PMe$_3$b** the binding of the ethylene ligand to **24PMe$_3$a** leads to a significant stabilization of -93.6 kJmol^{-1} in free energy respectively -40.1 kJmol^{-1} compared to **24PMe$_3$**. Therefore type **33** complexes are expected to be the prevailing species in presence of a suitable olefin, which is indeed in agreement with the observation of **33PPh$_3$**. A transition state **33PMe$_3$TS** for the reductive elimination of ethane from **33PPh$_3$** was found, which is +116.6 kJmol^{-1} higher in free energy than **33PMe$_3$** and +76.5 kJmol^{-1} higher than **24PMe$_3$**. Compared to the reductive elimination from **24PMe$_3$aTS** this route is favored -5.2 kJmol^{-1} but it is still too high to play an important role in efficient catalysis. However, the calculated barrier heights have to be critically assessed, since the reductive elimination from the closely related **33PPh$_3$** occurs slowly under ambient conditions. This speaks for lower barriers in the real systems.

Figure 6: Diagrams of the optimized structures of **24PMe$_3$aTS**, **33PMe$_3$a** and **33PMe$_3$TS** and their relative free energies with respect to **24PMe$_3$**.

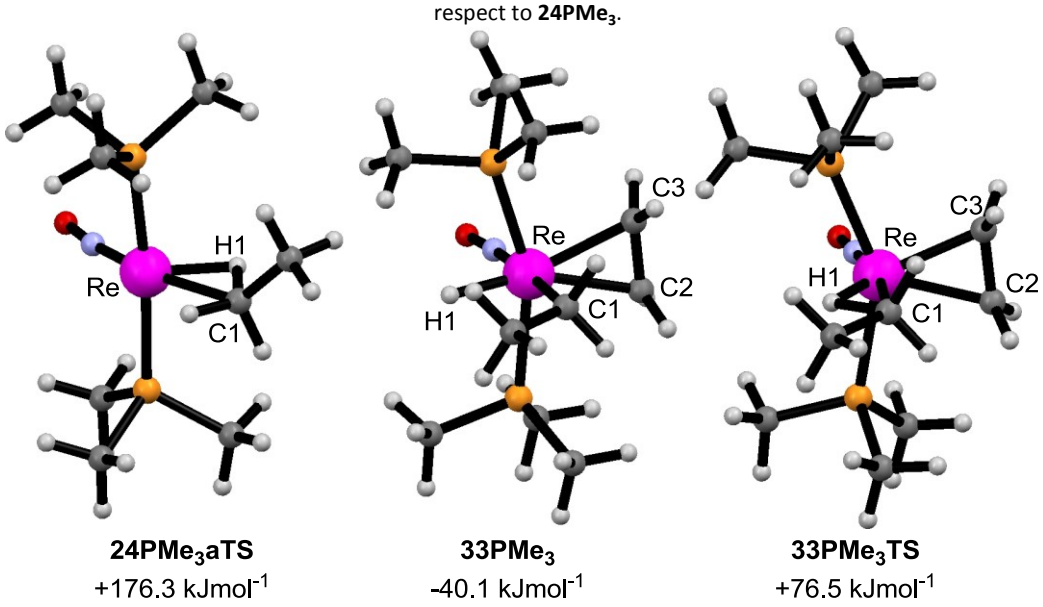

Selected bond lengths [Å]: **24PMe$_3$aTS** C1-H1 1.445, C1-Re 2.257, H1-Re 1.741; **33PMe$_3$** C1-H1 2.627, C1-Re1 2.259, C2-C3 1.422, C2-Re 2.263, C3-Re 2.263, H1-Re 1.702; **33PMe$_3$TS** C1-H1 1.480, C1-Re 2.477, C2-C3 1.438, C2-Re 2.213, C3-Re 2.213, H1-Re 1.719. Selected bond angels [°]:**24PMe$_3$aTS** C1-Re-H1 39.8; **33PMe$_3$** C1-Re-H1 81.8; **3PMe$_3$TS** C1-Re-H1 35.9.

Structurally **33PMe$_3$** resembles the dihydride complex **24PMe$_3$** (Figure 5, Figure 6). It also features an ethylene ligand bound with the C=C axis parallel to the P-P vector. The C1-C2 (1.445 Å) bond is elongated and the Re-C2 (2.2623 Å) and ReC3 (2.263 Å) bonds are in the same range as the Re-C1

(2.259 Å) single bond. The Re-H1 (1.702 Å) bond is also in the range of typical Re-H bonds and the H1-C1 (2.627 Å) distance and the H1-Re-C1 (81.8°) angle do not indicate any H1-C1 interaction. In contrast, **33PMe$_3$TS** already shows beginning C1-H1 interactions. The C1-H1 (1.480 Å) distance is shortened and the C1-Re-H1 (35.9°) angle is compressed. At the same time the C1-Re (2.477 Å) is elongated while the C2-C3 (1.438 Å), C2-Re (2.213 Å), C3-Re (2.213 Å) and the Re-H1 (1.179 Å) bonds remain almost unchanged. Again this transition state retains most of its *cis*-hydrido-alkyl character and is therefore best characterized as early transition state.

Comparing **33PMe$_3$TS**, **24PMe$_3$TS** and **24PMe$_3$bTS** reveals some common features. In all cases, the Re-H distances remain almost unchanged, while the Re-C distances are more variable (from +0.05 Å in case of **24PMe$_3$TS** to +0.22 Å in case of **33PMe$_3$TS**). For all transition states the sharpening of the C-Re-H angle from 80-90° to less than 40° is apparently more important than the changing of bond lengths. The reductive elimination of ethane from the model compounds is kinetically hindered in all cases. However, it is surprising that the reductive elimination from the 16e- complex **24PMe$_3$TS** is the least favorable, as one would assume that a 16e- complex is generally more electron deficient than an 18e- complex. Obviously the ethylene ligand in **33PMe$_3$TS** drains off more electron density from the Re center via π-back-bonding than it donates via σ-donor-bonding. However both pathways are disfavored compared to the reductive elimination from **24PMe$_3$b**. This is explained with the favorable change of the Re oxidation state from Re(+III) to Re(+I).

This DFT study reveals some pivotal points, which are reflected in the experimental results as well. The probably most important point is the fact that the performance of catalysts of the general form [ReH$_2$(olefin)(NO)(PR$_3$)$_2$] is limited by:

- β-shift of the Re-H to the olefin to form a 16e- alkyl complex
- reductive elimination of the products

This can be interpreted in terms of a too high electron density on the metal center since it

- increases the rotational barrier of the ethylene ligand
- disfavors the reductive elimination

Therefore the most promising approach to overcome these limitations is to tune the electron density of the complex. This could be achieved via the variation of the phosphines or alternatively by a more fundamental change of the system (e.g. by changing to a 16e- system like the [ReH$_2$(CO)(olefin)(PR$_3$)$_2$]$^+$ system). This might also help to overcome the possible problem of catalyst inhibition caused by substrate binding to type **24a** complexes to form type **33** complexes.

3. Ethylene binding in $[ReX_2(\eta^2\text{-}C_2H_4)(NO)(PPh_3)_2]$.

3.1 Synthesis of $[ReX_2(\eta^2\text{-}C_2H_4)(NO)(PPh_3)_2]$ complexes

The ability of a hydrogenation catalyst to bind and activate H_2 and the acceptor substrate is crucial for efficient catalysis. Therefore we decided to analyze the ethylene binding in Re-NO complexes in-depth. Complexes of the form $[ReBr_2(\eta^2\text{-}C_2H_4)(NO)(PR_3)_2]$ (**17PCy$_3$**, **17P*i*Pr$_3$**) and $[ReH_2(\eta^2\text{-}C_2H_4)(NO)(PR_3)]$ (**24PCy$_3$**, **24P*i*Pr$_3$**) have already been prepared and investigated. We wanted to extend this series with a phosphine with lower donor capability. Therefore we approached the preparation of the PPh_3 derivatives **17PPh$_3$**. In the case of the PCy_3 and P*i*Pr$_3$ derivatives the ethylene complexes were obtained either from dihydrogen complexes of the form $[ReBr_2(\eta^2\text{-}H_2)(NO)(PR_3)_2]$ (R=Cy: **17PCy$_3$**; R=*i*Pr: **17P*i*Pr$_3$**) or the acetonitrile complexes of the form $[ReBr_2(MeCN)(NO)(PR_3)_2]$ (R=Cy: **35PCy$_3$**; R=*i*Pr: **35P*i*Pr$_3$**) by exposing them in solution to ethylene[72] (Scheme 33).

Scheme 33: Synthesis of type **17** complexes

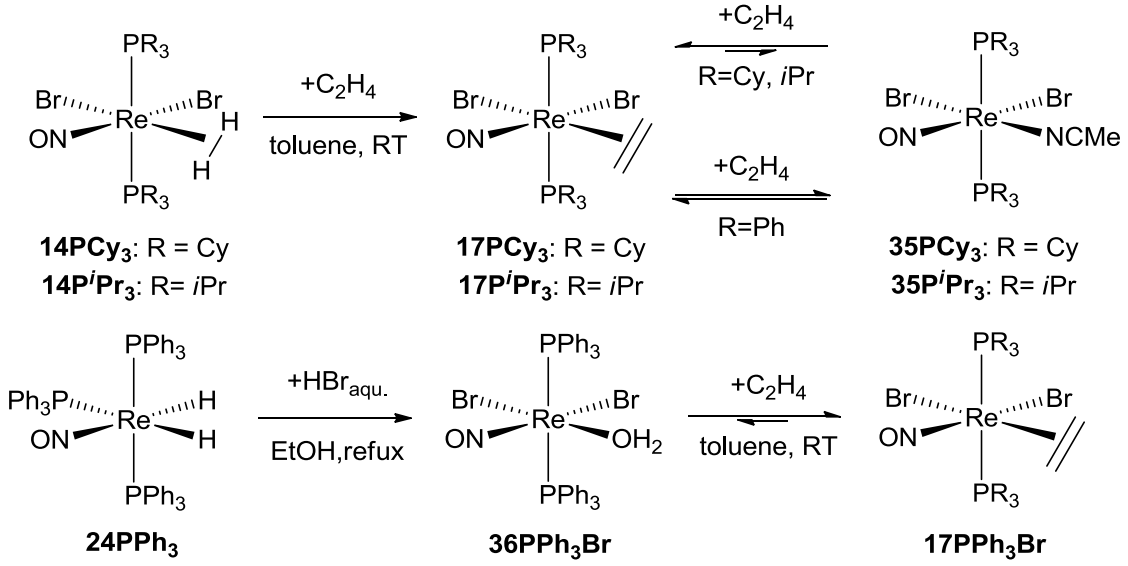

As the dihydrogen complex **14PPh$_3$** could not be prepared[66], the acetonitrile complex **35PPh$_3$** remained the most promising starting material. However, the attempt to substitute the acetonitrile ligand of **35PPh$_3$** with ethylene was not successful. Although the ethylene complex could be observed in the ^1H and ^{31}P NMR spectra of ethylene saturated reaction solutions, the isolation was not possible, because the equilibrium between **35PPh$_3$** and **17PPh$_3$** was shifted to **35PPh$_3$** when the ethylene concentration decreased. Nevertheless, the ethylene complex **17PPh$_3$Br** could be obtained from the H_2O complexes **36PPh$_3$Br** presented in the subsequent section.

We were also interested in preparing rhenium complexes of the form $[ReX_2L(NO)(PPh_3)_2]$ with the halides Cl, Br and I. Therefore the reactions of aqueous HCl, HBr and HI with **24PPh$_3$** were explored. In the case of the already known reaction with HCl_{aq} in refluxing ethanol suspension, the $[ReCl_2(NO)(PPh3)2]$ **37PPh$_3$** complex is obtained in ca. 60% yield[77]. Due to the introduction of the halides their *cis*-labilization effect gets into play. **37PPh$_3$** is much more reactive in ligand substitution reactions than the analogue hydride complex **24PPh$_3$**[77]. This is also manifests in their $^{31}P\{^1H\}$ NMR spectra. The spectrum of **24PPh$_3$** shows the signals of an AB_2 system at 28.3 (d, $^2J_{PP}$ = 8 Hz, 2 P) and 20.2 ppm (t, $^2J_{PP}$ = 8 Hz, 1 P) with a clearly resolved coupling pattern. In contrast, the chlorine derivative **37PPh$_3$** shows only two broad multiplet resonances without defined coupling pattern at -2 ppm and at -5 ppm. This can be interpreted in terms of phosphine exchange, which proceeds in the range of the NMR time scale for **37PPh$_3$**, while the same process is significantly slower for the hydride complex **24PPh$_3$**. This exchange would probably be initiated by the loss of a weakly bound ligand. Then the ligand sphere of the five coordinate intermediate would undergo a complex rearrangement of the ligand sphere and subsequently the dissociated ligand would recoordinate (Scheme 34). As this rearrangement is initiated by a ligand dissociation step, the increased *cis*-labilization[78] effect of the chlorides would explain the higher rate of this process for **37PPh$_3$**.

Scheme 34: Proposed mechanism for the dynamics observed for the $^{31}P\{^1H\}$ spectra of **37PPh$_3$**

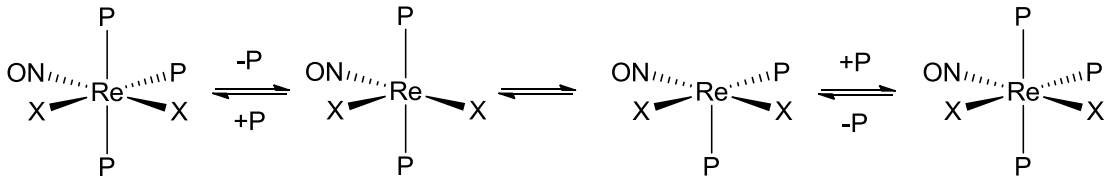

Unlike the reaction with HCl_{aq}, the reactions with HBr_{aq} and HI_{aq} furnished water complexes of the form $[ReX_2(NO)(OH_2)(PPh_3)_2]$ with X=Br (**36PPh$_3$Br**) and I (**36PPh$_3$I**) in 60-70% yield. This is probably due to the increased *trans*-effect of these halides, which labilizes the PPh_3 ligand in *trans* position. Furthermore the increased acidity of HBr and HI together with the higher solubility of $[HPPh_3][Br/I]$ salts might also facilitate the exchange of the PPh_3 with water. A single crystal X-ray diffraction study on **36PPh$_3$Br** revealed a slightly disturbed octahedral structure with a H_2O *trans* to NO arrangement (Figure 7).

[77] Cameron, T. S.; Grundy, K. R.; Robertson, K. N. Nitrosyl complexes of rhenium. Synthesis of some fluoro complexes of rhenium(I), including the novel cationic complex fluorocarbonylnitrosyltris(triphenylphosphine)rhenium(I) tetrafluoroborate. *Inorganic Chemistry* **1982**, *21,* 4149–4155.

[78] Atwood, J. D.; Brown, T. L. Cis labilization of ligand dissociation. 3. Survey of group 6 and 7 six-coordinate carbonyl compounds. The site preference model for ligand labilization effects. *J. Am. Chem. Soc.* **1976**, *98,* 3160–3166.

Figure 7: ORTEP diagram of **36PPh$_3$Br** draw at 50% probability not in hydrogen bonding involved THF molecules omitted.

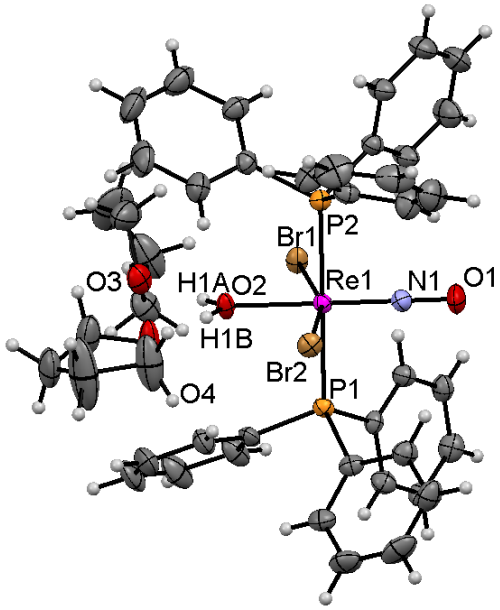

Selected bond lengths [Å]: Br1-Re1 2.572, Br2-Re2 2.557, N1-Re1 1.737, N1-O1 1.200, O2-Re1 2.134, O3-H1A 1.849, O4-H1B 1.847, P1-Re1 2.456, P2-Re2 2.440. Selected bond angles [°]: Br1-Re1-Br2 161.0, N1-Re1-O2 179.2, O1-N1-Re2 178.8, O2-H1A-O3 165.0, O2-H1B-O4 167.8, P1-Re2-P2 179.0.

This arrangement can be explained by the relative *trans*-effect of the ligands (H_2O < Br < NO). Furthermore the *cis*-labilization from the Br ligands weakens the H_2O-Re bond further. This is not only reflected in the kinetically weak H_2O-Re bond (the H_2O ligand exchanges on the NMR time scale) but also thermodynamically in the bending of the Br ligands towards the H_2O ligand. This bending allows a better π-donation from the Br ligands to the metal and compensates for the weakened H_2O-Re bond. The ^{1}H NMR spectra of **36PPh$_3$Br** and **36PPh$_3$I** displayed the typical resonances of the PPh_3 ligand and a signal assigned to the H_2O protons. The chemical shift of the H_2O protons depends on the concentration of the complex , the concentration of H_2O and the solvent. In the NOESY spectrum a cross-peak of the bound H_2O and the free H_2O indicates an exchange on the NMR time scale. In the $^{31}P\{^1H\}$ NMR signals were detected at 8.5 ppm (**36PPh$_3$Br**) and at 9.3 ppm (**36PPh$_3$I**). Strong ν(NO) bands in the IR spectrum at 1670 cm^{-1} (**36PPh$_3$Br**) and at 1668 cm^{-1} (**36PPh$_3$I**) indicated the presence of the NO ligands. As the water ligand is much weaker bound to the Re center compared to the acetonitrile ligand, the reaction with ethylene was expected to proceed quantitatively. And indeed, the ethylene complex **17PPh$_3$** was obtained in 83% yield by stirring **36PPh$_3$Br** in a THF suspension under an atmosphere of ethylene. The ^{1}H NMR spectrum of **17PPh$_3$Br** in THF consists of the signals attributed to the PPh_3 ligand at 7.926 ppm (m, 12 H) and 7.345 ppm (m, 18 H) and a resonance assigned to the protons of the ethylene ligand at 2.370 ppm (t, J_{PC} = 3.0 Hz, 4 H, 300 MHz). Because the environment of the ethylene ligand is asymmetric, a signal pattern of lower symmetry was expected, as it is observed for the PCy_3 and P*i*Pr$_3$ derivatives **17PCy$_3$** and **17P*i*Pr$_3$**[72]. Since this was not the case, fast rotation of the ethylene ligand around the Re-(ethylene)

axis on the NMR timescale is the most likely explanation for the observed signal pattern. Therefore a VT-NMR series of spectra was recorded, which actually showed temperature dependence and therefore revealed that the ligand ligand rotates on the NMR time scale (Figure 8). In the $^{13}C\{^1H\}$ NMR spectrum, the ethylene ligand caused a signal at 49.4 ppm. This can be interpreted either in terms of the ethylene being symmetrically bound or in terms of the fast exchange of two inequivalent carbon nuclei. In the IR spectrum an intense band at 1704 cm^{-1} was attributed to the ν(NO) vibration. **17PPh$_3$Br** is expected to possess an octahedral structure of type **A** (Scheme 35):

Scheme 35: The three possible constitutional isomers, which are in agreement with the $^{31}P\{^1H\}$ NMR spectrum of **17PPh$_3$**

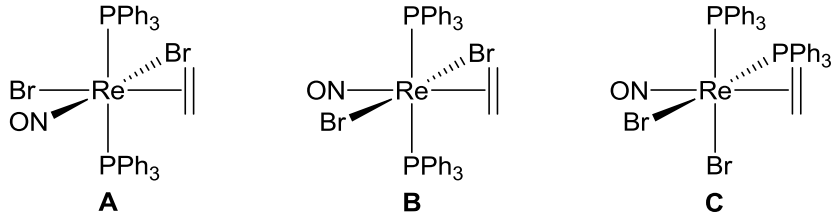

Although all of the isomeric forms **A**, **B** and **C** would be in agreement with the observed NMR spectra, **A** is expected to prevail, since in **B** and **C** the strong π-acceptors NO and ethylene would be arranged in *trans* positions, whereas in **A** the π-acceptors are *trans* to the bromide ligands, which act as π-bases forming a "push-pull' system (Scheme 36). This is also in agreement with the structures found for the analogous compounds **17PCy$_3$** and **17P*i*Pr$_3$**[79]. For comparison also the chloride derivative **17PPh$_3$Cl** was analogously prepared from **37PPh$_3$** and obtained in 90% yield. The spectroscopic features of **17PPh$_3$Cl** parallel those of **17PPh$_3$Br**. In the $^{31}P\{^1H\}$ NMR spectrum a singlet at -2.0 ppm is observed indicating a symmetric arrangement of the phosphines. In the ^1H NMR spectrum the PPh_3 ligand caused multiplets at 7.889 ppm (12 H) and 7.306 ppm (18 H). In contrast to the bromide analogue, the signals of the ethylene ligand are not in the fast exchange regime (THF, 23°C, 300 MHz). Therefore a set of clearly resolved higher order multiplets is observed at 2.192 ppm (2 H) and at 2.143 ppm (2 H). In the $^{31}C\{^1H\}$ NMR spectrum the ethylene ligand gives rise to one resonance at 50.2 ppm, which indicates that either the two carbon nuclei are in a chemically equivalent arrangement or in fast exchange. In the IR spectrum a sharp ν(NO) band at 1699 cm^{-1} indicates the presence of an NO group. The fact that the PPh_3 ligand in **37PPh$_3$** is easily replaced by ethylene, while the MeCN ligand of **35PPh$_3$** cannot be exchanged with ethylene in preparative experiments, reveals that the halides in the system have a crucial influence on the ethylene binding. An explanation for this behavior is the different degree of the "π-push-pull" effect[80] exerted by the halides. Since the Cl^-

[79] A. Choualeb, Unpublished results.
[80] Poulton, J. T.; Folting, K.; Streib, W. E.; Caulton, Kenneth G. Spectroscopic assessment of the degree of π-stabilization of unsaturation in ruthenium complex, RuH(X)CO(P-tert-$Bu_2Me)_2$. *Inorg. Chem.* **1992**, *31,* 3190–3191.

ligand is the better π-base[81] than Br^-, the Cl^- pushes the d-electrons with its lone pairs to the opposite site, where they are readily absorbed in the back donation to the ethylene ligand[82] (Scheme 36). A similar effect on the back bonding of the H_2 ligand by bending the phosphine ligands away from the π-acceptor ligands in the H_2 complexes **14PCy$_3$** and **14P*i*Pr$_3$** has already been discussed in literature[66]. However this "π-push-pull" concept should not be confused with the "π-push-pull" effect often encountered in the literature concerning photochemistry, where it denotes an intramolecular charge transfer process similar to a metal-to-ligand charge transfer. The term "push-pull" effect, as it is used in this work, refers not to a charge transfer, but rather to a polarization of the d-electrons involved in the backbonding to π-acceptor ligands.

Scheme 36: Qualitative model for the back bonding of ethylene to a metal center conjugated π-base and the Dewar Chatt and Duncanson model.

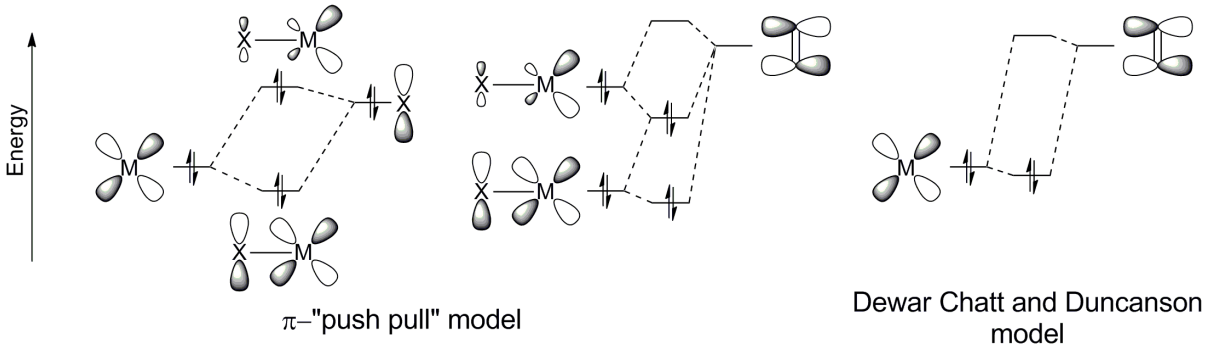

Therefore it is not surprising that the iodide analogue **17PPh$_3$I** does not form a stable ethylene complex, as the iodide ligand is known to be less π-basic than chloride or bromide ligands, while it is attributed a higher trans effect than chloride and bromide ligands.

3.2 Properties of [ReX$_2$(η^2-C$_2$H$_4$)(NO)(PPh$_3$)$_2$] complexes

The ethylene ligand in compound **17PPh$_3$Br** and **17PPh$_3$Cl** is not rigidly bound to the metal center. Nevertheless it is known for such complexes that the ethylene C-C vector has a preferential orientation along the P-Re-P axis[72]. Unlike in the case of the PCy_3 or P*i*Pr_3 derivatives, no signal overlap between the ethylene signals and the phosphine signals complicated the quantitative analysis of the site exchange process. Therefore a VT-NMR series in THF was recorded, which allowed to estimate the exchange rate of the ethylene ligand at various temperatures by NMR simulation with the gNMR program package. The observed rates were interpreted with the help of the transition state theory and the activation parameters for the ethylene rotation processes in **17PPh$_3$Br** and **17PPh$_3$Cl** could be obtained (**17PPh$_3$Br**: $\Delta H^{\ddagger}$ = 49 kJmol^{-1}, $\Delta S^{\ddagger}$ = -58 Jmol^{-1}K^{-1}; **17PPh$_3$Cl**: $\Delta H^{\ddagger}$ = 93 kJmol^{-1}, $\Delta S^{\ddagger}$ = 53 Jmol^{-1}K^{-1}).

[81] Keith Fagnou; Mark Lautens. Halide Effects in Transition Metal Catalysis. *Angew. Chem. Int. Ed.* **2002**, *41,* 26–47.
[82] Chatt, J.; Duncanson, L. A. Olefin Coordination Compounds 3. Infra-Red Spectra and Structure - Attempted Preparation of Acetylene Complexes. *J. Chem. Soc.* **1953**, 2939–2947.

Figure 8: ^{1}H NMR (THF-d8, 300 MHz, 22°C) spectra of **17PPh$_3$Br** and the ethylene section at selected temperatures

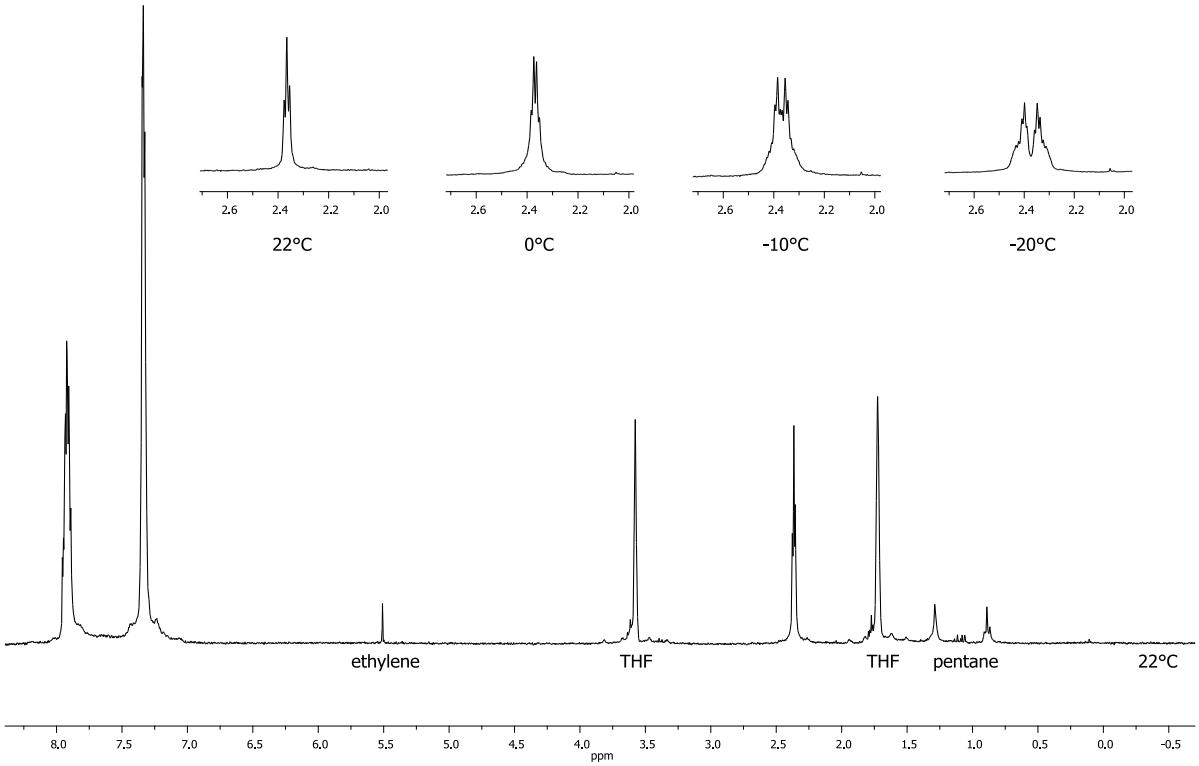

The difference of these two sets of activation parameters suggests that the character of the mechanism of the ethylene rotation process for the complexes **17PPh$_3$Br** and **17PPh$_3$Cl** differ. In the case of **17PPh$_3$Br** the activation entropy is positive. This suggests a highly ordered transition state. The rotation of the ethylene ligand of **17PPh$_3$Br** does not require the ligand to dissociate, but rather to rotate with largely intact metal ethylene bond. This is also in agreement with the relatively low value of $\Delta H^{\ddagger}$. For the chloride derivative **17PPh$_3$Cl** $\Delta S^{\ddagger}$ is negative. This might point to a dissociative ethylene proton exchange process. This is also in agreement with the higher $\Delta H^{\ddagger}$ value. Consequently we can postulate two different mechanisms for the observed rotation of the ethylene ligands. For **17PPh$_3$Br** the rotation seems to proceed via a highly ordered intermediate, in which the rhenium-ethylene bond is partly intact, while for **17PPh$_3$Cl** the rotation has dissociative character. As we were also interested in the thermodynamics of the rhenium-ethylene bond, we tried to find an equilibrium between **17PPh$_3$Br**/**17PPh$_3$Cl** and the corresponding unsaturated species and free ethylene using NMR spectroscopy. However, this proved to be difficult, as the ethylene is in both cases very strongly bound and the unsaturated [ReX$_2$(NO)(PPh$_3$)$_2$] could not be characterized due to its low solubility. This is probably caused by the dimerization to [{ReX(η^2-X)(NO)(PPh$_3$)$_2$}$_2$] or the polymerization to higher oligomers. Therefore we approached this question with DSC/TG experiments. The thermolysis of **17PPh$_3$Br**/**17PPh$_3$Cl** (Scheme 37) was found to be endothermic with a ΔH of 70kJmol^{-1} for both

derivatives. This is surprising, as the kinetics of the ethylene rotation in **17PPh$_3$Br**/**17PPh$_3$Cl** suggests a different binding situation for both derivatives.

Scheme 37: Thermolysis of **17PPh$_3$Br**/**17PPh$_3$Cl** to halide bridged products.

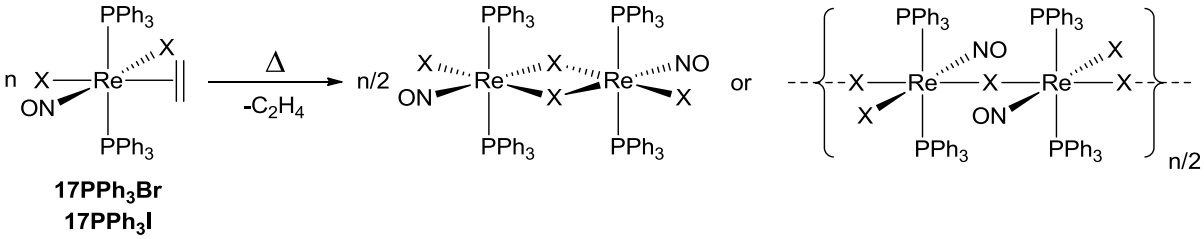

17PPh$_3$Br
17PPh$_3$I

However, the observed ΔH is plausible although it is somewhat lower than the $\Delta H^{\ddagger}$ of the ethylene rotation of **17PPh$_3$Cl**. This can be explained with the short-lived unsaturated intermediate occurring during the ethylene rotation, which is not stabilized by bridging chlorides or solvent molecules. In contrast to that the thermolysis product is expected to be stabilized by di-/oligomerization. Moreover we can conclude that the ethylene binds strongly to the rhenium center. In fact exchange experiments showed that it binds even stronger than the H_2 ligand, which indeed is expected to bind strongly to such electron rich rhenium centers.

4. Approaching the monohydride mechanism - the [ReHX(η^2-C_2H_4)(NO)(PR_3)$_2$] systems

To complete the series of rhenium ethylene complexes, we approached the preparation of hydride compounds of the form [ReHX(η^2-C_2H_4)(NO)(PPh_3)$_2$] (**18PPh$_3$Cl**, **18PPh$_3$Br** and **18PPh$_3$I**). These monohydride compounds caught our interest, because of two reasons. First of all, the olefin monohydride complexes are closely related to the dihydride species in chapter 2. The main difference between them is the fact that the monohydrides could only enter the Re(+I)/Re(+III) cycle (Scheme 30). Therefore the investigation of the monohydride compounds in catalytic hydrogenation reactions is promising - in particular in comparison to the dihydride compounds **24PPh$_3$/33PPh$_3$**. The second, interesting aspect is the comparison of the ethylene binding in the dihalide complexes of type **17**, the halide-hydride complexes of type **18** and the dihydride complexes of type **24**.

4.1 Preparation of [ReHX(η^2-C_2H_4)(NO)(PR_3)$_2$] (X=Br, Cl, I) complexes

In order to prepare [ReHX(η^2-C_2H_4)(NO)(PR_3)$_2$] (X=Br, Cl, I) complexes, two straight forward strategies might be followed. The first one starts from the readily accessible dihydride compound **21PPh$_3$** (Scheme 38). Substitution of one hydride with a halide leads to complexes of the form [ReHX(NO)(PPh_3)$_3$]. The replacement of PPh_3 with ethylene, would finally lead to the desired **18PPh$_3$** compounds. Nevertheless the selective exchange of a hydride with a halide by directly applying HX (X = Cl, Br, I) turned out to be difficult.

Scheme 38: The dihydride approach to compounds of type **18**.

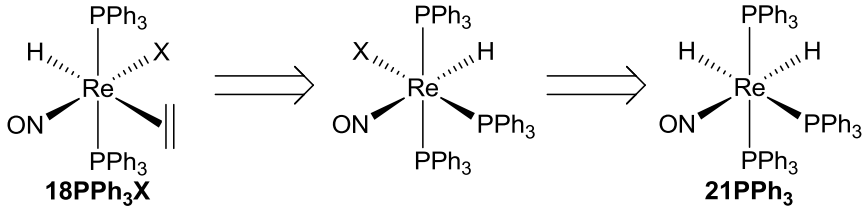

Hence the second strategy, which starts from the dihalide complexes **36PPh$_3$Br**, **36PPh$_3$I** and **37PPh3**, was pursued (Scheme 39). Since strong hydride sources, such as $NaBH_4$ are known to convert the related acetonitrile complexes of type **35** to the corresponding η^2-BH_4 complexes of type **23**[67], a mild hydride source is necessary to substitute selectively one halide with a hydride. Because $HSiEt_3$ is known to react with the dihydrogen complexes **14PCy$_3$** and **14P*i*Pr$_3$** exclusively to the monohydride complexes **15PCy$_3$** and **15P*i*Pr$_3$**, $HSiEt_3$ was considered a suitable reagent[68]. Therefore **36PPh$_3$Br**, **36PPh$_3$I** and **37PPh$_3$** were reacted in suspensions of toluene and $HSiEt_3$ in the presence of ethylene at 80°C resulting in the formation of the expected products in high yields (Cl, 81%; Br 70%; I, 64%). In

Scheme 39 a mechanism for the formation of **18PPh$_3$Cl**, **18PPh$_3$Br** and **18PPh$_3$I** is proposed. It starts with the loss of a ligand from **36PPh$_3$Br**, **36PPh$_3$I** and **37PPh3** to form the unsaturated intermediate [ReX$_2$(NO)(PPh$_3$)$_2$] complexes **38PPh$_3$Cl**, **38PPh$_3$Br** and **38PPh$_3$I** which add HSiEt$_3$ to form the intermediate hepta-coordinated [ReX$_2$H(SiEt$_3$)(NO)(PPh$_3$)$_2$] complexes **39PPh$_3$Cl**, **39PPh$_3$Br** and **39PPh$_3$I**. These complexes eliminate either HSiEt$_3$ in the back reactions or XSiEt$_3$ to form the [ReHX(NO)(PPh$_3$)$_2$] species **15PPh$_3$Cl**, **15PPh$_3$Br** and **15PPh$_3$I**.

Scheme 39: Proposed mechanism for the formation of type **18** compounds.

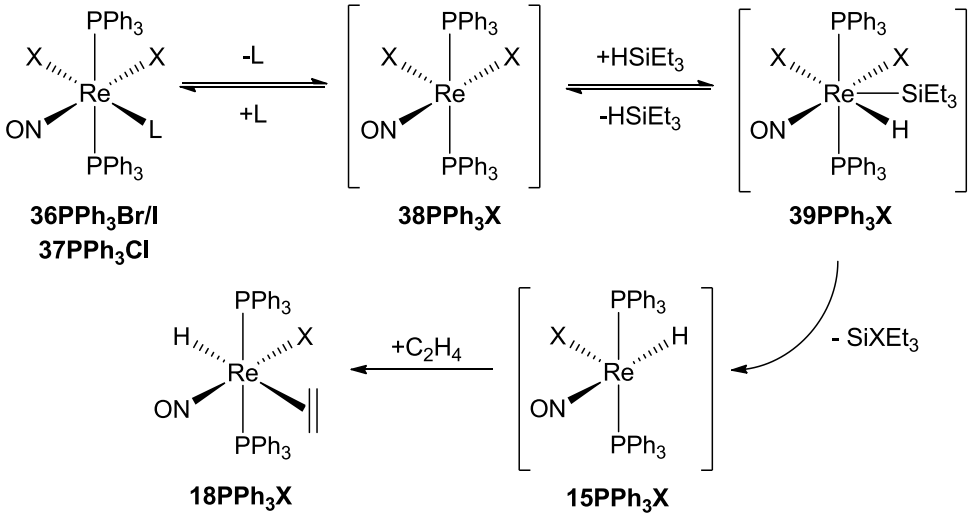

In the latter step XSiEt$_3$ is formed, which is supposed to be the thermodynamic driving force of the reaction, since the H-SiEt$_3$ bond is thermodynamically much less stable than the X-SiEt$_3$ bond. The resultant 16e- hydride complexes are known to be isolable in case of the PCy$_3$ and P*i*Pr$_3$ derivatives **15PCy$_3$Br** and **15P*i*Pr$_3$Br**. However under the applied conditions the 16e- complexes **15PPh$_3$Cl**, **15PPh$_3$Br** and **15PPh$_3$I** are intermediates, which bind ethylene to form the desired **18PPh$_3$Cl**, **18PPh$_3$Br** and **18PPh$_3$I**. In contrast to the thermodynamically unstable diiodide compound **17PPh$_3$I** the iodide hydride ethylene complex **18PPh$_3$I** is stable and can be isolated the same way as the Br and Cl derivatives.

The spectroscopic features of the compounds **18PPh$_3$Cl**, **18PPh$_3$Br** and **18PPh$_3$I** are very similar. In the ^{1}H NMR spectrum they show the expected signals of the PPh$_3$ ligand in the aromatic chemical shift region. The ethylene ligands give rise to sets of multiplets (**18PPh$_3$Cl**: 2.660 ppm (m, 2 H), 1.816 ppm (m, 2 H); **18PPh$_3$Br**: 2.729 ppm (m, 2 H), 1.888 ppm (m, 2 H); **18PPh$_3$I**: 2.782 ppm (m, 2 H), 2.035 ppm (m, 2 H)). The hydride ligands cause sharp resonances at 4.932 ppm (t, $^2J_{PH}$ = 31.0 Hz, **18PPh$_3$Cl**), at 4.485 ppm (t, $^2J_{PH}$ = 22.2 Hz, **18PPh$_3$Br**) and at 3.744 ppm (t, $^2J_{PH}$ = 29.8 Hz, **18PPh$_3$I**). The ^{1}H NMR spectrum did not provide any evidence for dynamic behavior. In the ^{31}P{^{1}H} NMR spectrum sharp signals were observed at 16.6 ppm (**18PPh$_3$Cl**), at 11.4 ppm (**18PPh$_3$Br**) and 5.0 ppm (**18PPh$_3$I**),

which indicated the presence of chemically equivalent PPh_3 groups. In the IR spectrum sets of characteristic bands are assigned to ν(ReH) and to ν(NO). The ν(ReH) increases in the order **18PPh$_3$Cl** (1905 cm^{-1}) < **18PPh$_3$Br** (1906cm^{-1}) < **18PPh$_3$I** (1912 cm^{-1}) while the ν(NO) bands decrease in wave numbers in the order **18PPh$_3$Cl** (1683 cm^{-1}) > **18PPh$_3$Br** (1682 cm^{-1}) > **18PPh$_3$I** (1676 cm^{-1}). In contrast to the dihalide complexes of type **17** or the dihydride complexes of type **24**, totally three types of constitutional isomers of **18PPh$_3$** bearing *trans*-arranged phosphines can be envisaged (Scheme 40).

Scheme 40: The three constitutional isomers of **18PPh$_3$Cl**, **18PPh$_3$Br** and **18PPh$_3$I** with trans phosphines.

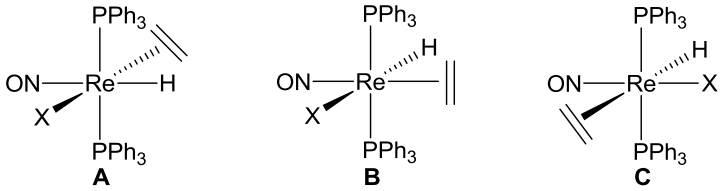

As in case of **17PPh$_3$Cl** and **17PPh$_3$Br** the *trans*-influence of the ligands can be used to estimate the thermodynamically most favorable isomer. In this case the *trans* influence declines in the row NO > C_2H_4 > H > Br[75]. Therefore **C** is most likely the thermodynamically favored structure. This interpretation is also in agreement with the known structure of the analogous styrene complex [ReHBr(η^2-styrene)(NO)(P*i*Pr$_3$)$_2$][68] and the DFT study presented in Scheme 42.

4.2 Properties of [ReHX(η^2-C_2H_4)(NO)(PR$_3$)$_2$] (X=Cl, Br, I) complexes

The complexes **18PPh$_3$Cl**, **18PPh$_3$Br** and **18PPh$_3$I** were employed in catalytic hydrogenation experiments. Although the hydride and an olefin ligands of these complexes would formally permit a monohydride mechanism (Scheme 24), no noteworthy hydrogenation activity was observed. We therefore concluded that the spatial arrangement of the ligands in **18PPh$_3$Cl**, **18PPh$_3$Br** and **18PPh$_3$I** is unfavorable. This is not surprising, since the hydride and the olefin ligands are in *trans* position in the proposed structures of these compounds. Therefore the initiation of the catalytic cycle requires first a rearrangement of the ligand sphere. This could proceed analogously to the rearrangement course proposed for compound **37PPh$_3$** in Scheme 34 and must involve an initial ligand dissociation step followed by complex rearrangement of the ligand sphere. Furthermore, this rearrangement is then followed by the migration of the hydride to the olefin ligand, before H_2 can be oxidatively added to the alkyl intermediate. Obviously one or both of these initial steps are energetically unfavored. Therefore the tuning of the **24PPh$_3$**/**33PPh$_3$** system to a catalytic monohydride system failed.

As mentioned above, none of the ^{1}H NMR spectra of **18PPh$_3$Cl**, **18PPh$_3$Br** and **18PPh$_3$I** showed any signs of exchange. Furthermore even the iodide derivative **18PPh$_3$I** was stable and could be isolated. This contrasts the binding of the ethylene ligand in the dihalide complexes **17PPh$_3$Cl** and **17PPh$_3$Br**,

where dynamics were observable in the ^{1}H NMR spectra. In order to compare the rhenium ethylene bond in **18PPh$_3$Cl**, **18PPh$_3$Br** and **18PPh$_3$I** we attempted DSC-TG experiments with these compounds. However **18PPh$_3$Cl**, **18PPh$_3$Br** and **18PPh$_3$I** did not release ethylene like the dihalide compounds **17PPh$_3$Cl** and **17PPh$_3$Br,** but decomposed completely. Therefore it might be concluded that the rhenium ethylene bond is much more stable in the hydride complexes of type **18** than in the dihalide complexes **17PPh$_3$Cl** and **17PPh$_3$Br**. The increased stability of these complexes is attributed to an increased level of back bonding to the ethylene ligand. This is caused by the increased electron density on the metal center originating from the hydride ligand. This is also reflected in the positions of the ν(NO) bands observed for the respective olefin complexes (Table 3).

Table 3: ν(NO) and ν(NO)from selected rhenium ethylene complexes:

Compound	ν(NO) [cm^{-1}]	ν(ReH) [cm^{-1}]	Compound	ν(NO) [cm^{-1}]	ν(ReH) [cm^{-1}]
24PPh$_3$/33PPh$_3$	1630	1959, 1897, 1815	**18PCy$_3$Br**[68]	1668	2089
24P*i*Pr$_3$[67]	1619	1843	**18P*i*Pr$_3$Br**[68]	1665	2024
24PCy$_3$[67]	1614	1858	**17PPh$_3$Cl**	1699	
18PPh$_3$Cl	1683	1905	**17PPh$_3$Br**	1704	
18PPh$_3$Br	1682	1906	**17PCy$_3$Br**	1696	
18PPh$_3$I	1676	1912	**17P*i*Pr$_3$Br**	1693	

Table 3 shows clearly that the ν(NO) vibrations of the [Re(X$_2$(η^2-C$_2$H$_4$)(NO)(PR$_3$)$_2$] complexes depend strongly on the nature of the X-ligand. Exchanging a halide with a hydride is connected with shifts of the ν(NO) bands in the range of 20-40 cm^{-1}. The kind of halide ligand has not such a large influence (5-6 cm^{-1}). In contrast, the donor capabilities of the phosphines have a larger influence with shifts up to 14 cm^{-1}. However, it should be mentioned that the electronic tuning potential could be exploited further. The list of employed phosphines encompasses merely PPh$_3$, PCy$_3$ and P*i*Pr$_3$, of which PCy$_3$ and P*i*Pr$_3$ have very similar donor capabilities. The same is true for the X-ligands. So far, no attempts have been undertaken to substitute the halides with other one electron donors, such as alkoxides or pseudo-halides. But as it became obvious in case of the type **24** compounds, electronic tuning of the phosphines can change the reactivity significantly. The same was observed for the dihalide compounds of type **17** where the stability and the dynamics of the compounds depend not only on the phosphines, but also on the halides. Therefore this section can be finished with the conclusion that the limits of the hydride as well as the dihydride systems for catalytic hydrogenations are still not fully explored and that these systems might be further optimized by directed tuning of the ligand sphere.

5. Optimizing the coordination geometry - the bisphosphine complexes [ReBrX(L)(NO)(P∩P)]

Chapter 5 is based on a manuscript for a publication. It has to be mentioned that the experimental work on the Sixantphos complexes presented in this chapter was conducted by Rajesh Kunjanpillai with my support as a kind of introduction into this field of research and the laboratory. The results originating from this work are included in this chapter, since they contribute to the overall understanding of the [ReBrX(L)(NO)(P∩P)] system.

As already mentioned in the previous sections, electronic tuning is expected to be a key to improve the catalytic performance of the $[ReH_2(olefin)(NO)(PR_3)_2]$ systems. Furthermore, we assume some potential for improvement for the hydrides of the form $[ReHX(olefin)(NO)(PR_3)_2]$ by the appropriate tuning of the X and PR_3 ligands as well. However, we expected the highest potential for optimization of the Re-NO based hydrogenation catalysts in changing of the coordination pattern. To rationalize this approach the factors governing the structure and reactivity of type **18** compounds should be analyzed with special stress on the influence of the stereochemistry.

5.1 Effects determining the structure of $[ReHX(\eta^2\text{-}C_2H_4)(NO)(PR_3)_2]$ compounds and their effect on hydrogenation catalysis

In the sections 3.1 and 4.1 we reasoned on the structures of type **17** and **18** compounds. We argued with the help of the *trans*-influence and the closely related "push-pull" concept for *trans*-arranged π-donors and π-acceptors (As mentioned in 2.1 the term "push-pull" effect is not referred to an intra-molecular charge-transfer process, but rather to the polarization of the d-electrons towards a π-acceptor). Employing these concepts we proposed the thermodynamically favored constitutional isomer should possess the structure of the model compound **18PMe$_3$Br** (Scheme 42), which is also in agreement with the structure found for the related styrene complex $[ReHBr(\eta^2\text{-styrene})(NO)(P\textit{i}Pr_3)_2]$[68]. Furthermore we assumed that the C=C vector of the ethylene ligand is parallel to the P-Re-P axis, because the phosphines are believed to polarize the d-electrons involved in the backbonding of the ethylene in a favorable way similar to the described "push-pull" effect (The interested reader is referred to lit. 72 for an in-depth discussion of this effect). Indeed in all reported X-ray structures of compounds bearing a $Re(olefin)(NO)(PR_3)_2$ fragment the olefin is coordinated with the C=C axis collinear to the P-Re-P axis ($[ReHBr(\eta^2\text{-styrene})(NO)(P\textit{i}Pr_3)_2]$[68], $[ReH(BF_4)(\eta^2\text{-}C_2H_4)(NO)(PCy_3)_2]$[67] and $[ReCl_2(\eta^2\text{-}C_2H_4)(NO)(PR_3)_2]$ (R=Cy, *i*Pr)[83]). Moreover the rotational barriers,

[83] Choualeb, A.; Blacque, O.; Schmalle, H. W.; Hiltebrand, T.; Berke H. CCDC 297766, CCDC 297767

which result from this effect were found to amount up to 90 kJmol^{-1} (**17PPh$_3$Cl)** and are expected to be higher for the monohydride compounds of type **18.**

Summing up all these effects results in the stabilization of the NO-Re-Br and the P-Re-P axis, as well as in stabilization of the collinear orientation of the C=C vector of the ethylene ligand and the P-Re-P axis. With respect to the application in hydrogenation catalysis, this has far reaching consequences for the initiation of the catalytic cycle (Scheme 41).

Scheme 41: Initiation of the catalytic cycle with type **18** catalysts.

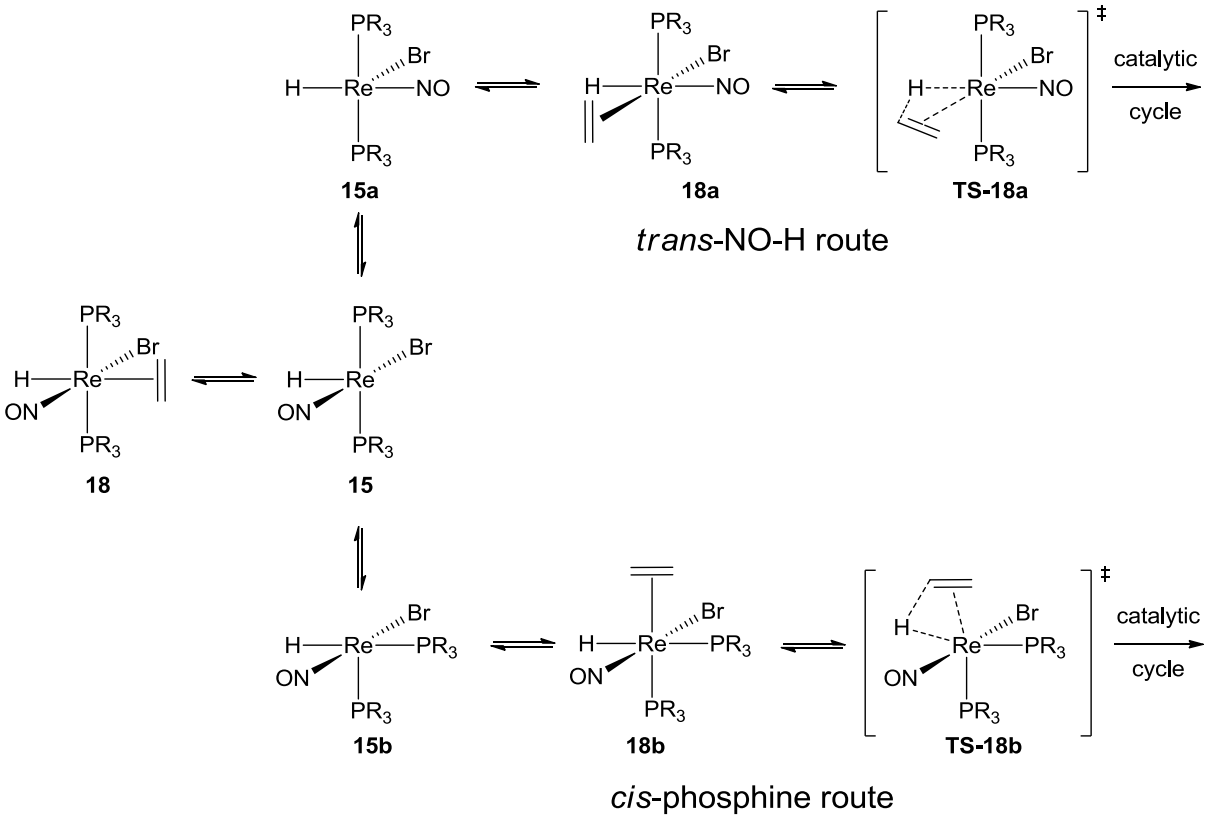

Since any common hydrogenation mechanism in the catalytic hydrogenation of olefins requires an olefin-*cis*-H arrangement, either the Br-Re-NO axis or the P-Re-P axis of type **18** compounds have to be broken, to initiate the catalysis via a monohydride mechanism (Scheme 41). The NO-Re-Br axis can principally be broken either by going to a NO-*trans*-H or a NO-*trans*-olefin arrangement to obtain the desired H-*cis*-olefin arrangement. However the NO-*trans*-olefin arrangement is not considered, because these ligands are both strong π-acceptors, which would compete in this arrangement for the same d-electrons. Moreover NO and olefins have a stronger *trans*-effect than the H and the Br ligand. Therefore only the NO-*trans*-H and the *cis*-phosphine route were considered in Scheme 41. Following either the *cis*-phosphine or the NO-*trans*-H route, the first step would be the dissociation of the ethylene ligand, which is according to DFT calculations (Scheme 42) the weakest bound ligand in the **18PMe$_3$Br** model system. The resulting five coordinate 16e- complex of type **15** undergoes a

rearrangement of the ligand sphere to form either the NO-*trans*-H complex **15a** or the *cis*-phosphine complex **15b**. Subsequently **15a** and **15b** re-coordinate the ethylene ligand in *cis*-position to the hydride ligand forming compounds of type **18a** and **18b**. These compounds can now be feed into the catalytic hydrogenation cycle according to Scheme 24. However, it has to be noted that the initial β-hydride shift over **TS-18a** is hindered, because the ethylene C=C axis is collinear to the P-Re-P axis. Thus **TS-18a** is expected to be energetically less accessible than **TS-18b**, for which no such rotational barrier is expected due to favorable orientation of all ligands. Since the above made considerations are of qualitative nature, the relative energy differences of the representative PMe_3 model compounds **16PMe$_3$Br**, **18PPMe$_3$Br**, **18PaPMe$_3$Br** and **18bPMe$_3$Br** were calculated employing the same DFT methodology as Liu et al. used[70] to elucidate the mechanism of the $[ReH_2(olefin)(NO)(PR_3)_2]$ catalysts.

Scheme 42: Comparison of the PMe_3 model compounds **16PMe$_3$Br**, **18PPMe$_3$Br**, **18PaPMe$_3$Br** and **18bPMe$_3$Br**

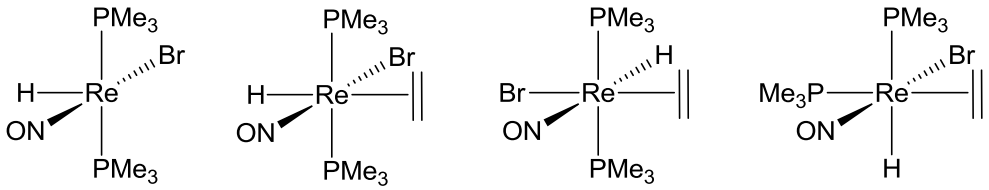

16PMe$_3$Br +70 kJmol^{-1} | **18PMe$_3$Br** 0 kJmol^{-1} | **18aPMe$_3$Br** +58 kJmol^{-1} | **18bPMe$_3$Br** +27 kJmol^{-1}

These calculations revealed that **18PMe$_3$Br** is the thermodynamically most favored constitutional isomer. This is in accordance with our qualitative assessment of the isomers. Nevertheless **18a** (+58 kJmol^{-1}) and **18b** (+27 kJmol^{-1}) would still be accessible under mild conditions, if a kinetically suitable pathway would allow the isomerization of these three constitutional isomers. But since at least in the case of the compounds **18PPh$_3$Cl**, **18PPh$_3$Br** and **18PPh$_3$I** no significant catalytic hydrogenation activity could be observed, we conclude that the formation of the reactive intermediates of type **18a** and **18b** is not taking place. This lack of catalytic activity originates probably in the high calculated ethylene affinity of **16PMe$_3$Br**, which might retard the formation of the reactive isomers (Scheme 41). An alternative isomerization mechanism leading to the **18aPMe$_3$** or **18bPMe$_3$** via a heptagonal pyramid or trigonal prism is unlikely because of the ligands steric demands.

Therefore the most promising approach to permit a monohydride hydrogenation mechanism with a compound of the $[ReHX(\eta^2\text{-}C_2H_4)(NO)(PR_3)_2]$ family is the direct synthesis of type **18a** or **18b** complexes. In case of type **18a** compounds this can only be achieved by electronic tuning of the X ligand and therefore the synthesis of new type **18a** complexes is difficult to plan. However the

synthesis of **18b** complexes can be achieved straight forward by simply using appropriate chelating bisphosphine. Therefore we approached the synthesis of [ReBrX(L)(NO)(P∩P)] compounds bearing a diphosphine ligand, which forces the formation of a type **18b** complex.

5.2 Preparation of [ReBrX(L)(NO)(P∩P)] complexes

Bidentate diphosphine ligands are characterized in electronic terms by their donicity[84] and in size by their bulk[85] including their bite angle[86]. The preferred bite angle of a certain diphosphine becomes obvious in the statistical analysis of X-ray diffraction study data. The histograms in Figure 9 illustrate that the range of the bite angle, which can be adopted by a diphosphine can be quite narrow.

Figure 9: Statistical analysis of the bite angle of bidentate phosphine with different backbones (CCSD data from 1.1.2009)

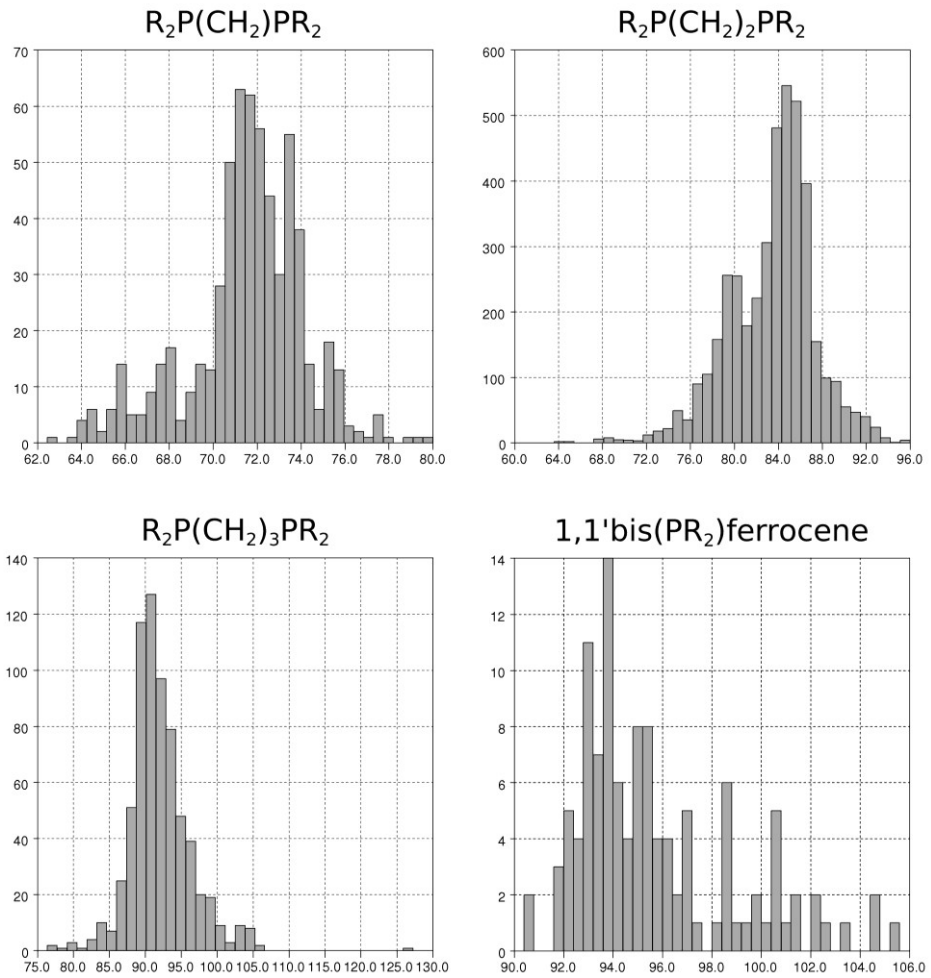

[84] Tolman, C. A. Electron Donor-Acceptor Properties of Phosphorus Ligands - Substituent Additivity. *J. Am. Chem. Soc.* **1970**, *92,* 2953-2956.
[85] Tolman, C. A. Steric Effects of Phosphorus Ligands in Organometallic Chemistry and Homogeneous Catalysis. *Chem. Rev.* **1977**, *77*, 313–348.
[86] Casey, C. P.; Whiteker, G. T. The Natural Bite Angle of Chelating Diphosphines. *Isr. J. Chem.* **1990,** *30,* 299–304.

Hence it turned that for proper catalytic performance the chelate diphosphines require an exact fit of their stereoelectronic properties to those of the metal fragment[87,88]. Preliminary DFT calculations on the stereochemically "relaxed" $[ReBr_2(MeCN)(NO)(PMe_3)_2]$ model suggested a phosphine angle of 97° to be optimal for strong binding. Translating this finding into a bite angle of a diphosphine we approached the initial preparation of "large bite angle" $[ReBr_2(MeCN)(NO)(P\cap P)]$ complexes bearing the chelates P∩P = 1,1'-bis(diphenylphosphino)ferrocene (dppfc) and bis(diisopropylphosphino)-ferrocene (diprpfc), which perfectly match the calculated 97° of the model. We approached the synthesis of the $[ReBr_2(MeCN)(NO)(P\cap P)]$ complexes via ligand substitution reactions starting from the $[Re(+I)Br_2(MeCN)_3(NO)]$ and $[Re(+II)Br_5(NO)][NEt_4]_2$ complexes (Scheme 43).

Scheme 43: Synthetic access to $[ReBr_2(MeCN)(NO)(R_2P\cap PR_2)]$ complexes.

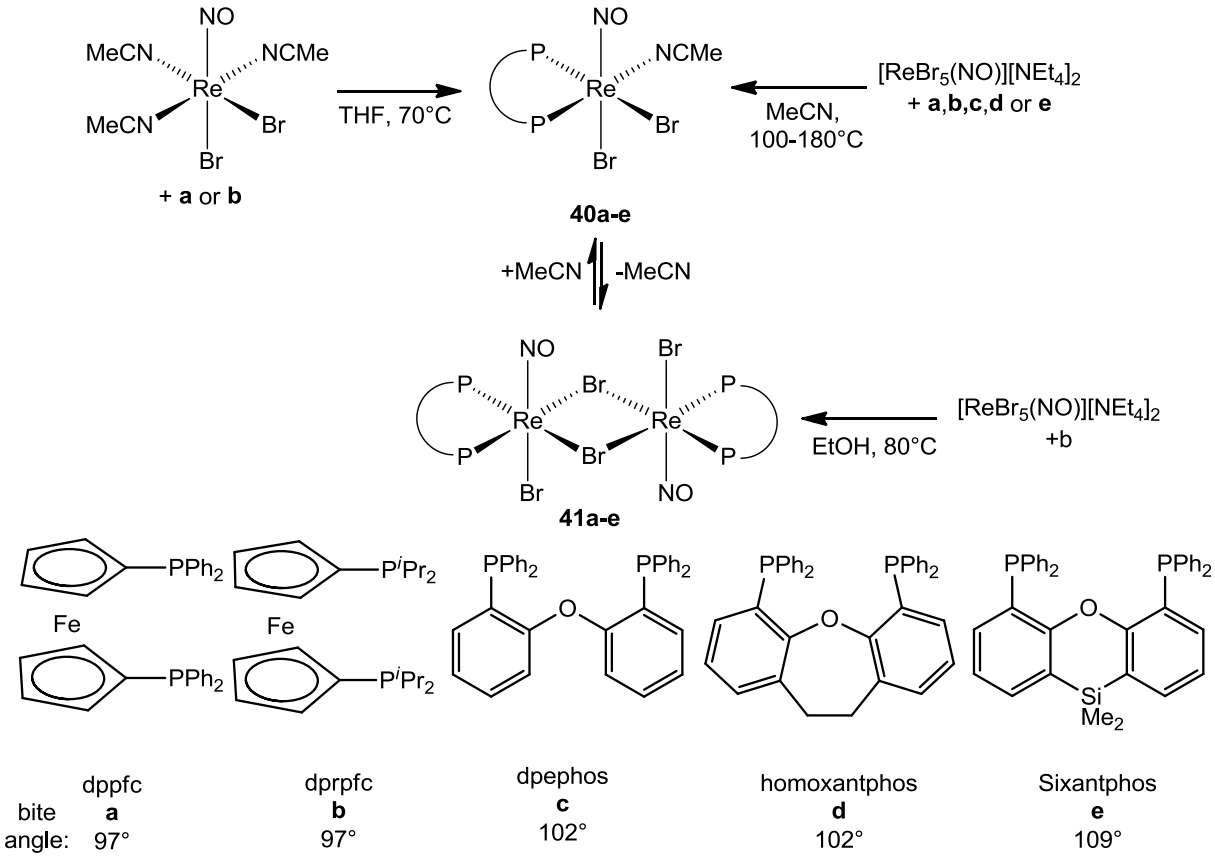

In contrast to the known substitution reactions with monodentate phosphine ligands[67], only low yields were obtained in the substitution processes of $[ReBr_2(MeCN)_3(NO)]$ with the ferrocenyl

[87] Saito, T.; Yokozawa, T.; Ishizaki, T.; Moroi T.; Sayo, N.; Miura, T.; Kumobayashi, H. New Chiral Diphosphine Ligands Designed to have a Narrow Dihedral Angle in the Biaryl Backbone. *Adv. Synt. Catal.* **2001**, *343,* 264–267.

[88] Kranenburg, M.; van der Burgt, Y. E. M.; Kamer, P. C. J.; van Leeuwen, P. W. N. M.; Goubitz, K.; Fraanje, J. New Diphosphine Ligands Based on Heterocyclic Aromatics Inducing Very High Regioselectivity in Rhodium-Catalyzed Hydroformylation: Effect of the Bite Angle. *Organometallics* **1995,** *14,* 3081–3089. van der Veen, L. A.; Keeven, P. H.; Schoemaker, G. C.; Reek, J. N. H.; Kamer, P. C. J.; van Leeuwen, P. W. N. M.; Lutz, M.; Spek, A. L. Origin of the Bite Angle Effect on Rhodium Diphosphine Catalyzed Hydroformylation. *Organometallics* **2000,** *19,* 872–883.

diphosphines yielding [$ReBr_2$(MeCN)(NO)(dppfc)] (**40a**) (60%) and [$ReBr_2$(MeCN)(NO)(diprpfc)] (**40b**) (31%). Following the synthetic route to the [$ReBr_2(\eta^2\text{-}H_2)(NO)(PR_3)_2$] (R = *i*pr, cy) complexes[66] we then attempted the reaction of an excess of the diphosphines with [$ReBr_5$(NO)][NEt_4]$_2$ in ethanol at 80-85°C. In case of the diprpfc ligand the reduction process of the Re(+II) species led to the bromide bridged dinuclear compound [(ReBr(μ^2-Br)(NO)(diprpfc))$_2$] (**41b**) in 78% yield. The dinuclear nature of **41b** was verified by an X-ray diffraction study. Stirring **41b** at room temperature in DCM/MeCN resulted in the splitting of the bromide bridges and quantitative formation of the acetonitrile complex **40b**. The reaction of [$ReBr_5$(NO)][NEt_4]$_2$ with excess of dppfc in a 7:3 mixture of MeCN and THF furnished **40a** in 74% yield. In these reactions the diphosphines dppfc and diprpfc functioned as ligands, as well as reducing agents (producing presumably brominated P(+V) compounds of the type [PR_3Br]Br or [PR_3Br_2][89]). This facile access to **40a** and **40b** prompted us to attempt the preparation of other related complexes with large bite angle diphosphines in the same way as for **40a,b** (Scheme 43).To increase the bite angle of the bidentate phosphine, while keeping the donicity of the ligand approximately constant, we selected dpephos, homoxantphos and Sixantphos from the van Leeuwen's large bite angle 2,2'-bis(diphenylphosphino)phenylethers ligand series[88] (Scheme 43).Unlike the ferrocene based ligands, dpephos, homoxantphos and Sixantphos were found to withstand temperatures of 180-200°C. In this range of temperatures the ligands **c-e**, as well as the [$ReBr_5$(NO)][NEt_4]$_2$ salt became soluble in acetonitrile and the combined redox and substitution reactions analogous to **40a** and **40b** went to completion within 3 h to 5 h to yield the desired Re(+I) substitution products [$ReBr_2$(MeCN)(NO)(dpephos)] (**40c**, 88%), [$ReBr_2$(MeCN)(NO)(homoxantphos)] (**40d**, 72%) and [$ReBr_2$(MeCN)(NO)(Sixantphos)] (**40e**, 56%).

For octahedral complexes bearing a rigid bidentate ligand various constitutional and conformational isomers are expected to exist[90]. But since the *trans* arrangement of the NO and one Br ligand is favored due to a strong "push pull" interaction, the *cis*-arrangement of the diphosphines to this axis is the natural consequence. Furthermore the bromide and acetonitrile ligands have to be *trans* to the diphosphine. Therefore only one constitutional isomer of **40a-e** with a chiral rhenium center is expected to exist. However, since the backbone of the diphosphine ligand can adopt either an "**up**", "**down**" or "**twisted**" conformation, this could result in up to four diastereomers as depicted Scheme 44. **Up**, **down** and **twisted** refer to the relative positions of the ligand backbone with respect to the NO ligand. In Figure 10 and Figure 11 the ORTEP diagrams of **40a** and **42f** present examples for **twisted** conformers while in Figure 13 and Figure 14 the ORTEP diagrams of **44d(up/down)** and

[89] Godfrey, S. M.; McAuliffe, C. A.; Mushtaq, I; Pritchard, R. G.; Sheffield, J. M. The structure of R_3PBr_2 compounds in the solid state and in solution; geometrical dependence on R, the crystal structures of tetrahedral ionic Et_3PBr_2 and molecular trigonal bipyramidal (C_6F_5)PBr_2. *J. Chem. Soc., Dalton Trans.* **1998**, 3815-3818.

[90] Zelewsky, A. von. *Stereochemistry of coordination compounds.* Inorganic chemistry; Wiley: Chichester u.a., 1995.

48e(up/down) present typical examples of complexes with the ligand backbone in either **up** or **down** conformation.

Figure 10: ORTEP diagram of **40a** drawn at 50% probability. THF molecule omitted.

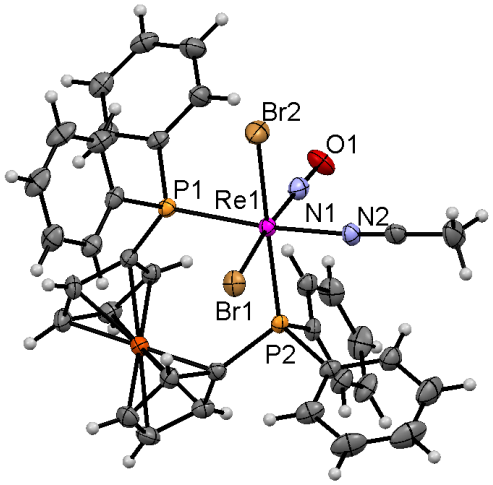

Selected bond lengths [Å]: Re1-Br1 2.576, Re1-Br2 2.604, Re1-N1 1.777, Re1-N2 2.122, Re1- P1 2.437, Re1-P2 2.417, N1-O1 1.146. Selected bond angels [°]: P1-Re-P1 98.9, Br2-Re1-P2 169.8, N2-Re-P1 170.1, Br1-Re1-N1 173.5, O1-N1-Re1 176.1.

The complexes **40a, 41b, 40c** and **40e** were characterized by X-ray diffraction studies. In the case of **40a** the **twisted** diastereomer was found, while in the cases of **40c** and **40e** as well as in the case of the dinuclear complex **41b** the **up** (**40c**: 10%, **40e**: 14%, **41b** 8%) as well as **down** (**40c**: 90%, **40e**: 86%, **41b**: 92%) conformers were found. The analysis of the structure revealed that in general the **down** conformation is more favorable due to steric reasons, as otherwise (in the **up** conformation) the Br ligand would get closer Van der Waals contact with the diphosphine substituents.

Scheme 44: Isomerism in [ReXYBr(NO)(P∩P)] complexes.

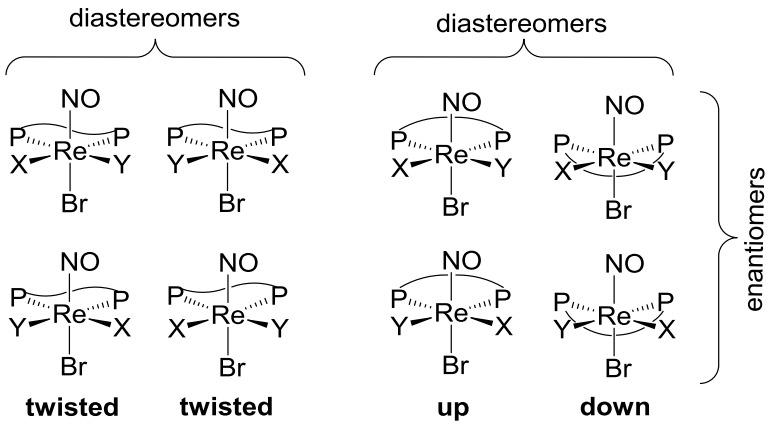

Furthermore the X-ray studies revealed that despite the fact that dppfc (97°), dpephos (102°) and Sixantphos (109°) possess different natural bite angles[88,86], in **40a** (98°), **40c** (100°) and **40e** (98°) the P-Re-P angles were found to be almost equal. This reveals on the one hand a high degree of conformational flexibility for the diphosphine backbones and on the other hand this reveals the

action of a strong driving force, which results from the optimization of the orbital overlap between the rhenium center and the diphosphine. Thus it appears that the optimization of the orbital overlap outweighs the deformation of the ligands backbone. Since the observed bite angle of the Sixantphos ligand in derivative **40e** is ca. 10° smaller than its natural bite angle, **40e** is believed to be considerably less stable than **40a** with respect e.g. to chelate opening. To a smaller extent this consideration would hold also for the dpephos derivative **40c** and the homoxantphos derivative **40d**. The ^{31}P-NMR spectra of compounds **40a-c** consist of sets of two broad resonances in 1:1 an integration ratio, for which no coupling patterns were resolved. The broadness is explained by assuming the exchange of the inequivalent sides of the diphosphine ligand via formation of μ^2-bromo bridged intermediates (**41a-e**). These intermediates are assumed to be symmetrical as **41b** and therefore the μ^2-Br bridges are cleaved randomly (Scheme 45). The two ways of splitting lead to both enantiomers of **40a-c** with virtual exchange of the diphosphine sides and racemization. The rates of these processes are apparently close to the NMR time scale. An additional ^{31}P NMR signal was observed for **40c** and **40e**. As these signals disappeared upon addition of acetonitrile, we propose the existence of the bromide bridged dimers **41d** and **41e** in equilibrium with the acetonitrile complexes (Scheme 43). From these observations we concluded that the μ^2-bromo bridged dinuclear compounds of type **41** are present in solutions of **40a-e** in varying concentrations and that the acetonitrile ligands are in all cases kinetically labile. The "steric pressure" imposed on the acetonitrile ligand by the bulky large bite angle diphosphines might by one reason for this lability.

Scheme 45: Proposed racemization/phosphorus exchange mechanism for **40a-e**.

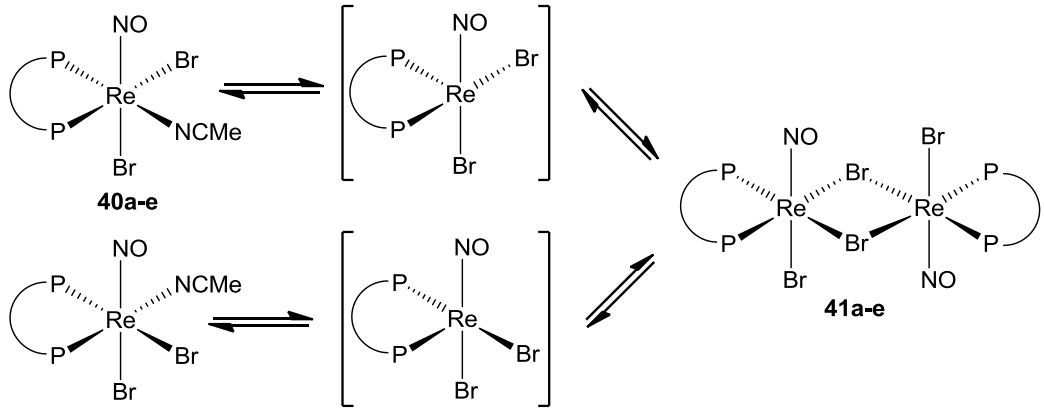

5.3 Preparation of [ReBrH$_2$(SiR$_3$)(NO)(P∩P)] complexes

Based on a well established hydride chemistry of the unstrained *trans* phosphine complexes [ReH(η^2-BH$_4$)(NO)(PR$_3$)$_2$] (R=cy, *i*Pr, p-tolyl)[66] we attempted the transformation of **40a-e** to related rhenium hydrides applying hydride reagents such as [NBu$_4$][BH$_4$], LiAlH$_4$, KH and KH/18-crown-6 in THF. Despite extensive variations of the temperatures and the stoichiometries of the reactants the reaction courses were found to be complex and inseparable mixtures were produced. However using

$HSiEt_3$ as a hydride source to react with **40a-e**, we obtained dihydride silyl complexes **42a-e** (Scheme 46), for which we propose a pentagonal bipyramidal structure with the hydrides, the silyl moiety and the diphosphine in the pentagonal plane in analogy to **42f** (*vide infra,* Figure 11). **42a**, **42c**, **42d** and **42e** were found to be stable in solution only in the presence of an excess of $HSiEt_3$ and could therefore only be characterized by their NMR spectra, which were in the hydride part analogous to that of **42f.**

Scheme 46: Synthesis and reactivity of the mono hydride fragment [ReHBr(NO)(P∩P)].

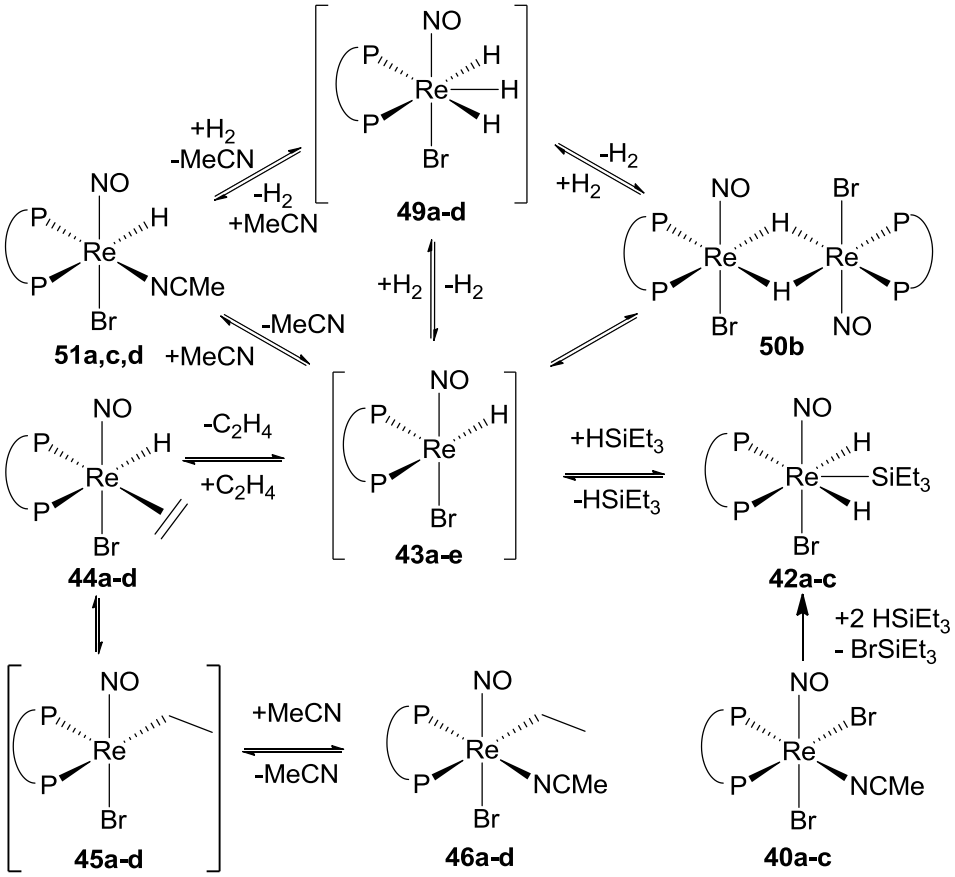

Attempts to isolate **42a**, **42c**, **42d** and **42e** led to the formation of brick red, insoluble and probably polynuclear precipitates. No structure of these solids could be established, but if dinuclear complexes are formed, their structure might be related to the μ^2-H bridged complex **50b** (*vide infra*). In contrast to this, **40b** bearing the more electron donating phosphine ligand diprpfc reacted to a stable seven-coordinate $[ReBr(H)_2(SiEt_3)(NO)(diprpfc)]$ (**42b**) complex. Because of the liquid nature of **42b**, the $SiMe_3$ derivative **42f** was prepared (92% yield) analogously applying $HSiMe_3$. **42f** was structurally characterized by an X-ray diffraction study (Figure 11). To probe the influence of the silicon substituents the $SiCl_3$ analogue **42g** was prepared as well. The formation of **42g** was accompanied by a partial bromide/chloride exchange yielding a mixture of products. Since this mixture could not be separated, NEt_4Cl was added to the reaction solution to achieve a quantitative Cl/Br exchange.

Chromatographic work up yielded pure **42g** (66%). In order to compare the structures of **42g** and **42f** (Figure 11) an X-ray diffraction study on single crystals of **42g** was performed. As expected, the Si-Re distance in **42g** (2.395 Å) is significantly shorter than in **42f** (2.525 Å) due to the increased π-acceptor capability of the $SiCl_3$ moiety. This reflects also in the ν(NO) bands of **42f** (1678 cm^{-1}) and **42f** (1718 cm^{-1}). Therefore we can conclude that the substituent effects on the silicon ligands are comparable to those on the phosphorus ligands[85]. Moreover the significantly shorter Re-Si bond in **42f** indicates drastically increased bond strength of the Re-Si bond for the $SiCl_3$ group which is not desirable for pre-catalysts. Therefore we did not prepare further SiR_3 derivatives of **1a-e**. However such $SiCl_3$ species might be interesting to immobilize organometallic compounds on various oxides such as Al_2O_3 or SiO_2.

Figure 11 : ORTEP diagrams of **42f** and **42g**, ellipsoids drawn at 50% probability. NO-Br disorder omitted in both structures.

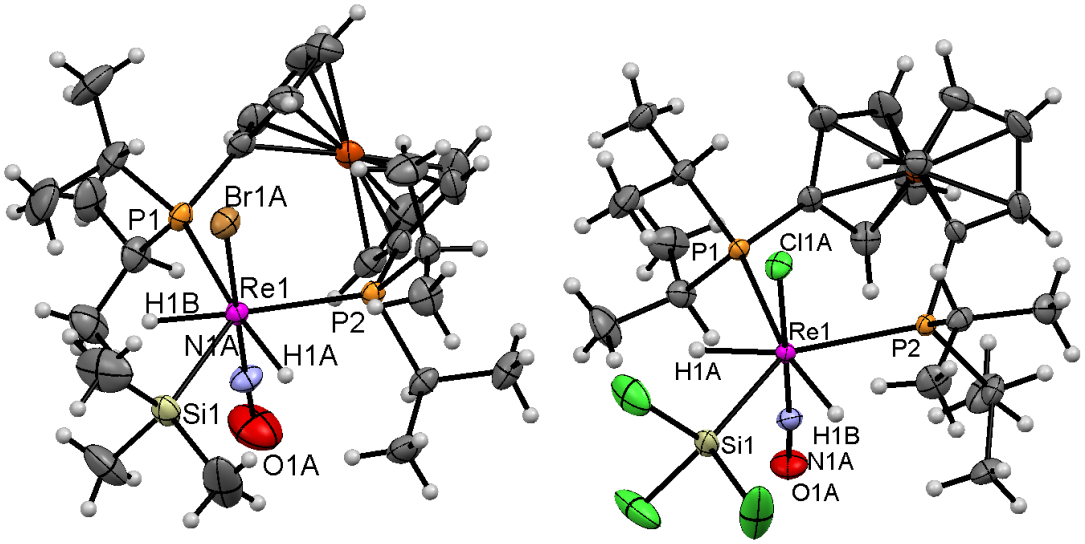

42f: Selected bond lengths [Å]: Br1A-Re1 2.514, H1A-Re1 1.655, H1B-Re1 1.586, N1A-Re1 1.744, N1A-O1A 1.309, P1-Re1 2.527, P2-Re1 2.505, Re1-Si1 2.520. Selected bond angels [°]: Br1A-Re1-N1A 177.3, P1-Re1-P2 102.4, P1-Re1-Si1 131.7, P2-Re1-Si1 125.6, P1-Re1-H1B 69.3, P2-Re1-H1A 73.4, Re1-N1A, O1A 178.5. **42g**: Selected bond lengths [Å]: Cl1-Re1 2.411, H1a-Re1 1.551, H1B-Re1 1.565, N1A-Re1 1.787, O1A-N1A 1.182, P1-Re1 2.543, P2-Re1 2.510, Re1-Si1 2.395. Selected bond angels [°]: Cl1A-Re1-N1A 178.6, H1A-Re1-Si1 57.8, H1B-Re1-Si1 69.1, O1A-N1A-Re1A 176.9, P2-Re1-R1 102.1.

5.4 Preparation of [ReBrH(η^2-C_2H_4)(NO)(P∩P)] complexes

As mentioned before, the hydride complexes **51a-e** turned out to be not accessible via the reaction of any of the employed ionic hydrides. One cause for this was the instability of the intermediately formed 16e- complexes [ReBrH(NO)(P∩P)] **43a-e**, which were suspected to undergo various types of side reactions. Therefore we attempted the bromide/hydride exchanges with $HSiEt_3$ in the presence of ethylene as an additional ancillary ligand. Ethylene was considered an ideal auxiliary to stabilize the 16e- [ReBrH(NO)(P∩P)] species **43a-e**, because of its small size and good binding abilities to electron rich Re(+I) centers[72]. Furthermore in view of the potential application of the ethylene hydride compounds as pre-catalysts, the ethylene ligand was anticipated to be quickly hydrogenated

to ethane gas under catalytic conditions leaving **43a-e** ready to be fed into the catalytic cycle. The reactions of **40a** and **40b** with an excess of $HSiEt_3$ in the presence of 2 bar ethylene proceeded smoothly forming the [ReBrH(η^2-C_2H_4)(NO)(P∩P)] complexes **44a** and **44b**. Monitoring the reaction by ^{31}P NMR showed almost quantitative conversions, but crystallization of **44a** and **44b** from dichloromethane/hexane solutions reduced the isolated yields (**44a:** 70%; **44b** 61%). Based on their spectroscopic properties **44a** and **44b** were assigned pseudo octahedral structures with *trans* Br and NO ligands. Additionally the IR spectra of **44a** and **44b** provided evidence for the presence of the hydride and the NO ligands revealing distinct ν(ReH) and ν(NO) bands. In accordance with the proposed structure the $^{31}P\{^1H\}$ NMR spectra of **44a** and **44b** displayed each a set of two sharp doublets. Hence, in contrast to **40a** and **40b**, **44a** and **44b** are not fluxional on the NMR time scale. However, the ^1H NMR spectrum of **44a** and **44b** showed exchange of the H_{Re} atom with two of the ethylene protons at room temperature. As the signals of the ethylene protons and the Re hydride of **44b** overlap with those of the isopropyl groups, the exchange could not be analyzed in greater detail. For further insight the ^1H NMR spectra of **44a** were recorded in a temperature range from 220 to 300 K in 10 K intervals (Figure 12). At 240 K the signals of the four ethylene protons and the hydride are no longer in exchange.

Figure 12: $^1H\{^{31}P\}$ spectrum of the ethylene hydride region of **44a** (CD_2Cl_2, 500 MHz).

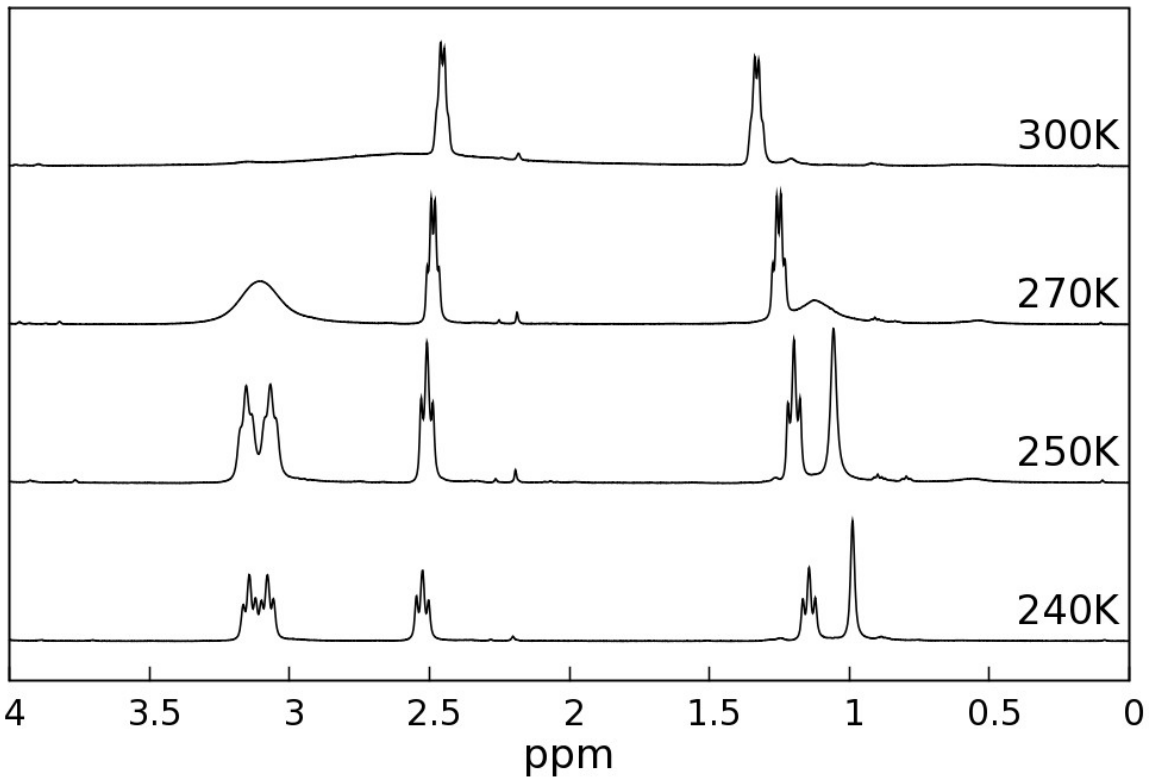

With the aid of an HSQC experiment the different sets of ethylene protons could be attributed to the respective $C_{ethylene}$ nuclei. The two protons at 3.03 and 2.98 ppm, which are involved in the exchange showed correlation with the $C_{ethylene}$ nucleus at 36.7 ppm, while the two other ethylene protons at 2.49 and 1.21 ppm showed correlation with the $C_{ethylene}$ nucleus at 40.0 ppm. This suggests that the rhenium hydride and the ethylene carbons lie in the same plane with one carbon close to the hydride. Warming the NMR sample up caused first broadening of the ethylene protons at 3.03 and 2.98 ppm and the rhenium hydride at 0.88 ppm. At approx. 300 K these signals reached coalescence. The signals of the two other ethylene protons at 2.49 and 1.21 ppm remained sharp and were apparently not affected by the exchange. Modeling the exchange with the help of the gNMR program package allowed extracting the exchange rate at temperatures ranging from 240 to 300 K. The activation parameters were then determined according to the transition state theory[91] amounting to $\Delta H^{\ddagger}$ = 62 kJmol^{-1} and $\Delta S^{\ddagger}$ = 31 Jmol^{-1}K^{-1}. Scheme 47 shows this process, but it also refers to a second process of the ethyl group changing sides. This principally constitutes a racemization process like the rearrangement of the dibromides **41a-e** and results also in a virtual phosphine exchange.

Scheme 47: The mechanisms for the hydride and the phosphine exchange. The phosphine exchange results in the racemization within the NMR time scale.

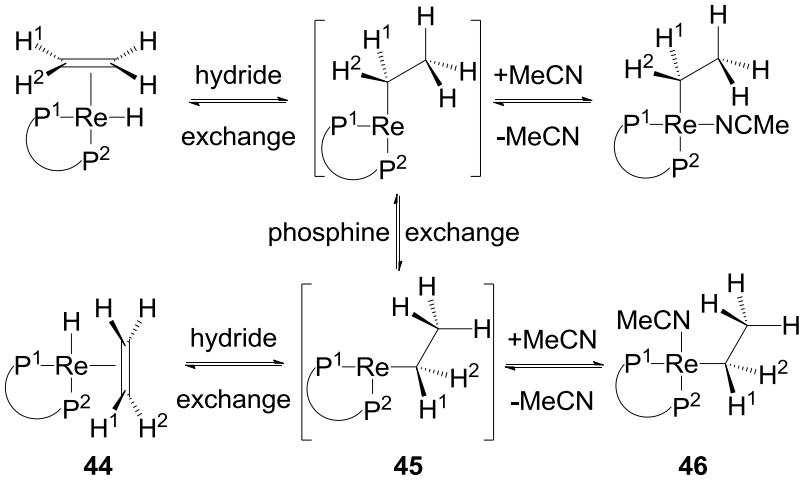

Experimentally this could be observed only for **44d** (*vide infra*). If the ethylene rotation is hindered, the exchange process denoted as hydride exchange in Scheme 47 leads only to an exchange of H_{Re} with one side of the ethylene ligand. This special situation is indeed in accordance with the dynamic NMR study, which showed only the exchange with the protons attached to the $C_{ethylene}$ at 36.7 ppm. The ethylene hydride complex **44a** was thus spectroscopically identified as the ground state and the unsaturated, not observable ethyl [ReBr(CH_2CH_3)(NO)(dppfc)] (**45a**) complex as the excited state of the given exchange process. The equilibrium constant for the **44a**/**45a** interconversion could not be determined. But it would be natural to assume, that the energy difference between the two isomers

[91] Eyring, H. The Activated Complex in Chemical Reactions. *J. Chem. Phys.* **1935,** *3*, 107–115.

cannot be more than the value of 62 kJmol^{-1} of the kinetic barrier. Comparing this barrier of 62 kJmol^{-1} between **44a** and **45a** to the value of 87 kJmol^{-1} calculated by Liu et al.[70] for the *trans* phosphine [$ReH_2(\eta^2\text{-}C_2H_4)(NO)(PMe_3)_2$] system shows that a change of the ligand pattern from *trans* to *cis* by aid of chelating diphosphines facilitates the initiation step of the catalytic hydrogenation significantly.

The reaction of the dpephos derivative **40c** suspended in a mixture of toluene and $HSiEt_3$ in the presence of 2 bar ethylene allowed the isolation of analytically pure [$ReBr(CH_2CH_3)(MeCN)(NO)$(dpephos)] (**46c**) in 61% yield directly by filtration from the toluene suspension. The formation of **46c** can be rationalized according to Scheme 46. The attempt to remove the coordinated acetonitrile by repeated dissolution of **46c** in THF or DCM followed by fast evaporation of the solvent failed. However in various solvents free acetonitrile was detected by ^{1}H NMR spectroscopy indicating the partial dissociation of the acetonitrile ligand. In the ^{31}P NMR spectrum a set of doublets at 1.6 and -12.7 ppm was assigned to **44c** and two sharp singlets at 6.0 and -9.0 ppm were eventually attributed to **46c**. This assignment was further substantiated by addition of MeCN to the sample, which led to an increase of the signals for **46c**. The fact that the phosphorus nuclei of **46c** did not reveal coupling was interpreted in terms of an exchange of the ligands *trans* to the diphosphine unit. A mechanism with a labile acetonitrile ligand and a rearrangement according to the phosphine exchange depicted in Scheme 47 is assumed. The relative intensities of the ^{31}P NMR signals revealed a **44c**/**46c** ratio of approximately 1:3 at room temperature in $CDCl_3$. In benzene the methyl group of the acetonitrile ligand gave rise to two resonances for the bound (0.56 ppm) and the free (0.53 ppm) molecules, also in an approximately 1:3 ratio. Signals at 2.30, 2.73 and 3.65 ppm in 3:1:1 ratio were assigned to the ethyl moiety of **46c**. A COSY experiment revealed that these signals constitute an A_3BC spin system. A similar spin system was observed at 3.64, 2.42 and 2.15 ppm in a 3:1:1 ratio assigned either to the 16e- complex **43c** or the 18e- ethylene hydride complex **44c**. Although the DEPT 135 and the HSQC experiments suggested the signal pattern to be associated with complex **43c**, this seems from a more general point of view unlikely, as heavy metal centers in low oxidation states like Re(+I) prefer the olefin hydride complexes over the 16e- alkyl complexes. With this assumption it is more likely that the observed pattern originates from the averaging of signals of **44c**. This interpretation would also be supported by the extraordinary low $^1J_{CH}$ coupling constant of 98 Hz of the methyl protons[73]. Since a VT-NMR study of the exchange process by cooling the sample was not possible due to either an inappropriate melting point of the solvent or an unfavorable signal overlapping and the drastic shift of the **44c**/**46c** equilibrium towards **46c** at low temperatures, the true nature of the complex could not be fully established via NMR spectroscopy. As IR spectroscopy possesses an intrinsically higher time resolution, the IR spectrum of the compound was recorded in benzene solution. As expected the ν(NO) band of **46c** at 1653 cm^{-1}, which is the only one visible ν(NO) band in the solid state IR spectrum, was observed. In addition two ν(NO)

bands attributed to two isomers of **44c** appeared at 1704 cm^{-1} and 1683 cm^{-1}. This is also in agreement with the two distinct ν(H) bands at 2014 cm^{-1} and 1954 cm^{-1}, which indicate the presence of two hydride species. The addition of acetonitrile to the solution led to a drastic increase of the ν(NO) band of the acetonitrile complex **46c** at 1653 cm^{-1}, while the other ν(NO) and ν(ReH) bands disappeared. It can be concluded from these observations that the ethylene hydride compound **44c** is the ground state structure and not the unsaturated ethyl complex **45c**. Moreover we associate the two distinct sets of ν(H) and ν(NO) bands to **44c** in the isomeric forms **44c(up)** and **44c(down)** (Scheme 48) in analogy to the observed isomerism in the $[ReBr_2(MeCN)(NO)(P\cap P)]$ compounds **40a**, **40c** and **40e** (Scheme 44).

Scheme 48: The proposed up/down isomerism for **44c**.

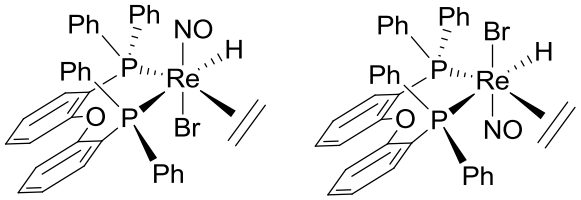

44c(down) **44c(up)**

The increase of the natural bite angle of the diphosphine from 95° in **44a** and **44b** to 102° in **44c** and **46c** apparently leads to a stabilization of the ethyl acetonitrile complex **46c**. Nevertheless the unsaturated 16e- ethyl complex **45c** could not be traced by any spectroscopy applied. Further attempts were directed towards tuning the backbone strain by preparing the homoxantphos derivative. Although this ligand has also a natural bite angle of 102°, the dpephos and the homoxantphos ligands differ considerably in backbone rigidity. Molecular dynamics simulation[86,88] revealed bite angles of 86-120° for dpephos and 92-120° for homoxantphos to be accessible within 12.6 $kJmol^{-1}$. Hence the strain in the homoxantphos complex is expected to be higher, which was presumed to lead to a further destabilization of the ethylene hydride species **44d**. The preparation of the homoxantphos derivative $[ReBrH(NO)(\eta^2\text{-}C_2H_4)(homoxantphos)]$ **44d** was achieved in the same manner as for **46c**. The product was isolated from the reaction suspension in 81 % yield. The IR spectrum of the isolated solid featured apart from a strong ν(NO) band at 1673 cm^{-1} a sharp and strong ν(ReH) band at 2008 cm^{-1}. This suggests the formation of the ethylene hydride species **44d**. High quality single crystals of **44d** were obtained suitable for an X-ray diffraction study. The supposed ethylene hydride structure displaying the hydride and the ethylene ligand in *cis* position could be verified (Figure 13). As expected the ethylene axis is parallel to the Re-H vector. The $(C\text{-}C)_{ethylene}$ bond is expanded to 1.401 Å indicating strong back donation from the rhenium center. The Re-C bond lengths of 2.242 Å and 2.216 Å are in the typical range of Re-C single bonds. The phosphines

comprise an angle of 95°, which is 7° lower than the ligand's preferred bite angle. The structural analysis of **44d** revealed also a disorder between the NO and the Br ligands in the ratio of approx. 15:85 originating from co-crystallization of **44d(up)** and **44d(down)**. In case of the more populated **44c(down)** isomer the bromide points into the pocket formed by the 10,11-dihydro-dibenzo[b,f]oxepine moiety, while the NO ligand points towards two diphosphine phenyl groups and *vice versa* for the less populated **44d(up)** isomer.

Figure 13: ORTEP diagram of **44d(NO-down)** is 85% populated and **44d(NO-up**) is 15% populated drawn at 50% probability.

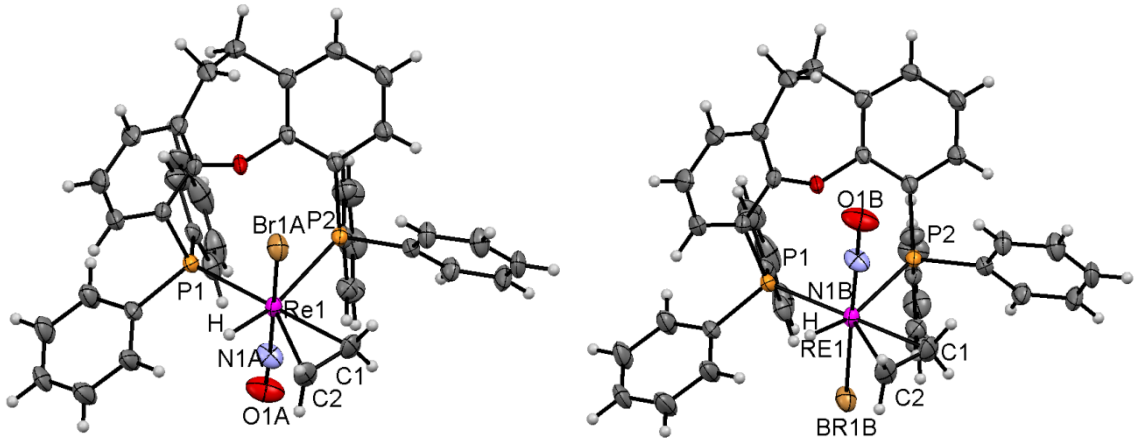

Selected bond lengths [Å]: Br1A-Re1 2.555, C1-Re1 2.241, C2-Re2 2.216, C1-C2 1.401, H-Re1 1.594, N1A-Re1 1.771, N1A-O1A 1.184, P1-Re1 2.460, P2-Re1 2.569. Selected bond angles [°]: Br1A-Re1-N1A 171.8, Br1A-Re-Br1B 168.8, C1-Re-C2 36.6, C1-Re-P2 83.7, C2-Re-H 65.7, H-Re1-P1 80.2, P1-Re1-P2 95.2

An isomerization between these complexes would require either the diphosphine backbone to flip over or the dissociation of one ligand leg and the rearrangement of the now fivefold coordinated intermediate with a flip over of the Re-bound leg followed by the re-coordination. As the backbone of homoxantphos is relatively rigid and all of the ligands are tightly bound to the rhenium center, the backbone conformers **44d(up)** and **44d(down)** are indeed expected to be kinetically stable. It might be speculated that the diphenyl ether and ferrocene backbones of **44a**-**c** are more flexible and allow isomerization between the isomeric forms. In the ^{31}P NMR spectrum of **44d** only one extremely broad phosphorus resonance originating from the coalescing signals of the two chemically different phosphorus nuclei was observed in benzene at 300 K (Scheme 47). This is in contrast to **44a-c** where no phosphine exchange was detectable in the ^{31}P NMR spectra. Cooling the sample to 285 K leads to a set of slightly broadened singlets. As all ligands in **44d** are tightly bound, the mechanism is anticipated to proceed via the formation of the 16e- ethyl complex [ReBr(CH_2CH_3)(NO)(homoxantphos)] (**45d**) according to the phosphine exchange depicted Scheme 47. This phosphine exchange results in racemization of **44d**. The phosphine site exchange according to Scheme 47 is not observable for **44a-c**. This could mean that an increasing strain originating from the diphosphine leads either to the destabilization of the ethylene hydride complex **44d** or to the

lowering of the barrier for the flip-over process of the 16e- ethyl complex **45e**. The phosphorus exchange of **44d** according to Scheme 47 is slowed by the addition of an excess of acetonitrile via the formation of **46d**. The affinity of **45d** to acetonitrile is lower than the affinity of **45c** to this ligand. Shifting the **44d**/**46d** equilibrium towards **46d** by addition of acetonitrile leads to two sharp singlets for **46d(down)** at 18.1 ppm and at -5.1 ppm accounting for approx. 85 % of the overall intensity and a set of two slightly shifted signals for **46d(up)** at 20.0 and 1.5 ppm accounting for the residual 15 % of the signal intensities in the $^{31}P\{^{1}H\}$ NMR spectrum. This ratio for **46d(up)** and **46d(down)** reflects the isomer ratio observed in the structural analysis of **44d(up)** and **44d(down)**. As the ratio of the isomers did not change during the VT-NMR study between 285 K and 330 K it was concluded that the isomers of **46d** are kinetically stable. The ^{1}H NMR spectrum of **44d** in benzene consists apart from the signals originating from the homoxantphos ligand only of a set of broad signals at 3.01 ppm (m, 3 H, $ReCH_2CH_3$) and at 2.32 ppm (m, 2 H, $ReCH_2CH_3$). Heating the sample to 320 K focuses the signals and a COSY experiment revealed them to be an A_2B_3 spin system ($^{3}J_{HH}$ = 7 Hz). Unlike in the **44a**,**b** and **44c** complexes the methylene protons of **44d** give rise to only one signal, which indicates the rotation of the ethyl moiety of the intermediate **45e** via the mechanism in Scheme 47. Since this mechanism would also result in the exchange of the diphosphine nuclei, the dynamic ^{31}P NMR spectra of **44d(up)** and **44d(down)** provide further evidence for the isomerization process according to Scheme 47. As in the case of **44c** the found $^{1}J_{CH}$ coupling of the apparent methyl group protons to the α-carbon nucleus ($^{1}J_{CH}$ = 97 Hz) is significantly lower than the characteristic value (120-130 Hz) for a typical methyl group[73]. Therefore it seems likely that the observed spectrum results again from averaging of signals via fast exchange of the rhenium hydride with the adjacent $CH_{2ethylene}$ group via the unsaturated ethyl complex. Further support of this interpretation was achieved with help of the IR spectrum of **44d** recorded in benzene. It shows a very broad ν(ReH) band at 2015 cm^{-1} and an also markedly broadened ν(NO) band at 1679 cm^{-1}. This again speaks for the ethylene hydride **44d**. Nevertheless it can be concluded that the activation barrier for the interconversion of **44d** and the unsaturated ethyl complex **45d** must be significantly smaller than the one of the **44b**/**45b** system. As kinetic barriers set the upper limits for the thermodynamics, the energy gap between **44d** and **45d** is presumably smaller.

The applied ligand tuning by increasing the diphosphine's bite angle thus induced the destabilization of the ethylene hydride complexes **44c** and **44d**. To push this bite angle effect even further we tried to prepare the corresponding Sixantphos ethylene hydride analogue. Reacting **40e** with $HSiEt_3$ and ethylene led the *ortho*-metallated species [ReBr(η^2-C_2H_4)(NO)(η^3-*ortho*-metallated-Sixantphos)] (**48e**). It bears an ethylene ligand, but neither a hydride nor an ethyl ligand was detected in the IR/NMR spectra. **48e** could be crystallized and an X-ray diffraction study revealed the Sixantphos ligand to coordinate tridentate with two P atoms and the *ortho*-metallated C_{phenyl} atom (Figure 14).

The structure of **48e** revealed in addition the presence of **48e(up)** and **48e(down)** isomers in the ratio 3:7 similar to the homoxantphos derivative **44d**.

Figure 14: ORTEP diagrams of **48e(down)** and **48d(up)** drawn at 50% probability.

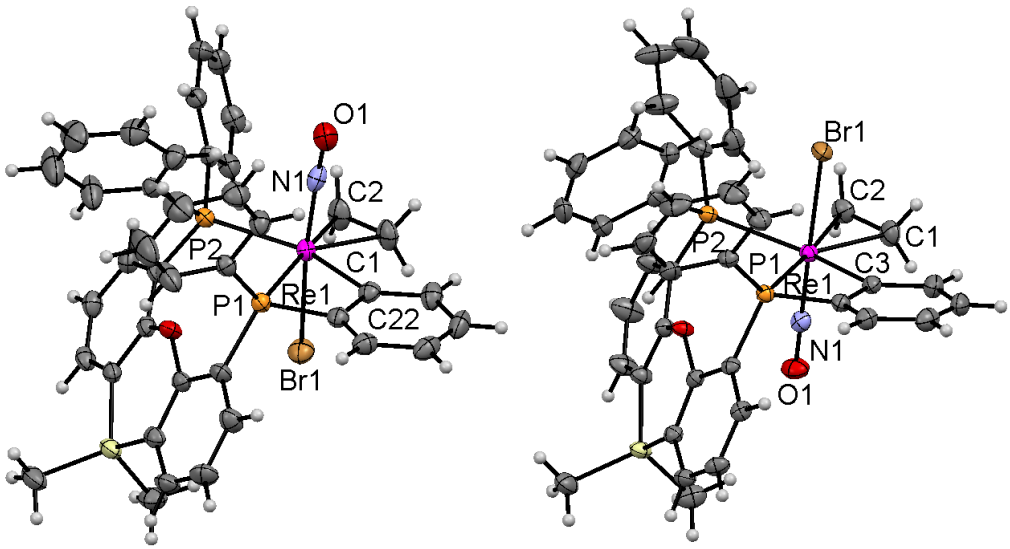

Selected bond lengths of **48e(down)** [Å]: Br1-Re1 2.582, C1-Re1 2.194, C2-Re1 2.225, C1-C2 1.400, C22-Re1 2.165, N1-Re1 1.819, N1-O1 1.073, P1-Re1 2.504, P2-Re1 2.561. Selected bond angels [°]: Br1-Re1-N1 174.4, C1-Re1-C2 36.9, C1-Re1-C22 81.7, C2-Re1-P2 82.2, C22-Re1-P1 64.6, P1-Re1-P2 94.4. Selected bond lengths of **48e(up)** [Å]: Br1-Re1 2.591, C1-Re1 2.199, C2-Re1 2.235, C1-C2 1.412, C3-Re1 2.177, N1-Re1 1.747, N1-O1 1.198, P1-Re1 2.502, P2-Re1 2.574. Selected bond angels [°]: Br1-Re1-N1 179.0, C1-Re1-C2 37.1, C1-Re1-C3 81.3, C2-Re1-P2 84.9, C3-Re1-P1 64.7, P1-Re1-P2 91.7.

Again the bromide ligand of the preferred conformer **48e(down)** points into a pocket formed by the ligand backbone. The ratio of the two isomers in the crude product mixture was determined by ^{31}P NMR spectroscopy to be 3:7 **48e(up)**:**48e(down)** and it turned out to be invariant to temperature changes indicating a high kinetic barrier of interconversion. The two isomers could be separated by column chromatography yielding 41% **48e(down)** and 16% **48e(up)**. The isolated compounds showed distinct sets of doublets in the ^{31}P{^{1}H} NMR spectra (**48e(down)** : -12.7, -69.4; **48e(up)** -22.8, -76.2) and in the ^{1}H NMR spectra the signals of the four ethylene protons at 3.13 (q, *J* = 9 Hz, 2 H, C_2H_4), at 2.72 (m, 1 H, C_2H_4) and at 1.76 (q, *J* = 9.0 Hz, 1 H, C_2H_4) ppm for **48(down)** respectively at 3.09-2.97 (m, 2 H, C_2H_4), at 2.66 (m, 1 H, C_2H_4) and at 1.99 (q, 1H, *J* = 8.0 Hz, C_2H_4) ppm for **48(up)** were visible apart from the Sixantphos proton signals. In contrast to **44a,b,d** and **46c** no dynamic behavior could be detected in the NMR spectra of the **48e(up/down)** species. In the IR spectra of both isomers strong ν(NO) bands were found at 1680 cm^{-1} for **48(down)** and at 1686 cm^{-1} for **48e(up)**. Attempts to influence the ratio of the formed products by changing the reaction temperature, reaction time and solvent were not successful.

5.5 Properties of [ReBrH(η^2-C_2H_4)(NO)(P∩P)] complexes

5.5.1 Acetonitrile affinity of the [ReBrH(η^2-C_2H_4)(NO)(P∩P)] complexes

Motivated by the fact that the acetonitrile complex **46c** was obtained under the same conditions as the complexes **44a**, **44b** and **44d** we studied also their acetonitrile affinity (Table 4). The quantitative analysis of the VT-NMR spectra of **44a-c** in the presence of controlled amounts of MeCN allowed the measurement of the dissociation constants (K_d) for the [ReBr(CH_2CH_3)(MeCN)(NO)(P∩P)] complexes **44a-c** at temperatures ranging from 285 K to 325 K and allowed the determination of the thermodynamic parameters of the association process (Table 4).

Table 4: Thermodynamic parameters of the equilibrium between **44a**,**b**,**c** and **46a**,**b**,**c**.

reaction	K_d at 300K	ΔH [kJmol^{-1}]	ΔS [Jmol^{-1}K^{-1}]
7a ⇆ **5a**+MeCN	0.91	+18.1	+60
7b ⇆ **5b**+MeCN	29.81	+12.5	+71
7c ⇆ **5c**+MeCN	0.035	+30.8	+74

However, the dissociation constants of **44d** and **48e** could not be determined due to unfavorable signal overlap in the ^{1}H-NMR spectra and the broad nature of the ^{31}P NMR signals of **44d** and the difficulty to transform **48e** into **44e** under the employed conditions. The positive entropies of the processes (60-74 kJmol^{-1}K^{-1}) reflect the dissociative character of the reaction. The reaction enthalpies range from 12.5 to 30.8 kJmol^{-1}. Comparing the relative stability of the ethylene hydride complexes of the diprpfc derivative **44b** with those of the corresponding dppfc and dpephos derivatives **44a** and **46c** revealed that larger bite angles, as well as smaller donor capabilities of the diphosphines, cause a decrease in the relative stabilization of the ethylene hydride complexes.

5.5.2 Reactivity of the 44a,b,d 45c and 48e towards H_2 and 1-hexene

H_2 affinity studies were then approached for **44a**, **44b**, **44d**, **46c** and **48e** to explore the potential of these complexes to act as hydrogenation catalysts. Exposing **44a**, **44b**, **44d**, **46c** and **48e** to 2 bar of H_2 led in all cases to hydrogenation of the ethylene ligand generating ethane, which could be monitored by NMR spectroscopy. In any case the presumed 16e- hydride complexes **43a-e** could not be detected. In the case of **44a** and **44d** hardly soluble red solids precipitated from the reaction solution. Their structures are yet unknown but can be assumed to be analogous to **50b**. Nevertheless the reaction of H_2 with **44b**, **46c** and **48e** furnished identifiable products. The reaction of a benzene solution of **44b** under an atmosphere of H_2 afforded the hydride bridged dimer **50b** after 1 day at room temperature as hardly soluble red single crystals containing 2 equivalents of benzene per molecule **50b**. Due to its low solubility **50b** was characterized only by an X-ray diffraction study (Figure 15), elemental analysis and IR spectroscopy.

Figure 15: ORTEP diagram of **50b** drawn at 50% probability..

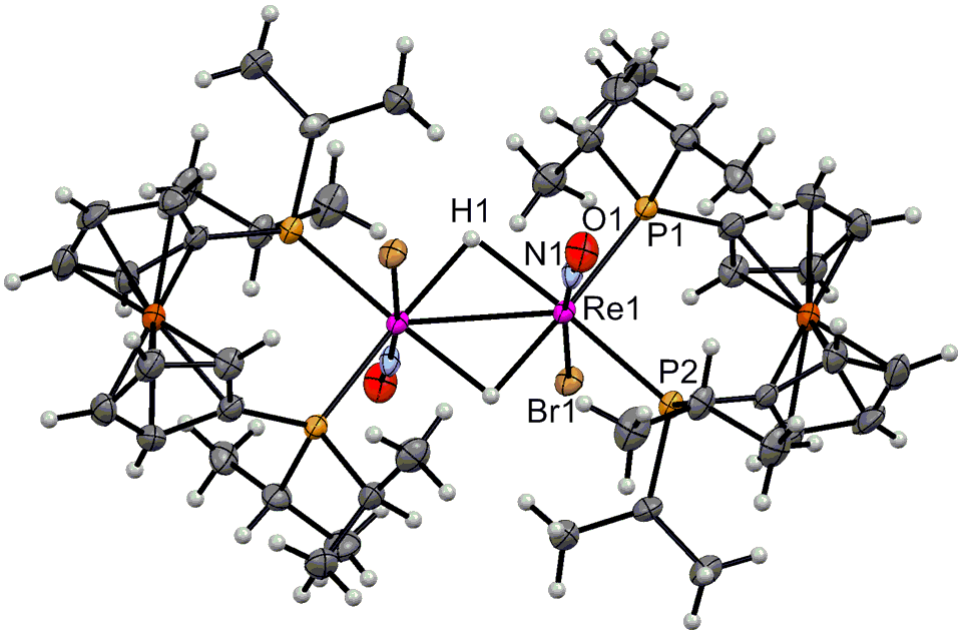

Selected bond lengths [Å]: Br1-Re1 2.604, H-Re1 1.948/2.061, N1-Re1 1.754, N1-O1 1.184, P1-Re1 2.449, P2-Re1 2.430, Re1-Re1 2.847. Selected bond angels [°]: Br1-Re1-N1, H-Re1-P1, O1-N1-Re 1 1.74.8, P1-Re1-P1

In the X-ray diffraction study, the Re-H distances were found to be quite long and slightly asymmetric with bond lengths of 1.948 Å (Re_1-H_1, Re_2-H_2) and 2.061 Å (Re_2-H_1, Re_2-H_2). As the asymmetric unit comprises only one half of the molecule, the bonding situation is symmetric. The Re-Re distance was found to be 2.847 Å, which indicates a μ^2-H bridge supported metal-metal bond. Single crystals suitable for X-ray diffraction studies of the Sixantphos derivative **50e** could be obtained in a similar way as for **50b**. The solid state IR spectra of **50b** showed a strong sharp ν(ReH) band at 1982 cm^{-1} whereas the ν(ReH) band of **50e** at 1990 cm^{-1} was broad. The ν(NO) bands of **50b** (1672 cm^{-1}) and **50e** (1693 cm^{-1}) are in both cases strong and sharp. This is in contrast to the products of the reactions of **44a** and **44d** with H_2, which displayed only broad ν(NO) bands, but no ν(ReH) bands in the IR spectra. This might indicate structures different from **50b** and **50e** - supposedly oligomers of **43a** and **43d** with higher nuclearities .

The reaction of **46c** with hydrogen in benzene led immediately to the targeted complex [ReBrH(MeCN)(NO)(dpephos)] **51c**, which is however unstable in solution and could therefore not be isolated. In the ^{1}H NMR spectrum of **51c** a resonance at 1.95 ppm (dd, $^2J_{HP(trans)}$ = 96.0 Hz, $^2J_{HP(cis)}$ = 25.5 Hz) was attributed to a hydride ligand located in the plane formed by the two phosphorus nuclei and the rhenium center. In the ^{31}P NMR spectrum a broad resonance at 18.1 ppm (m, P_{cisH}) and a sharp signal at -5.1 ppm (d, $^2J_{HP(trans)}$ = 96.0 Hz, P_{transH}) were observed. Exposing a solution of **51c** to an atmosphere of ethylene leads instantly to the formation of **44c** and **46c**. The reactions of **44a** and **44d** with H_2 was anticipated to lead also to hydrides, which could probably also be stabilized by the

addition of acetonitrile (Scheme 46). Indeed reacting **44a** and **44d** in the presence of acetonitrile with H_2 led to the formation of the acetonitrile hydride complexes **51a** and **51d**. Their spectroscopic features parallel those of **51c**. Hydride signals appeared in the ^{1}H spectra of **51a** at 1.44 ppm (dd, $^2J_{HP(trans)}$ = 63.3 Hz, $^2J_{HP(cis)}$ = 23.7 Hz) and of **51d** at 2.01 ppm (dd, $^2J_{HP(trans)}$ = 72.0 Hz, $^2J_{HP(cis)}$ = 19.5 Hz). The ^{31}P NMR spectra of **51a** and **51d** consist of broad singlets at 19.5 ppm and at 25.4 ppm, assigned to the phosphine atoms *cis* to the rhenium hydride and doublets at -4.4 ppm (d, $^2J_{HP(trans)}$ = 63.3 Hz, $P_{trans\text{-}H}$) and at 2.0 ppm (d, $^2J_{HP(trans)}$ = 72.0 Hz, $P_{trans\text{-}H}$) assigned to the phosphine atoms *trans* to the rhenium hydride. As in the case of **51c** the hydride complexes **51a** and **51d** are not sufficiently stable to be isolated. The ethylene complexes **44a** and **44d** can be regenerated by exposing them to ethylene (Scheme 46). Exposing **51a**-**d** to a mixture of H_2/D_2 results in isotope scrambling within minutes, which was pursued using ^{1}H NMR spectroscopy. Therefore we propose the existence of a trihydride complex [ReBrH_3(NO)(P∩P)] **49a-d**, which allows the efficient H_2/D_2 scrambling according to the mechanism depicted in Scheme 49.

Scheme 49: Proposed mechanism for the observed HD exchange.

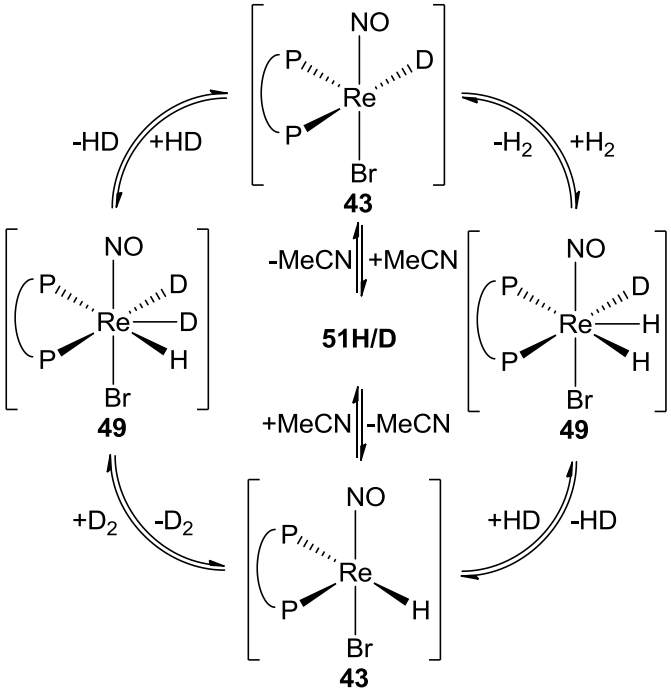

The olefin affinity of the 16e- complexes **43a**-**e** was qualitatively assessed by estimating the olefin exchange/isomerization rates of **44a**-**d**. For that purpose 1-hexene as a typical substrate was added to $CDCl_3$ solutions of **44a**,**b**,**d**, **44**/**46c** and **48e** at room temperature. Under these conditions isomerization of 1-hexene into Z-2-hexene and the thermodynamically more favorable E-2-hexene was observed (Scheme 50).

Scheme 50: Stepwise isomerization of 1-hexene.

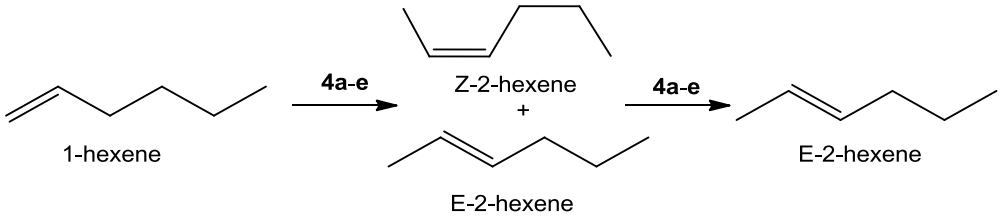

The pursuit of this reaction using ^{13}C NMR spectroscopy[92] revealed that there is neither a kinetic preference for the release of E-2-hexene, nor for the release of Z-2-hexene, since both are initially formed in equal amounts. But at the end of the isomerization process the thermodynamically favored E-2-hexene is exclusively found[93]. The thermodynamically highly favored Z- and E-3-hexenes were not formed. Quantitative NMR pursuit revealed that the 1-hexene isomerization depends on the catalysts concentration and is independent of the 1-hexene concentration, which was interpreted in terms of kinetically preferred coordination of terminal olefins to **43a-d** and a rate limiting elimination of the isomerized olefin ligand. The homoxantphos catalyst **44d** proved to be the fastest catalyst in the isomerization process with a TOF of ca 14 h^{-1} followed by the dpephos derivatives **44c**/**46c** with a TOF of ca 5 h^{-1}. The two bisphosphinoferrocene complexes **44a**,**b** were about equally active with a TOF of ca. 0.3 h^{-1}. The Sixantphos complexes **48e(up)** or **48e(down)** were inactive in this process of 1-hexene to E-2-hexene isomerization - presumably because of the absence of a hydride ligand in these complexes. From these experiments we concluded that ethylene dissociation from **44a**,**b**,**d** and **44**/**46c** is a slow process, supporting the assumption that all the ligands are quite strongly bound to the rhenium center. The 45 fold increase in the isomerization activity of the homoxantphos derivative **44d** compared to the bisphosphinoferrocene derivatives **44a** and **44b** also reflects diphosphine bite angle dependence. Since the 16e- hydride complexes **43a-d** preferably bind terminal olefins, a high selectivity for the hydrogenation of terminal olefins can be expected.

5.5.3 Hydrogenation catalysis of 44a,b,d, 46c and 48e

44a,b,d, 46c and **48e** turned out to be (pre-) catalysts for the hydrogenation of olefins comparable in activity to Wilkinson or Osborn type Rh catalysts[31,38,94]. To explore the catalytic capabilities of **44a,b,d, 46c** and **48e** in catalytic hydrogenations of olefins under H_2 pressure, we employed a press gas flow controller for quantitative kinetic monitoring.

[92] Forsyth, D. A.; Hediger, M.; Mahmoud, S. S.; Giessen, B. C. Quantitative Analysis of Alkene Alkane Mixtures by ^{13}C Nuclear Magnetic Resonance Spectroscopy. *Anal. Chem.* **1982,** *54,* 1896–1898.
[93] Wiberg, K. B.; Wasserman, D. J. Enthalpies of Hydration of Alkenes. 1. The n-Hexenes. *J. Am. Chem. Soc.* **1981,** *103*, 6563–6566.
[94] Crabtree, R. H.; Gautier, A.; Giordano, G.; Khan, T. The preparation and some catalytic properties of a number of rhodium(I) diolefin complexes. *J. Organomet. Chem.* **1977,** *141,* 113-121.

Table 5: Results of catalytic reactions using **44a**,**b**,**d**, **46c** and **48e(up/down)** as catalysts.

catalyst	loading (mol%)	substrate (mL)	solvent (mL)	additive (µL)	temp. (°C)	$p(H_2)$ (bar)	TOF (h^{-1})	TON
44a	0.14	1-hexene (1)	THF (2)		23	10	290 a)	700
44a	0.10	styrene (1)	THF (2)		23	10	386 a)	900
44b	0.50	1-hexene (1)	Toluene (8)		23	10	22 b)	500
44b	0.42	1-hexene (2)	THF (10)		60	10	144 a)	240
44b	0.42	1-hexene (2)	THF (10)		80	10	750 a)	240
44c/46c	0.08	1-hexene (1)	THF (2)		23	10	1248 a)	1200
44c/46c	0.09	styrene (1)	THF (2)		23	10	823 a)	1000
44d	0.06	1-hexene (1)	THF (2)	MeCN (0.3)	23	10	1050 a)	1600
44d	0.09	styrene (1)	THF (2)	MeCN (0.3)	23	10	1020 a)	1100
48e(up)	0.005	hexene (15)	toluene (10)	$HSiEt_3$ (100)	80	10	4120 a)	5000
48e(up)	0.004	styrene (15)	toluene (10)	$HSiEt_3$ (100)	80	10	2961 a)	24100
48e(up)	0.004	cyclohexene (15)	toluene (10)	$HSiEt_3$ (100)	120	10	1230 a)	10200
48e(up)	0.005	α-methylstyrene (15)	toluene (10)	$HSiEt_3$ (100)	120	10	1940 a)	20000
48e(up)	0.003	dimethylitaconate (5)	toluene (5)	$HSiEt_3$ (100)	140	50	600 c)	24400
48e(down)	0.005	hexene (15)	toluene (10)	$HSiEt_3$ (100)	80	10	4870 a)	6300
48e(down)	0.004	styrene (15)	toluene (10)	$HSiEt_3$ (100)	80	10	2414 a)	24100
48e(down)	0.004	cyclohexene (15)	toluene (10)	$HSiEt_3$ (100)	120	10	600 a)	6300
48e(down)	0.005	α-methylstyrene (15)	toluene (10)	$HSiEt_3$ (100)	120	10	1820 a)	20000
48e(down)	0.003	dimethylitaconate (5)	toluene (5)	$HSiEt_3$ (100)	140	50	500 b)	31500

a) The experiments were conducted with a Büchi press gas flow controller. The TOF's were determined in the first 10 minutes of the experiments. The products were identified by NMR spectroscopy. b) The TOF was measured *in situ* by ATR-IR spectroscopy in the range from 40-100 bar and extrapolated to 10 bar. c) The reactions were conducted in a closed autoclave without monitoring during the reaction. Instead the TOFs were calculated after the pressure did not further decline in autoclave. The conversion was determined by GC-MS.

The hydrogenations of 1-hexene and styrene were selected as benchmark processes to enable the comparison in catalytic activities. Kinetic isotope effects were also probed for **44a-d** in the hydrogenations/deuterations of 1-hexene using the same set up and k_{D2}/k_{H2} were found to be 1. The found reaction rates are listed in Table 5. The reaction rates were found to be independent of the substrate concentration and first order dependent on $p(H_2)$. In case of the hydrogenations of 1-hexene only slow decreases in activity were observed under the listed conditions. In the case of **44a,b** and **46c** replacement of THF with DCM led to a much faster decrease of the reaction rate, which was interpreted in terms of strongly progressing catalyst decomposition in this solvent. For **44d** it was found that the addition of small amounts of acetonitrile was crucial for proper catalytic performance. However, a too large amount of acetonitrile led also to lower TONs and TOFs presumably caused by competition of acetonitrile with the substrate. This showed that the catalytic activity is quite sensitive to the reaction media. In contrast to this catalytic reactions with **48e** were found to be less dependent on the type of solvent. Under "run to death" conditions TONs of more than 24000 could be reached for styrene. Nevertheless we noticed that the **48e(up)** and **48e(down)** catalysts were not as efficient for the hydrogenation of 1-hexene. This can be explained by the fact that under the employed reaction conditions, the isomerization of 1-hexene to Z/E -2-hexene was observed to proceed with a similar rate as the hydrogenation for **48e(up)** and **48e(down)**. We assume that Z/E-1-hexene binds less strongly to the metal and thus the substrate stabilization is lowered. As a consequence this leads to faster catalyst decay. The performance of the two isomers

48e(up) and **48e(down)** was found to differ slightly implying that the up-down isomerization does not take place under catalytic conditions. Furthermore we explored the catalytic potential of **44a,b,d, 46c** and **48e(up/down)** for the hydrogenation of the sterically more demanding substrates cyclohexene and α-methylstyrene. **44a,b,d** and **46c** showed virtually no activity for these substrates, while **48e(up/down)** was found to be still active - although the hydrogenations of these substrates with **48(up/down)** catalysts proceeded under generally lower TOFs and the TONs were found to be limited by progressive catalyst deactivation. It is presumed that the crucial catalytic species are the 16e- complexes **43a-e** and it is their supported or unsupported stability which restrict the TONs. The unsaturated Sixantphos complex **43e** is stabilized via *ortho*-metallation and accompanying H_2 release to form **47e**. *Ortho*-metallation is presumed to be the best mechanism of protection for the unsaturated [ReBrH(NO)(P∩P)] species. **48e(up/down)** are capable of hydrogenating bulkier olefinic substrates, such as α-methylstyrene, cyclohexene and dimethylitaconate. The deactivation of the catalyst is therefore substrate and catalyst precursor dependent and follows for olefins approximately the order of their metal binding abilities: 1-hexene < styrene << cyclohexene. The attempt to identify the catalyst's remains from the reaction solutions after the hydrogenation experiments with **44a,b,d, 46c** and **48e** failed and none of the species described from the reactions of **44a,b,d** and **46c** with H_2 could be identified. This could be explained on the basis of the previously described compounds **51a**, **51c** and **51d**, which were also unstable. Moreover these remains were not active in further hydrogenation experiments and are therefore not "living" systems.

5.5.4 The proposed catalytic cycle

Based on the catalytic hydrogenation scheme (Scheme 51) the precursor complexes **44a,b,d, 46c** and **48e(up/down)** are first transformed into the 16e- species **43a-e**. The *in situ* formed hydride complexes of type **43** enter then the depicted cycle. The course of the catalytic reaction follows in great parts the Osborn type hydrogenation mechanism (Scheme 11). The absence of kinetic isotope effect suggests that the initial insertion of the olefin into the Re-H bond (k_1) is rate limiting as the splitting of the D_2 molecule (k_2) is expected to show a high KIE. The k_2 step appears to be a connected oxidative addition/reductive elimination via a dihydride alkyl transition. Furthermore the binding of the olefin in **44a**, **44b**, **44c** and **44d** is so strong that it can be considered irreversible on the time scale of the catalytic hydrogenation. Therefore the rate of the catalytic hydrogenation is independent of the substrate concentration. The acetonitrile complexes of type **46** and **51**, the olefin hydride complexes of type **44** and the *ortho*-metallated compounds of type **48** are the resting states of the catalytic cycle.

Scheme 51: The proposed catalytic cycle for hydrogenations with **44a**,**b**,**d**, **46c** and **9e**. **44**, **46** and **51** are resting states.

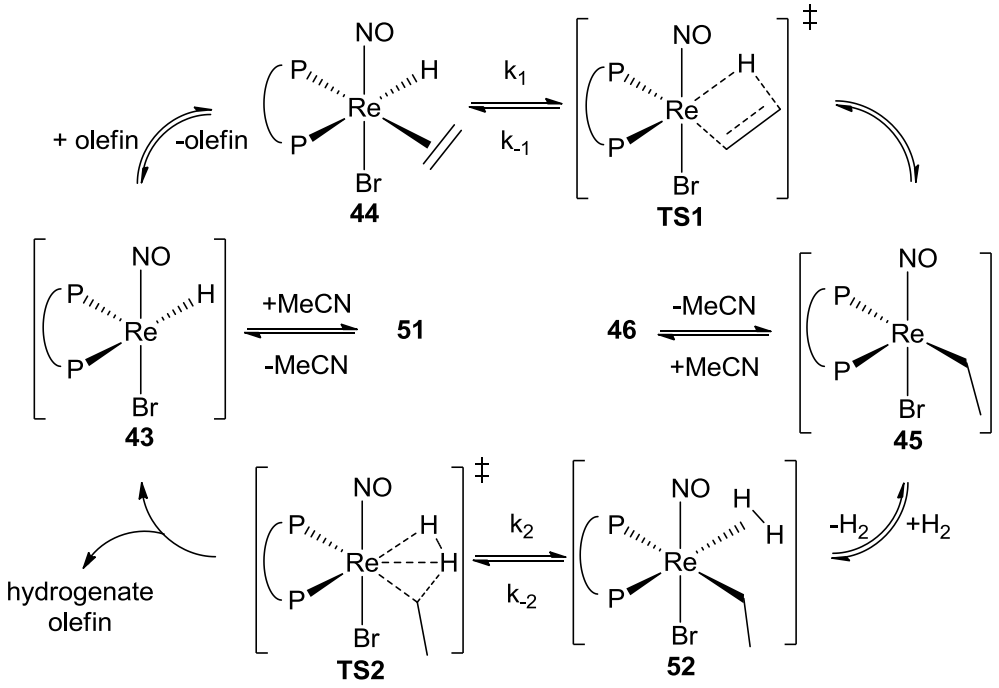

5.6 DFT model study of the ethylene hydrogenation using a [ReBrHL(NO)(PMe_3)$_2$] system

To support the proposed catalytic cycle of Scheme 51, we applied DFT calculations using a model, in which we replaced the bidentate ligands of Scheme 43 with two *cis* **PMe_3** groups. The respective PMe_3 substituted structures of type **43-45**, and **52** shown in Scheme 51 were optimized without geometrical constraints as the given model species **43PMe_3-45PMe_3** and **52PMe_3**. Their calculated energies are shown in Figure 18. They are given in the order of their appearance along the Osborn type reaction-path together with the calculated main transition states **TS1** connecting **44PMe_3** with **45PMe_3** and **TS2** connecting **52PMe_3** with **43PMe_3**. The calculations revealed two substantial barriers ΔE_1 and ΔE_2 to reach **TS1** and **TS2**, respectively. ΔE_1 denotes the calculated energy for the β-hydride shift (rate constant k_1) and ΔE_2 denotes the calculated energy for the combined steps of oxidative H_2 addition/reductive alkane elimination (rate constant k_2) in Scheme 51. ΔE_1 amounts to 41.4 kJmol^{-1} and ΔE_2 amounts to 28.5 kJmol^{-1}. According to the calculations, ΔE_1 would thus stand for the rate determining step of such a catalytic cycle. ΔE_1 is somewhat lower than the experimentally determined 62 kJmol^{-1} for the process of **44a** to **45a**. The lower barrier of the calculated system is attributed to the fact that **44PMe_3** is based on two monodentate ligands, which are more flexible to adjust to the steric needs in **TS1**. As the preferred bite angle of dppfc is 97°, we expect a considerable "steric pressure" for the transition state on going from **44a** to **45a**, since the dppfc chelate does apparently not admit opening of the P-Re-P angle to the extent necessary for a relaxed transition state (P-Re-P = 101.5°). Although the barriers for the β-hydride shifts (migratory insertion of the

olefin into the Re-H bond) of **44b-44e** could not be measured as single steps, we anticipate that the β-hydride shift from **44b** to **45b** has a similar barrier as the one form **44a** to **45a**, since the bite angles of dppfc and diprpfc are almost identical. For **44c**, **44d** and **44e**, we expect a barrier deviating much less from the calculated ΔE_1, since the bite angles of dpephos, homoxantphos and Sixantphos are closer to the P-Re-P angle of **TS1**. Thus, the dpephos and the homoxantphos compounds can be considered "more activated" due to the larger bite angles. This would be in accordance with the spectroscopic features of **44d** and **46c**, which indicate a much faster $H_{Re}/H_{ethylene}$ atom exchange than it is observed for **44a** and **44b**. Comparing **TS1** with **44PMe$_3$** (Figure 13) reveals that the Re-H (+0.07 Å), the Re-C1(ethylene) (+0.07 Å), Re-C2(ethylene) (-0.07 Å) and the C-C(ethylene) (+0.04 Å) bonds are only slightly changed. However the H1-Re-C1 angle is compressed from P-Re-P 71.8° in **44PMe$_3$** to 40.4° in **TS1**. At the same time the remaining the P1-Re-P2, P2-Re-H1 and the P1-Re-C2 angles are increased (Figure 16). The NO-Br axis remains largely unaffected by the β-hydride shift. Taking these structural changes in account, we therefore suggest **TS1** to be an early transition state, since the rhenium hydride character remains largely intact in **TS1**, which also would cope with a small normal KIE.

With the given model the formed unsaturated ethyl complex **45PMe$_3$** is preceded by an intermediate, which is stabilized by β-agostic interaction between the rhenium and the H_{CH3} atoms. This species is omitted in Figure 18 as **45PMe$_3$** is more stable and the energy barrier towards **45PMe$_3$** is only 1 kJmol^{-1}. For **45PMe$_3$** the DFT calculations revealed a H_2 affinity of -3.6 kJmol^{-1}. In the resulting H_2 complex, the H-H bond length is slightly stretched to 0.84 Å with Re-H distances of 1.85 Å (Re-H1) and 1.84 Å (Re-H2) (Figure 16). After binding of H_2 to form the H_2 complex **52PMe$_3$**, **TS2** has to be passed (ΔE_2), which has a 28.4 kJmol^{-1} higher energy than **52PMe$_3$**. Since ΔE_2 is 12.9 kJmol^{-1} lower than ΔE1, **52PMe$_3$** is not expected to accessible experimentally (Figure 18 and Table 6).

Based on the theoretical analysis, the P-Re-P bite angles of **52PMe$_3$** (99.8°) and **TS2** (95.5°) (Table 6) are smaller than the relaxed ones of **TS1** (101.5°) and **43PMe$_3$** (102.4°). This indicates that super large bite angle diphosphines (i.e. ≥ 110°) could cause a higher barrier in reductive eliminations of real catalytic systems, even so high that k_2 (Scheme 51) could exceed the value of k_1 and could become rate determining. In **TS2** the H_2 molecule is oxidatively added to form a 7 coordinate species with a non bonding H1-H2 (1.75 Å) distance, an elongated Re-C1 (2.39 Å) distance and Re-H distances of 1.64 Å (Re-H1) and 1.68 Å (Re-H2), from which the product alkane is reductively eliminated. **TS2** and the trihydride **51PMe$_3$** possess structural similarities.

Figure 16: The optimized structures of the DFT model compounds **43-45PMe$_3$**, **52PMe$_3$**, **TS1** and **TS2**.

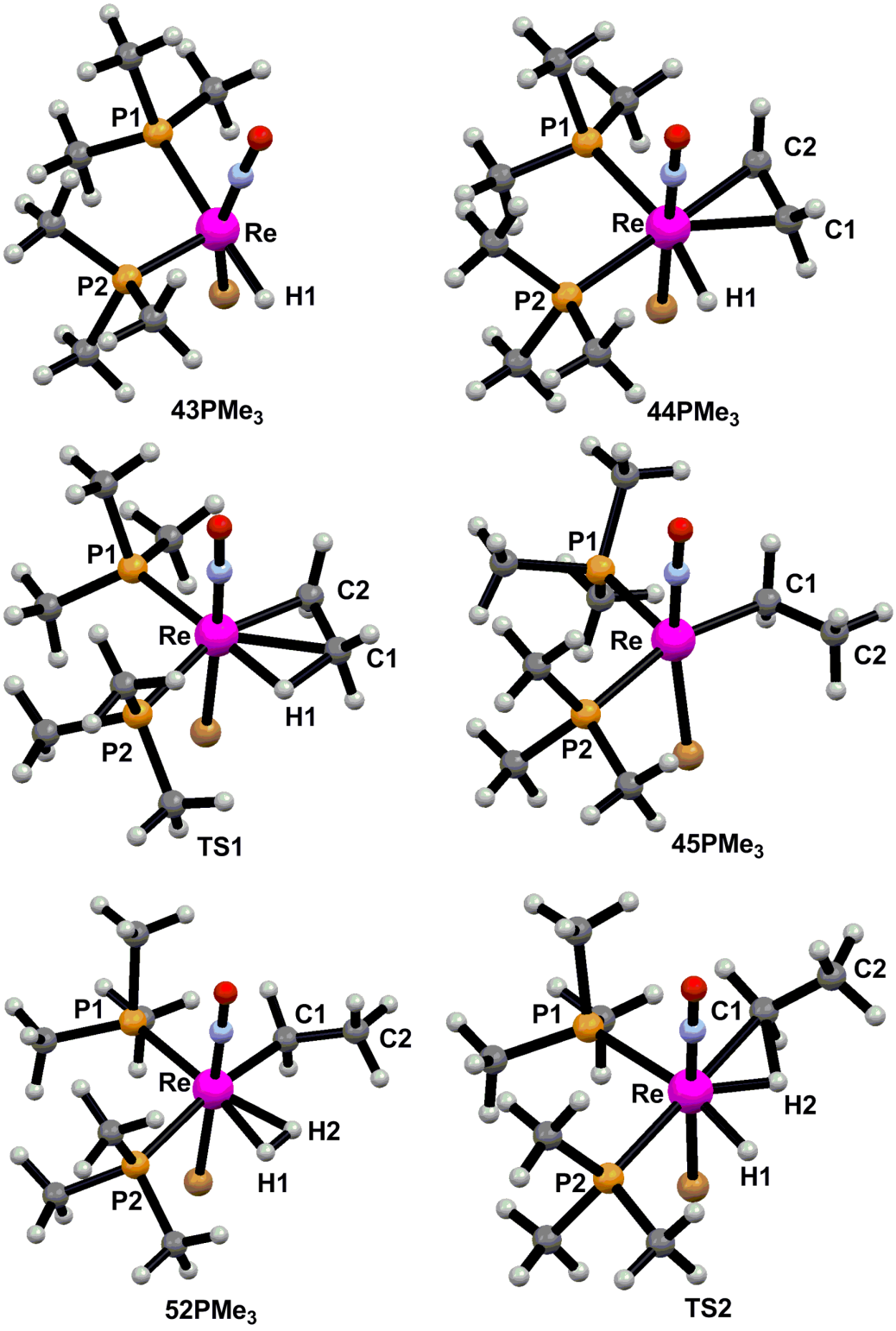

Selected bond lengths [Å]: **43PMe$_3$**: H1-Re 1.69; **44PMe$_3$** C1-C2 1.41, C1-Re 2.25, C2-Re 2.29, H1-Re 1.68; **45PMe$_3$**: C1-Re 2.18, C1-C2 1.54; **49PMe$_3$**: H1-Re 1.68, H2-Re 1.66, H3-Re 1.68; **51PMe$_3$**: H1-Re 1.69, N1-Re 2.09; **52PMe$_3$**: C1-Re 2.22, H1-H2 0.84, H1-Re 1.85, H2-Re 1.84; **TS1** C1-C2 1.45, C1-H1 1.51, C1-Re 2.32, C2-Re 2.22, H1-Re 1.75; **TS2** C1-Re 2.39, C1-H2 1.63, H1-H2 1.75, H1-Re 1.64, H2-Re 1.68. Selected bond angles [°]: **43PMe$_3$**: P1-Re-P2 C2-Re-C1, **44PMe$_3$**: C1-Re-H1 71.8, P1-Re-P2 95.1; **45PMe$_3$**: P1-Re-P2 102.4; **49PMe$_3$**: H1-Re-H2 60.0, H2-Re-H3 60.6, P1-Re-P3 94.7; 12PMe3: P1-Re-P2 99.2; **52PMe$_3$**: H1-Re-H2 26.4, H2-Re-C1 74.5, P1-Re-P2 99.8; **TS1**: C1-Re-C2 37.1, C1-Re-H1 40.5, P1-Re-P2 1.1.5;**TS2**: C1-Re-H2 42.9, H2-Re-H1 63.6, P1-Re-P2 95.5.

In both cases the P-Re-P angle is compressed to 94.7° (**49PMe$_3$**) and 95.5° (**TS2**), respectively (Figure 16, Figure 17). However, **49PMe$_3$** is not a transition state, but a minimum on the potential energy surface. Furthermore the binding of the three hydrides resembles the binding of the two hydrides and the alkyl moiety with the only difference that the alkyl moiety is pressed away by PMe_3 to the central hydride resulting in a C1-Re-H2 angle of 42.9°, which is comparable to the H1-Re1-C1 angle in **TS1**. Therefore **TS2** would represent neither an early nor a late transition state but rather a transient species, in which the oxidative addition of H_2 is accomplished proceeding along the lines of a concerted process.

Figure 17: The optimized structures of the DFT model compounds **49PMe$_3$** and **51PMe$_3$**.

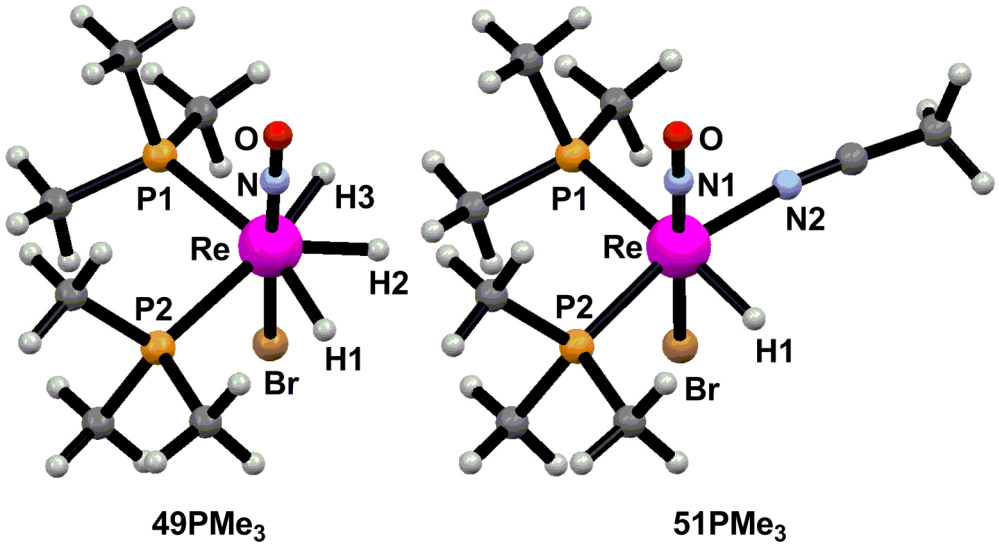

Selected bond lengths [Å]: **49PMe$_3$**: H1-Re 1.68, H2-Re 1.66, H3-Re 1.68; **51PMe$_3$** H1-Re 1.69, N2-Re 2.09 .Selected bond angles [°]: **49PMe$_3$**: H1-Re-H2 60.0, H1-Re-P2 72.5, H2-Re-H3 60.6, H3-Re-P1 71.2, P1-Re-P2 94.7; **51PMe$_3$**: H1-Re-N2 83.6, P1-Re-P2 99.2.

The DFT calculations allowed also assessing the stabilization of **43PMe$_3$** by the addition of H_2 or MeCN. In case of the addition of H_2 the trihydride **49PMe$_3$** is formed, which is -30.9 kJmol^{-1} stabilized compared to **43PMe$_3$**. In the case of the addition of MeCN (**51PMe$_3$**) the stabilization is much higher (-73.4 kJmol^{-1}) than that of the addition of H_2 (**49PMe$_3$**). However the stabilization of **43PMe$_3$** by the addition of ethylene (-88.0 kJmol^{-1}) leading to **44PMe$_3$** exceeds the stabilization energy of H_2 and MeCN complexations in order that H_2 and MeCN are easily displaced by ethylene. The stabilization energy of **43PMe$_3$** by dimerization has not been investigated, since one of the main aspects here are the steric congestions of the diphosphines, which cannot be modeled with two PMe_3 ligands. Nevertheless the results of the H_2-affinity experiments revealed that the MeCN complexes are thermodynamically favored over the formation of the dinuclear compounds of type **50** (Scheme 46).

Figure 18: Calculated energies of the structurally optimized model species of Scheme 51. The transition states **TS1** connect **44PMe$_3$** with **45PMe$_3$** and **TS2** connect **52PMe3** with the **43PMe$_3$**. For energetic comparison the various species are modified by the total energies the molecules indicated in the scheme.

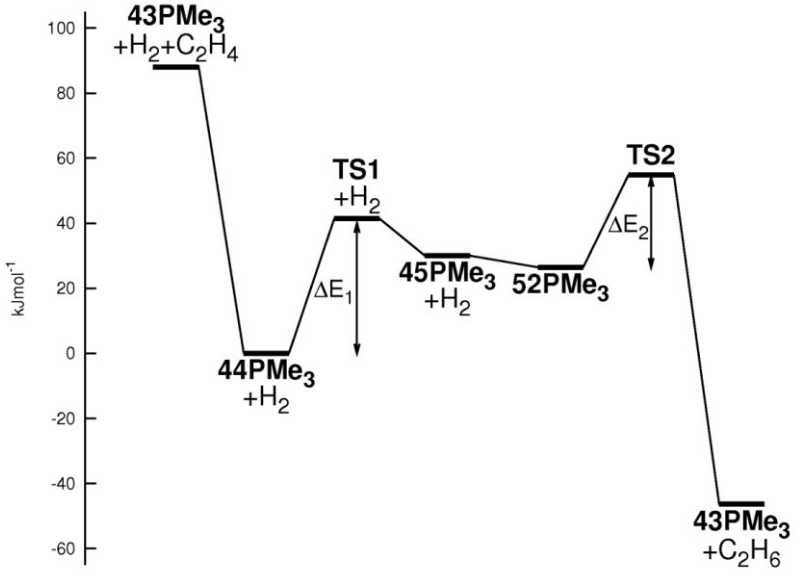

Table 6: P-Re-P angles and energies of selected structures of the catalytic cycle relative to **44PMe** + H_2.

Compound	Energy [kJmol^{-1}]	P-Re-P angle [°]
43PMe$_3$ + C_2H_4 + H_2	88.0	103.5
44PMe$_3$ + H_2	0.0	95.1
TS1 + H_2	41.4	101.5
45PMe$_3$ + H_2	30.0	102.4
52PMe$_3$	26.4	99.8
TS2	54.9	95.5
$\Delta E_{Hydr.}$	134.3	

6. Investigations on complexes bearing the Re(CO)(NO)(IMes)$_2$ fragment

6.1 The development of the [ReCl$_2$(CO)(NO)(IMes)$_2$] system

The chemistry of the [ReCl$_2$(CO)(NO)(IMes)$_2$] (**53**) system has been explored by M. Tymcio in her dissertation[95]. The main focus of her work was directed toward synthetic aspects. Therefore a few questions connected to the reactivity of **53** and related compounds remained. As we were interested in particular in the reactivity of these complexes towards H_2 and in their application in catalysis, we investigated the following aspects:

- Heterolytic H_2 activation with [ReCl(CO)(NO)(IMes)$_2$][BAr$^F{}_4$] (**54BAr$^F{}_4$**).
- The reactivity of the trichloroaluminoxy-(methylidene) complex [ReCl(C(OAlCl$_3$)CH$_3$)(NO)(IMes)$_2$] **55** towards H_2.
- The structure of the methyl complex [ReCl(Me)(CO)(NO)(IMes)$_2$] (**56**).

An introductory overview over selected parts of the known chemistry of **53** is given in Scheme 52.

Scheme 52: Synthesis and reactivity of **53**

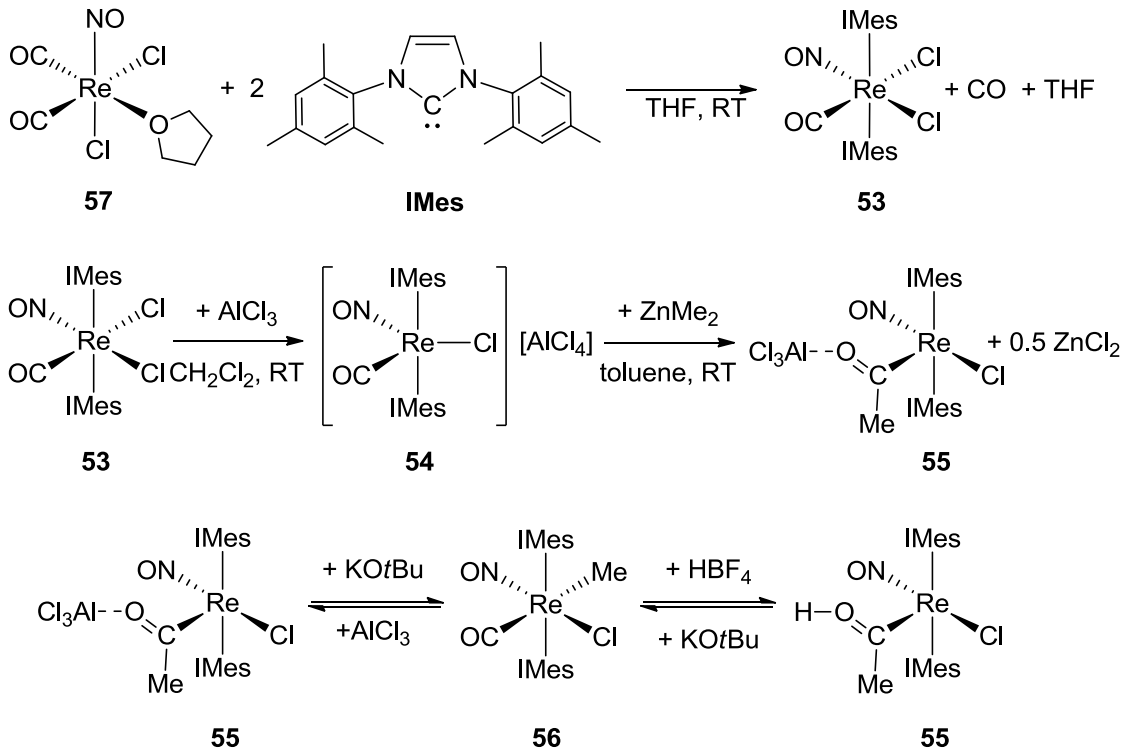

[95] Tymcio, M. A New Family of Nitrosyl Rhenium Complexes bearing the N-Heterocyclic Carbene Ligand IMes. Ph.D. Dissertation, University of Zürich, Zürich, 2007.

53 is obtained from the reaction of the readily accessible $[ReCl_2(CO)_2(NO)(THF)]$ (**57**) complex[96] by ligand substitution in >70% yield (Scheme 52). **53** turned out to be inert and needs thus chemical activation for further reactions. This activation is achieved by chloride abstraction with $AlCl_3$ to form the cationic 16e- complex $[ReCl(CO)(NO)(IMes)_2][AlCl_4]$ (**54**). **54** was shown to possess a high affinity to donor ligands. For example **54** reacts with MeCN to the cationic 18e- complex $[ReCl(CO)(MeCN)(NO)(IMes)_2][AlCl_4]$ (**58**). This illustrates the highly electrophilic character of the rhenium center. However the reaction with $ZnMe_2$ afforded not directly the expected methyl complex $[ReCl(Me)(CO)(NO)(IMes)_2]$ (**57**), but the trichloroaluminoxy-(methylidene) complex **55**. The formation of **55** can be explained with intermediate formation of **56** under the release of $AlCl_4^-$ and 0.5 Zn^{2+}. Under the given conditions the $AlCl_4^-$ anion is not stable and undergoes a metathesis reaction with Zn^{2+} forming $AlCl_3$ and $ZnCl_2$. $AlCl_3$ reacts subsequently with the intermediately formed **56** to **55**. However **56** was obtained by removing the $AlCl_3$ with KO*t*Bu from **55**. This reaction was shown to be reversible. Moreover the analogues behavior was found for the electrophiles H^+ ($[H(OEt_2)_x][BF_4]$) and Et^+ ($[OEt_3][BF_4]$).

Scheme 53: Hypothetic reactions of **54** with H_2

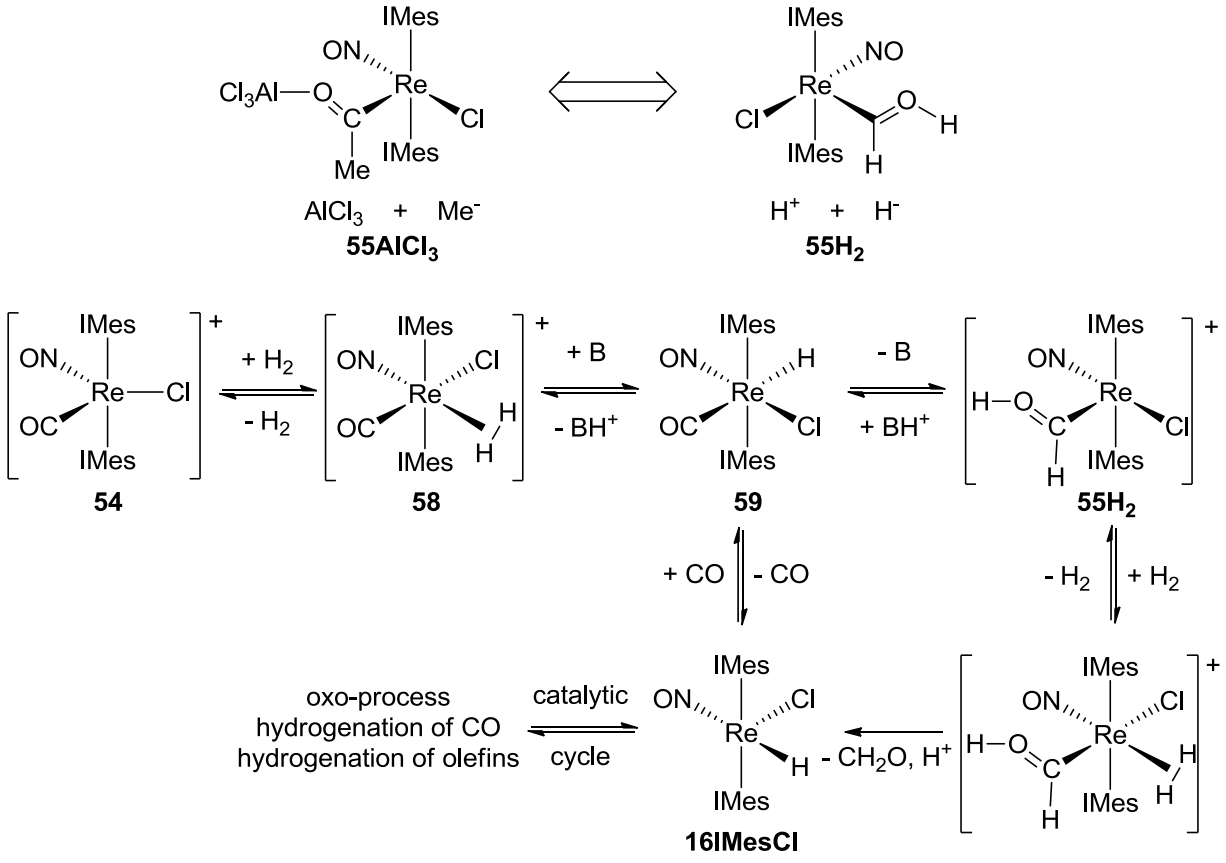

[96] Hund, H. U.; Ruppli, U.; Berke, H.. Chemistry of (Carbonyl)(nitrosyl)[bis(phosphorus donor)]rhenium Complexes. *Helv. Chim. Acta* **1993** *76,* 963–975.

This behavior prompted us to the question, whether we can substitute the Me group (acting as nucleophile) and $AlCl_3$ (acting as electrophile) with formal H^+ and H^- (Scheme 53). This might also give way to the catalytic reactions such as the CO reduction indicated in Scheme 53 and eventually preparative access to **16IMesCl**. Therefore we approached the hydrogen chemistry of **54**.

6.2 The reactivity of the $[ReCl(CO)(NO)(IMes)_2]^+$ cation towards H_2

Because **54** is difficult to crystallize/purify and since it has a high affinity to donor solvents, such as MeCN or THF, it is most conveniently prepared *in situ*. However the procedure with $AlCl_3$ is not suited for that purpose due to practical reasons (difficulty to weight small quantities and low solubility). Therefore Kobayashi's salt sodium tetrakis[3,5-bis(trifluoromethyl)phenyl]borate ($Na[BAr^F_4]$)[97] was employed to generate the unsaturated $[ReCl(CO)(NO)(IMes)_2][BAr^F_4]$ (**54BAr$^F_4$**) complex by a simple and very clean metathesis reaction (Scheme 54).

Scheme 54: The generation of **54BAr$^F_4$** by a simple metathesis reaction

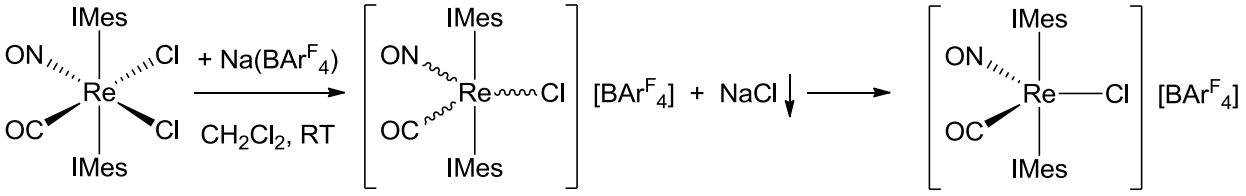

53 **54BAr$^F_4$A** **54BAr$^F_4$**

The reaction of **53** with $Na[BAr^F_4]$ in CH_2Cl_2 or toluene is very fast at room temperature. However it leads first to an intermediate compound (**54BAr$^F_4$A**), which is slowly converted to the final product **54BAr$^F_4$**. The intermediate **54BAr$^F_4$A** could not be isolated, but it posses distinct IR and NMR spectra (Table 7). The fact that the formation of **54BAr$^F_4$A** is accompanied by the formation of a precipitate (NaCl) indicates that **54BAr$^F_4$A** is an isomer of **54BAr$^F_4$** - especially since no precipitate is formed anymore during the isomerization of **54BAr$^F_4$A** to **54BAr$^F_4$**. The rate of isomerization depends on the concentration of the sample. A typical NMR sample with a concentration of approx. 25 $mmoL^{-1}$ is fully isomerized in 16 h at room temperature. More concentrated samples were found to isomerize faster.

Table 7: Selected spectroscopic data of **54**, **54BAr$^F_4$**, **54BAr$^F_4$A**

compound	IR (CH_2Cl_2) [cm^{-1}]		^{1}H-NMR (CD_2Cl_2): δ [ppm]					
	ν(NO)	ν(CO)	s, 4 H	s, 8H	s, 4H	s, 12 H	s, 12 H	s, 12 H
54BAr$^F_4$A	1750	1996	6.94	6.91	6.90	2.33	2.06	2.01
54BAr$^F_4$	1755	2012	7.09	6.94	6.91	2.41	1.93	1.86
54	1756	2011	7.12	6.95	6.92	2.42	1.93	1.86

[97] H. Nishida; N. Takada; M. Yoshimura; T. Sonoda; H. Kobayashi. Tetrakis[3,5-bis(trifluoromethyl)phenyl]borate. Highly Lipophilic Stable Anionic Agent for Solvent-extraction of Cations *Bull. Chem. Soc. Jpn.* **1984**, *57,* 2600–2604.

The spectroscopic features of **54BAr$^F_4$** parallel those of **54**. This indicates that the $AlCl_4^-$ counter ion of **54** is not coordinating to the complex and that **54BAr$^F_4$** and **54** have a similar structure. The structure of the intermediate **54BAr$^F_4$A** is unclear. However it might be speculated that it arises either from the isomerization of square pyramidal structure to the trigonal bipyramidal structure found for **54** or from rotation of the IMes ligands from the staggered conformation found in **53** to the eclipsed conformation found in **54** (Scheme 55)

Scheme 55: Possible isomerization processes from **54BAr$^F_4$A** to **54BAr$^F_4$**

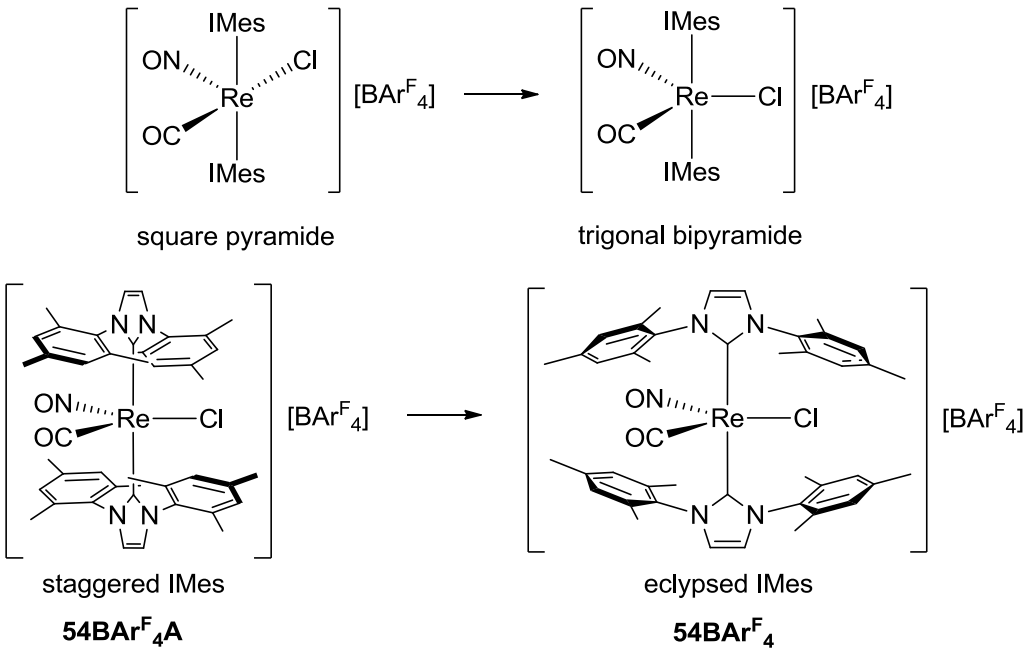

Exposing **54BAr$^F_4$** to H_2 leads to the slow formation of an inseparable mixture of decomposition products. In the NMR spectrum of **54BAr$^F_4$** in the presence of H_2, a remarkable broadening of the H_2 signal could be observed. The broadness and the chemical shift of the signal were found to depend on the H_2 and **54BAr$^F_4$** concentrations, as well as on the temperature. The NOE experiment revealed that upon saturation of the broadened H_2 signal, the IMes *o*-methyl groups showed a negative NOE effect. This indicates that a fraction of the H_2 molecules is bound to the rhenium center. Obviously a H_2 complex of the form $[ReCl(CO)(\eta^2\text{-}H_2)(NO)(IMes)_2][BAr^F_4]$ (**58**) is present. However the concentration of **58** could not be determined, as the NMR spectrum of **54BAr$^F_4$** in toluene in the presence of H_2 does not show any changes of the signals, which could be attributed to **58**. Attempts to slow down the observed H_2 exchange by lowering the temperature to 200 K failed, as well. Therefore the H_2 complex **58** could not be fully characterized by NMR spectroscopy. The strong dependence of the T1-relaxation time on the H_2 concentration (which could neither be determined, nor reliably adjusted) also prohibited T1-relaxation measurements. No spectroscopic evidence for the existence of the expected hydroxy carbene complex **60** was found either. As the H_2 complex is subject to side reactions, we attempted to trap it by deprotonation with a sterically hindered base.

Indeed the postulated H_2 complex **58** is deprotonated in the presence of stoechiometric amounts of 1,1,5,5-tetramethylpiperidine or 1,3,5-tri(*t*butyl)pyridine and two isomeric monohydrides **59a** and **59b** in approx. 4:5 ratio are formed.

Scheme 56: The formation of the monohydrides **59a** and **59b**

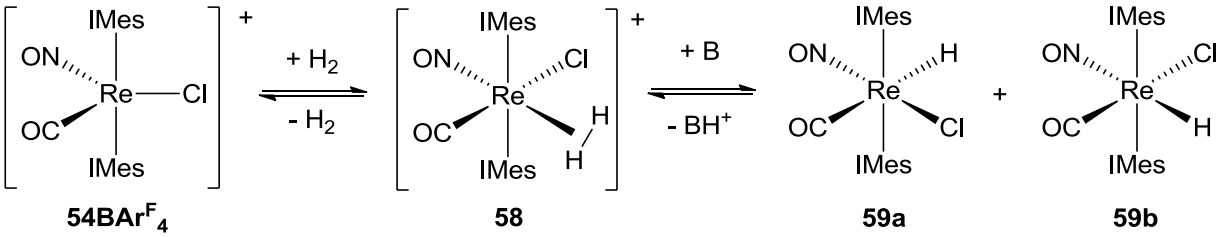

54BAr$^F_4$ **58** **59a** **59b**

The formation of the two isomers **59a** and **59b** was surprising, as one would expect that they are thermodynamically inequivalent due to their different structure. **59a** and **59b** could be separated by column chromatography on silica gel with 97:3 toluene/diethylether as eluent to obtain **59a** in 52% yield and **59b** in 39% yield. Alternatively **59a** can be obtained by the reaction of $[NBu_4][BH_4]$ and **54BArf-a** in 50% yield. The IR and the NMR spectra of **59a** and **59b** in toluene differ significantly (Table 8).

Table 8: Selected spectroscopic data of **59a** and **59b**

compound	IR (CH_2Cl_2) [cm^{-1}]		^{1}H-NMR (CD_2Cl_2): δ [ppm]					
	ν(CO)	ν(NO)	s, 4 H	s, 8H	s, 4H	Re-H	s, 12 H	s, 24 H
59a	1999	1657	6.67	6.09		4.77	2.21	2.11
59b	1926	1664	6.71	6.69	6.03	3.49	2.18	2.11

The IR spectra of **59a** and **59b** can be interpreted with help of the *trans*-influence concept. Since the hydride ligand induces a strong *trans*-effect, the ligand *trans* to the hydride would be more weakly bound compared to the same ligand *trans* to the chloride. In case of the NO and CO ligands, this would translate into a blue shift of the ν(CO) band or the ν(NO) band. Therefore the blue shift of the ν(CO) band in the IR spectra of **59a** indicates that the hydride ligand in **59a** is *trans* to the CO ligand, while in the case of **59b** the hydride ligand is in *trans* position to the NO ligand. The shift of the ν(NO) band of 7 cm^{-1} is not as pronounced as in case of the ν(CO) band, but it is consistent with respect to the assigned structures. Although the proton spectra of **59a** and **59b** differ significantly they cannot be interpreted in the same way. In order to further support the proposed structures an X-ray diffraction study has been carried out on single crystals of **59a** which indeed confirmed the structure assignment of **59a** and **59b** (Figure 19). Due to their different structures, **59a** or **59b** must be thermodynamically unequal. Therefore the isomerization of **59a** or **59b** is expected to occur, if a kinetically favorable mechanism exists. However samples of both isomers were found to be stable in solution indicating a high kinetic barrier for the isomerization process. Since an isomerization mechanism for octahedral coordinated complexes bearing bulky ligands usually cannot proceed over

an intermediate with a trigonal prismatic or a pentagonal pyramidal structure and all ligands of **59a** and **59b** are tightly bound, the kinetic stability of **59a** or **59b** towards isomerization is not surprising. Therefore $B(C_6F_5)_3$ was added as a catalyst to solutions of **59a** and **59b**. And indeed the isomerization of either **59a** or **59b** to mixtures of approx. 1:1 **59a**/**59b** could be observed. For this isomerization we suggest a mechanism according to Scheme 57.

Figure 19: ORTEP diagram of **59a** ellipsoids drawn at 50% probability, NO-Cl disorder omitted.

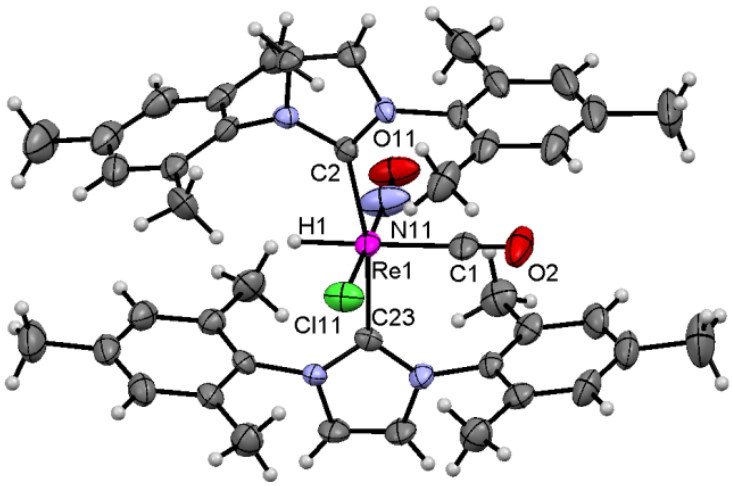

Selected bond distances [Å]: C1-Re1 1.980, C1-O2 1.143, C2-Re1 2.165, C23-Re1 2.164, Cl11-Re1 2.347, H1-Re1 1.490, N11-Re1 1.852, N11-O11 1.218. Selected bond angles [°]: C1-Re1-H1 176.3, C2-Re1-C23 168.9, Cl11-Re1-N11 178.7, O11-N11-Re1178.2, O2-C1-Re1 179.2.

This reaction is anticipated to proceed via reversible chloride abstraction from **59a**/**59b** and formation of the cationic hydride $[ReH(CO)(NO)(IMes)_2]^+$ (**61**). In **61** the hydride is expected to be flexibly and/or symmetrically bound to the rhenium center and thus the abstracted chloride can reenter the coordination sphere randomly forming either **59a** or **59b**. To further support this hypothesis, we approached the synthesis of **61** by irreversible chloride abstraction with Kobayashi's salt.

Scheme 57: The $B(C_6F_5)_3$ catalyzed isomerization of **59a/59b** via the cationic **61**.

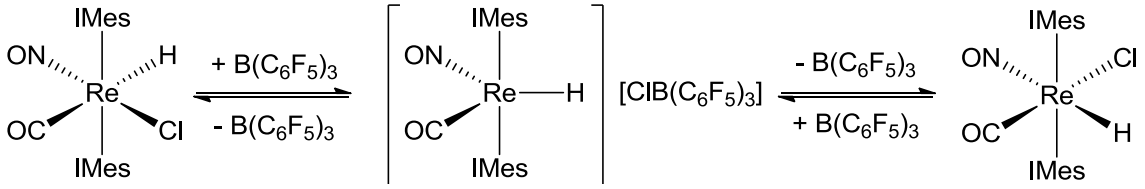

Indeed **61BAr$^F_4$** could be obtained in quantitative yield by the reaction of **59a/59b** with Kobayashi's salt. In the IR spectrum of **61BAr$^F_4$** a strong ν(CO) at 2016 cm^{-1} and a strong ν(NO) at 1694 cm^{-1} indicated the presence of the CO and the NO ligands. In the ^1H NMR spectrum, the expected signals

of the IMes ligand and the BAr^F_4 counter ion were observed. The rhenium hydride caused a broad resonance at 0.22 ppm. Hydrogenation experiments with ethylene and ethylene/CO were not successful. However **61BAr$^F_4$** was found to be an active catalyst for the H_2/D_2 isotope scrambling under mild conditions (80°C, 0.5 bar H_2, 0.5 bar D_2, 1 mg **61BAr$^F_4$**, 0.5 ml benzene, 30 min.).

Scheme 58: Synthesis of **61BAr$^F_4$**

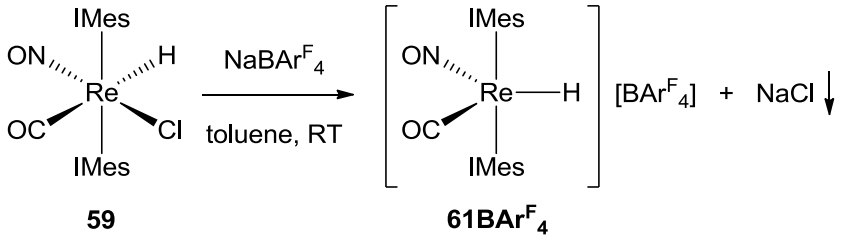

59 **61BAr$^F_4$**

To close this section on the H_2 activation a short interpretation of the found reactivity should be given. First of all, the NMR experiments and the heterolytic activation of H_2 with **54BAr$^F_4$** in the presence of a base clearly indicate the presence of the H_2 complex **58**. The fact that it can be deprotonated easily also reveals a kinetic pathway to form the desired hydroxy-carbene complex **55H$_2$**. As this complex could not be found in the reaction mixtures, it seems quite likely that it is thermodynamically disfavored. This is interesting, since the methyl analogue **55H$^+$** was prepared and characterized by M. Tymcio in our group. The only difference between those complexes is the substitution of the Me group in **55H$^+$** with a hydride in **55H$_2$**. Formally only a C-CH_3 bond is exchanged to a C-H bond. And since these bonds are usually thermodynamically comparable **55H$^+$** and **55H$_2$** are expected to be energetically comparable. And indeed the hypothetical model reactions of CO with H_2 or C_2H_6 to formaldehyde or acetone (calculated from tabulated $\Delta H_f^\ominus$ values) reveal only a difference of approx. 12.5 kJmol^{-1} in favor for the C-C bond.

$$CO(g) + H_2(g) \leftrightarrows CH_2O(g) \quad \Delta H = +1.9\ kJmol^{-1}\ [2]$$

$$CO(g) + 2\ C_2H_6(g) \leftrightarrows OC(CH_3)_2(g)\ \Delta H = -23.2\ kJmol^{-1}\ [2]$$

This demonstrates a tendency to weakly favor the formation of an acetyl-group over a formyl-group. However the binding situation in the rhenium complex is different since the acetyl/formyl group is protonated and the C=O bond is delocalized (Scheme 59). Therefore the hypothetical H_2/CH_4 exchange reaction was calculated employing the imidazolylidene model compounds (Scheme 59). The calculation revealed that neither **55ImH$^+$** nor **55ImH$_2$** are thermodynamically stable. Therefore it is not surprising that **55BAr$^F_4$H$_2$** could not be detected in solutions of **54BAr$^F_4$** and H_2.

Scheme 59: Various cationic model species and their energies relative to **55Im**.

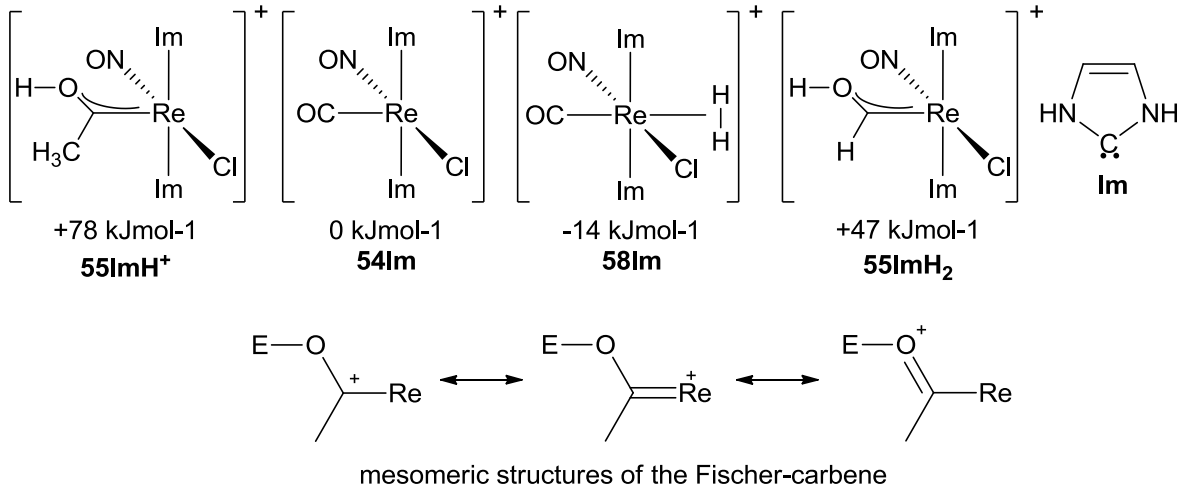

mesomeric structures of the Fischer-carbene

Furthermore these calculations suggest that the formation of **55H**$^+$ by the protonation of **56** is a kinetically controlled process. This is not surprising, since the oxygen lone pairs of the CO and the NO ligands are the only ones accessible. Protonation of the metal followed by reductive elimination of methane is unlikely, since all ligands are tightly bound to the metal and the IMes ligands shield the metal core very efficiently (Scheme 60).

Scheme 60: Rhenium in a nut shell ;-)

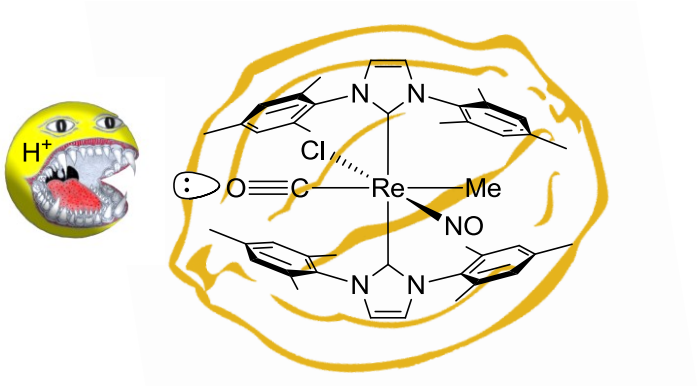

6.3 The attempted reaction of [ReCl(C(OAlCl$_3$)CH$_3$)(NO)(IMes)$_2$] with H$_2$

As shown in Scheme 52 the trichloroaluminoxy-(methylidene) complex **55** is obtained by the reaction of the cationic **54** complex with $ZnMe_2$. M. Tymcio showed that this complex possesses the structure of a distorted square pyramid. She synthesized a series of analogous complexes with different electrophiles on the oxygen via the direct reaction of **56** with these electrophiles and characterized them by X-ray diffraction studies.

Scheme 61: The reaction of **56** with the electrophile E (E=H^+, Et^+, $AlCl_3$) and the mesomeric structures of **56** compounds

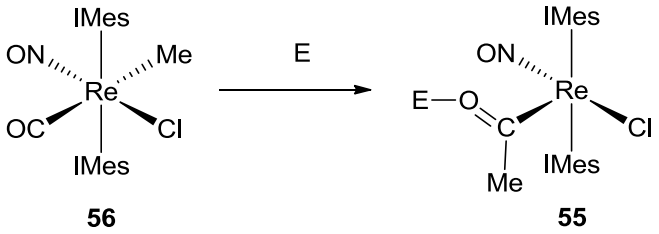

56 **55**

This series of compounds revealed that the electrophile on the oxygen has an enormous influence on the bonding of the Fischer carbene moiety to the rhenium center.

Table 9: Selected bond lengths for **56** compounds[95]

Compound	Re-C(OE)(Me) [Å]	ReC(-OE)(Me) [Å]
55AlCl$_3$	1.938	1.292
55H$^+$	1.922	1.342
55Et$^+$	1.911	1.422

From the data given in Table 9 it can be seen that $AlCl_3$ is the least electron withdrawing electrophile in the series with the CO bond still closer to the C=O double bond (approx. 1.2 Å) than to the C-O single bond (approx. 1.4Å)[2]. This encouraged us to probe the reactivity of **55AlCl$_3$** towards H_2. However the experiment showed that **55AlCl$_3$** did not react in the presence of H_2. This can be interpreted in terms of a very stable Fischer-carbene metal bond with strong backbonding. Moreover the geometry of **55** type compounds is unfavorable for the hydrogenolysis of the rhenium Fischer-carbene bond, since no *cis* coordination of H_2 is possible. Obviously the sum of all these factors prohibits the desired hydrogenolysis of the Re-(C(OE)(Me)) bond.

Another remaining question related to **55AlCl$_3$** is connected to the structure of **56**. Although **56** was fully characterized and no spectroscopic evidence for the presence of two isomers of **56** was found, an X-ray diffraction study suggested the presence of two isomeric forms analogous to the isomerism observed for the hydride complexes **59a** and **59b**[95]. Therefore the X-ray study on **56** was repeated. Since the crystals were previously obtained from THF/pentane, new crystals were grown from other solvent combinations. Finally the crystallization from toluene/pentane yielded X-ray suitable crystals, which clearly revealed that only the CO-*trans*-Me isomer **56a** is formed by the reaction of **55AlCl$_3$** with KO*t*Bu in THF (Figure 20). This is also in accordance with the DFT calculations performed on the [ReClMe(CO)(NO)(imidazolylidene)] model, which revealed the Me-*trans*-CO isomer to be ca. 6 $kJmol^{-1}$ more favorable than the Me-*trans*-NO isomer[95]. With the assumption that both isomers possess similar entropy, this energy difference would translate to K≈0.9 in favor for the CO-*trans*-Me isomer.

However the energy difference for the real system must be bigger in order to obtain solely the isomer **56a**.

Figure 20: ORTEP diagram of **56**, ellipsoids drawn at 50% probability , CO-Me disorder omitted.

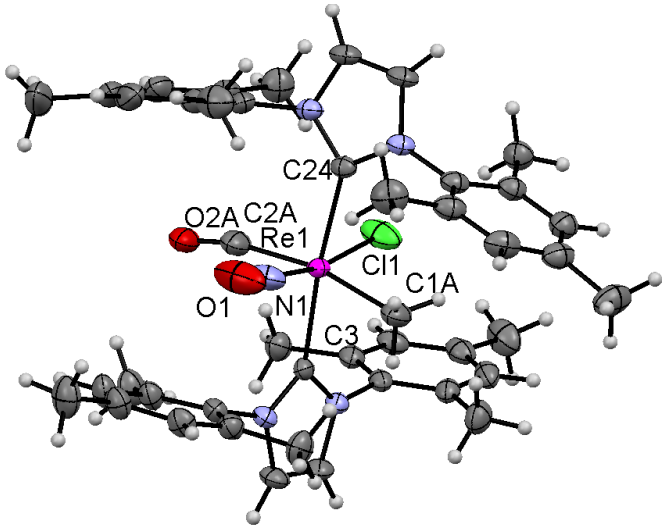

Selected bond lengths [Å]: Re1-C1A 2.095, Re1-C2A 1.931, Re1-C3 2.205, Re1-C24 2.210, Re1-Cl1 2.454, Re-N1 1.961, C2A-O2A 1.136, N1-O1 1.075. Selected bond angles [°]: C1A-Re-C2A 166.6, C3-Re1-C24 173.7, Cl1-Re1-N1 169.5, O1-N1-Re1 174.0, O2A-C2A-Re1 167.8.

In Addition to these thermodynamic considerations, the kinetic aspects of the formation of **56a** must not be omitted. The formation of the Me-*trans*-CO complex is from the kinetic point of view not the most favorable product, as one would expect the migration of the Me group to a *cis*-CO position. Therefore another isomerization step is required to form the final product **56a**. As this reaction occurs in the presence of $AlCl_3$, it seems likely that this isomerization proceeds in a similar way, as in case of the closely related **59** hydride complexes via reversible chloride abstraction and intermediate formation of a $[ReMe(CO)(NO)(IMes)_2]^+$ cation as depicted in Scheme 57.

7. Experimental Part

General considerations

All manipulations were performed under an atmosphere of dry nitrogen using either standard Schlenk techniques or an M-Braun glove box. All solvents were dried, distilled and degassed according to standard lab procedures. The diphosphine ligands, $[ReBr_5(NO)][NEt_4]_2$ and $[ReBr_2(MeCN)_3(NO)]$ were prepared according to published methods[66,67,88]. 1-hexene, styrene, α-methylstyrene and cyclohexene have been purchased from Sigma Aldrich and were dried, distilled and degassed according to standard lab procedures. Hydrogen and Deuterium were purchased from Pan Gas. NMR spectra were recorded on a Bruker AV-2 400/500 or a Varian Gemini 300 spectrometer. Chemical shifts are expressed in parts per million (ppm) and referenced to the solvents residual signals or in case of $^{31}P\{1H\}$ to the external standard 85% H_3PO_4 at δ = 0.0 ppm. NMR spectra simulation has been performed with the gNMR program package. IR spectra were recorded on a Bio Rad Excalibur spectrometer. Microanalyses were carried out at the Anorganisch-Chemisches Institut of the University of Zürich.

Computational methods: The model calculations were performed analogously to the investigations on the related *trans*-phosphine system $[ReH_2(\eta^2\text{-}C_2H_4)(NO)(PMe_3)_2]$ investigated by Liu et al.[70] using the B3LYP functional[98] in combination with a G6-31*+ basis[99] for the elements H-P and a Hay and Wadt ECP basis[100] with f polarization functions for Re and Br. The gamess[101] program package was employed for these calculations. Solvent effects were neglected. The character of the stationary points was verified by a normal mode analysis. All ZPE corrections are included in the energies. Free energies were calculated at 25°C.

Kinetic measurements/catalysis: Kinetic measurements were monitored via the gas consumption by means of a Büchi press gas flow controller attached to a 45 mL steel autoclave with a resolution of 0.045 mmol. The temperature was controlled with a large oil or water bath. The products were identified by NMR spectroscopy.

---

[98] Lee, C.; Yang, W.; Parr, R. G. Development of the Colle-Salvetti correlation-energy formula into a functional of the electron density. *Phys. Rev. B* **1988,** *37,* 785–789.
Miehlich, B.; Savin, A.; Stoll, H.; Preuss, H. Results obtained with the correlation energy density functionals of becke and Lee, Yang and Parr. *Chem. Phys. Lett.* **1989,** *157,* 200–206.

Becke, A. D. Density-functional thermochemistry. III. The role of exact exchange. *J. Chem. Phys.* **1993,** *89,* 5648–5653.

[99] Hariharan, P. C.; Pople, J. A. The influence of polarization functions on molecular orbital hydrogenation energies. *Theor. Chim. Acta* **1978,** *28,* 213–312.

[100] Hay, J. P.; Wadt, W. R. Ab initio effective core potentials for molecular calculations. Potentials for K to Au including the outermost core orbitals. *J. Chem. Phys.* **1985,** *82*, 299–311.

[101] Schmidt, M. W.; Baldridge, K. K.; Boatz, J. A.; Elbert, S. T.; Gordon, M. S.; Jensen, J. H.; Koseki, S.; Matsunaga, N.; Nguyen, K. A.; Su, S. J.; Windus, T. L.; Dupuis, M.; Montgomery, J. A. *J. Comput. Chem.* **1993,** 14, 1347-1363.

$[ReBr_2(\eta^2\text{-}C_2H_4)(NO)(PPh_3)_2]$ (17PPh$_3$Br)

A suspension of $[ReBr_2(NO)(OH_2)(PPh_3)_2] \cdot 2$ THF (0.200 g, 0.18 mmol) in THF (5 mL) in a 50 mL Young Schlenk tube with a magnetic stirring bar was stirred for 16 h under 2 bar of ethylene. During this time a pale, light brown solid formed. Hexane (5 mL) was then added carefully and the mixture was allowed to rest over night. The solid was filtered off and dried *in vacuo* to yield $[ReBr_2(\eta^2\text{-}C_2H_4)(NO)(PPh_3)_2] \cdot$ THF (0.157 g, 0.16 mmol, 83%).

IR (cm^{-1}, KBr pellet): 1704 (s, ν(NO)). ^{1}H NMR (THF-d8, 295K, 300 MHz): δ = 8.0-7.8 (m, 12 H, PPh_3), 7.4-7.3 (m, 18 H, PPh_3), 2.370 (t, $^3J_{PH}$ 3Hz, 4 H, C_2H_4) ppm. $^{13}C\{^1H\}$-NMR (THF-d8, 295K, 300 MHz): δ = 135.8 (t, J_{PC} = 4 Hz, PPh_3), 132.4 (t , J_{PC} = 24 Hz, PPh_3), 130.8 (s, PPh_3), 128.4 (t , J_{PC} = 5 Hz, PPh_3), 49.4 (s, C_2H_4) ppm. $^{31}P\{^1H\}$ NMR (THF-d8, 295K, 121 MHz): δ = – 12.2 (s, PPh_3) ppm. Anal. Calcd. for $C_{43}H_{51}N_5O_2Re$ (928.65): C, 53.84; H, 3.92; N, 1.65. Found: C, 53.69; H, 4.00; N, 1.62.

$[ReCl_2(\eta^2\text{-}C_2H_4)(NO)(PPh_3)_2]$ (17PPh$_3$Cl)

A suspension of $[ReCl_2(NO)(PPh_3)_3]$ (0.550 g, 0.52 mmol) in toluene (10 mL) in a 50 mL Young Schlenk tube with magnetic stirring bar was stirred for 8 h at RT under an atmosphere of 2 bar ethylene. During this time the yellow $[ReCl_2(NO)(PPh_3)_3]$ dissolved and a pale solid was formed. A layer of hexane (10 mL) was carefully added and the mixture was allowed to stand overnight. The precipitate was filtered off, rinsed with hexane (3×5 mL) and dried *in vacuo* to yield $[ReCl_2(\eta^2\text{-}C_2H_4)(NO)(PPh_3)_2]$ (0.400 mg, 0.47 mmol, 90%).

IR (cm^{-1}, KBr pellet): 1699 (s, ν(NO)). ^{1}H NMR (THF-d8, 295K, 300 MHz): δ = 8.0-7.8 (m , 12H, PPh_3), 7.4-7.3 (m, 18 H, PPh_3), 2.250-2.050 (m, C_2H_4) ppm. $^{13}C\{^1H\}$ NMR (THF-d8, 295K, 75 MHz): δ = 135.8 (t, J_{PC} = 4 Hz, PPh_3), 132.0 (t, J = 24 Hz, PPh_3), 130.9 (s, PPh_3), 128.9 (t, J_{PC} = 5 Hz, PPh_3), 50.2 (s, C_2H_4) ppm. $^{31}P\{^1H\}$ NMR (THF-d8, 295K, 121 MHz): δ = – 2.0 (s, PPh_3) ppm. Anal. Calcd. for $C_{43}H_{51}N_5O_2Re$ (839.11): C, 54.35; H, 4.08; N, 1.67. Found: C, 54.14; H, 4.00; N, 1.56.

$[ReHCl(\eta^2\text{-}C_2H_4)(NO)(PPh_3)_2]$ (18PPh$_3$Cl)

$[ReHCl(\eta^2\text{-}C_2H_4)(NO)(PPh_3)_2]$ was obtained analogously to $[ReHBr(\eta^2\text{-}C_2H_4)(NO)(PPh_3)_2]$ in 81% yield.

IR (cm^{-1}, KBr pellet): 1905 (s, ν(ReH)), 1683 (s, ν(NO)). ^{1}H NMR (THF-d8, 295K, 300 MHz): δ = 7.736 (m, 12 H, PPh_3), 7.393 (m, 18 H, PPh_3), 4.932 (t, $^3J_{PH}$ = 31.0 Hz, 1 H, ReH), 2.660 (d, J = 10.5 Hz, 2 H, C_2H_4), 1.816 (d, J = 10.5 Hz, 2 H, C_2H_4) ppm. $^{13}C\{^1H\}$ NMR (THF-d8, 295K, 75 MHz): δ = 135.4 (t , J_{PC} = 4.8 Hz, PPh_3), 133.9 (t, J_{PC} = 24.5 Hz, PPh_3), 131.0 (s, PPh_3), 128.8 (t, J_{PC} = 4.9 Hz) 50.6 (s, C_2H_4) ppm. $^{31}P\{^1H\}$ NMR (THF-d8, 295K, 121 MHz): δ = 13.6 (s, PPh_3) ppm. Anal. Calcd. for $C_{38}H_{35}ClNOP_2Re$ (805.30): C, 56.68; H, 4.38; N, 1.74. Found: C, 56.55; H, 4.18; N, 1.57.

[ReHBr(η^2-C_2H_4)(NO)(PPh_3)$_2$] (18PPh_3Br)

Representative procedure for [$ReBr_2(OH_2)(NO)(PPh_3)_2$]: A suspension of [$ReBr_2(NO)(OH_2)(PPh_3)_2$] · 2 THF (0.250 g, 0.24 mmol) in toluene (5 mL) and $HSiEt_3$ (1 mL, 5.78 mmol) was placed in a 50 mL Young Schlenk with magnetic stirring bar. The suspension was then stirred 16 h at 80°C under 2 bar of ethylene. After cooling to room temperature, the volatiles were removed *in vacuo*. The solid residue was washed with pentane (3×3 mL) and recrystallized from toluene/pentane to yield [ReHCl(η^2-C_2H_4) (NO)(PPh_3)$_2$] (143 mg, 70%) as pale solid.

IR (cm^{-1}, KBr pellet): 1906 (s, ν(ReH)), 1682 (s, ν(NO)). ^{1}H NMR (THF-d8, 295K, 300 MHz): δ = 7.585 (m, 12 H, PPh_3), 7.464 (m, 18 H, PPh_3), 4.485(t, $^3J_{PH}$ = 22.2 Hz, 1 H, ReH), 2.729 (d, *J* = 10.5 Hz, 2 H, C_2H_4), 1.888 (d, *J* = 10.5 Hz, 2 H, C_2H_4) ppm. ^{13}C{^{1}H} NMR (THF-d8, 295K, 75 MHz): δ = 135.8 (t , J_{PC} 4.8 Hz, PPh_3), 133.8 (t, J_{PC} = 24.0 Hz, PPh_3), 130.9 (s, PPh_3), 128.7 (t, J_{PC} = 4.6 Hz, PPh_3) 49.5 (s, C_2H_4) ppm. ^{31}P{^{1}H} NMR (THF-d8, 295K, 121 MHz): δ 11.4 (s, PPh_3) ppm. Anal calcd for $C_{38}H_{35}BrNOP_2Re$ (849.75): C, 53.71; H, 4.15; N, 1.65. Found: C, 53.69; H, 4.00; N, 1.62.

[ReHI(η^2-C_2H_4)(NO)(PPh_3)$_2$] (18PPh_3I)

[ReHCl(η^2-C_2H_4) (NO)(PPh_3)$_2$] was obtained analogous to [ReHCl(η^2-C_2H_4) (NO)(PPh_3)$_2$] in 64% yield.

IR (cm^{-1}, KBr pellet): 1912 (s, ν(ReH)), 1676 (s, ν(NO)). ^{1}H NMR (THF-d8, 295K, 300 MHz): δ = 7.971 (m, 12 H, PPh_3), 7.402 (m, 18 H, PPh_3), 3.744 (t, $^3J_{PH}$ = 29.8 Hz, 1 H, ReH), 2.782 (d, *J* = 11.0 Hz, 2 H, C_2H_4), 2.035 (d, *J* = 11.0 Hz, 2 H, C_2H_4) ppm. ^{13}C{^{1}H} NMR (THF-d8, 295K, 75 MHz): δ = 135.5 (t, J_{PC} = 9.4 Hz, PPh_3), 134.1 (t, J_{PC} = 24.9 Hz, PPh_3), 131.0 (s, PPh_3), 128.7 (t, J_{PC} = 4.8 Hz, PPh_3), 47.5 (s, C_2H_4) ppm. ^{31}P{^{1}H} NMR (THF-d8, 295K, 121 MHz): δ 5.0 (s, PPh_3) ppm. Anal calcd for $C_{38}H_{35}INOP_2Re$ (896.75): C, 50.90; H, 3.93; N, 1.56. Found: C, 51.02; H, 3.98; N, 1.51.

[ReH_2(η^2-C_2H_4)(NO)(PPh_3)$_2$] (24PPh_3) and [ReH(Et)(η^2-C_2H_4)(NO)(PPh_3)$_2$] (33PPh_3)

A suspension of [ReH(η^2-BH_4)(NO)(PPh_3)$_2$] (0.250 g, 0.33 mmol) in THF (5 mL) in a Young Schlenk tube with magnetic stirrer was stirred at 0°C for 15 min. under an atmosphere of 2 bar ethylene. The orange suspension turned into a bright yellow solution during this time. The solvent was removed *in vacuo* leaving the products as yellow foam. The yellow foam was twice dissolved in 2 mL THF and dried *in vacuo* yielding a bright yellow oil.

NMR spectroscopic data of [ReH_2(η^2-C_2H_4)(NO)(PPh_3)$_2$]: ^{1}H NMR (C_6D_6, 300K, 500 MHz): δ = 7.860 (m, 12 H, PPh_3), 7.25-6.90 (m, 18 H, PPh_3), 2.844 (m, 2 H, C_2H_4), 2.763 (m, 2 H, C_2H_4), 1.507 (td, J_{PH} = 36.5 Hz, J_{HH} = 7.4 Hz, 1 H, ReH), -3.287 (td, J_{PH} = 27.6 Hz, J_{HH} = 7.4 Hz, 1 H, ReH) ppm. ^{13}C{^{1}H} NMR (C_6D_6, 295K, 125 MHz): δ = 136.89 (t, J_{PC} = 25.0 Hz, PPh_3), 134.6 (t, J_{PC} = 5.0 Hz, PPh_3), 130.0, 128.2-127.5 (m, PPh_3 and C_6D_6), 35.8 (s, C_2H_4) ppm. ^{31}P NMR (C_6D_6, 300K, 200 MHz): δ = 28.5 (dd, J_{HP} = 36.5 Hz, J_{HP} = 27.6 Hz, PPh_3) ppm.

NMR spectroscopic data of [ReH(Et)(η^2-C_2H_4)(NO)(PPh_3)$_2$]: ^{1}H NMR (C_6D_6, 300K, 500 MHz): δ = 7.956 (m, 12 H, PPh_3), 7.25-6.90 (m, 18 H, PPh_3), 2.939 (d, J_{HH} = 10.2 Hz, 2 H, C_2H_4), 2.908 (t, J_{PH} = 31.8 Hz, 1 H, ReH), 2.117 (d, J_{HH} = 10.2 Hz, 2 H, C_2H_4), 0.675 (t, $^3J_{HH}$ = 7.3 Hz, 3 H, ReEt), -1.168 (t br, $^3J_{HH}$ = 7.3 Hz, 2 H, ReEt) ppm. ^{13}C{^{1}H} NMR (C_6D_6, 295K, 125 MHz): δ = 136.89 (t, J_{PC} = 25.0 Hz, PPh_3), 134.8 (t, J_{PC} = 5.0 Hz, PPh_3), 131.2 (s, PPh_3), 128.2-127.5 (m, PPh_3 and C_6D_6), 42.9 (s, C_2H_4), 20.0 (s, ReEt), 19.0 (s, ReEt) ppm. ^{31}P NMR (C_6D_6, 300K, 200 MHz): δ = 20.4 (d, J_{HP} = 31.8 Hz, PPh_3) ppm.

IR spectroscopic data of [ReH_2(η^2-C_2H_4)(NO)(PPh_3)$_2$] and NMR spectroscopic data of [ReH(Et)(η^2-C_2H_4)(NO)(PPh_3)$_2$]: IR (cm^{-1}, KBr pellet): 1959 (m, ν(ReH)), 1897 (m, ν(ReH)), 1815 (m, ν(ReH)), 1630 (s, ν(NO)).

[ReH_2(η^2-C_2H_4)(η^4-butadiene)(NO)(PPh_3)] (34PPh_3)

[ReH(η^2-BH_4)(NO)(PPh_3)$_2$] (0.010 g, 0.013 mmol) was placed in a NMR-tube with a Young Teflon cap and THF (0.6 mL) was added. An atmosphere of 2 bar ethylene was established in the tube and the sample was vigorously shaken until it completely dissolved. After 16 h, the formation of [ReH_2(η^2-C_2H_4)(η^4-butadiene)(NO)(PPh_3)] was complete.

IR (cm^{-1}, KBr pellet): 1640 (s, ν(NO)). ^{1}H NMR (C_6D_6, 300K, 500 MHz): δ =7.7-6.9 (m, 30 H, free and bound PPh_3) 5.748 (q, J_{HH} = 6 Hz, 1 H, CH_2=C*H*-CH=CH_2), 5.423 (q, J_{HH} = 6.5 Hz, 1 H, CH_2=C*H*-CH=CH_2), 2.497 (t, J_{HH} = 9.5 Hz, 1 H, C_2H_4), 2.233 (m, 2 H, C*H*$_2$=CH-CH=CH_2, C_2H_4), 1.660 (d, J_{HH} = 7.7 Hz, 2 H, C_2H_4), 0.149 (m, 1 H, C*H*$_2$=CH-CH=CH_2), -0.532 (dd, J_{HH} = 6.5, J_{HH} = 3.5 Hz, 1 H, C*H*$_2$=CH-CH=CH_2), 1.551 (dd, , J_{HH} = 7.1, J_{HH} = 3.9 Hz, 1 H, C*H*$_2$=CH-CH=CH_2) ppm. ^{13}C{^{1}H} NMR (C_6D_6, 300K, 125 MHz): δ =134.2 (d, J_{PC} = 20 Hz, PPh_3), 133.6 (d, J_{PC} = 10 Hz, PPh_3), 129.9 (d, J_{PC} = 3 Hz, PPh_3), 128.9-128 (overlapping m, PPh_3, C_6D_6), 100.8 (s, CH_2=*C*H-CH=CH_2), 83.0 (s, C*H*$_2$=CH-CH=CH_2), 43.5 (d, J_{PC} = 3.8 Hz, *C*H_2=CH-CH=CH_2), 35.7 (d, J_{PC} = 6.3 Hz, *C*H_2=CH-CH=CH_2), 31.3 (d, J_{PC} = 7.5 Hz, *C*$_2H_2$), 25.3 (d, J_{PC} = 3.8 Hz, *C*$_2H_2$) ppm. ^{31}P{^{1}H} NMR (C_6D_6, 300K, 200 MHz): δ = 22.4 (s, bound PPh_3), -5.3 (free PPh_3) ppm.

[$ReBr_2$(NO)(OH_2)(PPh_3)$_2$]·2 THF (36PPh_3Br)

To a refluxing suspension of [ReH_2(NO)(PPh_3)$_2$] (1.0 g, 1.00 mmol) in ethanol (20 mL) aqueous 48% HBr (0.5 ml, 4.40 mmol) was added drop wise. The evolution of H_2 was observed immediately and the color of the solid changed from yellow to brick-red. After gas evolution ceased, the suspension was kept refluxing for additional 15 min. and was then allowed to cool to room temperature before the solid was filtered off. The solid was rinsed with ethanol (3×10 mL) and recrystallized from THF/hexane to yield [$ReBr_2$(NO)(OH_2)(PPh_3)$_2$] · 2 THF (0.7 g, 0.66 mmol, 66 %).

IR (cm^{-1}, KBr pellet): 1670 (s, ν(NO)). ^{1}H NMR (THF-d8, 295K, 300 MHz): δ = 7.8-7.7 (m, 12H, PPh_3), 7.4-7.2 (m, 18 H, PPh_3), 5.476 (s, 2 H, H_2O), 3.7-3.6 (m, 8 H, THF), 1.8-1.6 (m, 8 H, THF) ppm. ^{13}C{^{1}H} NMR (THF-d8, 295K, 75 MHz): δ = 135.0 (t, J_{PC} = 5 Hz, PPh_3), 133.6 (t , J_{PC} = 22.0 Hz, PPh_3), 129.6 (s,

PPh_3), 127.4 (t, J_{PC} = 4 Hz, PPh_3), 68-66 (m, THF), 28-24 (m, THF) ppm. $^{31}P\{^1H\}$ NMR (THF-d8, 295K, 121 MHz): δ = 8.5 (s, PPh_3) ppm. Anal. Calcd. for $C_{43}H_{51}N_5O_2Re$ (1060.80): C, 49.72; H, 4.55; N, 1.32. Found: C, 49.57; H, 4.49; N, 1.25.

$[ReI_2(NO)(OH_2)(PPh_3)_2]\cdot 4$ THF (36PPh_3I)

$[ReH_2(NO)(PPh_3)_3]$ (0.500 g, 0.50 mmol) was suspended in ethanol (5 mL) in a 50 mL Schlenk tube with a magnetic stirring bar. Aqueous 67% HI (0.150 mL, 1.54 mmol) solution was added drop wise to the stirred suspension in the dark. Immediately gas evolution was observed and the color changed from bright yellow to pale olive green. The suspension was allowed to stir additional 16 h before the solid was filtered off and washed with ethanol (3×10 mL). The solid was then recrystallized from THF/pentane to afford [ReI2(OH2)(PPh3)2] · 4 THF (0.380 mg, 0.31 mmol, 62%) as olive green powder.

IR (cm^{-1}, KBr pellet): 1668 (s, ν(NO)). ^1H NMR ($CDCl_3$, 300K, 500 MHz): δ = 7.85-7.75 (m, 12 H, PPh_3), 7.38-7.7.32 (m, 18 H, PPh_3), 3.627 (m, 18 H, THF), 1.829 (m, 2 H, OH_2), 1.748 (m, 18 H, THF) ppm. $^{13}C\{^1H\}$ NMR ($CDCl_3$, 300K, 125 MHz): δ = 134.7 (t, J_{CP} = 5.1 Hz, PPh_3), 133.8 (t, J_{CP} = 23.5 Hz, PPh_3), 129.9 (s, PPh_3), 128.2 (t, J_{CP} = 4.9 Hz, PPh_3), 68.0 (s, THF), 67.2 (m, THF), 25.6 (s, THF), 24.6 (s, THF) ppm. $^{31}P\{^1H\}$ NMR ($CDCl_3$, 200 MHz, 300 K): δ = 9.3 ppm. Anal. Calcd. for $C_{52}H_{64}I_2NO_6P_2Re$ (1301.03): C, 48.00; H, 4.96; N, 1.08. Found: C, 47.86; H, 4.96; N, 1.14.

$[ReBr_2(MeCN)(NO)(dppfc)]$ (40a)

Method 1: $[ReBr_2(MeCN)_3(NO)(THF)]$ · 2 THF (0.240 g, 0.356 mmol) and 1,1' -bisdiphenylphosphinoferrocene (0.224 g, 0.404 mmol) were suspended in THF (10 mL) in a Schlenk tube with magnetic stirring bar. The mixture was stirred 5 h at 60°C. The resulting precipitate was filtered of, washed with a minimum of THF and dried *in vacuo* yielding (0.250 g, 0.239 mmol, 67%) **40a**·2 THF.

Method 2: A mixture of $[ReBr_5(NO)][NEt_4]_2$ (1.003 g, 1.1 mmol) and 1,1´-bisdiphenyl-phosphinoferrocene (1.250 g, 2.3 mmol) were suspended in THF (3 mL) and MeCN (7 mL) in a 50 mL Schlenk tube with magnetic stirrer. The suspension was stirred for 12 h at 80°C. The precipitate was filtered off and the solid residue was washed with 3 mL portions of EtOH until it was bright yellow. After drying *in vacuo* **40a** · 2 THF (0.910 g, 0.8 mmol, 74%) was obtained as a bright yellow powder.

IR (cm^{-1}, KBr pellet): 1685 (s, ν(NO)). ^1H NMR (500 MHz, $CDCl_3$, 27°C): δ = δ 8.09 (m, 2 H, phenyl), 7.00 (m, 2 H, phenyl), 7.53 (m, 4 H, phenyl), 7.43 (s, 4 H, phenyl), 7.32 (m, 8 H, phenyl), 5.82 (s, 1 H, cp), 4.50 (s, 1 H, cp), 4.44 (s, 1 H, cp), 4.38 (s, 1 H, cp), 4.24 (s, 1 H, cp), 4.22 (s, 2 H, cp), 3.91 (s, 1 H, cp), 2.24 (s, 3 H, acetonitrile) ppm. $^{31}P\{^1H\}$ NMR (202 MHz, $CDCl_3$, 27°C): δ = 4.95 (s broad, 1 P); -0.71

(s broad, 1 P) ppm. Anal. Calcd. for $C_{40}H_{39}Br_2FeN_2OP_2Re$ (1043.56 $gmol^{-1}$): C, 46.04; H, 3.77; N, 2.68. Found: C, 46.00; H, 3.75; N, 2.59.

[$ReBr_2$(MeCN)(NO) (d*i*prpfc)] (40b)

Method 1: A solution of [$ReBr_2(MeCN)_2(NO)(THF)$] · 2 THF (0.100 g, 0.148 mmol) and 1,1'-bisdiisopropylphosphinoferrocene (0.068 g, 0.162 mmol) in DCM (5 mL) was stirred 4 h at room temperature in a 20 mL scintillator vial . Then hexane (10 mL) was added and the solvent was removed *in vacuo*. The remaining dark brown solid was washed with THF (3×0.5 mL) and dried *in vacuo* to yield **40b (**0.044 g, 0.053 mmol, 32%) as a yellow powder.

Method 2: A suspension of [{$ReBr_2$(d*i*prpfc)(NO)}$_2$] (0.300 g, 0.38 mmol), DCM (10 mL) and acetonitrile (1 mL) was stirred for 4 h at room temperature in a 20 mL. During this time the solid dissolved and a yellow solution formed. The solvent was removed *in vacuo* and **40b** was obtained quantitatively.

IR (cm^{-1}, KBr pellet): 1683 (s, ν(NO)). ^{1}H NMR (500 MHz, $CDCl_3$, 27°C): δ = 4.886 (s, 1 H, cp), 4.588 (s, 1 H, cp), 4.392 (s, 1 H, cp), 4.371 (s, 4 H, cp), 4.274 (s, 1 H, cp), 3.719 (s, 1 H, *i*pr C*H*$(CH_3)_2$), 3.199 (s, 1 H, *i*Pr C*H*$(CH_3)_2$), 3.007 (s, 1 H, *i*Pr C*H*$(CH_3)_2$), 2.769 (m, 1 H, *i*Pr C*H*$(CH_3)_2$, 3 H, C*H*$_3$CN), 1.633-1.102 (m, 24 H, *i*Pr CH(C*H*$_3)_2$) ppm. ^{31}P{^{1}H} NMR (202 MHz, $CDCl_3$, 28°C): δ = δ 2.27 (s, broad); 0.86 (s, broad) ppm. Anal. Calcd. For $C_{24}H_{39}Br_2FeN_2OP_2Re$ (835.39 $gmol^{-1}$): C, 34.51; H, 4.71; N, 3.35. Found: C, 34.33; H, 4.63; N, 3.19.

[$ReBr_2$(MeCN) (NO) (dpephos)] (40c)

A Mixture of [$ReBr_5(NO)][NEt_4]_2$ (1.000 g, 1.14 mmol) and 2,2´-bisdiphenylphosphinodiphenylether (1 g, 1.85 mmol) in MeCN (3 mL) in a Büchi pressure tube with magnetic stirring bar was stirred for 3 h at 180°C. During this time an orange crystalline solid formed. The reaction mixture was allowed to rest 16 h at room temperature before filtering off the solid which was washed with EtOH (3×2 ml) and dried *in vacuo* to yield **40c** (0.960 g, 0.90 mmol, 88%) as orange crystals.

IR (KBr pellet, cm^{-1}): 1693 (s, ν(NO)). ^{1}H NMR (500 MHz, $CDCl_3$, 28°C): δ = 8.1-7.1 (overlapping multiplets, 26 H, dpephos H), 6.84 (s, 1 H, dpephos H), 6.72 (s, 1 H, dpephos H), 6.63 (s, 1 H, dpephos H), 6.02 (s, 1 H, dpephos, H), 2.07 (s, 3 H, MeCN H) ppm. ^{31}P{^{1}H} NMR (125 MHz, THF-d8, 28°C): δ = -2.8 (s broad, 1 P), -5.0 (s broad, 1 P) ppm. Anal. Calcd. for $C_{38}H_{31}Br_4N_2O_2P_2Re$ (955.63): C, 47.63; H, 3.27; N, 2.93. Found: C, 47.63; H, 3.22; N, 2.97.

[$ReBr_2$(MeCN)(NO)(homoxantphos)] (40d)

A Mixture of [$ReBr_5(NO)][NEt_4]_2$ (1.000 g, 1.14 mmol) and homoxantphos (1.000 g, 1.77 mmol) in MeCN (3 mL) in a Büchi pressure tube with magnetic stirring bar was stirred for 5 h at 180°C. During

this time the reaction mixture turned dark and an orange solid separated. The product was allowed to rest 16 h at room temperature. The crystals were filtered off and washed with EtOH (3×2 ml) and dried *in vacuo* to yield **40d** (0.810 g, 0.83 mmol, 72%) as orange crystals.

IR (cm^{-1}, KBr pellet): 1680 (s, ν(NO)). ^{1}H NMR (500 MHz, $CDCl_3$, 28°C): δ = 8.0-6.8 (overlapping multiplets, 28 H, arom. H), 3.2-2.9 (overlapping multiplets, 4 H, ethylene bridge), 2.4-1.9 (overlapping singlets, 3 H, $NCCH_3$) ppm. $^{31}P\{^{1}H\}$ NMR (125 MHz, THF-d8, 28°C): δ = 25.3 (s, broad), 1.2 (s broad), -0.3 (s broad) ppm. Anal. Calcd. for $C_{40}H_{33}B_2N_2O_2P_2Re$ (981.66): C, 48.94; H, 3.39; N, 2.85. Found: C, 48.69; H, 3.58; N, 2.97.

$[(ReBr_2(di prpfc)(NO))_2]$ (41b)

$[ReBr_5(NO)][NEt_4]_2$ (1.000 g, 1.14 mmol), 1,1'-bisdiisopropylphosphinoferrocene (1.00 g, 2.39 mmol) and abs. EtOH (10 mL) were placed in a 150 mL Schlenk tube with magnetic stirring bar. The suspension was stirred 16 h at 80°C. During this time an orange precipitate forms gradually and the supernatant turns dark brown. The orange precipitate was filtered off and washed with EtOH (3×5 mL). After drying *in vacuo* **41b** (0.720 g, 0.45 mmol, 78%) is obtained as yellow powder.

IR (cm^{-1}, KBr pellet): 1693 (s, ν(NO)). Anal. Calcd. for $C_{44}H_{72}Br_4Fe_2N_2O_2P_4Re_2$ (1585.90): C, 33.26; H, 4.57; N, 1.76. Found: C, 33.20; H, 4.64; N, 1.82.

$[ReBrH_2(SiEt_3)(NO)(P\cap P)]$ (42)

Representative procedure for **42c**: A NMR tube was charged with a suspension of **40c** (10 mg, 0.01 mmol) in $HSiEt_3$ (50 µL, 0.28 mmol) and THF-d6 (500 µL). The NMR tube was sonicated at 50°C for 1 h before measuring the ^{1}H and $^{31}P\{^{1}H\}$ NMR spectra. The solution was quickly evaporated under high vacuum and the remaining solid was used for IR spectroscopy.

Spectroscopic data of **42a**: IR (cm^{-1}, KBr pellet): 1968 (m, broad, ν(ReH)), 1684 (s, ν(NO)). ^{1}H NMR (500 MHz, THF, 28°C): δ = 8.45-7.00 (m, 20 H, phenyl), 5.152 (s, 1 H, cp), 4.656 (s, 1 H, cp), 4.525 (s, 1 H, cp), 4.43-4.30 (m, 5 H, cp), 1.154 (m, 2 H, ReH) 1.18-0.54 (overlapping signals $HSiEt_3$ and $ReSiEt_3$) ppm. $^{31}P\{^{1}H\}$ NMR (125 MHz, THF-d8, 28°C): δ = 3.9 ppm.

Spectroscopic data of **42b**: IR (cm^{-1}, KBr pellet): 1981 (m, broad, ν(ReH)), 1671 (s, ν(NO)). ^{1}H NMR (500 MHz, THF, 28°C): δ = 4.766 (s, 2 H, cp), 4.434 (s, 2 H, cp), 4.354 (s, 4 H, cp), 2.752 (m, 2 H, *i*Pr), 2.610 (m, 2 H, *i*Pr), 1,6-0.5 (overlapping multiplets, 41 H, *i*Pr, ReH) ppm. $^{31}P\{^{1}H\}$ NMR (125 MHz, THF-d8, 28°C): δ = 12.0 ppm.

Spectroscopic data of **42c**: IR (cm^{-1}, KBr pellet): 2004 (m, broad, ν(ReH)), 1678 (s, ν(NO)). ^{1}H NMR (500 MHz, THF, 28°C): δ = 6.670 (m, 3 H, phenyl), 7.50-7.25 (m, 14 H, phenyl), 7.196 (m, 3 H, phenyl),

7.075 (m, 4 H, phenyl), 6.70 (m, 3 H, phenyl), 1.17-0.51 (overlapping signals $HSiEt_3$ and $ReSiEt_3$), 0.688 (m, 2 H, ReH) ppm. $^{31}P\{^1H\}$ NMR (125 MHz, THF-d8, 28°C): δ = -5.0 ppm.

Spectroscopic data of **42d**: IR (cm^{-1}, KBr pellet): 2008 (m, broad, ν(ReH)), 1683 (s, ν(NO)). ^1H NMR (500 MHz, THF, 28°C): δ = 6.648 (t, *J* = 9.0 Hz, 4 H, phenyl), 7.35-7.05 (m, 18 H, phenyl), 6.901 (t, *J* = 7.5 Hz, 2H), 6.513 (t, *J* = 8.0 Hz, 2 H, phenyl), 3.25-3.05 (m, 4 H, homoxantphos-CH_2CH_2), 1.17-0.51 (overlapping signals $HSiEt_3$ and $ReSiEt_3$), 0.755 (m, 2 H, ReH) ppm. $^{31}P\{^1H\}$ NMR (125 MHz, THF-d8, 28°C): δ = -0.2 ppm.

[$ReBrH_2$(d*i*prpfc)(NO)($SiMe_3$)] (42f)

A suspension of [($ReBr_2$(d*i*prpfc)(NO))$_2$] (0.105 g, 0.07 mmol) and 15% $HSiMe_3$ in THF (0.4 mL, 0.57 mmol) in THF (10 mL) was stirred 6 h at room temperature in a 50 mL Schlenk tube with magnetic stirring bar. The resulting turbid orange solution was filtered through a short plug of celite and dried in vacuo to yield **42f** (0.095 g 0.12 mmol, 92%) as yellow powder.

IR (cm^{-1}, KBr pellet): 1974 (m, ν(ReH)), 1678 (s, ν(NO)). ^1H NMR (500 MHz, C_6D_6, 28°C): δ = 4.660 (s, 2 H, Cp), 4.190 (s, 2 H, Cp), 3.975 (s, 4 H, Cp), 2.652 (d heptett, $^3J_{HH}$ = 7 Hz, $J_{P,H}$ = 9.5, 2 H, *i*Pr CH), 2.350 (d heptett, $^3J_{HH}$ = 7 Hz, $J_{P,H}$ = 8.5, 2 H, *i*Pr CH), 1.839 (m, 2 H, ReH), 1.644 (dt, $^3J_{HH}$ = 7 Hz, $^3J_{PH}$ = 15 Hz, 6 H, *i*Pr CH), 1.484 (dt, $^3J_{HH}$ = 7 Hz, $^3J_{P,H}$ = 14.5 Hz, 6 H, *i*Pr CH), 1.220 (s, 9 H, $Si(CH_3)_3$), 1.091 (m, 6 H, *i*Pr CH) ppm. $^{31}P\{^1H\}$ NMR (125 MHz, THF-d8, 28°C): δ = 16.30 ppm. Anal. Calcd for $C_{25}H_{47}BrFeNOP_2ReSi$ (733.79). C, 38.03; H, 6.00; N, 1.77. Found: C, 37.88; H, 5.90; N, 1.71.

[$ReClH_2$(d*i*prpfc)(NO)($SiCl_3$)] (42g)

[($ReBr_2$(d*i*prpfc)(NO))$_2$] (0.100 g, 0.06 mmol), tetraethylammonium chloride (0.250 g, 1.5 mmol) and DCM (10 mL) were placed in a 50 mL Schlenk tube. The suspension was stirred 2 h at 39°C. Trichlorosilane (5 mL, 39.4 mmol) was added to the bright yellow solution and stirring was continued 2 h at 39°C. The solvent was removed *in vacuo* and the residue was extracted with THF. The remaining solid was filtered off and filtrate dried *in vacuo*. The yellow solid was dissolved in a minimum of DCM and chromatographed on silica gel with DCM as eluent. A bright yellow fraction was collected and the solvent was removed *in vacuo* yielding **19b** (0.065 g, 0.08 mmol, 66%) as bright yellow powder.

IR (cm^{-1}, KBr pellet): 2001, 1938 (m, ν(ReH)), 1718 (s, ν(NO)).^1H NMR (500 MHz, THF-d8, 28°C): δ = 4.789 (s, 2 H, Cp), 4.560 (s, 2 H, Cp), 4.539 (s, 2 H, Cp), 4.514 (s, 2 H, Cp), 3.005 (m, 2 H, ReH), 2.759 (m, 2 H, *i*Pr CH), 2.712 (m, 2 H, *i*Pr CH), 1.636 (dd, $^3J_{HH}$ = 7.0 Hz, $^3J_{HP}$ = 8.5 Hz, *i*Pr CH_3), 1.611 (dd, $^3J_{HH}$ = 7.0 Hz, $^3J_{HP}$ = 8.5 Hz, *i*Pr CH_3), 1.310 (dd, $^3J_{HH}$ = 7.0 Hz, $^3J_{HP}$ = 7.5 Hz, *i*Pr CH_3), 1.305 (dd, $^3J_{HH}$ = 7.0 Hz, $^3J_{HP}$ = 7.5 Hz, *i*Pr CH_3) ppm. $^{31}P\{^1H\}$ NMR (125 MHz, THF-d8, 28°C): δ = 24.01 ppm. Anal. Calcd for $C_{22}H_{38}Cl_4FeNOP_2ReSi$ (806.44). C, 32.77; H, 4.75; N, 1.74. Found: C, 32.69; H, 4.81; N, 1.76.

[ReBrH(η^2-C_2H_4)(dppfc)(NO)] (44a)

[$ReBr_2$(MeCN)(NO)(dppfc)] · 2 THF (0.800 g, 0.72 mmol), triethylsilane (1 mL, 6.26 mmol) and DCM (5 mL) were placed in a 50 mL Young Schlenk tube. The Young Schlenk tube was then charged with 2 bar ethylene. The yellow suspension was stirred 24 h at 60°C. The solvent was reduced *in vacuo* to ca. 3 mL and a layer hexane (3 mL) was added. After 3 h the precipitate was separated from the supernatant, washed with pentane (3×2 mL) and dried *in vacuo* to yield **44a** (0.440g, 0.50 mmol, 70%) as a yellow powder.

IR (KBr pellet, cm^{-1}): 1960 (m, ν(ReH)), 1685 (s, ν(NO)). ^{1}H NMR (500 MHz, $CDCl_3$, 28°C): δ = 7.90 (m, 2 Phenyl H), 7.74 (m, 2 Phenyl H), 7.67 (m, 2 H, Phenyl H), 7.47-7.24 (m, 14 H, Phenyl H), 5.38 (s, 1 H, Cp H), 4.65 (s, 1 H, Cp H), 4.51 (s, 1 H, Cp H), 4.37 (s, 2 H, Cp H), 4.24 (s, 2 H, Cp H), 4.09 (s, 1 H, Cp H), 2.59 (s, 3 H, ReH, η^2-C_2H_4 coalescent), 2.42 (m, 1 H, η^2-C_2H_4), 1.21 (m, 1 H, η^2-C_2H_4). ^{31}P{^{1}H} NMR (125 MHz, $CDCl_3$, 28°C): δ = 10.8 (d, $^2J_{PP}$ = 34Hz), 6.49 (d, $^2J_{PP}$ = 34Hz). Anal. Calcd for $C_{36}H_{33}BrFeNOP_2Re$ (879.56). C, 49.16; H, 3.78; N, 1.59. Found: C, 49.08; H, 3.93; N, 1.56.

[ReBrH(η^2-C_2H_4)(diprpfc)(NO)] (44b)

A suspension of [$ReBr_2$(MeCN)(NO)(diprpfc)] (0.70 g, 0.88 mmol) in DCM (20 mL) and $HSiEt_3$ (1 mL, 6.3 mmol) was placed in a Young Schlenk tube with magnetic stirring bar. The Young Schlenk tube was charged with ethylene (2 bar). The suspension was then stirred 24 h at 40°C. The resulting dark brown solution was filtered through a short plug of celite and reduced *in vacuo* to a volume of 3 mL. A layer of hexane (3 mL) was then placed on the concentrated solution. After 16 h **44b** (0.39 g, 0.54 mmol, 61%) was obtained as a microcrystalline pale orange solid.

IR (KBr pellet, cm^{-1}): 1974 (m, ν(ReH)), 1678 (s, ν(NO)). ^{1}H NMR (400 MHz, C_6D_6, 28°C): δ = 4.636 (s, 1 H, cp – H), 4.548 (s, 1 H, cp – H), 4.363 (s, 1 H, cp – H), 4.119 (s, 1 H, cp – H), 4.008 (s, 4 H, cp – H), 3.1-2.4 (overlapping multiplets, 9 H, 4 ethylene H, 1 Re–H, 4 *i*Pr CH), 1.961 (dd, $^2J_{PH}$ = 15.7, $^3J_{HH}$ = 6.7 Hz, 3 H, *i*Pr CH_3), 1.740 (dd, $^2J_{PH}$ = 14.4, $^3J_{HH}$ = 7.5 Hz, 3 H, *i*Pr CH_3), 1.539 (dd, $^2J_{PH}$ = 13.8, $^3J_{HH}$ = 7.4 Hz, 3 H, *i*Pr CH_3), 1.439 (s broad, 3 H, *i*Pr CH_3), 1.403 (dd, $^2J_{PH}$ = 13.9, $^3J_{HH}$ = 7.5 Hz, 3 H, *i*Pr CH_3), 1.10-0.98 (overlapping multiplets, 6 H, *i*Pr CH_3), 1.048 (dd, $^2J_{PH}$ = 11.5, $^3J_{HH}$ = 7.5 Hz, 3 H, *i*Pr CH_3) ppm. ^{31}P{1H} NMR (125 MHz, THF-d8, 28°C): δ = 24.2 (d, $^2J_{pp}$ = 33Hz), -6.2 (s, broadened by exchange). Anal. Calcd for $C_{24}H_{41}BrFeNOP_2Re$ (743.49). C, 38.77; H, 5.56; N, 1.88. Found: C, 38.73; H, 5.53; N, 1.80.

[ReBrH(η^2-C_2H_4)(NO)(homoxantphos)] (44d)

[$ReBr_2$(MeCN)(NO)(homoxantphos)] (0.500g, 0.51 mmol), $HSiEt_3$ (2 mL, 12.5 mmol) and toluene (4 mL) were placed in a 100 mL Young Schlenk tube. The tube was charged with ethylene (2 bar). The yellow suspension was then stirred for 160 h at 50°C. During this time the suspended solid changed its color from bright to pale orange. The solid was then collected by means of centrifugation and

washed with toluene (1 mL). After drying in vacuo **44d** (0.370 g, 0.42 mmol, 82%)was obtained as a pale orange solid.

IR (KBr pellet, cm^{-1}): 2009 (m, ν(ReH)),1673 (s, ν(NO)). ^{1}H NMR (500 MHz, C_6D_6, 28°C): δ = 7.934 (d, *J* = 7.5 Hz, 3 H, arom. H), 7.334 (d, *J* = 7.0 Hz, 3 H, arom. H), 7.13-6.75 (overlapping multiplets, 13 H, arom. H), 6.734 (d, *J* = 5 Hz, 2 H, arom. H), 6.592 (t, J = 7.5 Hz, 3 H, arom. H), 3.028 (t, $^{2}J_{HH}$ = 7 Hz, 3 H, ReH and η^2-CH_2CH_2 in coalescence), 2.706 (m, 4 H, homoxantphos CH_2CH_2), 2.294 (q, $^{2}J_{HH}$ = 7 Hz, 2 H, η^2-CH_2CH_2) ppm. $^{31}P\{^{1}H\}$ NMR (203 MHz, $CDCl_3$ with 5% $NCCH_3$, 28°C): δ = 20.1 (s, 0.18 P), 18.44 (s, 0.82 P), 1.36 (s, 0.18 P), -4.82 (s, 0.82 P) ppm. Anal. Calcd for $C_{40}H_{35}BrNO_2P_2Re$ (889.77). C, 53.99; H, 3.96; N, 1.57. Found: C, 53.80; H, 4.08; N, 1.80.

[ReBr(CH$_2$CH$_3$)(MeCN)(NO)(dpephos)] (46c)

[$ReBr_2$(MeCN)(NO)(dpephos)] (0.500 g, 0.52 mmol), $HSiEt_3$ (0.7 mL, 4.39 mmol) and DCM (3 mL) were placed in a 100 mL Young Schlenk tube. The tube was charged with ethylene (2 bar). The yellow suspension was stirred 24 h at 60°C. The yellow solid was separated by means of centrifugation, washed with pentane (2 mL) and dried *in vacuo* to yield **46c** (0.290 g, 0.32 mmol, 61 %) as a yellow powder. From the supernatant a fraction of less pure **46c** (0.140 g, 0.15 mmol, 29 %) can be obtained by removing the solvent *in vacuo* followed by repeated pentane washes.

IR (cm^{-1}, KBr pellet): 1686 (w, ν(NO)),1653 (s, ν(NO)). ^{1}H NMR (500 MHz, $CDCl_3$ with 5% $NCCD_3$, 28°C): δ = 7.676 (m, 2 H, arom. H), 7.5-6.8 (overlapping multiplets, 22 H, arom. H), 6.711 (m, 1 H, arom. H), 6.594 (m, 1 H, arom. H), 6.429 (m, 1 H, arom. H), 5.872 (m, 1 H, arom. H), 2.738 (m, 1 H, Re$CH_2$$CH_3$), 1.86 (s, 3 H, $NCCH_3$), 1.726 (m, 1 H, Re$CH_2$$CH_3$), 1.197 (s, 3 H, $ReCH_2CH_3$) ppm. $^{31}P\{^{1}H\}$ NMR (203 MHz, $CDCl_3$ with 5% $NCCD_3$, 28°C): δ = 24.2 (d, $^{2}J_{pp}$ = 33Hz), -6.2 (s, broadened by exchange). Anal. Calcd for $C_{40}H_{36}BrN_2O_2P_2Re$ (904.78). C, 53.10; H, 4.01; N, 3.10. Found: C, 53.10; H, 4.01; N, 3.10.

[(ReBr(*μ2*-H)(NO)(d*i*prpfc))$_2$] (50b)

In a NMR tube with Young Teflon cap [ReBrH(η^2-C_2H_4)(diprpfc)(NO)] (0.02 g, 0.03 mmol) was dissolved in a minimum of benzene. The tube was charged with H_2 (1 bar) and allowed to rest until **50b** fully crystallized. **50b** was obtained as large dark red crystals bearing 2 equivalents benzene in quantitative yield.

IR (KBr, cm^{-1}): 1982 (s, ν(ReH)) 1672 (s, ν(NO)). Anal. Calcd. for $C_{56}H_{86}Br_2N_2O_2P_4Re_2$ (1587.10): C, 42.38; H, 5.46; N, 1.77. Found: C, 42.40; H, 5.39; N, 1.78.

[ReBrH(MeCN)(NO)(dppfc)] (51a)

A solution of [ReBrH(η^2-C_2H_4)(dppfc)(NO)] (10 mg, 0.011 mmol) in C_6D_6 and MeCN (10 µL, 0.19 mmol) in a NMR tube with Teflon valve was degassed with tree freeze, pump and taw cycles. The NMR tube

was charged with H_2 (2 bar) and the sample was shaken vigorously. The reaction completed before an NMR spectrum could be obtained.

^{1}H NMR (500 MHz, C_6D_6, 28°C): δ = 8.468 (t, *J* = 9.3 Hz, 2 H, dppfc-ph), 8.197 (t, *J* = 7.5 Hz, 2 H, dppfc-ph), 8.058 (t, *J* = 7.5 Hz, 2 H, dppfc-ph), 7.596 (m, 2 H, dppfc), 7.20-6.95 (overlapping multiplets, 12 H, dppfc), 6.145 (s, 1 H, dppfc), 4.744 (s, 2 H, dppfc), 4.204 (s, 1 H, dppfc), 4.002 (s, 1 H, dppfc), 3.951 (s, 1 H, dppfc), 3.871 (s, 2 H, dppfc), 1.435 (dd, J_{PcisH} = 23.4 Hz, $J_{PtransH}$ = 86.7 Hz, 1 H, ReH), 0.625 (s, 3 H, MeCN) ppm. ^{31}P{^{1}H} NMR (203 MHz, C_6D_6, 28°C): δ = 19.5 (s), -4.4 (s) ppm.

[ReBrH(MeCN)(NO)(dpephos)] (51c)

A solution of [ReBr(CH_2CH_3)(MeCN)(NO)(dpephos)] (10 mg, 0.011 mmol) in C_6D_6 in a NMR tube with Teflon valve was degassed with tree freeze, pump and taw cycles. The NMR tube was charged with H_2 (2 bar) and the sample was shaken vigorously. The reaction completed before an NMR spectrum could be obtained.

^{1}H NMR (500 MHz, C_6D_6, 28°C): δ = 8.458 (s, 2 H, dpephos), 8.115 (s, 2 H, dpephos), 7.598 (s, 2 H, dpephos), 7.500 (s, 2 H, dpephos), 7.15-6.85 (m, 17 H), 6.465 (s, 1H, dpephos), 6.399 (s, 1 H, dpephos), 6.065 (s, 1 H, dpephos), 1.952 (dd, J_{PcisH} = 25.5 Hz, $J_{PtransH}$ = 96.0 Hz, 1 H, ReH), 0.571 (s, 3 H, MeCN) ppm. ^{31}P{^{1}H} NMR (203 MHz, C_6D_6, 28°C): δ = 18.1 (s), -5.1 (s) ppm.

[ReBrH(MeCN)(NO)(dpephos)] (51d)

A sample of **51d** was prepared analogously to **51a**.

^{1}H NMR (500 MHz, C_6D_6, 28°C): δ = 8.478 (s, 2 H, homoxantphos), 7.959 (m, 2 H, homoxantphos), 7.003 (s, 2 H, homoxantphos), 7.503 (s, 2 H, homoxantphos), 7.284 (s, 2 H, homoxantphos), 7.12-6.60 (m, 16 H, dpephos), 3.169 (m, homoxantphos), 2.890 (m, 1 H, homoxantphos), 2.710 (m, 1 H, homoxantphos), 2.470 (m, 1 H, homoxantphos), 2.005 (dd, J_{PcisH} = 19.5 Hz, $J_{PtransH}$ = 91.5 Hz, 1 H, ReH), 0.645 (s, 3 H, MeCN) ppm. ^{31}P{^{1}H} NMR (203 MHz, C_6D_6, 28°C): δ = 25.38 (s), -2.0 (s) ppm.

[ReCl(CO)(NO)(IMes)$_2$][BAr$^F_4$] (54BAr$^F_4$A)

[$ReCl_2$(CO)(NO)(IMes)$_2$] (20 mg, 0.019 mmol) and NaBAr$^F_4$ (19 mg, 0.021 mmol) were stirred in DCM (1 mL) for 30 min. The immediate formation of a fine white precipitate was observed and the solution changed color from yellow/green to light orange. The reaction mixture was filtered through a short plug of celite and the filtrate dried *in vacuo* yielding [ReCl(CO)(NO)(IMes)$_2$][BAr$^F_4$] (33 mg, 0.017 mmol, 90%) as a light orange semi solid.

IR (cm^{-1}, DCM): 1996 (s, ν(CO)), 1750*s* (s, ν(NO)). ^{1}H NMR (CD_2Cl_2, 295K, 300 MHz): δ = 7.73 (s, 8 H, BAr$^F_4$), 7.56 (s, 4 H, BAr$^F_4$), 6.94 (s, 4 H, mes), 6.91 (s, 4 H, N-C*H*=C*H*-N), 6.90 (s, 4 H, mes), 2.33 (s, 12 H, mes), 2.06 (s, 12 H, mes), 2.01 (s, 12 H, mes) ppm. ^{13}C{^{1}H} NMR (CD_2Cl_2, 295K, 125 MHz): δ = 203.5

(s, CO), 169.3 (s, IMes), 162.1 (q, $^{1}J_{BC}$ = 50Hz, $BAr^{F}{}_{4}^{-}$), 140.0 (s, mes), 138.0 (s, mes), 137.5 (s, mes), 136.8 (s, mes), 135.2 (s, $BAr^{F}{}_{4}$), 129.8 (q, ^{3}J = 30 Hz, $BAr^{F}{}_{4}$ C), 128.8 (s, mes), 128.7 (s, mes), 125.8 (s, NCH=CHN), 124.9 (q, $^{1}J_{CF}$ = 272Hz, $BAr^{F}{}_{4}$), 117.9 (m, $BAr^{F}{}_{4}$), 21.1 (s, mes), 18.8 (s, mes), 18.6 (s, mes) ppm.

Isomerization of $[ReCl(CO)(NO)(IMes)_2][BAr^{F}{}_{4}]$ (54$BAr^{F}{}_{4}$)

A sample of freshly prepared $[ReCl(CO)(NO)(IMes)_2][BAr^{F}{}_{4}]$ (20 mg, 0.011 mmol) was dissolved in DCM (1 mL) and left for 16 h. During this time the color of the solution changed from light orange to dark red. The solvent was then removed *in vacuo* quantitatively yielding isomerized $[ReCl(CO)(NO)(IMes)_2][BAr^{f}{}_{4}]$.

IR (cm^{-1}, DCM): 2012 (s, ν(CO)), 1755 (s, ν(NO)). ^{1}H NMR (CD_2Cl_2, 295K, 300 MHz): δ = 7.73 (s, 8 H, $BAr^{F}{}_{4}$), 7.56 (s, 4 H, $BAr^{F}{}_{4}$), 7.09 (s, 4 H, N-C*H*=C*H*-N), 6.94 (s, 4 H, mes), 6.91 (s, 4 H, mes), 2.41 (s, 12 H, mes), 1.93 (s, 12 H, mes), 1.86 (s, 12 H, mes) ppm. $^{13}C\{^{1}H\}$ NMR (CD_2Cl_2, 295K, 125 MHz): δ = 193.5 (s, CO), 180.1 (s, IMes), 162.1 (q, $^{1}J_{BC}$ = 50Hz, $BAr^{F}{}_{4}^{-}$), 140.9 (s, mes), 136.0 (s, mes), 135.9 (s, mes), 135.2 (s, $BAr^{F}{}_{4}$), 133.7 (s, mes), 130.1 (s, mes), 130.0 (s, mes), 129.8 (q, $^{3}J_{BC}$ = 30 Hz, $BAr^{F}{}_{4}$), 125.8 (s, NCH=CHN), 124.9 (q, $^{1}J_{FC}$ = 272Hz, $BAr^{F}{}_{4}$), 117.9 (m, $BAr^{F}{}_{4}$ C), 21.3 (s, mes), 18.0 (s, mes), 17.7 (s, mes) ppm. Anal. calcd. for $C_{75}H_{60}BClF_{24}N_5O_2Re$ (1751.37): C, 51.36; H, 3.56, N 3.99. Found: C, 51.07; H, 3.21; N, 3.68.

$[ReClH(CO)(NO)(IMes)_2]$ (58)

$[ReCl_2(CO)(NO)(IMes)_2]$ (40 mg, 0.045 mmol), $NaBAr^{F}{}_{4}$ (38 mg, 0.045 mmol) and toluene (5 mL) were stirred in an 100 mL Young Schlenk tube with a stirring bar for 16 h. During this time the reaction mixture turned red and a white precipitate was formed. Then 2,2,6,6-tetramethylpiperidin (10 mg, 0.071 mmol) was added and a 2 bar H_2 atmosphere was established in the Young Schlenk tube. The mixture was stirred additional 16 h before removing the volatiles *in vacuo*. The remaining solids were then chromatographed on silica with toluene/diethylether 97:3. Two yellow fractions were collected and the solvent was evaporated *in vacuo* to yield **58a** (20 mg, 0.024 mmol, 52%) and **58b** (14 mg, 0.018 mmol, 39%).

H-*cis*-NO $[ReClH(CO)(NO)(IMes)_2]$ (**58a**): IR (cm^{-1}, toluene): 1999 (s, ν(CO)), 1657 (s, ν(NO)), ^{1}H NMR (C_6D_6, 295K, 300 MHz): δ = 6.76 (s, 8H, mes), 6.09 (s, 4 H, NCHCHN), 4.77 (s, 1 H, Re-H), 2.21 (s, 12 H, mes), 2.11 (s, 24 H, mes) ppm. $^{13}C\{^{1}H\}$ NMR (C_6D_6, 295K, 125 MHz): δ = 207.6 (s, CO), 176.9 (s, IMes), 139.2 (s, mes), 137.3 (s, mes), 136.4 (s, mes), 136.2 (s, mes), 129.2 (s, NCHCHN), 122.8 (s, mes), 21.2 (s, mes), 18.7 (s, mes), 18.7 (s, mes) ppm. Anal Calcd. for $C_{43}H_{51}N_5O_2Re$ (891.33): C, 57.93; H, 5.77; N 7.86. Found: C, 57.60; H, 5.63; N, 7.61.

H-*trans*-NO [ReClH(CO)(NO)(IMes)$_2$] (**58b**): IR (cm^{-1}, toluene): 1926 (s, ν(CO)), 1664 (s, ν(NO)). ^{1}H NMR (C_6D_6, 295K, 300 MHz): δ = 6.71 (s, 4 H, mes), 6.69 (s, 4 H, mes), 6.03 (s, 4 H, NCHCHN), 3.49 (s, 1 H, ReH), 2.18 (s, 24 H, mes), 2.11 (s, 12 H, mes) ppm. ^{13}C{^{1}H} NMR (C_6D_6, 295K, 75 MHz): δ = 221.8 (s, CO), 180.3 (s, IMes), 138.5 (s, mes), 137.2 (s, mes), 136.4 (s, mes), 135.8 (s, mes), 129.2 (s, NCHCHN), 123.1 (s, mes), 21.2 (s, mes), 18.8 (s, mes), 18.7 (s, mes) ppm. Anal. Calcd. for $C_{43}H_{51}N_5O_2Re$ (891.33): C, 57.93; H, 5.77; N, 7.86. Found: C, 58.15; H, 5.84; N, 7.84.

[ReH(CO)(NO)(IMes)$_2$][BAr$^f_4$] (61BAr$^F_4$)

H-*cis*-NO [ReClH(CO)(NO)(IMes)$_2$] (30 mg, 0.034 mmol), NaBAr$^F_4$ (29 mg, 0.034 mmol) and benzene (0.5 mL) were stirred in a 20 mL scintillation counter vial with a magnetic stirring bar for 30 min. The reaction mixture was then filtered through a short plug of celite and the solution was lyophilized to yield [ReH(CO)(NO)(IMes)$_2$][BAr$^F_4$] (57 mg, 0.033 mmol, 97%).

IR (cm^{-1}, toluene): 2016 (s, ν(CO)), 1694 (s, ν(NO)). ^{1}H NMR (Toluen-d8, 295K, 500 MHz): δ = 8.259 (s, 8 H, BAr$^F_4$), 7.632 (s, 4 H, BAr$^F_4$), 6.530 (s, 4 H, mes), 6.470 (s, 4 H, mes), 5.947 (s, 4 H, N-C*H*=C*H*-N), 2.063 (s, 12 H, mes), 1.791 (s, 12 H, mes), 1.706 (s, 12 H, mes), 0.220 (s, 1 H, Re-H) ppm. ^{13}C{^{1}H} NMR (C_6D_6, 295K, 125 MHz): δ = 203.5 (s, CO), 172.1 (s, IMes), 162.7 (q, $^1J_{BC}$ = 50Hz, BAr$^F_4$$^-$), 139.8 (s, mes), 137.8 (s, mes), 137.7 (s, mes), 136.0 (s, mes), 135.5 (s, BAr$^F_4$) 130.1 (q, $^3J_{BC}$ = 31 Hz, BAr$^F_4$), 129.6 (s, mes), 125.3 (q, $^1J_{FC}$ = 272 Hz, BAr$^F_4$), 123.7 (s, NCHCHN), 118.2 (m, BAr$^F_4$), 20.8 (s, mes), 18.3 (s, mes), 17.5 (s, mesityl *o*-CH_3) ppm. Anal. Calcd. for $C_{43}H_{51}N_5O_2Re$ (1718.31): C, 52.39; H, 3.63; N, 4.07. Found: C, 52.02; H, 3.69; N 3.97.

Appendix

List of abbreviations

BAr^F_4	tetrakis(bis(trifluromehyl)phenyl)borate
COSY	correlation spectroscopy
DCM	dichloromethane
dpephos	2,2'-bis(diphenylphosphineo)phenylether
diprpfc	1,1'-bis(diisopropylphosphineo)ferrocene
dppfc	1,1'-bis(diisopropylphosphineo)ferrocene
homoxantphos	10,11-dihydro-4,5-bis(diphenylphosphino)dibenzo[b,f]oxepine
HMBC	heteronuclear multiple bond coherence spectroscopy
HSQC	heteronuclear single quantum coherence spectroscopy
IMes	2,5-dimesithylenimidazoylidene
IR	infra red
MeCN	acetonitrile
Sixantphos	4,6-bis(diphenylphosphino)-10,10-dimethylphenoxasilin
THF	tetrahydrofuran
NMR	nuclear magnetic resonance
NOESY	nuclear Overhauser effect spectroscopy
PPh_3	triphenylphosphine
$P\mathit{i}Pr_3$	triisopropylphosphine
PCy_3	tricyclohexylphosphine
VT NMR	variable temperature NMR
ZPE	zero point energy

Crystal structure determinations

Relevant details about structure refinements are given in Table 10. Intensity data were collected at 183(2) K an Oxford Xcalibur diffractometer (4-circle kappa platform, Ruby CCD detector, and a single wavelength Enhance X-ray source with MoK_α radiation, $\lambda = 0.71073$ Å).[102] The selected suitable single crystals were mounted using polybutene oil on the top of a glass fiber fixed on a goniometer head and immediately transferred to the diffractometer. Pre-experiment, data collection, data reduction and analytical absorption corrections[103] were performed with the Oxford program suite CrysAlisPro[104]. The crystal structures were solved with SHELXS-97[105] using direct methods. The structure refinements were performed by full-matrix least-squares on F^2 with SHELXL-97[105]. All programs used during the crystal structure determination process are included in the WINGX software[106]. The program PLATON[107] was used to check the result of the X-ray analyses. Crystallographic data for **40a**, **40c**, **40e**, **41b**, **42f**, **44d**, **48e(up)**, **48e(down)**, **50b** and **50e** have been deposited with the Cambridge Crystallographic Data Center as CCDC-787668-787677. These data can be obtained free of charge from The Cambridge Crystallographic Data Centre via www.ccdc.cam.ac.uk/data_request/cif and are also available as Supporting Information.

[102] Xcalibur CCD System; Oxford Diffraction Ltd: Abingdon, Oxfordshire, England, 2007.
[103] R. C. Clark and J. S. Reid *Acta Cryst.* **1995**, *A51*, 887-897.
[104] *CrysAlisPro* (versions 1.171.32.34d-55), Oxford Diffraction Ltd, Abingdon, Oxfordshire, England.
[105] G. M. Sheldrick *Acta Cryst.* **2008**, *A64*, 112-122.
[106] L. J. Farrugia *J. Appl. Cryst.* **1999**, *32,* 837.
[107] A. L. Spek *J. Appl. Cryst.* **2003**, *36*, 7-13

Table 10 Crystallographic data for **36PPh$_3$Br**, **40a**, **40c**, **40e**, **41b**, **42f, 42g**, **44d**, **48e(up)**, **48e(down)**, **50b**, **50e, 56** and **59a**.

	36PPh$_3$Br	**40a**	**40c**
CCDC deposition number		787668	787669
empirical formula	$C_{36}H_{32}Br_2NO_5P_2$ Re, 3(C_4H_8O)	$C_{36}H_{31}Br_2FeN_2OP_2$ Re, C4H8O	$_2$($C_{38}H_{31}Br_2N_2O_2P_2Re$), 0.33($CH_2Cl_2$), C_4H_8O
formula weight (g·mol^{-1})	1134.89	1043.53	2012.18
temperature (K)	183(2)	183(2)	183(2)
wavelength (Å)	0.71073	0.71073	0.71073
crystal system, space group	monoclinic, *P 21*/c	monoclinic, *P 21*/n	trigonal, *R -3*
a (Å)	12.3663(2)	9.9650(1)	44.9814(5)
b (Å)	19.8224(4)	32.0257(4)	44.9814(5)
c (Å)	19.7817(5)	12.1774(2)	11.4942(1)
α (deg)	90	90	90
β (deg)	104.979(2)	99.971(1)	90
γ (deg)	90	90	120
volume (Å^3)	4684.31(17)	3827.55(9)	20140.7(4)
Z, *density (calcd) (Mg·m^{-3})*	4, 1.609	4, 1.811	9, 1.493
abs coefficient (mm^{-1})	4.414	5.748	4.625
F(000)	2264	2040	8838
crystal size (mm^3)	0.39 x 0.31 x 0.20	0.31 x 0.17 x 0.06	0.20 x 0.11 x 0.09
θ range (deg)	2.31 to 30.51	2.43 to 30.51	2.59 to 27.10
reflections collected	46853	38549	37156
reflections unique	14218 / R_{int} = 0.036	11676 / R_{int} = 0.057	9889 / R_{in}= 0.031
completeness to θ (%)	99.4	99.9	99.9
absorption correction	analytical	analytical	analytical
max/min transmission	0.461 and 0.327	0.760 and 0.279	0.622 and 0.364
data / restraints / parameters	9660 / 0 / 540	8661 / 0 / 452	7864 / 15 / 468
goodness-of-fit on F^2	1.029	0.934	1.120
final R_1 and wR_2 indices [$I > 2\sigma(I)$]	R_1 = 0.028, wR2 = 0.059	R_1 = 0.032, wR2 = 0.060	R_1 = 0.030, wR2 = 0.096
R_1 and wR_2 indices (all data)	R_1 = 0.058, wR_2 = 0.070	R_1 = 0.054, wR_2 = 0.064	R1 = 0.042, wR2 = 0.098

	40e	**41b**	**42f**
CCDC deposition number	787670	787671	787672
empirical formula	$C_{40}H_{35}Br_2N_2O_2P_2ReSi$, $2(CH_2Cl_2)$	$C_{44}H_{72}Br_4Fe_2N_2O_2P_4Re_2$, $4(CH_2Cl_2)$	$C_{25}H_{47}BrFeNOP_2ReSi$
formula weight ($g \cdot mol^{-1}$)	1181.59	1928.34	789.63
temperature (K)	183(2)	183(2)	183(2)
wavelength (Å)	0.71073	0.71073	0.71073
crystal system, space group	monoclinic, *P 21*/n	triclinic, *P* -1	triclinic, *P* -1
a (Å)	11.2933(2)	11.0458(3)	9.0686(3)
b (Å)	27.3351(4)	12.3739(4)	9.7069(2)
c (Å)	14.7027(2)	13.1814(5)	17.3971(5)
α (deg)	90	84.950(3)	80.684(2)
β (deg)	92.782(2)	68.289(3)	82.148(3)
γ (deg)	90	74.162(3)	85.390(2)
volume ($Å^3$)	4533.43(12)	1610.11(10)	1494.40(7)
Z, *density (calcd) ($Mg \cdot m^{-3}$)*	4, 1.731	1, 1.989	2, 1.755
abs coefficient (mm^{-1})	4.813	7.139	6.034
F(000)	2312	936	784
crystal size (mm^3)	0.17 x 0.10 x 0.06	0.14 x 0.07 x 0.05	0.35 x 0.33 x 0.16
θ range (deg)	2.6 to 26.4	2.31 to 25.68	2.39 to 30.51
reflections collected	37598	18890	26135
reflections unique	9254 / R_{in}= 0.049	6022 / R_{int} = 0.054	9111 / R_{int} = 0.042
completeness to θ (%)	99.9	98.6	99.9
absorption correction	analytical	analytical	analytical
max/min transmission	0.792 and 0.625	0.72 and 0.46	0.46 and 0.18
data / restraints / parameters	6232 / 13 / 528	4778 / 1 / 337	7631 / 2 / 337
goodness-of-fit on F^2	0.85	0.901	0.994
final R_1 and wR_2 indices [$I > 2\sigma(I)$]	R_1 = 0.032, wR_2 = 0.047	R_1 = 0.029, wR_2 = 0.058	R_1 = 0.028, wR_2 = 0.059
R_1 and wR_2 indices (all data)	R1 = 0.061, wR2 = 0.050	R_1 = 0.042, wR_2 = 0.060	R_1 = 0.037, wR_2 = 0.061

	42g	**44d**	**48e(up)**
CCDC deposition number		787673	787674
empirical formula	$C_{22}H_{38}Cl_4FeNOP_2ReSi$	$C_{40}H_{35}BrNO_2P_2Re$	$C_{40}H_{35}BrNO_2P_2ReSi$
formula weight (g·mol-1)	806.42	889.74	917.83
temperature (K)	183(2)	183(2)	183(2)
wavelength (Å)	0.71073	0.71073	0.71073
crystal system, space group	triclinic, *P-1*	monoclinic, *P 21*/c	monoclinic, *P 21*/c
a (Å)	8.8694(1)	19.7393(3)	18.0902(1)
b (Å)	9.7012(2)	9.2862(1)	9.6663(1)
c (Å)	17.2600(3)	19.8067(3)	20.1922(2)
α (deg)	79.778(2)	90	90
β (deg)	82.725(1)	108.782(2)	93.795(1)
γ (deg)	84.055(1)	90	90
volume ($Å^3$)	1444.77(4)	3437.30(9)	3523.17(5)
Z, *density (calcd) (Mg·m^{-3})*	2, 1.854	4, 1.719	4, 1.730
abs coefficient (mm^{-1})	5.227	4.828	4.745
F(000)	796	1752	1808
crystal size (mm^3)	0.49 x 0.39x 0.33	0.31 x 0.17 x 0.11	0.20 x 0.12 x 0.05
θ range (deg)	2.49 to 32.50	2.45 to 30.51	2.57 to 30.51
reflections collected	27997	34427	68012
reflections unique	8821 / R_{int} = 0.0234	10489 / R_{int} = 0.030	10747 / R_{int} = 0.037
completeness to θ (%)	99.9	100.0	99.9
absorption correction	analytical	analytical	analytical
max/min transmission	0.31 to 0.18	0.660 and 0.398	0.813 and 0.532
data / restraints / parameters	8821 / 2 / 349	7811 / 3 / 438	8572 / 0 / 435
goodness-of-fit on F^2	1.046	0.934	0.946
final R_1 and wR_2 indices [$I > 2\sigma(I)$]	R_1 = 0.0203, wR_2 = 0.0463	R_1 = 0.0274, wR_2 = 0.0538	R_1 = 0.023, wR_2 = 0.045
R_1 and wR_2 indices (all data)	R_1 = 0.0237, wR_2 = 0.0470	R_1 = 0.0432, wR_2 = 0.0554	R_1 = 0.033, wR_2 = 0.046

	48e(down)	**50b**	**50e**
CCDC deposition number	787675	787676	787677
empirical formula	$C_{40}H_{35}BrNO_2P_2ReSi$	$C_{44}H_{74}Br_2Fe_2N_2O_2P_4Re_2$, $3(C_6H_6)$	$C_{38}H_{33}BrNO_2P_2ReSi$, $CHCl_3$
formula weight ($g \cdot mol^{-1}$)	917.83	1665.18	1011.16
temperature (K)	183(2)	183(2)	183(2)
wavelength (Å)	0.71073	0.71073	0.71073
crystal system, space group	monoclinic, *P 21/n*	monoclinic, *P 21/c*	orthorhombic, *P nma*
a (Å)	9.8141(1)	12.1375(2)	12.1307(3)
b (Å)	15.7671(2)	14.8890(2)	15.0103(3)
c (Å)	23.1408(3)	17.7830(2)	22.0714(4)
α (deg)	90	90	90
β (deg)	93.946(1)	98.118(1)	90
γ (deg)	90	90	90
volume ($Å^3$)	3572.32(7)	3181.46(8)	4018.88(15)
Z, *density (calcd)* ($Mg \cdot m^{-3}$)	4, 1.707	2, 1.738	4, 1.671
abs coefficient (mm^{-1})	4.680	5.639	4.361
F(000)	1808	1652	1984
crystal size (mm^3)	0.47 x 0.28 x 0.21	0.24 x 0.24 x 0.22	0.17 x 0.14 x 0.10
θ range (deg)	2.55 to 30.51	2.31 to 26.37	2.71 to 25.68
reflections collected	31733	45003	14069
reflections unique	10883 / R_{int} = 0.030	6493 / R_{int} = 0.063	3963 / R_{int} = 0.042
completeness to θ (%)	99.9	99.9	99.9
absorption correction	analytical	analytical	analytical
max/min transmission	0.524 and 0.287	0.46 and 0.30	0.734 and 0.626
data / restraints / parameters	8087 / 0 / 435	5584 / 0 / 355	2760 / 0 / 293
goodness-of-fit on F^2	0.985	1.183	0.962
final R_1 and wR_2 indices [$I > 2\sigma(I)$]	R_1 = 0.029, wR_2 = 0.066	R_1 = 0.039, wR_2 = 0.117	R_1 = 0.0319, wR_2 = 0.0694
R_1 and wR_2 indices (all data)	R_1 = 0.047, wR_2 = 0.069	R_1 = 0.046, wR_2 = 0.119	R_1 = 0.0555, wR_2 = 0.0724

	56	**59a**
CCDC deposition number		
empirical formula	$C_{44}H_{51}ClN_5O_2Re$	$C_{43}H_{49}ClN_5O_2Re$
formula weight ($g \cdot mol^{-1}$)	903.56	889.53
temperature (K)	183(2)	183(2)
wavelength (Å)	0.71073	0.71073
crystal system, space group	P 21/c	P 21/c
a (Å)	12.75330(10)	21.1079(8)
b (Å)	18.98400(10)	10.8793(3)
c (Å)	16.89000(10)	18.7037(7)
α (deg)	90	90
β (deg)	95.2683(4)	109.157(4)
γ (deg)	90	90
volume ($Å^3$)	4071.94(5)	4057.3(3)
Z, *density (calcd) ($Mg \cdot m^{-3}$)*	4, 1.474	4, 1.456
abs coefficient (mm^{-1})	3.092	3.102
F(000)	1832	1800
crystal size (mm^3)	0.34 x 0.25 x 0.12	0.44 x 0.33 x 0.25
θ range (deg)	2.3490 to 32.6937	2.2511 to 32.7127
reflections collected	120652	44055
reflections unique	12425 / R_{int} = 0.0289	12353 / R_{int} = 0.0456
completeness to θ (%)	100.0	99.8
absorption correction	analytical	analytical
max/min transmission	0.466 and 0.731	0.406 and 0.575
data / restraints / parameters	67388 / 4 / 488	7579 / 0 / 493
goodness-of-fit on F^2	1.066	1.008
final R_1 and wR_2 indices [$I > 2\sigma(I)$]	R_1 = 0.0226, wR_2 = 0.0590	R_1 = 0.0413, wR_2 = 0.0928
R_1 and wR_2 indices (all data)	R_1 = 0.0303, wR_2 = 0.0628	R_1 = 0.0837, wR_2 = 0.1168

The unweighted R-factor is $R_1 = \sum(Fo - Fc)/\sum Fo$; $I > 2\,\sigma(I)$ and the weighted R-factor is $wR_2 = \{\sum w(Fo^2 - Fc^2)^2/\sum w(Fo^2)^2\}^{1/2}$.

Coordinates of the optimized structures 43PMe$_3$, 44PMe$_3$, 45PMe$_3$, 49PMe$_3$, 51PMe$_3$, 52PMe$_3$, TS1 and TS2:

24PMe$_3$			
	X [Å]	Y [Å]	Z [Å]
RE	-0.000689	0.056484	-0.093575
P	-2.368171	0.219916	0.438773
P	2.365747	0.236221	0.438635
N	0.010523	-1.734891	-0.280695
O	0.020627	-2.933079	-0.309391
C	-0.716025	0.692140	-2.137958
C	0.704693	0.711213	-2.135840
H	1.243752	-0.079711	-2.653446
H	-1.257241	1.635447	-2.117126
H	1.218969	1.669330	-2.111959
H	-1.232448	-0.114006	-2.655225
H	-0.001488	0.084509	1.604152
H	-0.005818	1.764461	0.274545
C	2.850135	-0.538840	2.044551
C	3.044037	1.945314	0.596894
C	3.560642	-0.560185	-0.728819
C	-2.846682	-0.552730	2.047651
C	-3.559727	-0.585888	-0.725622
C	-3.055337	1.925867	0.593027
H	-3.926812	-0.483177	2.224882
H	-2.546035	-1.605675	2.046167
H	-2.306437	-0.050921	2.855617
H	-3.496513	-0.114804	-1.710981
H	-3.305385	-1.645566	-0.834869
H	-4.588396	-0.499235	-0.355460
H	-2.538010	2.447083	1.403637
H	-2.872433	2.477039	-0.334258
H	-4.132816	1.904027	0.796753
H	3.930777	-0.468166	2.217987
H	2.312339	-0.040034	2.856115
H	2.551165	-1.592281	2.041651
H	3.494943	-0.085858	-1.712478
H	4.589137	-0.470647	-0.358838
H	3.310574	-1.620467	-0.841765
H	2.860434	2.496858	-0.330037
H	2.522819	2.462868	1.407356
H	4.121174	1.927837	0.802610

24PMe$_3$TS			
	X [Å]	Y [Å]	Z [Å]
RE	-0.004250	0.038697	0.021406
P	-2.405599	0.070006	0.329809
P	2.400301	0.114501	0.170256
N	0.067623	-1.721194	-0.283866
O	0.183088	-2.911409	-0.422160
C	-0.321255	1.209094	-1.952296
C	0.097448	2.226170	-1.070611
H	1.131055	2.559134	-1.077661
H	-1.347915	1.205728	-2.310426
H	-0.603816	3.000704	-0.769621
H	0.403911	0.769697	-2.632634
H	-0.029684	0.063829	1.708532
H	0.058160	1.730467	0.612997
C	3.107053	-1.358066	1.037398
C	3.145055	1.513388	1.128115
C	3.430661	0.146142	-1.381258
C	-3.026070	-0.699506	1.892514
C	-3.406126	-0.847790	-0.931784
C	-3.241056	1.723335	0.361955
H	-4.121736	-0.676517	1.944184
H	-2.683638	-1.738256	1.936458
H	-2.607910	-0.172559	2.756578
H	-3.215228	-0.443937	-1.931376
H	-3.099147	-1.899532	-0.930116
H	-4.480709	-0.788038	-0.720362
H	-2.823223	2.324949	1.175600
H	-3.059989	2.250678	-0.581372
H	-4.324739	1.630046	0.505574
H	4.203410	-1.360553	1.000721
H	2.776985	-1.350050	2.081162
H	2.726657	-2.271611	0.570470
H	3.173957	1.023227	-1.986103
H	4.503690	0.174440	-1.155063
H	3.213225	-0.749883	-1.972674
H	2.976245	2.467898	0.617529
H	2.663281	1.563015	2.109405
H	4.224496	1.370529	1.258962

24PMe$_3$a			
	X [Å]	Y [Å]	Z [Å]
RE	0.000024	-0.002244	0.000381
P	-2.434128	0.012292	0.078625
P	2.434114	0.011812	0.077986
N	-0.000126	-1.784971	-0.052462
O	-0.000258	-2.940417	-0.402982
H	0.000115	0.045268	1.646667
C	0.000046	2.014203	-0.901859
C	3.170460	-0.040626	1.777599
C	3.419330	1.370781	-0.708446
C	3.197735	-1.481885	-0.707878
C	-3.170117	-0.040223	1.778391
C	-3.198162	-1.481235	-0.707177
C	-3.419260	1.371536	-0.707430
H	-4.261819	-0.145046	1.747378
H	-2.737778	-0.884704	2.323852
H	-2.911458	0.876869	2.318330
H	-2.961374	-1.496966	-1.776837
H	-2.778737	-2.386661	-0.259035
H	-4.287646	-1.483420	-0.581685
H	-3.180142	1.435073	-1.774336
H	-4.492204	1.176134	-0.598088
H	-3.183324	2.337041	-0.247702
H	4.262156	-0.145482	1.746401
H	2.911906	0.876497	2.317533
H	2.738204	-0.885072	2.323181
H	2.960820	-1.497574	-1.777510
H	4.287240	-1.484189	-0.582564
H	2.778280	-2.387257	-0.259656
H	3.179885	1.434318	-1.775283
H	3.183799	2.336381	-0.248714
H	4.492256	1.175098	-0.599441
C	0.000082	3.127358	0.177251
H	-0.873086	2.174452	-1.551818
H	0.873079	2.174539	-1.551923
H	-0.000520	4.134759	-0.269594
H	-0.878845	3.067165	0.833478
H	0.879716	3.067848	0.832596

24PMe$_3$a-ag			
	X [Å]	Y [Å]	Z [Å]
RE	-0.001844	0.005185	0.009850
P	-2.413630	0.075965	0.182808
P	2.415823	0.119746	0.227750
N	0.040850	-1.778344	-0.123671
O	0.050068	-2.961202	-0.338369
H	-0.015165	0.047594	1.670043
C	-0.101379	2.145151	-0.478098

C	3.069483	-0.359974	1.891752
C	3.273902	1.737691	-0.043979
C	3.363614	-1.011664	-0.892948
C	-3.158914	-1.528391	0.713835
C	-3.450986	0.499301	-1.300701
C	-3.088741	1.251233	1.443707
H	-4.254145	-1.475348	0.747895
H	-2.857935	-2.321393	0.021880
H	-2.776387	-1.787720	1.706175
H	-3.177252	1.489853	-1.679215
H	-3.272000	-0.233545	-2.095104
H	-4.519082	0.501732	-1.051273
H	-2.868401	2.283647	1.153421
H	-4.173222	1.135869	1.558223
H	-2.595574	1.057357	2.400925
H	4.165831	-0.333788	1.916733
H	2.670026	0.328285	2.643032
H	2.721912	-1.367906	2.139592
H	3.150969	-0.754131	-1.936183
H	4.444811	-0.946571	-0.719780
H	3.037473	-2.044300	-0.728531
H	3.037476	2.134436	-1.035981
H	2.929882	2.461278	0.702683
H	4.362357	1.632360	0.044896
C	0.017086	1.704756	-1.945940
H	0.712699	2.806246	-0.169399
H	-1.041777	2.673550	-0.291469
H	0.017781	0.568933	-2.064049
H	-0.831276	2.010345	-2.568088
H	0.947572	2.018052	-2.431639

24PMe$_3$aTS			
	X [Å]	Y [Å]	Z [Å]
RE	0.030505	0.002178	-0.009675
P	2.448553	0.111293	-0.186593
P	-2.392692	-0.035978	-0.086811
N	-0.021080	1.748831	0.248082
O	-0.047037	2.897234	0.620498
H	0.089776	-1.162658	1.283398
C	0.202524	-2.225767	0.309837
C	-3.426899	-0.737372	1.294649
C	-3.143148	-0.882078	-1.564845
C	-3.135123	1.652584	-0.211947
C	3.527332	-0.925460	0.920959
C	3.147468	1.793643	0.127794
C	3.177209	-0.284225	-1.852155
H	4.589549	-0.708601	0.753864
H	3.275751	-0.709410	1.964509
H	3.356927	-1.991710	0.741686
H	2.739081	2.502405	-0.599610
H	2.857534	2.133948	1.125751
H	4.240492	1.777405	0.047227
H	2.747744	0.390677	-2.599696
H	4.268978	-0.177007	-1.851723
H	2.920034	-1.310630	-2.137901
H	-4.496283	-0.601211	1.091438
H	-3.224867	-1.803291	1.430293
H	-3.168631	-0.223557	2.226709
H	-2.694145	2.187934	-1.057435
H	-4.223379	1.597397	-0.336921
H	-2.905956	2.217299	0.697385
H	-2.760686	-0.412010	-2.476717
H	-2.855464	-1.939688	-1.584298
H	-4.238334	-0.815052	-1.560380
C	-0.778898	-3.308512	0.758506
H	1.225825	-2.564279	0.490574
H	0.111954	-2.050798	-0.806573
H	-0.481944	-4.291223	0.369265
H	-0.793322	-3.380225	1.853528
H	-1.802375	-3.116292	0.424425

24PMe$_3$c			
	X [Å]	Y [Å]	Z [Å]
RE	-0.002066	0.065914	-0.022036
P	-2.388241	0.327279	0.004850
P	2.389353	0.305755	0.020548
N	0.008469	-1.709112	0.101773
O	0.016386	-2.889842	-0.137249
H	-0.013525	1.540714	-1.003852
H	0.000245	0.264092	1.611840
C	3.235706	-0.538167	1.435099
C	3.039200	2.033595	0.148441
C	3.329152	-0.351183	-1.438006
C	-3.309028	-0.810783	1.136841
C	-3.295218	0.081908	-1.594924
C	-2.999586	1.990711	0.538637
H	-4.394328	-0.683053	1.046423
H	-3.046616	-1.847886	0.901627
H	-3.007512	-0.612581	2.170608
H	-2.902106	0.775996	-2.345240
H	-3.129143	-0.939614	-1.954281
H	-4.374570	0.245097	-1.481144
H	-2.630073	2.210745	1.545524
H	-2.618524	2.757614	-0.142477
H	-4.095865	2.017940	0.543366
H	4.327324	-0.446408	1.379072
H	2.880626	-0.091423	2.368543
H	2.959216	-1.597922	1.441560
H	3.006432	0.165678	-2.348345
H	4.411131	-0.219998	-1.312925
H	3.111951	-1.418239	-1.557451
H	2.783361	2.583729	-0.762496
H	2.572978	2.542297	0.998028
H	4.127654	2.032815	0.280953

33PMe$_3$			
	X [Å]	Y [Å]	Z [Å]
RE	-0.005756	-0.073693	-0.129751
P	-2.397540	0.137893	0.367952
P	2.402028	0.033156	0.328312
N	-0.035288	-1.822298	0.261055
O	-0.040902	-2.972374	0.604677
C	-0.734952	-0.166121	-2.270370
C	0.685196	-0.240046	-2.277704
H	1.156899	-1.199462	-2.482782
H	-1.215002	0.759968	-2.577453
H	1.261486	0.624814	-2.597156
H	-1.312767	-1.065089	-2.477026
H	0.025601	0.434424	1.493504
C	0.053251	2.155016	-0.491362
C	2.822465	0.169250	2.122631
C	3.432360	1.378591	-0.408081
C	3.333833	-1.483714	-0.170559
C	-2.784813	0.216935	2.172149
C	-3.430638	-1.297517	-0.175938
C	-3.333951	1.580814	-0.304869
H	-3.862612	0.311692	2.354553
H	-2.416378	-0.694965	2.653933
H	-2.260352	1.064564	2.623281
H	-3.450637	-1.338019	-1.269622
H	-2.983887	-2.225171	0.193131
H	-4.458649	-1.214067	0.196461
H	-3.316971	1.558864	-1.399158
H	-4.376605	1.558923	0.034416
H	-2.867484	2.511180	0.027670
H	3.903983	0.099027	2.293514
H	2.452653	1.122637	2.512049
H	2.314949	-0.635075	2.663203

H	3.333545	-1.568667	-1.262163
H	4.371776	-1.451498	0.182403
H	2.839712	-2.369895	0.239554
H	3.398494	1.333642	-1.501382
H	3.058308	2.356822	-0.092668
H	4.474545	1.275450	-0.083173
C	0.090154	3.122868	0.702533
H	-0.807595	2.424554	-1.123952
H	0.922103	2.373038	-1.133517
H	0.113831	4.182514	0.396380
H	-0.781770	2.998385	1.360300
H	0.969676	2.951797	1.338927

H	4.419325	-1.270680	0.192457
H	2.950848	-2.287191	0.130174
H	3.347765	1.587353	-1.178494
H	2.855884	2.449554	0.292647
H	4.350795	1.477534	0.290161
C	0.027282	3.569298	0.193672
H	-0.898681	2.345293	-1.336388
H	0.867888	2.328532	-1.367930
H	0.020843	4.490647	-0.404785
H	-0.835775	3.609337	0.870882
H	0.924602	3.594038	0.826287
H	-0.005460	1.464694	0.497621

44PMe$_3$

	X [Å]	Y [Å]	Z [Å]
C	1.129200	-2.418120	1.997533
P	1.725266	-0.920638	1.104957
C	3.301667	-1.510792	0.346229
RE	0.252897	0.186950	-0.553871
N	1.396489	1.510115	-0.693048
O	2.166370	2.422313	-0.787452
P	-1.258470	1.271169	1.176432
C	-1.570140	0.364698	2.762534
C	2.380994	0.162157	2.458497
C	-0.643804	2.914853	1.769526
C	-2.998184	1.668209	0.694502
H	1.146423	-0.929462	-1.441240
BR	-1.502229	-1.828562	-0.370352
H	-1.324643	3.351335	2.510401
H	0.349261	2.807909	2.217522
H	-0.553066	3.603814	0.922823
H	-3.534668	2.124141	1.535159
H	-3.012143	2.358580	-0.153077
H	-3.508623	0.745436	0.400841
H	-2.293361	0.907797	3.381550
H	-1.972965	-0.623176	2.518421
H	-0.645590	0.237013	3.333182
H	3.978655	-1.912650	1.109546
H	3.080002	-2.286656	-0.392308
H	3.789457	-0.678538	-0.171016
H	3.102624	-0.378897	3.082288
H	2.878840	1.031268	2.014584
H	1.568656	0.524466	3.094907
H	1.909305	-2.804425	2.663756
H	0.232080	-2.183014	2.576181
H	0.853835	-3.179517	1.262940
C	-0.338223	0.371245	-2.713149
C	-1.251322	1.163028	-1.987465
H	-1.152437	2.247415	-1.992694
H	-2.251389	0.781754	-1.809528
H	-0.644959	-0.603640	-3.078750
H	0.471420	0.836389	-3.269303

33PMe$_3$TS

	X [Å]	Y [Å]	Z [Å]
RE	-0.002494	-0.104157	-0.204915
P	-2.341756	0.044893	0.455128
P	2.344793	0.055332	0.436810
N	0.007103	-1.755689	0.468876
O	0.019687	-2.876119	0.925865
C	-0.723486	-0.246842	-2.292392
C	0.714961	-0.244189	-2.295724
H	1.228454	-1.182978	-2.503869
H	-1.257352	0.624368	-2.677540
H	1.243188	0.628218	-2.685508
H	-1.235314	-1.187045	-2.497851
C	-0.003990	2.320765	-0.708717
C	2.672855	-0.014322	2.256500
C	3.321841	1.536245	-0.084727
C	3.392244	-1.337428	-0.186501
C	-2.664849	-0.241631	2.255262
C	-3.471270	-1.204821	-0.312020
C	-3.265806	1.615121	0.138558
H	-3.735511	-0.186996	2.491578
H	-2.282293	-1.229617	2.530167
H	-2.120720	0.507340	2.838291
H	-3.488629	-1.077084	-1.398874
H	-3.108794	-2.215353	-0.092310
H	-4.491359	-1.100146	0.076396
H	-3.249942	1.859463	-0.928260
H	-4.309166	1.517530	0.463195
H	-2.807464	2.443281	0.686707
H	3.744080	-0.111451	2.477324
H	2.286848	0.894612	2.729934
H	2.136565	-0.866909	2.686286
H	3.410089	-1.315160	-1.280233

43PMe$_3$

	X [Å]	Y [Å]	Z [Å]
C	-1.694934	2.143184	1.635956
P	-1.937291	0.486089	0.862046
C	-3.593091	0.619851	0.058633
RE	-0.198261	-0.076168	-0.554513
N	-1.053961	-1.516159	-1.087529
O	-1.579215	-2.508168	-1.506041
P	1.415426	-1.301717	0.948452
C	1.922882	-0.503524	2.539296
C	-2.313628	-0.607323	2.308741
C	0.874773	-2.987509	1.493014
C	3.061171	-1.665843	0.177508
H	-0.984434	0.949360	-1.646644
BR	1.527331	1.841354	-0.461495
H	1.674673	-3.507108	2.034438
H	-0.000835	-2.908199	2.145338
H	0.590803	-3.583953	0.619316
H	3.708145	-2.227131	0.862639
H	2.919092	-2.250323	-0.737909
H	3.548632	-0.722749	-0.089321
H	2.656126	-1.114421	3.079968
H	2.355770	0.476669	2.317261
H	1.045903	-0.355248	3.178137
H	-4.363548	0.896765	0.788170
H	-3.544357	1.373149	-0.732763
H	-3.855959	-0.338817	-0.400056
H	-3.185882	-0.244878	2.867099
H	-2.515438	-1.624114	1.955637
H	-1.451891	-0.640079	2.982736
H	-2.539508	2.382649	2.293287
H	-0.765948	2.155312	2.212753
H	-1.614096	2.898087	0.849371

45PMe$_3$

	X [Å]	Y [Å]	Z [Å]
RE	0.230239	0.011287	-0.508902
P	1.626039	0.474931	1.337275
P	-1.221216	-1.806446	0.378486

BR	-1.736124	1.553072	0.429576
N	1.453690	-1.067928	-1.160583
O	2.287109	-1.819204	-1.584067
C	0.700370	1.700135	-1.757314
H	0.435566	2.690192	-1.381561
H	1.705901	1.705506	-2.184606
C	-0.340814	1.109387	-2.695921
H	0.065780	0.753162	-3.647789
H	-0.845475	0.148295	-2.273104
H	-1.216472	1.746157	-2.852612
C	-1.788838	-1.827437	2.141350
C	-2.843500	-1.961841	-0.503304
C	-0.523689	-3.512393	0.178399
C	1.915883	-0.777939	2.675097
C	3.363263	0.809209	0.796890
C	1.204177	1.982460	2.309022
H	2.721517	-0.456197	3.346247
H	1.003011	-0.916061	3.262637
H	2.191183	-1.738605	2.226966
H	1.988589	2.180389	3.049546
H	1.107512	2.838150	1.635013
H	0.244008	1.848226	2.813836
H	4.002695	1.063234	1.651113
H	3.772029	-0.074339	0.295646
H	3.365393	1.637903	0.082777
H	-3.447057	-2.777993	-0.089181
H	-3.389008	-1.018424	-0.405763
H	-2.668075	-2.152137	-1.568434
H	-2.511439	-2.634239	2.317291
H	-0.935936	-1.971812	2.812482
H	-2.255787	-0.866030	2.375420
H	-1.238221	-4.272949	0.514654
H	-0.281580	-3.688259	-0.874456
H	0.401008	-3.610050	0.756397

52PMe$_3$			
	X [Å]	Y [Å]	Z [Å]
RE	-0.252080	-0.193252	0.480713
P	-1.293635	0.061852	-1.698683
P	2.054192	-1.036420	-0.237104
BR	0.918753	2.187728	0.143372
N	-0.925466	-1.798095	0.711791
O	-1.360595	-2.903897	0.851390
C	-2.060735	0.856587	1.234649
H	-1.857860	1.932690	1.163297
H	-2.923848	0.664511	0.579422
C	-2.500599	0.508195	2.665603
H	-3.421137	1.042941	2.952024
H	-1.738394	0.774240	3.412905
H	-2.701246	-0.565280	2.776270
C	2.927730	-0.462949	-1.768082
C	3.364028	-0.685769	1.025663
C	2.173035	-2.879988	-0.391733
C	-0.298724	-0.255368	-3.221624
C	-2.733214	-1.068292	-1.940805
H	-0.898849	-0.082801	-4.123503
H	0.567152	0.411205	-3.239142
H	0.051815	-1.293098	-3.228562
C	-1.990325	1.731887	-2.052699
H	-2.443057	1.746654	-3.050140
H	-2.744575	1.988857	-1.304208
H	-1.188292	2.472400	-1.994392
H	-3.190441	-0.913673	-2.924377
H	-2.405897	-2.109064	-1.853829
H	-3.481147	-0.884672	-1.163165
H	4.337604	-1.087091	0.718480
H	3.445303	0.397503	1.159950
H	3.082740	-1.134477	1.984707
H	3.969319	-0.805486	-1.762404
H	2.440478	-0.849215	-2.667649
H	2.911814	0.631132	-1.798422
H	3.207235	-3.192952	-0.576515
H	1.815843	-3.349961	0.530562
H	1.540871	-3.231055	-1.213852
H	0.785907	-0.238872	2.014717
H	0.056348	0.093565	2.271550

TS1			
	X [Å]	Y [Å]	Z [Å]
RE	0.194219	-0.202729	-0.540086
P	1.543215	1.073994	1.054348
P	-1.065723	-1.696152	0.965600
BR	-1.727471	1.585122	0.066778
N	1.459229	-1.377790	-0.852821
O	2.333798	-2.177427	-1.028854
C	0.652667	1.141273	-2.241120
H	0.375098	2.179765	-2.076955
H	1.663727	1.001411	-2.620413
C	-0.371330	0.251021	-2.748158
H	-1.361050	0.670779	-2.924825
H	-0.084154	-0.507619	-3.475501
H	-0.946223	-0.735358	-1.761054
C	-0.403602	-3.424196	0.976082
C	-1.267379	-1.375679	2.779663
C	-2.827432	-1.959294	0.466654
C	3.229436	0.373270	1.353209
C	1.933300	2.788386	0.483241
H	3.813547	1.023744	2.014812
H	3.151588	-0.621143	1.804587
H	3.755219	0.266861	0.399256
C	0.953600	1.406103	2.777339
H	1.626087	2.105810	3.288319
H	-0.053479	1.830572	2.738652
H	0.919079	0.473100	3.345808
H	2.518825	3.326902	1.238135
H	2.500550	2.746659	-0.451642
H	0.997866	3.324816	0.299063
H	-1.936526	-2.115514	3.237255
H	-0.294922	-1.437122	3.278994
H	-1.680565	-0.374875	2.936905
H	-0.384473	-3.816862	-0.045644
H	0.622864	-3.433252	1.356427
H	-1.024147	-4.077917	1.600484
H	-3.324594	-2.676587	1.130658
H	-3.356364	-1.002497	0.501798
H	-2.858841	-2.331735	-0.562164

TS2			
	X [Å]	Y [Å]	Z [Å]
RE	-0.196762	-0.245250	0.506289
P	-1.124117	0.204946	-1.847958
P	2.074815	-0.968991	-0.267067
BR	0.715934	2.254334	0.434300
N	-0.778096	-1.898043	0.633499
O	-1.168971	-3.024764	0.717167
C	-2.335765	0.611038	1.131016
H	-2.232585	1.693815	1.244034
H	-2.908947	0.419645	0.221079
C	-3.089154	-0.009425	2.315362
H	-4.122890	0.363059	2.354930
H	-2.611497	0.228529	3.273726
H	-3.135404	-1.102703	2.235234
C	2.109551	-2.578287	-1.182788
C	3.129204	0.126123	-1.314967
C	3.200514	-1.319662	1.151131
C	-0.044807	0.099435	-3.350314
C	-2.481182	-0.975184	-2.290298

H	0.706826	0.894731	-3.321731
H	0.464568	-0.867823	-3.393998
H	-0.642174	0.220847	-4.261947
C	-1.904687	1.858738	-2.114101
H	-2.345643	1.918099	-3.115271
H	-2.681045	2.040608	-1.365497
H	-1.135626	2.626307	-1.994785

H	-2.877874	-0.771485	-3.291418
H	-2.109437	-2.004987	-2.251638
H	-3.294409	-0.892106	-1.562021
H	4.109660	-0.337043	-1.476677
H	2.654892	0.305442	-2.283326
H	3.254484	1.090099	-0.814175
H	3.139277	-2.913988	-1.353157

H	1.575706	-3.340128	-0.605064
H	1.609231	-2.478035	-2.151443
H	4.182706	-1.666609	0.807207
H	3.320754	-0.407403	1.743689
H	2.746807	-2.082017	1.791405
H	0.714172	-0.326365	1.913454
H	-0.933528	0.259327	1.880805

Curriculum Vitae

Name	:	Dudle
First name	:	Balthasar
Date, place of birth	:	18.10.1979, St. Gallen
Natinality	:	Swiss
Citizen of	:	Bütschwil, SG
Education	:	
since 2006	:	Dissertation at the University of Zürich
2005-2006	:	Master of Science, University of Zürich in Chemistry
2002-2005	:	Bachelor of Science, University of Zürich in Chemistry
1997-2001	:	general qualification for university entrance, Gymnasium Friedberg, Gossau SG